APPSBX 22 1–342(1973)

Polymeric Materials for Unusual Service Conditions

Editors:
Morton A. Golub
and
John A. Parker

1973: an Interscience® Publication

APPLIED POLYMER SYMPOSIA NO. 22

Polymeric Materials for Unusual Service Conditions

Held at Ames Research Center, NASA, Moffett Field, California,
November 29, 30, and December 1, 1972

Sponsored Jointly by *National Aeronautics and Space Administration, Ames Research Center*, and the *University of California, San Diego*

Editors

Morton A. Golub
Ames Research Center, NASA
Moffett Field, California

John A. Parker
Ames Research Center, NASA
Moffett Field, California

an Interscience® Publication

published by **JOHN WILEY & SONS**
NEW YORK · LONDON · SYDNEY · TORONTO

JOURNAL OF APPLIED POLYMER SCIENCE
APPLIED POLYMER SYMPOSIA NO. 22

Morton A. Golub and John A. Parker have been appointed Editors by the Editorial Board of the *Journal of Applied Polymer Science* for this issue of *Applied Polymer Symposia.*

Published at irregular intervals by John Wiley & Sons, Inc. Publication Office at 20th and Northampton Streets, Easton, Pennsylvania 18042. Executive, Editorial, and Circulation Offices at 605 Third Avenue, New York, New York 10016. Subscription price $150.00 per volume. Foreign postage, $8.00 per volume.

Printed in U.S.A.

Preface

The Conference on Polymeric Materials for Unusual Service Conditions was held at Ames Research Center at Moffett Field, California on November 29, 30, and December 1, 1972. This conference, apparently the first of its kind, was organized with the aim of bringing together people interested in the development and utilization of polymers intended for an assortment of unusual or extreme service applications. The conference was divided into six sessions dealing with the following topics: polymers for aircraft and spacecraft structures, high temperature resins and composites, elastomers for high temperature applications, fire retardant materials, polymers for critical pollution control, and polymers for critical medical use.

The idea for this conference, as well as the choice for its locale, arose from the recognition that the dominant theme pervading most of the polymer programs in NASA for a number of years has, in fact, been the development of polymeric materials for unusual service conditions. Moreover, the search for new polymers to meet the critical demands imposed by advances in aeronautics and space missions has led to the creation at Ames Research Center of the Chemical Research Projects Office in which a variety of projects have been conducted on topics paralleling those represented in the sessions of this conference. Professor Herman Mark has given generously of his time in providing guidance for many of these endeavors, and it was he who urged and indeed inspired us to undertake the organization of this rather eclectic conference.

We would like to record our sincere appreciation to the various session chairmen (J. D. Ray, T. T. Serafini, J. Moacanin, C. J. Hilado, A. S. Michaels, and M. Goodman, drawn from other organizations) and co-chairmen (D. A. Kourtides, S. R. Riccitiello, G. M. Fohlen, T. Wydeven, and A. H. Heimbuch, all of Ames Research Center) who, besides conducting their respective sessions in the conference, aided us in the selection of the speakers; to Professor Mark, our honorary chairman, for his encouragement and support; and to the authors without whose important contributions there would not have been the conference nor this symposium issue.

Morton A. Golub
John A. Parker

Chemical Research Projects Office
Ames Research Center
National Aeronautics and Space Administration
Moffett Field, California 94035

Contents

Fire Retardant Materials

Polymers for Critical Pollution Control

Polymers for Critical Medical Use

NOVEL FOAMS AND POROUS STRUCTURES

I. O. SALYER, J. L. SCHWENDEMAN and G. L. BALL III

Monsanto Research Corporation,
Dayton Laboratory,
Dayton, Ohio 45407

SYNOPSIS

Five types of new foams, or foaming techniques, were investigated. These include ultra-light-weight foams, air-frothed epoxy foams, open-pore polyurethane (OPP), a new polyimide foam process, and instant polystyrene foam.

First, ultra-light-weight foams, having a density in the range of 0.08 lb/ft^3 were prepared using aqueous solutions of surfactant plus water soluble resin binders. The foams were generated by spraying a water solution of the resin-augmented surfactant on the back side of a suitable screen support through which air was blown to generate copious quantities of low density foam on the downstream side. Foam density was controlled by the concentration and quantity of surfactant and resin binder, plus the air volume. Potential application of these unusual light-weight foams for dust suppression in coal mines was studied in the laboratory. The systems and equipment developedfor this use and the results obtained were described.

Second, a new air-frothable epoxy resin foam system was developed. In this foam, air was dissolved or dispersed at ambient or elevated pressure in a proprietary epoxy composition which has surfactant properties built into it. With this process, foam having a shaving cream-like consistency is obtained which does not rise further during cure. The density of the product foam is an inverse linear function of the air pressure applied during frothing. Densities from 3 to 30 lb/ft^3 have been investigated. These air-frothed epoxy foams have considerable thixiotropic character, and can be troweled or sprayed into molds, or onto vertical surfaces, without flowing under their own weight. The foams cure in several hours at ambient temperature, or in 1 to 2 hr at elevated temperature. Uses foreseen for the air-frothed epoxies include packaging of items for shipment, building components, and entire buildings or shelters.

The third novel system, open pore polyurethane (OPP), was obtained by polymerizing specific polyol and isocyanate precursors in selected solvents, followed by evaporative removal of the solvent. The OPP which was formed consisted of chains of small spheres (1/2 μ) with throughgoing pores, formed by the space between the entangled chains of spheres. A very narrow distribution of pore sizes was observed, whose average size depends on the density of the product. Density, in the range of 6–25 lb/ft^3 was determined by the amount of solvent present during the polymerization. Fillers can be incorporated into the OPP if desired. Reaction kinetics of the polymerization were followed by infrared spectroscopy. Important uses are projected for open pore polyurethane in various types of filtering applications, and in chromatographic substrates, for either liquid or gas phase chromatography.

The fourth system developed was an improved process for molding all-aromatic polyimide foam. In this process, ultra-low density precursor foam (about 0.5 lb/ft^3) was prepared, shredded, and remolded with application of heat and pressure in a closed mold. Foams ranging in density from 2–20 lb/ft^3 have been prepared with excellent uniformity and reproducibility. These foams are highly resilient, 100% open-cell, and have good mechanical properties, and an abrasion-resistant skin. Polyimide foams of this type are non-burning in air, and with incor-

Applied Polymer Symposium No. 22, 1–2 (1973)

poration of additional proprietary additives, are also non-burning in an atmosphere of 70% oxygen at 6.2 psi. With the development of this new process, larger utilization of polyimide foam in a variety of high temperature and flame-retardant applications is expected.

The fifth novel foam system (instant foam) consists of any one of several soluble thermoplastic polymers (e.g., polystyrene) dissolved in a combination of low boiling solvents, nucleating agents, and surfactants. Density range is limited to about 1–3 lb/ft^3. Solvents constitute about 33% of the weight and volume of the foam solution. Foaming is achieved by depressurizing the solution through a suitable valve and die (for extruded shapes), or into a closed vented mold (for rigid moldings).

AIRPLANE NACELLE COMPOSITE STRUCTURE TECHNOLOGY

L. D. CHRISTENSEN* and R. N. HOLMES

Douglas Aircraft Company, McDonnell Douglas Corporation, Long Beach, California

SYNOPSIS

Current investigations of non-metallic composite materials for use in commercial jet airplane nacelles are reported. Both acoustical structure, for attenuation of sound in engine inlet and fan exhust ducts, and non-acoustical structure for use in other nacelle areas are under development. Unique composite development problems include sustained high-temperature operation and intermittent environmental operating extremes under flight loads, severe sonic fatigue conditions, fire burnthrough resistance, and sound attenuation requirements. A method of composite integral construction shows potential for satisfying many of these unique requirements. The development and application of a glass fiber/polyimide resin configuration is presented, as well as data on other configurations of interest. A full-scale glass/polyimide inlet acoustical liner for an advanced technology airplane has recently been built and acoustically tested on an engine test stand. Lightweight integral constructions of advanced fibers are in development and undergoing tests. Preliminary analyses show significant cost and weight savings potential. The need for improved polymer capability and fiber technology to realize this potential is discussed.

INTRODUCTION

This paper addresses the application of non-metallic composite materials technology to airplane jet engine nacelle structure. This is a limited use of a broad technology, yet it is among the most challenging and may be one of the most promising areas for composite materials use.

A jet engine nacelle is in essence a pod that encases the turbine engine. The nacelle is required to withstand duct pressures and loads imposed on it in flight and during ground handling. However, it structural load requirements are less severe than those of the primary airplane structure, such as the wings and fuselage.

The aerospace industry efforts involving composites technology have heavily emphasized primary structure with lesser attention given to lightly loaded structure applications such as may be found in the jet engine nacelle. A purpose of this paper is to increase awareness of the potential benefits of composite structure applications to nacelles.

* Present address: General Structures Corporation, Balboa, California

Applied Polymer Symposium No. 22, 3–19 (1973)

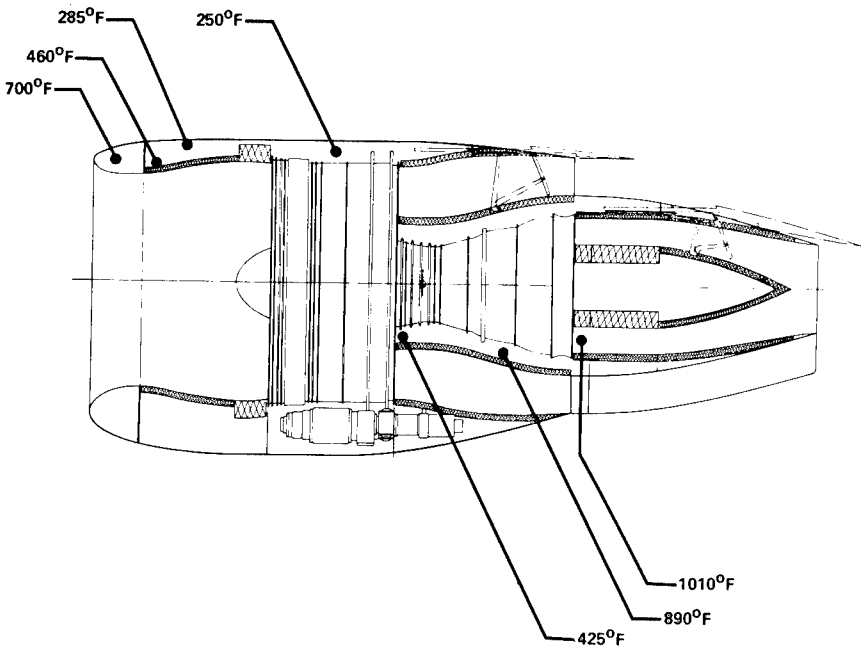

FIG. 1. Advanced technology engine.

The introduction of non-metallic composites in nacelle structure offers prospects of attractive weight and cost savings. Recent achievements in composites technology lend confidence that these prospective savings may be realizable. There is need, however, for sustained and continued research and for the development of improved fibers and high-temperature resins to achieve the potential.

Several recent developments in non-metallic composites technology appear to be of promise for application to nacelle design. These include the integral weaving of three-dimensional fabric structure of fiber glass and other yarns in a way which unifies the structure and precludes debonding or delamination; the development of new lightweight fibers with a variety of strength and temperature characteristics; and hybridizing techniques of combining integral structure and selected fibers to tailormake lightweight nacelle parts with the desired characteristics. Enough background has been accumulated with the production and testing of glass–polyimide composites to provide encouragement to proceed with advanced fibers and resins using similar structures and processes.

Based upon available technology and anticipated developments, it has become possible to define a nacelle that makes extensive use of non-metallic composites, and to estimate in some detail and with reasonable confidence the weight and cost savings that may be realized. This paper presents such an estimate, using an advanced technology conceptual engine to illustrate the benefits of using composites.

UNIQUE PROBLEMS OF COMPOSITE NACELLE DESIGN

The association of the nacelle with the engine imposes unique requirements and constraints upon nacelle design, which include strength, temperature, fire containment, noise reduction, sonic fatigue, and erosion.

Although structural loads are light, noise reduction requirements are increasingly important for commercial transports, and temperature and sonic fatigue environments are extreme. Near-sonic-velocity air flows impose erosion resistance requirements upon internal duct surfaces. Nacelle materials used in fire zones must survive a 2000°F flame for 15 minutes to pass certification requirements for commercial use. In addition, it is a continuing design objective to meet the requirements with minimum weight and cost.

Figure 1 illustrates a conceptual design for an advanced technology engine nacelle. Although this is a representative rather than an optimized design, the concept is a fair basis for the cost and weight comparisons which follow.

A preliminary thermal analysis, conducted concurrently with the conceptual design phase, considered potential materials and their conductivities as well as the configuration. With the selected composite parts, it was estimated that temperatures may reach as high as 460°F aft of the inlet lip section, 890°F on the back face of the fan exhaust duct inner wall, and 1010°F in the turbine exhaust duct, during a hot day (120°F) sea level takeoff.

Maximum temperatures throughout the nacelle are indicated on Figure 1. The inlet maximum temperatures shown assume that the ice protection system is operating during hot day sea level takeoff. These are extremes which would not often be encountered and which would not last long. Normal steady-state operating temperatures would be more than 100°F lower.

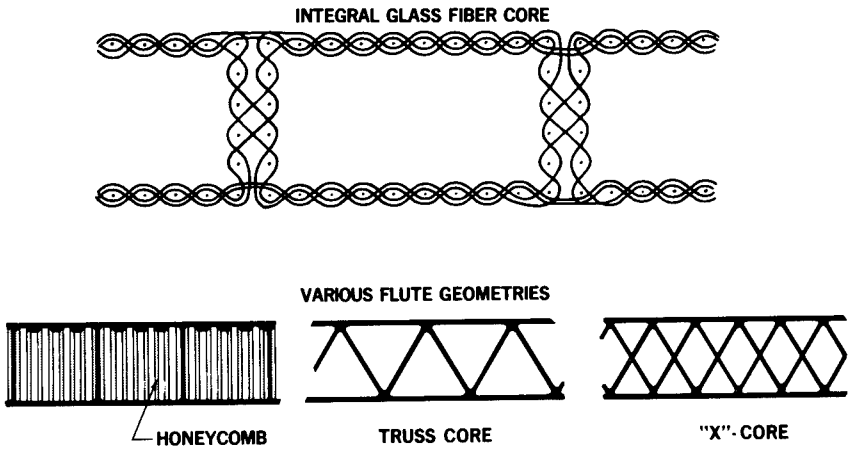

FIG. 2. Integrally woven core designs.

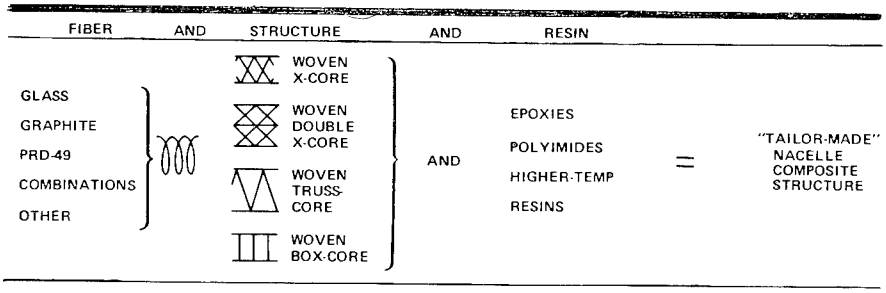

FIG. 3. Nacelle composite structure options.

It is expected that composites with polyimide or epoxy resins will operate satisfactorily in selected areas of the inlet and fan exhaust duct outer wall. In the fan exhaust duct inner wall, fibers and resins capable of steady-state temperatures above 500°F are desired. These temperatures are beyond the capabilities of polyimide or epoxy resins. In the turbine exhaust area the steady-state temperature requirements exceed 1000°F. Modified pyrolized graphite fibrous structure offers an approach to these temperature extremes, combining strength with light weight.

These requirements exemplify a fertile field for the development of high temperature polymers and resins that would provide structural versatility while maintaining light weight, fabricability, and relatively low cost, as glass/polyimide composites do.

Composite materials and processes are being developed which will meet most of the unique requirements of nacelle design, often with substantial weight and cost savings over present conventional metal materials. A nacelle built almost entirely of advanced composites is conceivable. However, for the weight and cost analyses presented later in this paper, composite nacelle parts selected were those which could be developed and demonstrated in the relatively near future.

DISCUSSION

Douglas Aircraft Company has developed a glass/polyimide integrally woven composite material which has been shown to be suitable for acoustical and fire-resistant applications. A sketch of some typical integrally woven construction designs is shown in Figure 2.

The woven structure is unique in that both faces are integral and interlocked with the core structure, unlike ordinary sandwich composite structure which has faces bonded to a core material. The integral construction precludes delamination or debonding. The structure is capable of being tailored to meet specific requirements of various parts of a nacelle. This tailoring ranges from filament selection and optimization, through the woven structure configuration design and resin selection and pre-impregnation, to the final curing stages, where the maximum-achievable high temperature properties of both the fibers and the resins are realized. Figure 3 illustrates a variety of combinations available for tailormaking a structure.

FIG. 4. DC-10 APU inlet duct part

To date, considerable development work has been done on integrally-woven glass-polyimide composites. This includes the acoustical evaluation of many configurations, full-scale ground static tests of the material in the fan exhaust duct of a JT3D engine, sonic fatigue tests, fire burnthrough tests, preliminary studies of installed weight and production costs, and service testing of specimens in the fan duct inner walls of JT3D engines. At present, the material is used for the Douglas DC-10 APU inlet duct shown in Figures 4 and 5.

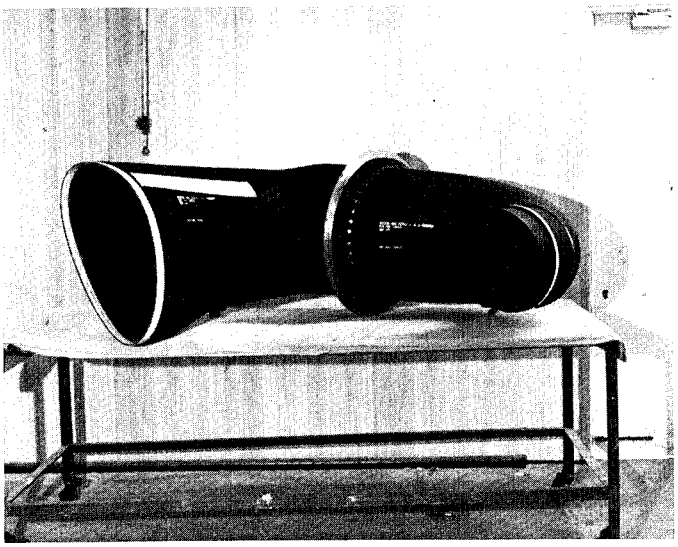

FIG. 5. Complete DC-10 APU duct.

Acoustic Properties

Preliminary acoustical evaluations have included flow resistance tests, duct transmission loss tests, and full-scale acoustical testing. These tests and their results are described in the following paragraphs.

Flow Resistance Tests

The capability of a structure to dissipate acoustic energy as heat in the pores of the material is directly related to its resistance to air flow, or flow resistance. For example, ordinary sandwich structure with porous face sheet, inpervious backing sheet, and impervious honeycomb core, dissipates acoustic energy in the porous face sheet only. Flow resistance measurements therefore provide an easy means of evaluating candidate porous structure for use in nacelles.

Flow resistance, in cgs rayls, is the ratio of the pressure drop across the sample, in dynes/sq cm, to the linear velocity of the airflow through the sample, in cm/sec. The flow resistance at an airflow velocity of 20 cm/sec is known as the nominal flow resistance, and the nonlinearity factor (NLF) is defined as the ratio of the flow resistance at an airflow velocity of 500 cm/sec to the nominal flow resistance. For applications in the nacelles of jet engines, it is often desirable to have porous material with a low NLF because this ensures that the characteristics of the material will have only minimum variation over the range of incident sound pressures and grazing airflow velocities encountered in a nacelle. This characteristic is most desirable when substantial noise reduction is desired over a wide range of engine operating conditions and when the sound field and grazing airflow velocities cannot be accurately predicted.

The development efforts on woven fiberglass/polyimide structures included flow resistance tests on several sample structures differing in type of weave, the number of plies, and the impregnation process. The purposes of these tests were: (1) to determine the relationship between flow resistance and the weaving–impregnating characteristics so that porous face sheets could be manufactured with specified acoustic properties; (2) to verify the repeatability of the flow resistance from one batch of material to another; and (3) to determine glass volume and resin content to aid in developing integrally woven face sheets that had given flow resistance characteristics without special requirements for orientation or stacking of several layers of individual plies.

Figure 6 shows representative flow resistance curves for three different types of porous sheet materials. The fibermetal material had the smallest NLF and would be the least sensitive to variations in the acoustic and flow fields in an engine nacelle. The NLF of the perforated plate specimen was approximately eight times that of the fibermetal sample. The polymide–fiberglass sample had a nominal flow resistance approximately equal to that of the fibermetal sample with a significantly smaller NLF than that of the perforated plate sample.

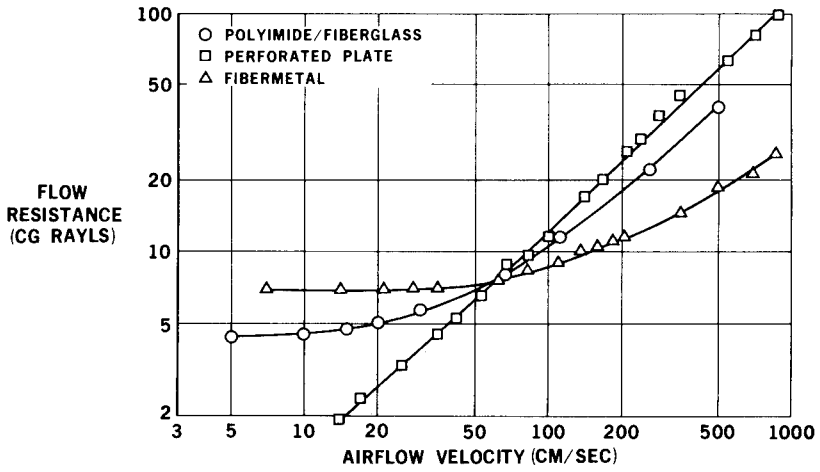

FIG. 6. Flow resistance vs airflow velocity for various materials.

Duct Transmission-Loss Tests

The transmission loss achieved with acoustical test panels installed on the walls of a special test duct was compared to the transmission loss achieved with hardwall panels. Several different types of acoustical structures were studied including perforated sheet over honeycomb and integrally-woven glass–polyimide composite structure. One general result was that the glass–polyimide structure could achieve larger noise attenuations over a wider range of frequencies than perforated sheet over honeycomb, for the same value of maximum attenuation. This result was especially marked when the core behind the porous face sheet was also porous. Several porous core constructions were tested, and the one that achieved the widest attenuation bandwidth had an X-shaped cross section. An X-core glass–polyimide composite construction was subsequently chosen for evaluation in a DC–10 full-scale inlet duct.

Figure 7 presents typical results from these duct transmission loss tests. The integrally-woven glass–polymide composite structure achieved approximately the same maximum attenuation as the perforated sheet linings, but significantly more attenuation at frequencies above the frequency of maximum attenuation. This is a desirable result because it means that larger reductions in turbomachinery noise can be obtained over a wider range of engine power settings and because the linings will be more effective at reducing the amplitude of harmonics of the fundamental blade-passage frequency. This characteristic of being able to achieve wider attenuation bandwidths for comparable maximum attenuation values is one of the chief acoustical advantages of integrally woven composite structures for absorptive duct linings compared to perforated sheet/honeycomb structures.

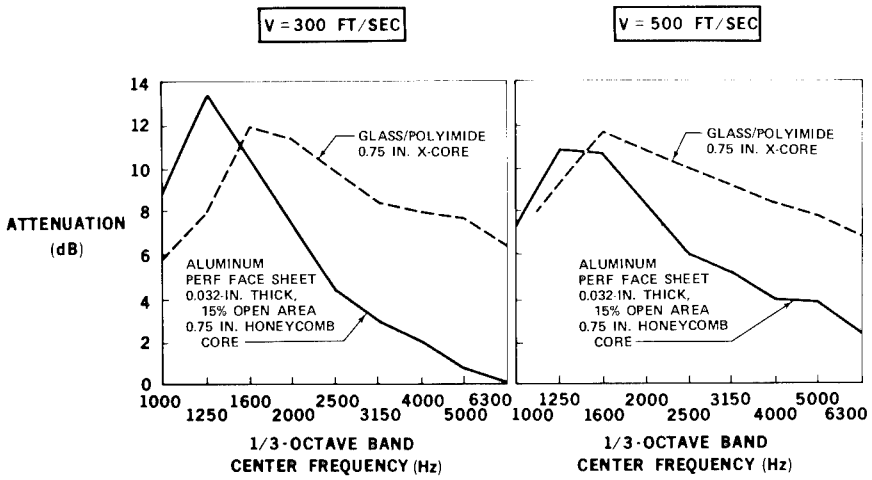

FIG. 7. Exhaust mode noise reduction for integrally-woven glass-polymide and perforated sheet-honeycomb.

Full-Scale Acoustic Tests

Noise reduction tests on a JT3D turbofan engine were conducted with two different types of linings installed in special 48-inch-long fan-exhaust ducts (see Fig. 8). The two types of linings consisted of: (1) integrally woven fiberglass structures with porous face sheets and impervious cores and backing sheets; and (2) perforated aluminum sheets bonded to impervious aluminum honeycomb with impervious back sheets.

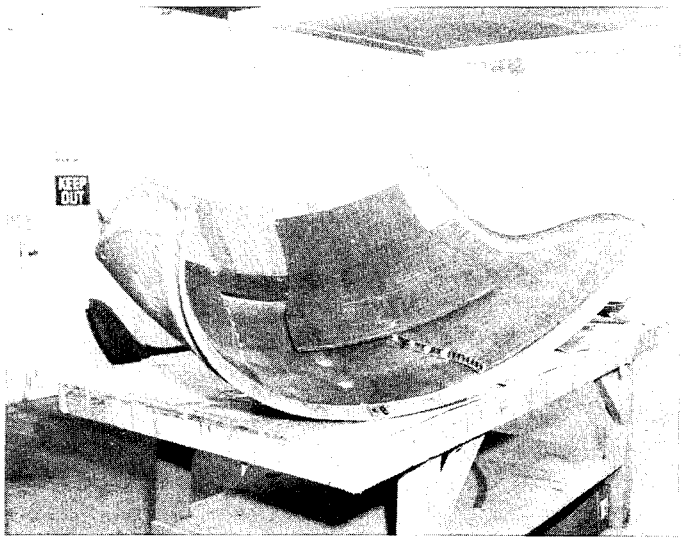

FIG. 8. Integrally woven JT3D fan exhaust duct.

Two configurations of each type of lining were tested: (a) the woven linings had face sheets with nominal 7 cgs rayl and nominal 15 cgs rayl flow resistances; and (b) the preforated sheet linings had face sheets with nominal 8.6 and nominal 15 percent open areas.

Noise reductions were determined by comparing the data obtained with hardwall, untreated fan ducts to the data obtained with acoustical linings installed in the ducts. At an engine power setting representative of a typical engine speed required by DC–8 airplanes during approach, the results showed that the maximum noise reduction, as a function of frequency, achieved by the better of the two woven structure linings was comparable to the maximum noise reduction achieved by the better of the two perforated sheet linings. However, the frequency range over which large noise reductions were achieved was wider with the woven structure linings than with the perforated sheet linings, corroborating the results of the duct-transmission-loss tests.

Sonic Fatique Properties

Sonic fatigue tests were performed on two flat integrally woven structural panels, 0.75 by 20 by 26.75 inches, simulating a fan exhaust duct. Panels were subjected to a random noise sound pressure level (SPL) spectrum that had the following variations of overall SPL and test time:

Overall SPL, dB	Total Exposure Time, Minutes	Inspection Time Interval, Minutes
150	120	30
153	60	30
156	60	15
159	60	15
162	60	15
165	240	15

Both panels withstood, without failure, the entire 10-hour exposure to random noise. Control panels duplicating conventional aluminum skin and stringer construction in fan duct walls (which have proved to be satisfactory in more than a generation of service) failed the same test in 110 minutes at 159 dB and 30 minutes at 165 dB, indicating that the test was severe.

Fire Resistance Properties

Acoustic duct walls in a fire zone area are required to have fire resistance as well as acoustic absorption properties, because of the proximity to the engines or auxiliary power units, and the requirements of certification that a nacelle must contain a fire of 2000°F for 15 minutes.

Four polyimide impregnated fiber glass panels were tested with an oxygen acetylene torch at 2000°F for 15 minutes. All panels passed the burn test with no panel burnthrough.

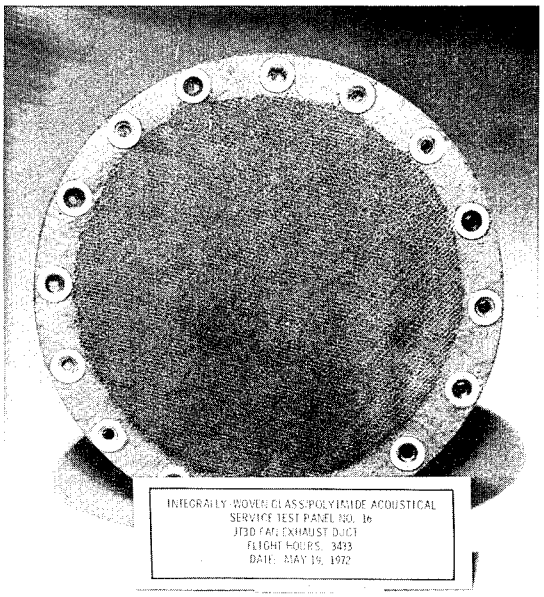

FIG. 9. Service test panel.

Service Testing

Integrally woven structure specimens 9 inches in diameter with bonded face sheets were exposed to the fan-exhaust duct environment of JT3D engines to determine the durability of the face-sheet material under actual service conditions. The specimens were designed to fit in the inner wall of the fan exhaust duct of the engines. Figure 9 shows a typical specimen.

As of this writing, two of the specimens had been in service for nearly 5000 flight hours. Inspection revealed no erosion or other service problems. There were two cases of foreign object damage with broken fibers in areas no greater than 1/8 square inch. Overall, performance of the specimens has been excellent.

Current Programs

Currently, a program is under way to develop the 3/4-inch integrally-woven glass–polyimide X-core composite, shown in Figure 10, for possible incorporation in the DC–10–30 engine nacelle inlets. A prototype full-scale DC–10 inlet liner has been fabricated of the material and is shown in Figure 11. This inlet performed successfully in ground static acoustical tests run by General Electric, and its acoustical performance was comparable to metal perforated plate honeycomb sandwich material.

A comprehensive laboratory test program is in progress to determine the mechanical allowables of the 3/4-inch material. In addition to the investi-

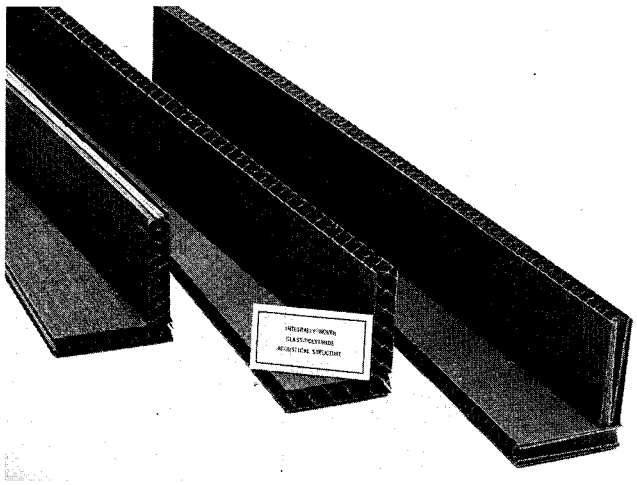

FIG. 10. X-core glass/polyimide structure.

gation of various configurations of woven glass–polyimide structure, research and development is under way on improved fibers to further reduce weight, increase load-carrying capability, improve sustained high temperature capability and fire resistance. Included in these studies are fibers of graphite and Du Pont PRD–49. Sandwich panels incorporating Du Pont PRD–49 on both the front and back face passed the FAA 15-minutes 2000°F fire burnthrough test. These results make the PRD–49 material a potential candidate for use in fire zone areas.

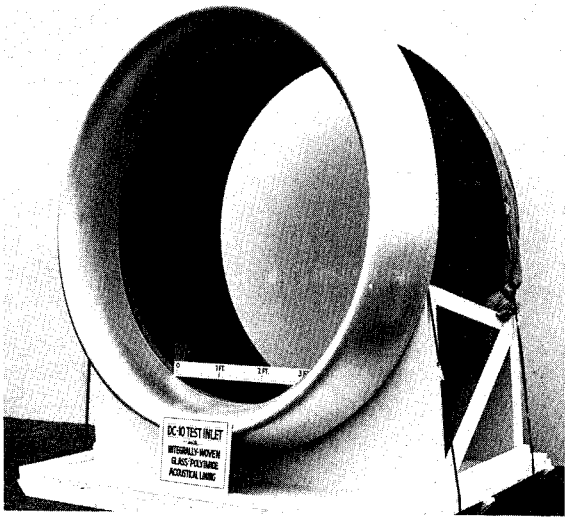

FIG. 11. DC–10 test inlet.

The Du Pont company has developed for this program a series of PRD–49 experimental yarns duplicating the glass yarns now being used. It has been demonstrated that these PRD–49 yarns can be woven on the same looms and to the same integral three-dimensional configurations as the glass yarns presently in use.

Non-Acoustical Composites

The development of non-acoustical configurations of integrally-woven composites parallels and follows the acoustical material. Its uses are intended to be in structural areas such as cowling, fairing, and bulkheads. We are presently in the process of making and evaluating glass–polyimide and glass–epoxy non-acoustical panels for testing. We expect weight and cost savings of the same order as the acoustical material, for the same reasons.

For maximum weight savings these non-acoustical composites also may utilize advanced lightweight filaments. Since large nacelle areas are non-acoustical, the development of non-acoustical composites is important for bringing the full benefits of composites technology to nacelle structure.

PRELIMINARY WEIGHT ANALYSIS

This analysis develops a measure of the engine nacelle weight that may be saved through the use of advanced composite parts, both acoustic and non-acoustic, in a representative advanced technology engine nacelle, shown in Figure 1. This considers the replacement of about half of the metal nacelle structure with advanced composite materials. The remaining metal parts (listed below) would be retained. The reason for selecting this level of composite application is that the weight benefit is significant, yet the level of composite use appears to be an achievable target through identifiable technology, with a reasonable and sustained research and development effort. The key findings may be summarized as follows:

Weight savings of advanced composite nacelle
55% on a part-for-part basis
30% of total bare nacelle (less engine)
11% of total installed nacelle and pylon

Acoustical treatment was used on the inlet inner barrel, fan duct walls, thrust reverser translating structures, tailpipe walls, and bullet. Nacelle weights were compared for a conventional metal configuration and for an advance composite configuration in which about half the parts of the conventional configuration (by weight) were replaced with advanced composite parts.

Table I lists the nacelle parts that would be built of advanced composites. It was assumed that fittings, fastenings, and associated hardware

would remain present technology (metallic); likewise, the inlet lip and the primary and secondary thrust reverser cascades, drive mechanisms, supporting structures, and attachments would remain unchanged.

Selection of the particular configuration of each advanced composite part involved a number of considerations. The sizing, depth, and internal structure was, in each case, selected to meet or exceed the structural loads requirements of the part, bearing in mind the strength and modulus of elasticity of the selected material. For the acoustical parts, representative face, depth, and cell characteristics were designated. High temperature requirements were met by the selection of high temperature materials such as modified pyrolized graphite fiberous structure.

Table II compares the weights of the nacelle built of conventional metal-parts with the estimated weights of the same nacelle using the indicated fourteen advanced composite parts.

The fourteen replaceable parts of metal construction weight 870 pounds. The same fourteen parts of the indicated advanced composite construction weigh 395 pounds, a saving of 475 pounds, or 55%, on a part-for-part basis.

With inclusion of the 718 pounds of metal parts in each configuration, the bare nacelle (without engine and pylon) weights 1588 pounds in the all-metal configuration, and 1113 pounds in the mixed configuration which has selected parts of advanced composites. The weight differential remains the same 475 pounds, which is 30 percent of the all-metal bare nacelle weight.

With inclusion of the engine, engine systems, and pylon, the total installed weight of the nacelle and pylon was 4,890 pounds for the conventional metal configuration, and 4,350 pounds for the advanced composite configuration. The same dry engine weights and engine systems weights were used for both configurations. Pylon weight was 74 pounds less for the lighter nacelle, since pylon weight is a function of the weight it supports. Ten pounds of lightning protection was added to the composite configuration. The saving in total installed weight of nacelle and pylon from the use of advanced composites was accordingly 539 pounds or 11%.

TABLE I
Nacelle Parts Built of Composites

NOSE COWL INSTALLATION:	EXHAUST SECTION:
OUTER BARREL	TAILPIPE
INNER BARREL	BULLET (PLUG)
BULKHEAD	FAN REVERSER INSTALLATION:
AFT SECTION COWL INSTALLATION:	OUTER SKIN
FAN ACCESS DOORS	FAN EXHAUST DUCTING
AFT COWL	TRANSLATING STRUCTURE
FAIRING	PRIMARY SPOILER INSTALLATION:
BULKHEAD	OUTER COWL
	TRANSLATING STRUCTURE

Table II
Preliminary Weight Comparisons (Per Nacelle)

1. REPLACEABLE PARTS (PART-FOR-PART COMPARISONS)	CONFIGURATION			
	NUMBER OF PARTS	PARTS BUILT OF METAL (LB)	SAME PARTS BUILT OF ADVANCED COMPOSITES (LB)	Δ WEIGHT (LB)
NOSE COWL INSTALLATION	3	169	81	88
AFT SECTION COWL INSTALLATION	4	133	34	99
EXHAUST SECTION	2	114	20	94
FAN REVERSER INSTALLATION	3	318	210	108
PRIMARY SPOILER INSTALLATION	2	136	50	86
TOTAL REPLACEABLE PARTS	14	870	395	475
PERCENTAGE SAVING: 475/870 = 55 PERCENT				

2. BARE NACELLE (WITHOUT ENGINE AND ENGINE SYSTEMS AND PYLON)	CONFIGURATION		
	ALL PARTS OF METAL (LB)	SELECTED PARTS OF ADVANCED COMPOSITES (LB)	Δ WEIGHT (LB)
REPLACEABLE PARTS (SEE ABOVE)	870	395	475
RETAINED METAL PARTS	718	718	–0–
TOTAL BARE NACELLE	1588	1113	475
PERCENTAGE SAVING: 475/1588 = 30 PERCENT			

3. INSTALLED NACELLE AND PYLON (ALL-UP COMPARISON)	CONFIGURATION		
	ALL PARTS OF METAL (LB)	SELECTED PARTS OF ADVANCED COMPOSITES (LB)	Δ WEIGHT (LB)
BARE NACELLE (SEE ABOVE)	1588	1113	475
ADD: DRY ENGINE	2570	2570	–0–
ENGINE SYSTEMS	167	167	–0–
PYLON	565	491	74
LIGHTNING PROTECTION	–0–	10	<10>
TOTAL INSTALLED NACELLE AND PYLON	4890	4351	539
PERCENTAGE SAVING: 539/4890 = 11 PERCENT			

PRELIMINARY COST ANALYSIS

This analysis develops a measure of the engine nacelle cost savings that may be possible through the use of advanced composite parts in an advanced technology engine nacelle. This analysis parallels the preceding

weight analysis and is based on the same engine, nacelle design, ground rules and assumptions. The conclusions may be summarized as follows:

Cost savings of advanced composite nacelle
65% on a part-for-part basis
48% of total bare nacelle (less engine)
12% of total installed nacelle and pylon

Table I identifies the nacelle parts where advanced composites might replace conventional metal construction. As with the weight analysis, it was assumed that fittings, fastenings, and miscellaneous hardware would remain conventional metal in both configurations.

The three composite parts in the nose cowl installation section are estimated to cost about 27% as much as the same three parts of conventional metal construction, a savings of 73%. Similarly, the four composite parts in the aft section cowl installation are estimated to cost about 56 percent less than the same parts in metal. Savings of 78% in the exhaust section, 63% in the fan thrust reverser installation, and 69% in the primary spoiler installation are estimated.

The savings range from 56 to 78, an average of 65% for the fourteen selected parts on a part-for-part basis. With inclusion of the common parts, which remain metal in both configurations, the savings become 48% of total bare nacelle cost. With inclusion of the engine, engine systems and pylon, the savings is still 12% of total installed nacelle and pylon cost.

CONCLUSIONS

The potential impact of non-metallic composites technology on airplane nacelle structures is illustrated in Figure 12. The application of existing glass–polyimide technology could reduce nacelle cost and weight, even though only the lower and intermediate temperature areas would be

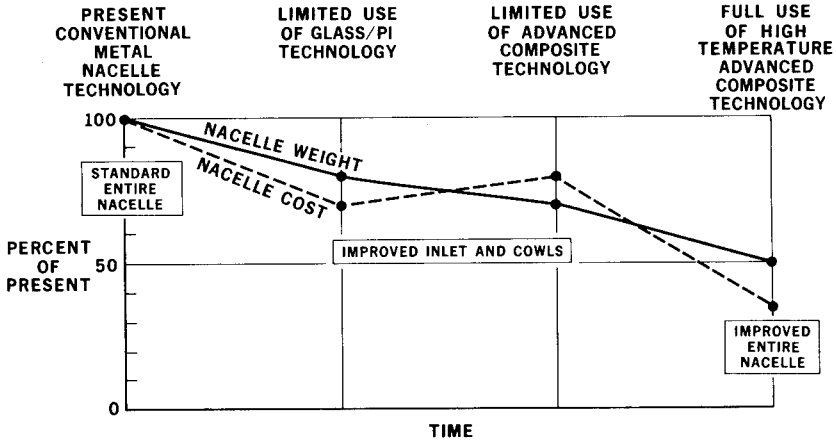

FIG. 12. Potential impact of composite nacelle technology.

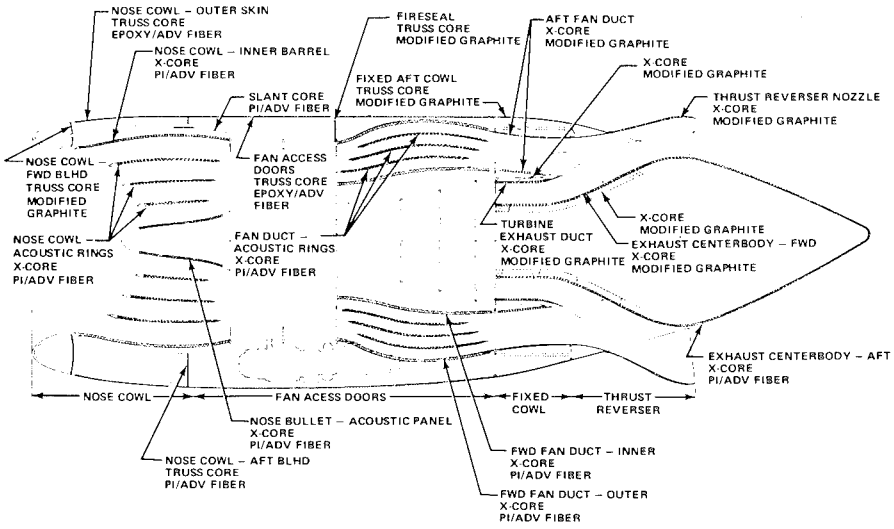

FIG. 13. Conceptual study–advanced composite nacelle.

benefited. The use of lighterweight, advanced fibers would further reduce overall nacelle weight, although costs would be more than for glass.

The ultimate potential of cost and weight savings would be realized with the use of advanced composite structures with high-temperature capabilities, permitting nearly the entire nacelle to be made of composites. Such a conceptual configuration is shown in Figure 13. Although modified carbon-bonded rather than resinbonded systems would be required in the extreme high temperatures of the jet exhaust, the fan duct and aft cowl areas of the nacelle, where temperatures exceed 500°F, could benefit from the development of higher temperature resistant resins.

REFERENCES

[1] R. L. Goble, "Advanced Transport Structures and Materials Technology," AIAA Paper No. 72–302, presented to AIAA/ASME/SAE 13th Structures, Structural Dynamics, and Materials Conference, San Antonio, Texas, April 10–12, 1972.

[2] Alan M. Lovelace, et. al., "Project Composites Recast, Executing Summary Report," Air Force Materials Laboratory, Air Force Systems Command, Wright-Patterson Air Force Base, Dayton, Ohio, August 1972.

[3] "Study of the application of Advanced Technologies to Long-Range Transport Aircraft; Volume II, Research and Development Requirements," General Dynamics, Convair Aerospace Division. Fort Worth Operation, prepared for National Aeronautics and Space Administration under contract No. NASL–10702, May 8, 1972.

[4] "Final Report–Study of the Application of Advanced Technologies to Long-Range Transport Aircraft; volume II, Advanced Technology Program Recommendations," The Boeing Company, Seattle, Washington, prepared for National Aeronautics and Space Administration under contract No. NASl–10703, May, 1972.

[5] N. A. Adrova, M. I. Bessonov, L. A. Laius, and A. P. Rudakov, "Polyimides, A New Class of Thermally Stable Polymers," Technomic Publishing Co., Inc., Stanford, Connecticut; Translated from Russian, Academy of Sciences of the USSR, by Kurt Gingold. August, 1969.

[6] "Conceptual Design of Advanced Composite Airframe and Propulsion Systems," Technical Proposal Report No. 71D-432T, Douglas Aircraft Company, Long Beach, California, December 17, 1971.

[7] James R. Courtright, "High Temperature Organic Polymers," Presented at American Institute of Chemical Engineers 62nd National Meeting, Salt Lake City, Utah, May 22, 1967.

[8] S. D. Bruck, "Thermal Degradation of Aromatic Polypyromellitimide in Air and Vacuum," Applied Physics Laboratory, The Johns Hopkin University.

[9] Alan H. Marsh, R. L. Frasca, D. Gordon, C. A. Henry, G. L. Laurie, and L. T. Kamei, "Investigation of DC-8 Nacelle Modifications to Reduce Fan-Compressor Noise in Airport Communities," Part II: Design Studies and Duct-Lining Investigations. NASA Contractor Report CR-1706, 1970.

[10] J. Manhart, D. A. Campbell, C. A. Henry, and E. M. Lowder, "Investigation of DC-8 Nacelle Modifications to Reduce Fan-Compressor Noise in Airport Communities. Part III:Static Tests of Noise Suppressor Configurations," NASA Contractor Report CR-1707, 1970.

PROPERTIES AND PROCESSING OF POLYIMIDAZOQUINAZOLINE COMPOSITES

REX B. GOSNELL, WALTER P. FITZGERALD, JR., and ROBERT J. MILLIGAN

Whittaker Corporation,
Research and Development Division,
San Diego, California 921123

SYNOPSIS

Efforts to prepare stable, high temperature resin systems based on the polyimidazoquinazoline (PIQ) structure have been successful. The most thermal oxidatively stable of these resins is code-named AF-R-530. Low void, high density, flat laminate samples using Modmor II unidirectional reinforcement have been fabricated whose flexural properties equal or exceed the levels of capability of conventional high-performance support resin systems (Table I).

To achieve this type of thermal oxidative stability, a designed cure-postcure schedule which included short term final exposures to temperatures exceeding 950°F (the approximate glass-transition temperature of the resin) was utilized. Such a schedule insures maximum reaction and subsequent cyclization to the PIQ units prior to immobilizing gelation of the highly cross-linked resin system. Lap-shear tensile strengths for the unfilled AF-R-530 systems on 17-7 PH stainless steel were modest (1000 psi) but constant after 1 hour and 50 hour exposures to

TABLE I
AF-R-530/MODMOR II Laminate High Temperature Flexural Performance Retention

Heat Aging	Flexural Strength (psi)	Modulus (10^6 psi)	% Retention of Initial Strength	Composite Weight Loss
Room Temperature	223,200	17.2	—	—
200 hr @ 600°F	181,000	16.7	81	1.5
500 hr @ 600°F	181,400	18.3	81	3.7
1000 hr @ 600°F	86,700	11.7	39	10.7
Room Temperature	281,500	17.2	—	—
1 hr @ 700°F	171,200	18.3	—	—
50 hr @ 700°F	172,000	16.9	100	3.1
100 hr @ 700°F	143,700	14.5	84	6.5
Room Temperature	234,300	16.8	—	—
1 hr @ 800°F	217,000	16.4	93	0
5 hr @ 800°F	143,000	14.8	61	1.5
10 hr @ 800°F	48,000	14.2	21	7.5
1 hr @ 900°F	171,100	16.0	73	3.0
1 hr @ 1000°F	91,100	9.1	39	10

Applied Polymer Symposium No. 22, 21-22 (1973)

700°F. It is believed these properties can be upgraded by formulation. Carbonization of these various systems, both as moldings and in Modmor-II laminates, to 1600°F under nitrogen produced structural, glassy-carbon ablated products with char yields of 78–84%. Recent efforts with PIQ polymers have uncovered another system, coded AF-R-553, whose properties may exceed the above described AF-R-530.

A UNIFIED VIEW OF THE PROCESSING OF ORGANIC MATRICES INTO STRUCTURAL COMPOSITES

IRA PETKER

Structural Composites Industries, Inc.,
Azusa, California 91702

SYNOPSIS

A necessary basis for a rational approach to the processing of high performance composites is dependent upon knowledge of the manner in which the matrix influences the mechanical properties of a composite, as well as identification of those properties of the composite itself relatable to processing, which also exert an influence. A brief summary of experimental data which provide such a basis is given initially. From this a view is developed from which a number of generalizations are derived concerning the processing of high performance structural composites, particularly in regard to the matrix. It is shown that considerable unity can be identified between apparently diverse processes and materials. A small number of physico-chemical properties control the processing behavior of a polymer. Predictable manufacture of organic matrix composites, as well as the achievement of high performance, is shown to depend upon the identification of proper levels of these properties and reproducible control of the levels.

INTRODUCTION

In 1965 I published a paper together with a group of co-workers which set forth a theory for the processing of structural composites [1]. The paper was substantially limited to composites based on addition-type polymers with data only on glass fiber reinforcements. To my knowledge this publication still remains as the singular attempt to deal in generalized fashion with a subject for which there have been numerous publications dealing with the specific processing of a specific material system.

Since 1965, the technology of structural composites has grown rapidly with the introduction of a variety of fibers, such as boron and graphite, which have added the very important new attribute of high modulus to the important attributes of high strength and light weight of the earlier structural composites. The new high modulus structural composites have come to be known as Advanced Composites. In addition, new organic polymers, especially the polyimides, which perform well at temperatures to 600°F, have become prominent and are beginning to compete with the earlier epoxy resins. These new organic polymers, cured during polymeriza-

Applied Polymer Symposium No. 22, 23–46 (1973)

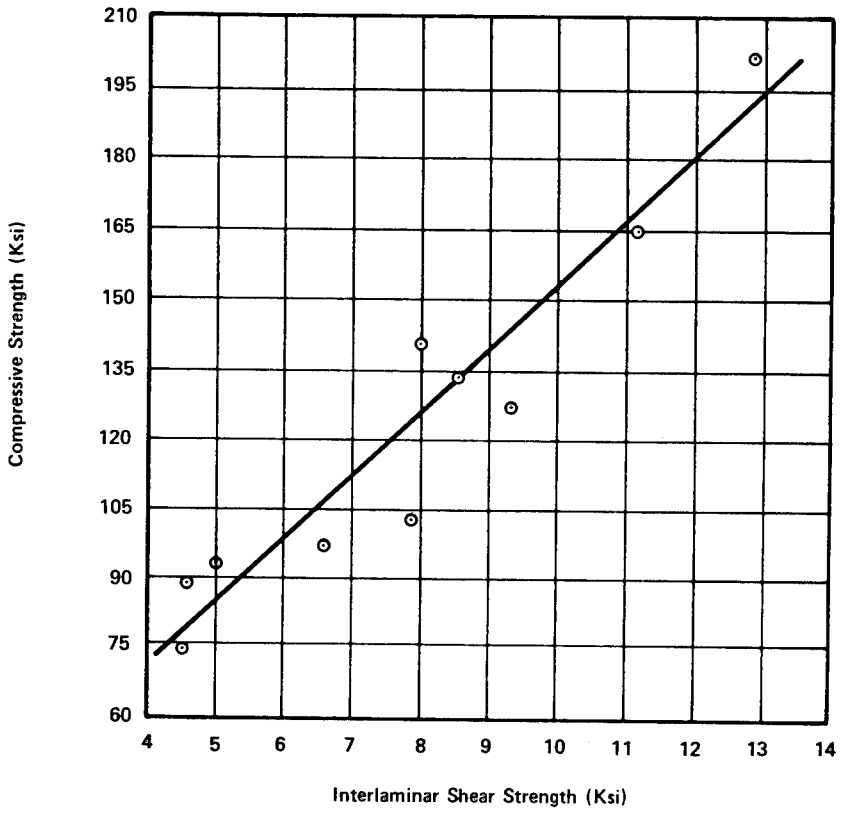

FIG. 1. Compressive strength as a function of interlaminar shear strength for glass-epoxy composites.

tion with condensation, liberated volatile matter after substantial polymerization had occurred, and required residual solvents for tractability. These factors significantly complicate their processing.

More recently, other polyimides, which polymerize by means of addition, have become important matrices for structural composites. These new polyimide materials simplify the processing problems of the earlier polyimides, but, because they still require residual solvent for tractability, they remain more difficult to process than the epoxies. They have similarities to both and therefore have an intermediate position in regards to the overall processing problem.

In this paper I will attempt to extend my earlier thoughts to polymers requiring residual solvents for processing and to those which produce volatile matter either during or after polymerication. My intent will be to develop a unified view that will encompass in a generalized manner all types of polymeric material of practical interest in the preparation of composites. I will use data published earlier and amplify them with new data. The primary attention will be given to the role of the matrix in the process of making a composite and will reserve for another time the role of the fiber.

Initially I will divert from the main subject in order to develop a basis for speculating upon just what it is that a composite process must achieve in order to realize the high strength potential of structural composite materials and the role played by the polymer. It seems to me that this would be a necessary prerequisite for setting forth a theory of processing.

MECHANICAL PROPERTY BASIS FOR PROCESSING

In Figures 1 through 5 empirical correlations are shown relating the compressive and flexural strength of glass, boron and graphite reinforced composites to the interlaminar shear strength (ISS) of the composite. All the data were obtained at room temperature, except those shown in Figure 5, which were measured at elevated temperatures between 250 and 600°F. The data are for a variety of epoxy and polyimide composites. These data, as well as most of the other data in this section, were published elsewhere recently [2], where they were discussed in detail. I will limit myself here to some pertinent highlights and extensions of the original discussion.

The tendency toward linear correlation in all of the data is quite good. Although there is insufficient information to explain the scatter quantitatively, a number of sources of scatter can be identified. In all the data shown, ISS was measured by the short beam shear method. Most current practice is to test by this method at a span-to-depth ratio of 4 to 1. However, ratios of up to 6 to 1 have been and are in use, and the level of certain types of failures in this test are influenced by the ratio. A more im-

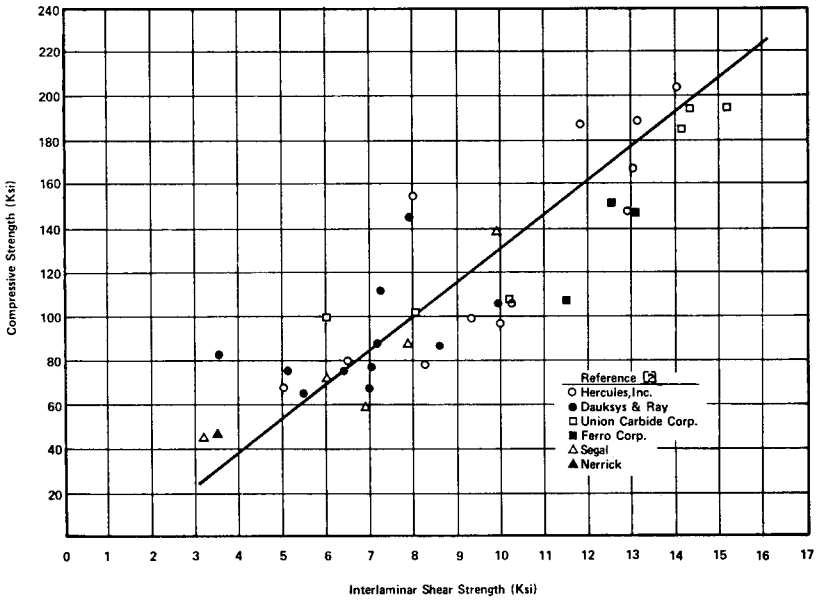

FIG. 2. Correlation of compressive strength with interlaminar shear strength for graphite composites.

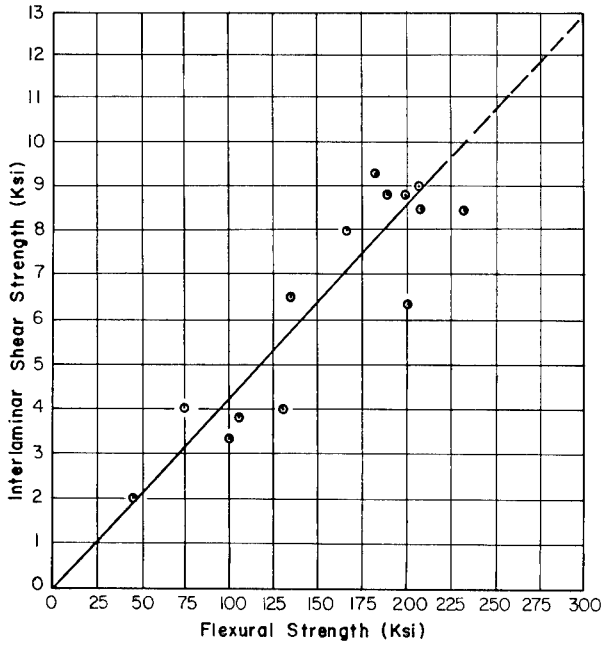

FIG. 3. Correlation between interlaminar shear strength and flexural strength for boron–polyimide composites.

portant factor, especially at elevated temperature and in the mid-and-low-ranges of shear, is the identification of the correct failing load. In Figure 6 are shown typical, generalized load-deflection curves observed in these shear tests. Generally at high failure loads, the break is sharp and clean, as shown in Figure 6A. Where yielding occurs, maximum load may be close to yielding load as in Figure 6B or at very different levels as in Figure 6C. It is not usual practice to record load-deflection curves in shear testing whereas it is usual to report data based on maximum load.

Another set of conditions are operative in short beam shear testing. There is no singular failure mechamism. Failure can occur within the matrix, between the matrix and reinforcement, and within the fibers. Generally the location of failure is not reported and where attempts are made to locate failure sites by direct observation, it is difficult to discriminate between the first and second types. However, in spite of all of these factors, the correlations are quite good, beyond coincidence, to the point where I consider it possible to predict the compressive and flexural strength of most composites from their ISS for reasonable regions of fiber strength and fiber loading. Conversely, if the compressive or flexural properties are not predictable from ISS, I believe strongly, suspiciously, that I am dealing with a unique composite material, with a unique failure mechanism.

Thus, ISS becomes a powerful and unique tool in studies of structural composites. If we can identify quantitative factors which influence the interlaminar shear properties and in turn relate them to the matrix be-

havior in the process, we will discover an objective basis for viewing processing.

In Figure 7 a correlation is shown between the matrix tensile strength* and the interlaminar shear strength (measured by bending a short beam) with glass fibers for a group of diverse epoxy resins. The tensile strength of these resins was determined from castings of the bulk resin. A condition imposed upon these composites was that they be essentially void free. Under this condition, the correlation is linear and passes through the origin. I consider this correlation to be one of the fundamental relations in structural composites and one that is rarely violated.

The zero void content interlaminar shear strength line suggests that for any given matrix there is a unique, maximum shear strength associated with its composites and this level is defined by the strength of the matrix. Although there are limited direct data, the correlation presented earlier and others strongly suggest that the relationship is applicable at all temperatures and the maximum shear strength of a composite will be defined by the instantaneous strength of the matrix. If a chemical reaction occurs at elevated temperature which increases or decreases the strength of the matrix, the composite shear strength will vary accordingly.

The highest tensile strength for an epoxy resin that I have observed directly or found in the literature [5] is for a cycloaliphatic resin (Union

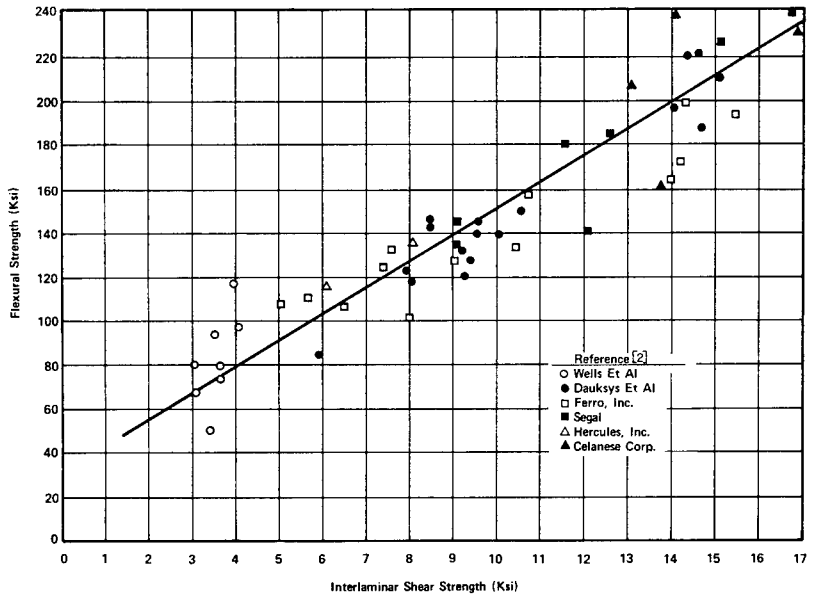

FIG. 4. Correlation of flexural strength with interlaminar shear strength for graphite–epoxy composites.

* Other matrix mechanical properties could have been used in place of tensile strength. Some of these are modulus, compressive yield strength, flexural strength, or shear strength. Most matrix materials for which data have been published tend to have mechanical properties which are internally correlated [3, 4]. Therefore, it is impossible to separate these empirically.

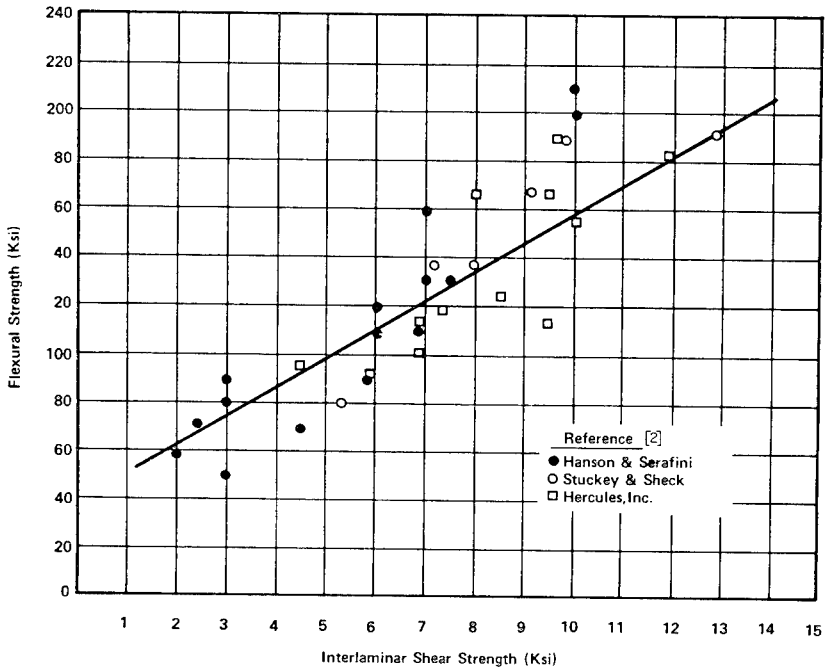

FIG. 5. Elevated temperature data—Graphite polyimide and graphite epoxy composites.

Carbide ERLA 4617) cured with an aromatic diamine. The value is about 20 ksi and we have measured limiting shear strength with glass of about 21 ksi with it. Practically all epoxy resins used in structural composites have tensile strengths between this level and about 10 ksi with the preponderant number between 12 and 15 ksi, a very narrow range, and yet this narrow range describes a range in flexural strength in boron or graphite composites of about 40 ksi, which is substantial.

Thus, high strength composites require high strength matrices and we can assign a range of polymer strength between 15 and 20 ksi as being very high strength within the context of current materials. When reviewing the literature on high performance, high temperature polymers and their composites, I can find values of shear strength as high as 18 ksi at 75°F. Polyimide materials, such as P13N (Geigy-CIBA Chemical Company) and Keramid 601 (Rhone-Poulenc) for which I have observed shear strengths of 16 to 18 ksi, produce very strong room temperature composites because their strength at room temperature is probably high, probably over 15 ksi. The chemistry of very high temperature polymers leads naturally to high inherent strength.

The data, however, on the tensile strength of these and most other polymers are extremely sparce and sometimes much lower than would be anticipated from their composite properties. This occurs for two reasons: Many students of composites do not consider neat resin and composite properties as intimately related as I have suggested, so that they are not vitally interested in determining precise data from neat resin. It is also difficult, sometimes virtually impossible, to prepare resins as testable

material in their neat form. Even with resins which are readily amenable to casting, great preparative care is necessary to eliminate defects. Tensile strength is an especially difficult measurement to make with precision. However, to the extent to which good data are vailable (data that is less than good generally is low), it tends to support the relationship.

Although it is impossible to achieve values of shear strength above the zero void content shear strength line, every value below the line is possible [6]. It is here that the process becomes crucial and the identification of the process factors which can affect the achievement of less than the maximum potential shear strength for any given matrix–reinforcement system is necessary if a rational approach towards processing is to be discovered.

The interlaminar shear strength is generally considered to be a measure of the force necessary to separate layers of reinforcement. It seems reasonable to conclude from the zero void content ISS line that with composites prepared from S–901 glass fibers and epoxy matrices with tensile strength to about 20 ksi, in the absence of voids, failure occurs within the matrix. Since 20 ksi is the highest value of strength identified for any matrix used in composites, it is possible to conclude further that with at least one fiber, a maximum and limiting level of structural performance for composites can be identified and shown to be achievable. There is nothing that a process can do to improve upon this level of performance, since the limitations are inherent in the characteristics of the constituent materials. The process can only negatively influence the achievement of the inherent,

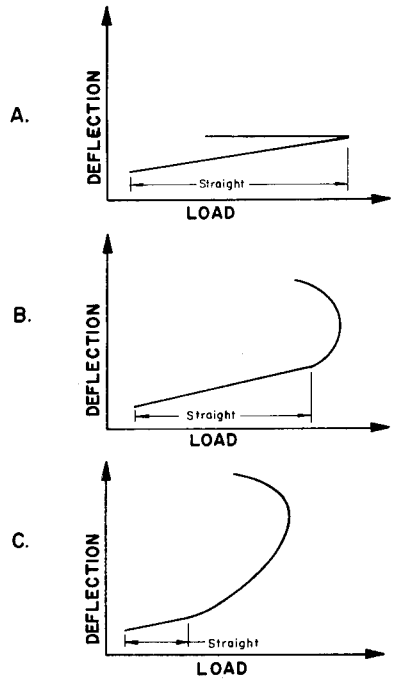

FIG. 6. Typical load–deflection curves in ISS test.

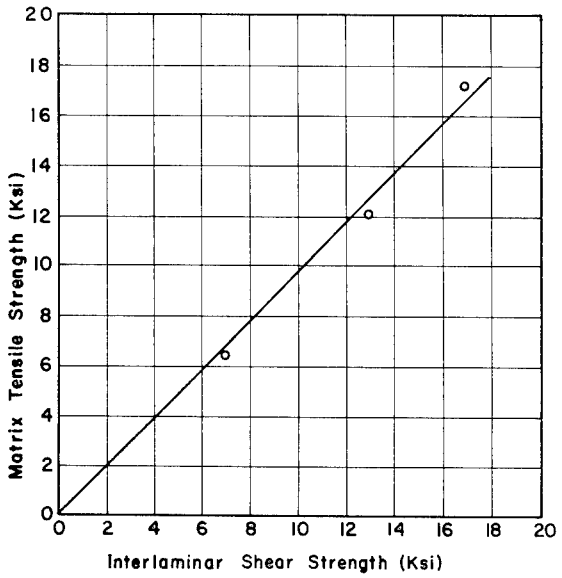

FIG. 7. Zero void content interlaminar shear strength line.

achievable, quantitatively identifiable structural performance. Higher performance requires constituent materials with higher performance potential already built into them.

When I consider the range of actual conditions that are used to process organic matrix composites, I find that it is virtually impossible for the process to cause chemical changes to occur in any of the reinforcements commonly used in structural composites.* Thus I feel comfortable in making the assumption that processing does not influence the properties of the fiber or change its inherent nature.

It is generally assumed, however, that an interaction takes place at the surface of a fiber, between it and the matrix, that this interaction results in adhesion or lack of adhesion or different levels in the degree of adhesion, and that the structural performance of the composite will respond accordingly. I have never found satisfying verification of this position in the literature even though it is very popular. Because of the sparcity of a good empirical basis for this view, I tend to ignore considerations of adhesion and try to get along without them. I do find, however, that if I make the contrary assumption, that adhesion is important, then a necessary condition for the existence of the zero void content ISS line is that all of the composites from which it was developed must have had matrix–fiber bonds stronger than the matrix. From the high levels of ISS achievable with certain graphite and boron fibers with certain epoxy and polyimide resins, I conclude that bond strengths between these materials are at least as strong

* Except for the very thermally stable polymers such as PQ, PPQ, and PIQ, processing temperatures are 600°F or less for relatively short periods of time. Under these conditions glass, graphite and boron fibers can be considered inert in the presence of most organic matter.

as those for the glass fiber composites discussed previously. I find it helpful to conclude, therefore, that processing does not affect the fiber, that adhesion, if it exists, always exists at a non-limiting level with current materials and, therefore, I can ignore potential negative influences of processing upon the fiber or fiber–matrix interaction.

The matrix, however, is a material that is newly created everytime a composite is prepared. It, therefore, is intimately related to processing. If it is processed in such a manner that its resultant characteristics vary from time to time, such that its strength also varies from time to time, then the strength of its composites will vary accordingly. Assuming chemical identity in the starting materials, then the primary processing factor that will influence the strength of a polymer is its thermal history starting with the time just after the preparation of the prepolymer and ending with the cured composite. Preimpregnation, storage conditions of the prepregs and resin, the time during composite fabrication, as well as the actual cure of the composite, are all part of the thermal history, and in a sense, therefore, are all part of the process in the preparation of the composite. It would seem probable that every different thermal past for any given polymeric material might result in some difference in the molecular constitution of the polymer and, therefore, different strength levels. However, I have not found this to be true and believe that it is the exception, rather than the norm, for this to occur.

I believe this for a simple reason. The range of matrix strength available to the composite engineer, from an apparently very widely ranging variation in molecular structure (based on the chemistry of polymeric materials used for composites), is very small, a variation of only 12 to 20 ksi, and yet the theoretical strength of any one of these matrices is at least two orders of magnitude greater than the achievable strength. Therefore, an organic matrix can be considered, under the best of conditions, a material that is so loaded down by molecular defects that its strength is essentially non-variant under most conditions of use. Most of the polymerization takes place during the final cure of the composite and this is one of the process steps that generally is controlled precisely and according to prior empirical data developed by resin chemists and the materials engineer himself. I do not consider variation in matrix strength, particularly at ambient temperature, to be a serious source of variation in composite strength, as well as a minor limitation upon the achievement of the maximum potential strength of any specific matrix–reinforcement system.

I find that the short diversion from the main subject is longer than I had anticipated. However, I find for myself that unless I follow the foregoing path, it is virtually impossible to arrive at a point of view relative to the processing of composites that is sufficiently restrictive and, therefore, amenable to a simple treatment. Otherwise the problem encompasses too many variables and is overly complicated.

If the hypothesis that the molecular structure of the matrix, and fiber, and the matrix–fiber interface are unaffected by processing is accepted, then the manner in which the structural performance of a composite is af-

fected by processing must be found in other characteristics confined solely to the composite itself. Two such characteristics have been identified: (a) resin content [7], and (b) void content [6, 8, 9]. The effect of voids in composites is well documented. The effect of resin content is less clear; it is obvious that there is a minimum for any given fiber diameter for which the interstices of the composite will not be filled. It is also obvious that there is a maximum above which the matrix will act simply as a diluent of the fiber properties. The precise region between these two limits for optimum composite structural performance is not obvious, nor is it well-explained in the literature. However, good guides can be found in readily available empirical data.

Voids, at any level, reduce composite structural performance. A composite material system capable of 20 ksi in ISS might have a shear strength of 14 ksi at 3 v/o voids and lower shear strength at higher void content. I have found that the presence or absence of voids is a singularly process-related characteristic.

Finally, the distribution of fiber, resin, and voids, the tendency towards and the size of local accumulations of each of them, also affect, in an interdependent fashion, structural performance. Again, there exist little empirical data concerning these phenomena or their interaction. If it is possible, however, to treat the problem of processing without a quantitative definition of an optimum composite condition, it is only necessary to understand that void content should be a minimum, fiber-matrix distribution should be a constant and resin content has an empirically-defineable optimum. These conditions are true for all structural composites. Any given fiber–matrix system will have maximum structural performance under these conditions. Therefore, their achievement is the object of processing.

PROCESSING AS A PROBLEM IN PHYSICO-CHEMISTRY

Processability

Processability can be defined as the summation of all the characteristics of a material which influence its ability to be transformed into a composite. Included within this definition are a multiplicity of characteristics including tack, flexibility, reactivity, softening and flow behavior and others. Each specific reinforcement makes a unique contribution to the processability of a composite material, but this contribution can be viewed as a constant for a given reinforcement. The contribution of the matrix is more complex since it is not only dependent upon the chemistry of the matrix and a potential for infinite variation in the molecular structure of any specific polymeric material, but also because all of the processability characteristics of a matrix are temperature-dependent. Since practically all organic matrices in structural composites are thermosetting materials, their processing requires more than simple changes in physical state. The contribution of the matrix, is therefore, dynamic and time-dependent. Thus it is only under

the unique condition of constant molecular structure and constant temperature that the processability of a composite material can be considered constant.

I will now make a hypothesis which can simplify this otherwise very complex problem. The hypothesis states that the contribution to the processability by the matrix is determined by its viscosity and the changes in its viscosity starting with the time that it is being laminated until the time that it is no longer capable of movement under the influence of external forces. For a given matrix–reinforcement system the tack of a prepreg is determined by the viscosity of the matrix, as is its band integrity, as is its flow, and all are a function of temperature since viscosity changes with temperature.

The importance of the hypothesis is that it relates a multitude of specific characteristics to a singular physico-chemical characteristic which is quantitatively determinable. It also eliminates the need for specific knowledge of molecular structure and considers chemical structure important only from the standpoint that it does influence viscosity. I shall clarify the significance of ". . . the influence of external forces", and the contribution of resin content later. I shall also submit data to support the hypothesis.

Process

The second definition defines the process as the summation of all the manipulations performed to a material, as well as all the conditions to which it is exposed in transforming it into a cured composite. It is important that the proper emphasis be given to the word "all". If an autoclave is used in a process, it is not the general term "autoclave" that is important, but it is the specific autoclave used, its size, heat transfer, and pressurization characteristics are part of the definition. Even more, the size of the mold, its construction, its position within the autoclave are part of the definition of a specific process. And anytime a change is made in anyone of these, it is no longer the same process. Another important point to stress is that, just as there is nothing about a process which is a priori unimportant, everything about a process is theoretically capable of a priori definition. For the engineer this is one of the important distinctions between the raw materials used in a process and the process itself. The basic raw material used in the preparation of high performance composites is generally a prepreg. It may always have the same processing characteristics or it may vary from time to time beyond the control of the processing engineer. However, since the process is the sum total of the things done to a material after it is received, it is within the control of the engineer to establish constancy or controlled variation from this point on. It is less important to know the best thing to do to a material in processing it, than it is to know exactly what will be and is done, and to be committed to constancy until there is clear evidence that a change is in order.

I find that all composite processes are composed of two primary stages. One is lamination when the fibers and resin are placed in a mold, or in

some other manner are given shape, and the cure stage when heat is applied to polymerize the matrix and give permanency to the shape. The compression molding of discontinuous fiber is the only true exception since the fiber and resin are handled as a mass and placed in the mold without regard necessarily to the final location of the materials. Room temperature curing might also be considered an exception since external heat is not applied, but it might more appropriately be considered a special case.

Composite processes tend to derive their name from a significant feature of the lamination or cure stage. Thus "filament-winding", "tape laying", and "hand layup" are methods for applying materials to a form, and "bag molding", "autoclave molding", "compression molding" are methods used to apply heat and/or pressure during cure. The names have limited use and tend to emphasize differences in processes. I find that there is one parameter which is common to all composite processes and my tendency is to categorize processes according to the level of this parameter, the manner in which it is used and the point or points in the process when it is introduced. The parameter is pressure, which is the basis for my second hypothesis: Pressure is the only unique and necessary characteristic common to all composite processes, with its level and manner of use, determining the quality of a composite.

As I said before, the quality of a composite is determined by its resin and void content and the distribution of resin and fiber. Insofar as the process is concerned, it is the pressure that exerts the controlling influence. Each composite process has its own means to accomplish this. In hand laminating, pressure is applied by hand and sometimes with the assistance of hand tools by the laminator as each ply is applied. In sprayup, where chopped fibers and resins are sprayed onto a mold, it is the impetus of the sprayed material followed by hand rolling techniques which apply pressure. If hand ironing is used during lamination, this operation applies pressure. In each of these processes, the amount and effect of the pressure is a variable factor in the process.

In more sophisticated processes, the amount of pressure is highly controlled. In bag molding, a flexible membrane is drawn tight over the composite by evacuating the air between the membrane and the mold. The pressure in this process is generally considered to be about 15 psi at "full" vacuum. Autoclave processing is a means to implement the pressure of simple bag molding and generally increases pressures to between 50 and 200 psi. Hydroclave molding is similar, except that 1000 psi or more pressure may be available. The fact that the composite material may be experiencing simultaneous negative pressure in bag processes must also be considered. The fact that these composites probably all experience some level or type of pressure during lamination can also be a significant part of its pressure history.

In compression molding, the broadest range of pressure is available for composite processing. Theoretically, any pressure can be achieved depending upon the capacity of the press and the size of the composite being molded. Pressures up to 20,000 psi are sometimes used for some molding

compounds and as low as 100 psi for laminated or otherwise preformed materials. Thus, when I think of composite processes as they relate to the matrix, I think of pressure and find that the practical limits range between near zero to 20,000 psi.

VISCOSITY–PRESSURE INTERACTION

To reduce composite processing to its ultimate simplicity, I believe that one can get by with the following two statements:

1. Processability (matrix contribution) is viscosity;

and

2. The process is pressure.

However, neither one alone is sufficient; rather it is their interaction. This leads to a third hypothesis: Given a defined composite material system and a means to laminate the material, there is a unique level of viscosity for each level of pressure.

The hypothesis suggests that an intimate, interdependent, interacting relationship exists between viscosity and pressure, that one cannot be defined in the absence of the other, that the definition of one constrains the limits of variation of the other, that once both are defined neither one can be allowed to vary if the desire is to prepare composites of optimum structural performance, reproducible structural performance, predictable structural performance.

The practical limits of pressure available to the processor are from just about zero to about 20,000 psi and composite processes can be categorized according to the pressure level available as long as attention is given to the manner of pressure application, as well as its level. It is not possible at this time to associate a quantitative viscosity level for each of the pressure levels since the basic work has not been done yet. It will be necessary, therefore, to deal more qualitatively with the problem than I would like to. Also I will not try to infer that one particular viscosity–pressure level or another is better generally for processing composites. All are "good" and it is also true that some are "better". The fundamental consideration that might lead one towards the design of processes for a particular viscosity–pressure region are not part of the substance of my intent in this paper. The composite responds structurally to its voids, resin content, and fiber distribution, not its processing history, and all viscosity–pressure regions, properly matched, are capable, theoretically, of preparing high quality composites.

All matrices used in high performance composites require temperatures above ambient in order to effect polymerization. Heat is a condition imposed upon the matrix. It is, therefore, by my definition, a part of the process. It is, however, unique among the many process factors, since except in the final stages of cure, its primary effect is to influence matrix viscosity, which is the primary processability characteristic. It is, in fact, the

only tool available to the process engineer, by which he can influence the properties of his raw materials and manipulate them advantageously to further his interests in preparing high quality composites. I view heat and the manner of its use as fundamental to processing, but less in terms of its role in the last stages of the process than in the intermediate stages.

I shall now present some examples of the kind of data which support the hypotheses starting with simple addition-type polymerization.

ADDITION POLYMERS

I was fortunate in the early 60's to be associated with one of the earliest intensive efforts to apply structural fibers in the form of preimpregnated rovings to truly high performance structures, filament-wound pressure vessels. The material system was S-glass coated with a mixture of simple and tetrafunctional bisphenol-A-type epoxy cured with methyl nadic anhydride and catalyzed with benzyl dimethyl amine. The formulation is commonly called 58–68R (from the page number of a Shell Chemical Company brochure on which it was printed), and has become the industry standard for prepreg rovings.

Some of the processability attributes that are desirable in a filament winding prepreg are that it has closely controlled and predictable band width, sufficient tack to prevent slip in non-geodesic winding paths, the ability to resist fraying and breaking, and minimal transference of resin to contact points.

Although these were the desirable attributes, they were not consistently realized at first and a host of others were observed. Sometimes the prepreg would have a good nominal bandwidth on the roll, but the bandwidth would narrow considerably during winding so that severe gappage occurred in the structure. Other times the severe band distortions that are often present at the turn around point of a waywind package would not be removed during winding and would also be cured into the structure causing fiber distortion, overlap and twist. Sometimes the roving would break with frustrating consistency and other times it would fray. Sometimes the rollers would be wet with resin and sometimes packed with powdered resin and fibers.

The striking fact about all of this multitudinous variety in processability behavior was that we were dealing with a constant material system. Attempts to rationalize the observation upon the fibers or the monomeric chemicals simply was unsatisfying and I undertook a series of investigations based on the assumption that we were really only observing the effect of different viscosity levels in the prepreg resin. The results of these studies have been published in detail [1].

One of the nice things about many epoxy resins is that they can be formulated to low viscosity at ambient temperature so that they do not require solvent for tractability. It can be assumed therefore that, for a given formulation, differences in the viscosity levels of the partial polymer can be

uniquely related to its degree of polymerization. We developed a solution viscosity (VI) procedure which responded to different levels in degree of polymerization. This was used to follow changes in the viscosity of the prepreg resin.

In Figure 8 is shown the changes in VI during exposure of 58–68R/S-glass prepreg to ambient temperature for a number of days. Plotted together with the curve are qualitative observations made of the prepreg while winding and simply feeling it during the period of exposure. We found that every processability attribute observed previously at various times with this prepreg was reproduced during this study. Prepreg which broke easily, transferred to rollers and narrowed down excessively was described by a low VI. The resin had low relative viscosity. Prepreg which frayed easily, from which the distortions were not removed during winding and deposited powdered resin and fiber onto the rollers, was described by high relative VI. The resin had high relative viscosity. There was also a region in-between in which the prepreg had all of the desirable attributes of a good winding material.

We conducted another study in which we wound a series of NOL rings from prepreg with different VI levels as the only variable. Winding was done at room temperature and all process factors were maintained constant. Figure 9 displays the results of this study. We found that ISS of the rings reached a maximum value of about 12.5 ksi at a VI of about 1.95. At a VI of 2.5 ISS was 9 ksi and at a VI of 3.0, it was barely 2 ksi. At a VI of 1.6, the interlaminar shear strength reduced to between 10 and 11 ksi. Later work showed that only the composites with shear strength about 12 ksi were void free, that the very low VI composites had void contents up to 3 v/o, the high VI composites had voids over 20 v/o. Here was a clear demonstration that for a specific, constant process there was a specific region of prepreg resin viscosity required for the preparation of void-free composites. These composites also had the best fiber–resin distribution. It is of interest to note also that the viscosity region for optimum winding characteristics and optimum composite quality were not exactly the same,

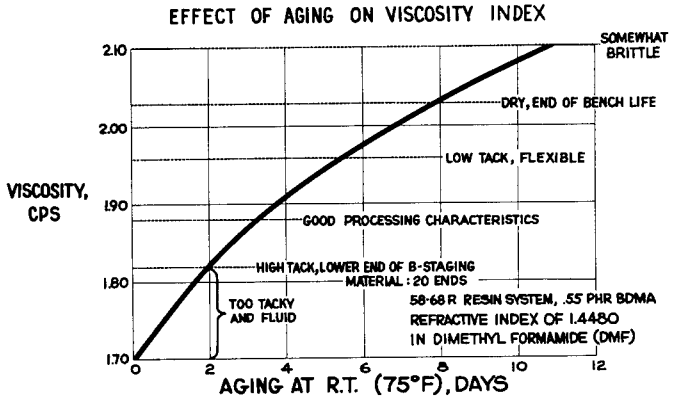

FIG. 8. Effect of aging on viscosity index.

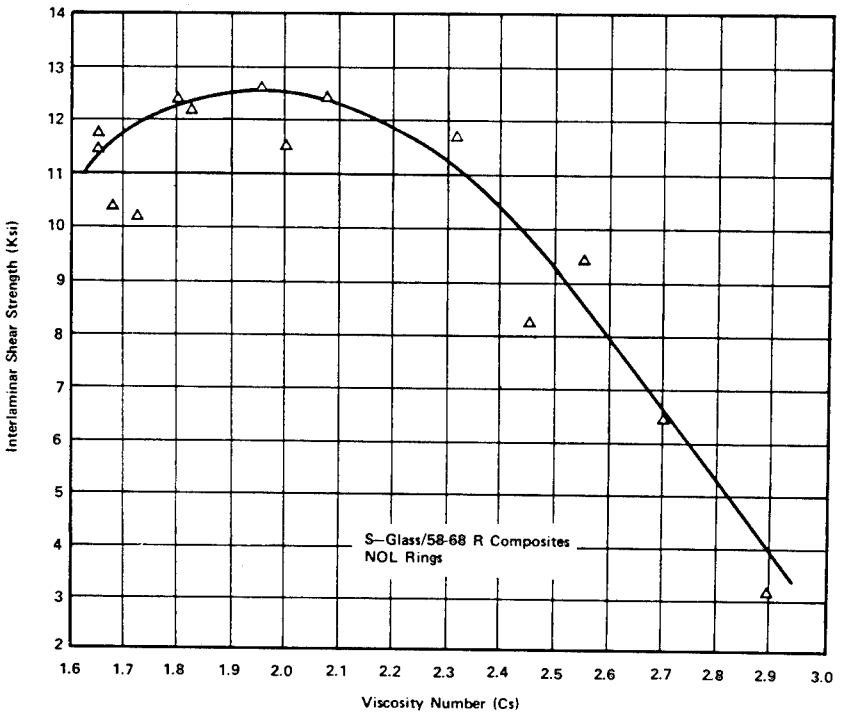

FIG. 9. Influence of processability on interlaminar shear strength.

but then, why should they be, when one is concerned only with the instantaneous viscosity at the time of winding and the other is concerned with viscosity changes during cure.

We prepared another series of rings described by the data in Figure 10. In this study we varied VI, but we also varied the process by heating the prepreg as it contacts the mandrel and adjusting the heat for the higher VI materials in order to duplicate, qualitatively at least, the same appearance of rings during winding when prepared from optimum VI material and wound at room temperature. As the VI became higher, a greater amount of heat was required so that, consistent with my definition of a process, a number of different processes are included in Figure 10.

Significantly, these process variations resulted in dramatic increases in ISS for high VI materials so that at a VI level of 2.9 an ISS over 12 ksi was observed, an improvement of about 400% over the process with no heat. I have heard comments about these data to the effect that the most significant conclusion demanded by the study is that heat be used during the filament winding of prepregs. Although such a conclusion would have merit over a broad range of VI, at the low and moderate VI range it could actually be detrimental. To me, what is much more important is the manner in which the data illustrate the high degree of interaction between processability and the process, between the raw material and the manipula-

tions carried out upon it. Each region of VI (or processability) required its own amount of heat (process) or lack of heat (process) for the preparation of a high quality composite. The converse is also true.

Throughout these studies the pressure was constant. Pressure is an inherent attribute of filament winding for surfaces of revolution as illustrated in Figure 11 and is created by the tension applied to the material during winding. Figure 11A shows how pressure, interacting with the viscosity of the resin, assists in keeping air out of or eliminating it from the laminated composite. If pressure had been allowed to vary for the room temperature processing, I am quite certain that we would have discovered a region of related curves, each with a similar level of maximum ISS. Since pressure did not vary, however, it was necessary to moderate the viscosity by means of different levels of heat in order to achieve a viscosity level at which the specific pressure used was effective. This heat, although a part of the process, functions primarily as a viscosity modifier and changes, thereby, the processability.

Figure 11B illustrates the condition in which pressure is not effectively used during the laminating process (the flat side). This also illustrates what occurs during most laminating processes. Depending upon the level of viscosity during lamination and the manner and level of pressure application

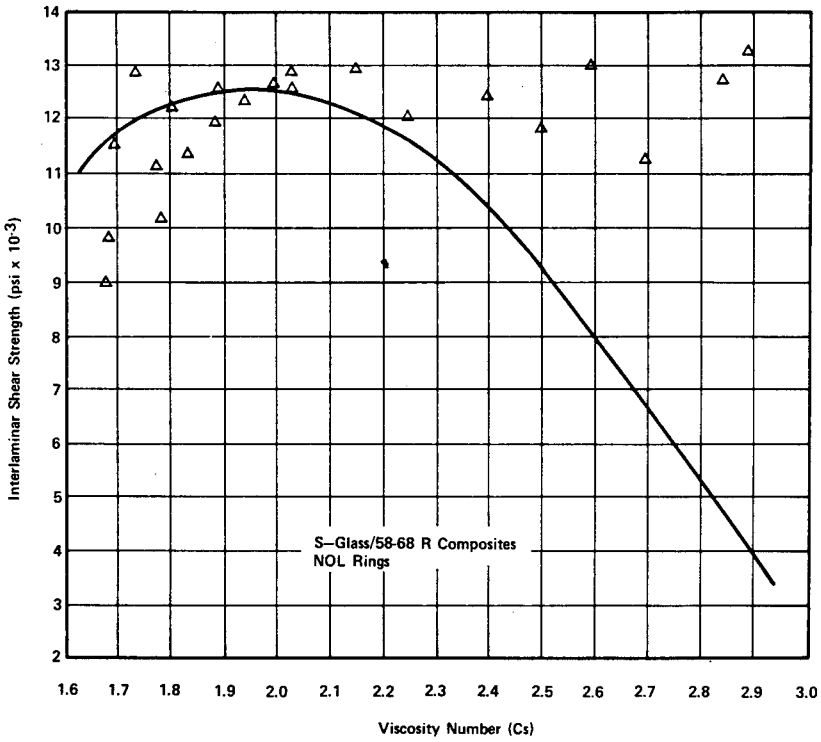

FIG. 10. Influence of heat during winding on interlaminar shear strength.

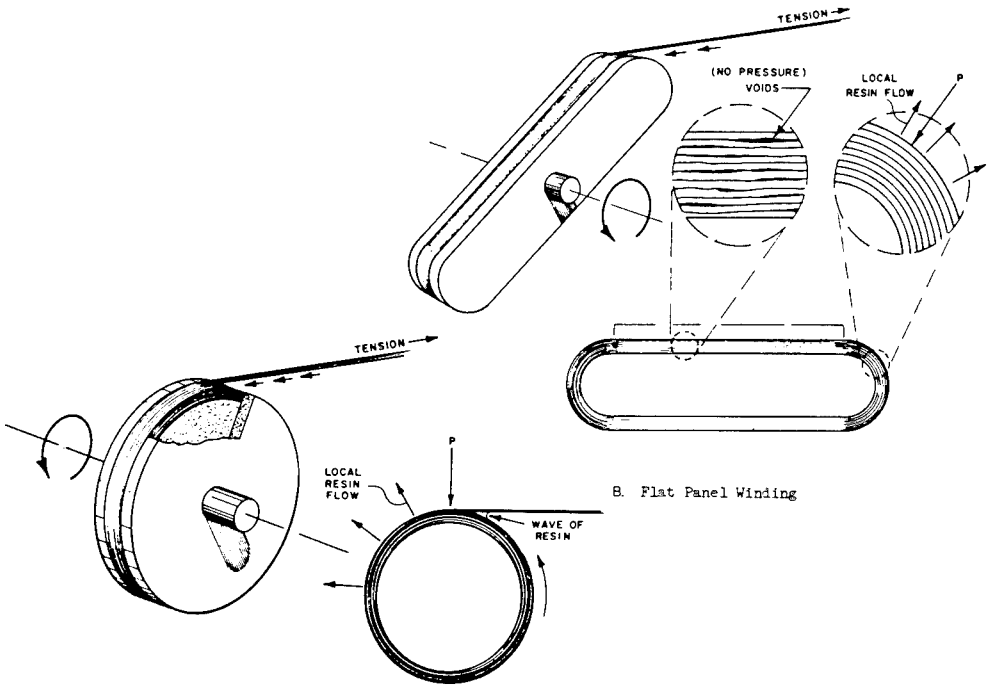

FIG. 11. Pressure–flow effects in filament winding.

during lamination (there is always some pressure present even if only hand pressure), more or less air is occluded in the laminate. In order to eliminate this, pressure must be applied during a succeeding stage in the process. This has given rise to many different processes including the use of vacuum bags, autoclaves, hydroclaves, pressure bags, and presses.

CONDENSATION POLYMER

In the late 1960's I was quite fortunate to become intimately involved in the early studies involving the new high modulus fibers. I was doubly fortunate since my first important problem dealt with a class of resins with which I had no previous experience, the polyimides. The superior thermal capabilities of this class of resin over the most thermally stable epoxies was well-documented, but nobody had been able to make a quality composite with them. The only polyimides curent at the time were the classical ones of the Skybond (Monsanto) and Pyralin (DuPont) types. These materials were solid at room temperature, formed solid polyamic acids quickly at low temperatures, thereby requiring high boiling solvents for tractability, and, finally, as if this was not enough, liberated low molecular weight products during imidization when polymer of appreciable molecular weight was al-

ready present. The usual composite prepared from these resins had void content typically over 20 v/o. It is obvious that these composites could not attain the ISS necessary for high performance.

I did not enter upon these studies with the belief that quality composite could be prepared from these polyimides. Rather I approached the problem from the standpoint that if a polyimide had the capacity to be manipulated into a high quality composite, it could only fall out of a series of experiments in which the viscosity and pressure were varied in some consistent fashion. Thus I went back to my basic learning derived from addition polymers.

Some of the structural results of this study have already been published [5]. Iwill relate now one particular result of the processing investigations which for me disclosed a great deal of fundamental information concerning the basic processing behavior of polymers which require solvents for tractability, as well as those which liberate volatile matter during the process.

Everything important can be shown by one illustration which is given in Figure 12. The figure shows the variation of ISS with prepreg volatile content (VC) for boron–polyimide (Skybond 703, Monsanto) composites. In this work, the boron–polyimide prepreg was conditioned for various periods of time at 225°F yielding prepreg with a variety of processability characteristics. We found that under these conditions the VC of the prepreg (which included both residual solvent and products of reaction) was suffi-

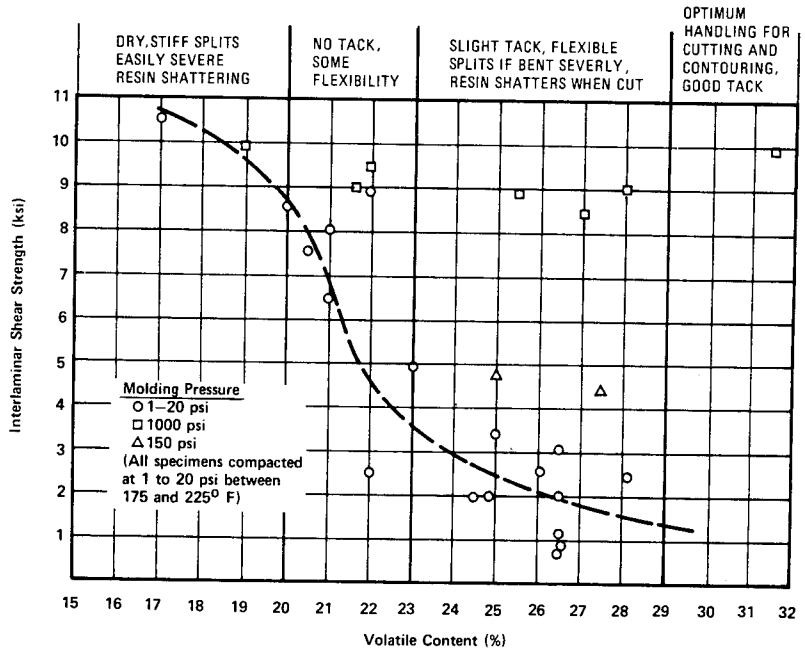

FIG. 12. Effect of volatile and molding pressure on interlaminar shear strength, boron–PI composites.

cient to describe and reproduce the processability of this matrix system so that it became a processability index similarily to the viscosity index for the epoxy material.

In this work we were dealing with sheet laminate processing and were interested in learning if low void content composites could be prepared from boron–polyimide and the minimum pressure necessary to achieve them. At the top of Figure 12 qualitative observations of processability are shown for regions of VC. Above a VC of 32 w/o, the prepreg tended to be wet, fibers were poorly held in place and support materials could not be stripped cleanly. Between a VC of 29 and 32 w/o, the prepreg had optimum processability for room temperature laminating. It had good bond integrity, fibers did not split out, it could be cut with little edge debris it could be contoured, and it had good tack. As VC reduced further, the prepreg took on more and more of the characteristics of a sold material until, in the VC region of 15 to 20 w/o, it was dry, could not be contoured without severe fiber breakout and splitting, could not be cut without severe resin shattering and fiber breakage, and obviously had no integrity between laminated layers.

Composites were prepared for various regions of VC by stacking plies, placing weights of 1–20 psi upon the stacks and placing the assembly in an oven at 175–225°F for 16 to 24 hours. The temperature was then raised for some of these specimens, without additional weight being placed upon them, to 350°F for several hours, at which time cure was considered complete. Others were cured in the same manner with pressure increased to 150 psi while others were cured at pressure of 1000 psi, both pressure levels being applied by a press. The process, therefore, for all the specimen panels can be called compression molding, although the pressure regions included those for simple vacuum bag and autoclave molding. All the resulting panels were post-cured to 600°F. Interlaminar shear strength at room temperature was then measured from sections of all panels.

Turning first to the very low pressure moldings (1–20 psi), I find that the data are best described by an S-shaped curve. I had never seen such a curve in any previous processing studies of composites, at first a frustration, but later a delightful discovery. I was so prejudiced against such a curve that I tried to make it into a simple curve, almost a straight line. Described by a simple curve the scatter in the data is not much more than with an S-shaped curve, but the necessary physical explanation to support it is much less satisfying to me than the one I will now describe.

An S-shaped curve requires that there be a change in the physical mechanism that underlies the relationship between the related parameters. For the data in Figure 12, one mechanism prevailed at VC's above about 24 w/o and another for VC's below about 21 w/o, with a transition region from one dominating mechanism to the other between these levels. Above a VC of 24 w/o, void contents were high in all of the composites, although the resin content for most of them were similar to lower VC composites.

For these composites voids either formed during the first compaction step or during the period of increasing temperature during the cure. In

either case, the resin had insufficient cohesive strength (or viscosity) to resist its displacement by volatile matter attempting to escape from it, but sufficiently high that the displacement was local. This resulted in voids permanently in the composite.

As VC was reduced, the cohesive strength (or viscosity) of the matrix increased until it was at a sufficiently high level to resist displacement. At some level of VC around 21 w/o, volatile matter attempting to escape was no longer a source of voids. Variation in void content became a function of the elimination of occluded air. This was dependent on specific viscosity/pressure levels and possibly the amount and position of the air originally entrapped. Void contents were below 5 v/o for all composites with ISS above about 8 ksi. All of these were processed at no higher than 20 psi and some at only 1 psi throughout the entire processing cycle. This was a truly astounding finding for this type of polymer. I should also note that throughout all of the processing described by all of the data in Figure 12, essentially all of the volatile matter in the starting prepreg was retained in the composites until post-cure, a type of processing that I have come to call "Trapped Volatile Processing". Therefore, no explanation of the phenomena can be based upon changes in volatile content nor differences in polymerization state since the thermal histories of all the composites are very similar.

The effect of pressure during cure is also shown in Figure 12. The application of 150 psi during cure raised ISS about 100% for similar VC composites cured at lower pressures, whereas the application of 1000 psi raised the ISS to 9 ksi or higher over the entire range of VC. This was the level of limiting ISS for most boron composites at the time [2] and required void contents below 3 v/o. Thus during cure the external force, the pressure, applied to the composite, either disallowed the appearance of new voids or eliminated those present before. The latter, I believe, is most correct. This could only occur if the matrix had some capability of movement during this phase of the process. The pressure had no effect at low VC and, therefore, it is not a truism that "the more the pressure, the better the composite" as is sometimes suggested.

I include Figure 13 to show how dramatically solvent content and temperature influence the viscosity of Skybond 703 solutions. These measurements were made on net resin solutions and a given solvent content does not duplicate exactly an equivalent VC for the prepregs. However, the severe trends must be present in the prepreg as well, and tend to explain the high degree of sensitivity displayed by the composite to VC levels.

SOME CLOSING THOUGHTS

I have two more bits of information to offer at this time. Both relate to the fundamental sources of the problems of making reproducible composites. The first is given in Figure 14 and derives from some studies we conducted of the preimpregnation process for glass rovings with a com-

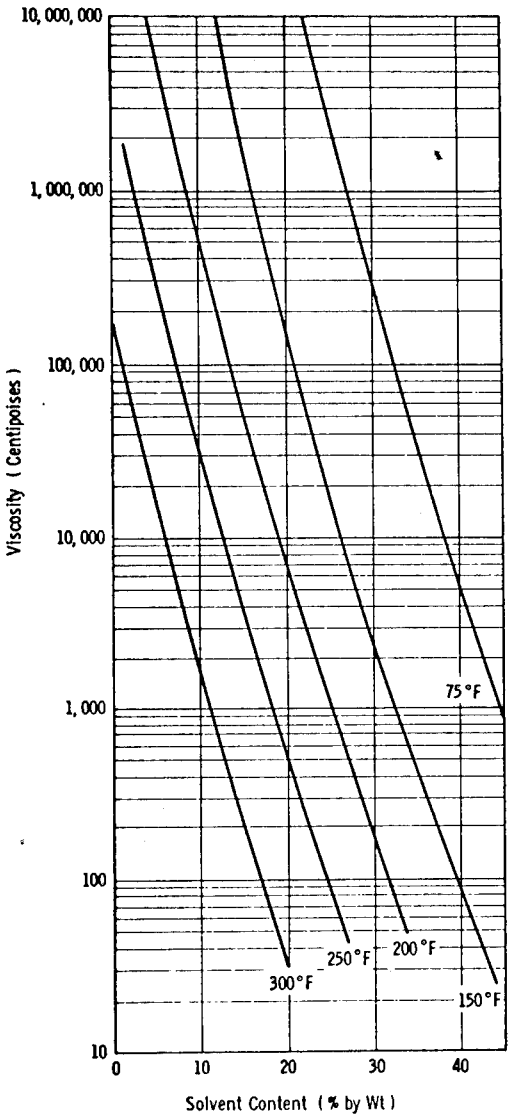

FIG. 13. Effect of solvent content on viscosity of Skybond 703.

mercial preimpregnator. Plotted are the changes in VI for 58–68R prepreg as a function of tower temperature at constant running speed. Recalling that the maximum range in VI for optimum processability during winding was no more than 0.1 VI units, we find that the maximum tolerable range in tower temperature is 20°F or ± 10°F from a nominal. Considering the fact that it is total thermal input that is most consequent, running speed variations superimpose upon temperature variations. There is a need for establishing an exact, optimum nominal level if maximum tolerable variation is to be allowed. Furthermore, there is continued, even if slowly, polymerization of the material after manufacture. It is no wonder that variation in

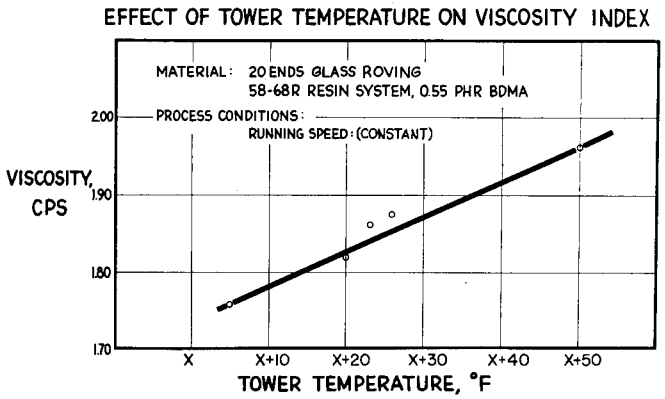

FIG. 14. Effect of tower temperature on viscosity index.

processability was observed. However, the preimpregnator in this instance learned to make a very reproducible material from which reproducible structures could be fabricated. But precision is required, often a greater degree of precision than that assumed to be necessary.

The second illustration is given in Figure 15 which depicts the temperature readings of an oven which we use in the preparation of prepreg. Figure 15A shows the temperature of the oven as a trace on a strip chart during a period when we experienced no difficulties with processing the material into void-free composites. Suddenly the oven broke down and while being repaired it was discovered that the oven temperature sensing and control systems were not functioning optimally. Everything was

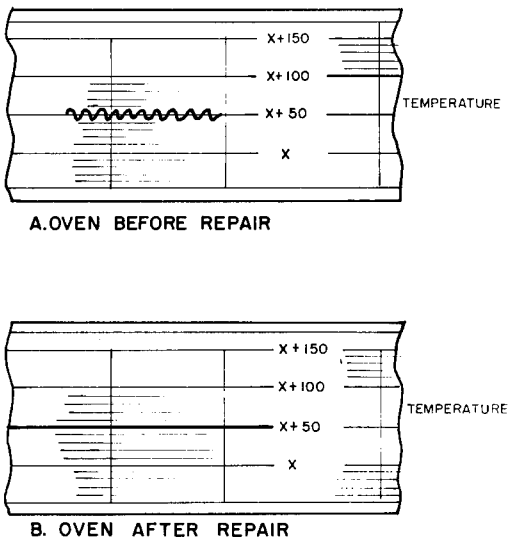

FIG. 15. Temperature traces for oven.

repaired or replaced and we started up again. Now the temperature trace was as shown in Figure 15B, with much improved precision and much better control. The only problem was that the materials prepared in the "improved" oven did not make a good composite. It was only when we re-corrected the oven back to its non-optimal, original condition that we made good composites again. Thus in this instance precision was less important than following the process precisely. I think that my professional life has been frustrated more by "improvements" to processes than any other single factor.

Finally, I believe that the data I have presented support the hypotheses. The case of the solid resin requiring solvent for tractability is really covered by the case of the condensation polymer. There are many other studies that I would like to conduct which would further clarify the role of the matrix in processing, as well as the fiber. Ultimately it should be possible to set down quantitative definitions for the levels in the physical properties of these materials and their processing which would transform the processing of composites, sometimes viewed as an art, into a science.

REFERENCES

[1] I. Petker et al. "Processability of Preimpregnated Materials, Parts I and II", *Mod. Plast., 42*, (9, 10), (September and October, 1965).

[2] I. Petker, "The Status of Organic Matrices in Advanced Composites—A Personalized View", *SAMPE, 2*, (1), March 1972.

[3] I. Petker, and D. H. Eilfort, "Resin Systems for High External Load-Bearing Systems", Proceedings of Reinforced Plastics, Composites Division, Society of the Plastics Industry, Vol. 20, February 1964.

[4] Weingart, O., "Development of Improved Processes for Filament-Wound Reinforced Plastic Structures", Proceedings of Reinforced Plastics, Composites Division, Society of the Plastics Industry, Vol. 21, February 1965.

[5] Union Carbide Corporation, "Bakelite Liquid Epoxy Resin, ERLA–4617, ERLB–4617, ERLC–4617, Product Information Bulletin F–43010, 1970.

[6] I. Petker, "The Influence of Resin Strength and Defects on the Interlaminar Shear Strength of Filament-Wound Composites", *Polymer and Engineering Science, 5* (1), January 1965.

[7] I. Petker, M. Segimoto, and R. T. Sakakura, "Low Void Content Polyimide Composites", Proceedings of Reinforced Plastics, Composites Division, Society of the Plastics Industry, Vol. 23, February 1968.

[8] J. T. Paul, Jr., and J. B. Thomson, "The Importance of Voids in the Filament-Wound Structures", Proceedings of Reinforced Plastics, Composites Division, Society of the Plastics Industry, Vol. 20, February 1965.

[9] W. Hand, "Quality Control of Filament-Wound Materials for Deep Submergence Vessels", Proceedings of Reinforced Plastics, Composites Division, Society of the Plastics Industry, Vol. 20, February 1965.

THERMALLY STABLE POLYMERS

CARL S. MARVEL

Department of Chemistry,
The University of Arizona,
Tucson, Arizona 85721

SYNOPSIS

Thermally stable polymers in my classification are those which are stable up to 500°C in a TGA test and have useful properties and reasonable life in air at 300°C or above. Most of the polymers which are stable in air to 500°C in a TGA test will oxidize slowly in air at temperatures a little above 300°C so that isothermal aging tests are important in evaluating their useful lifetime.

The types of polymers which have the best thermal stability seem to be aromatic in character, often with heterocyclic recurring units, low hydrogen content, and often with a two-strand structure. They are usually high melting and have relatively low solubility in common organic solvents, but do dissolve in sulfuric and methanesulfonic acid.

The more promising structures which have been studied are polyphenyls, polyimides, polyamides, polybenzimidazoles, polybenzoxazoles, polybenzothiazoles, polypyrrolones, polyquinoxalines, polyoxadiazoles, polytriazoles, anthraquinone derivatives with these recurring units built into the structure, some siloxane types, and some chelate structures.

DISCUSSION

There are two measurements of polymers that are important to determine in order to know how successfully they may be used at elevated temperatures. First we need to know the TGA behavior of the polymer in air and nitrogen to know the temperature at which pyrolytic decompositions become rapid. Then we need to determine its isothermal aging characteristics in air in order to learn about its slow oxidation and the time it may be expected to maintain a useful life under aerobic working conditions. It is our experience that polymers which stand up to 500°C in a TGA test will usually have a life of at least 200–300 hours in air at 300°C before they begin to have enough weight loss to be critical. This of course varies some with different types of structures.

The general types of polymers which have the best thermal properties are aromatic in character, often with heterocyclic recurring units, low hydrogen content, and often of a two-strand or so-called ladder structure. Such polymers are usually very high melting, have relatively low solubility in common organic solvents but generally are soluble in concentrated sulfuric

Applied Polymer Symposium No. 22, 47–56 (1973)

acid or methanesulfonic acid. As a result they are difficult to fabricate into useful shapes. Crosslinked polymers are often more stable at elevated temperatures than are linear polymers, but they are very difficult to fabricate into useful articles in most cases.

The reactions which produce the materials which show greatest promise in this area are condensation reactions. One big problem in synthesis is to get molecules of high enough molecular weight before some side reactions ends the polymer chain or crosslinking occurs through a side reaction to render the product completely intractable.

Poly-p-phenylene has been prepared by Kovacic [1] by the oxidative

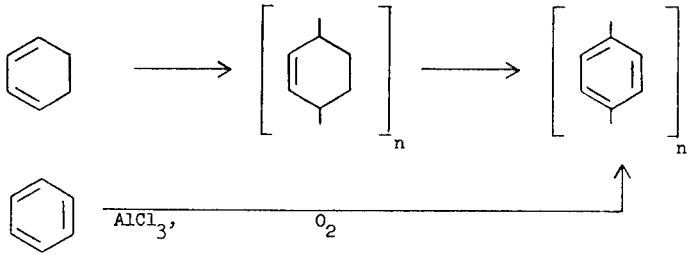

polymerizatiion of benzene. It is very stable to about 500–600°C and oxidizes very slowly. However, it is very high melting and very insoluble and its use is very limited for these reasons. By making an irregular polymer by condensing a mixture of benzene and terphenyl, a more tractable material has been made by Bilow and Miller [2]. This has found some uses as an ablative material. Thus far no other uses have been devised for these intractable materials.

DuPont's polyimides [3] and Monsanto's [4] regular aromatic polyamides have been industrially produced and are used as films and fibers in specialty uses. The polyimides are also used as wire coatings and have been fabricated into plastic shapes with difficulty. The polyamides have been converted to experimental fibers with interesting properties.

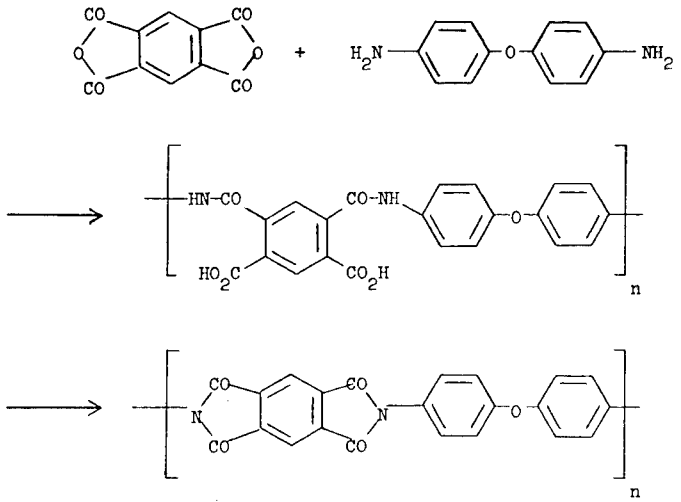

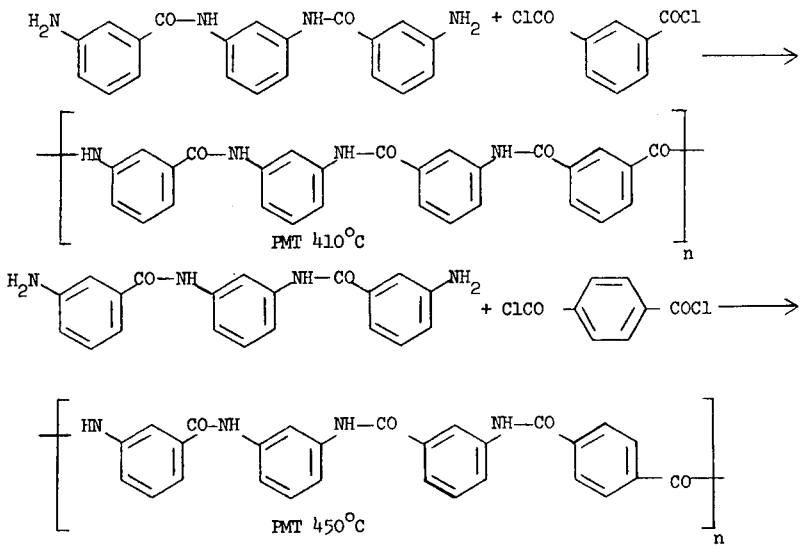

A series of polybenzimidazoles [5], polybenzooxazoles [6], polybenzothiazoles [7], polyoxadiazoles [8], polybenzotriazoles [9], and polysulfodiazoles [10] have been experimentally produced and converted by spinning into fibers of promise. All are useful at about 300°C in the air, but all are

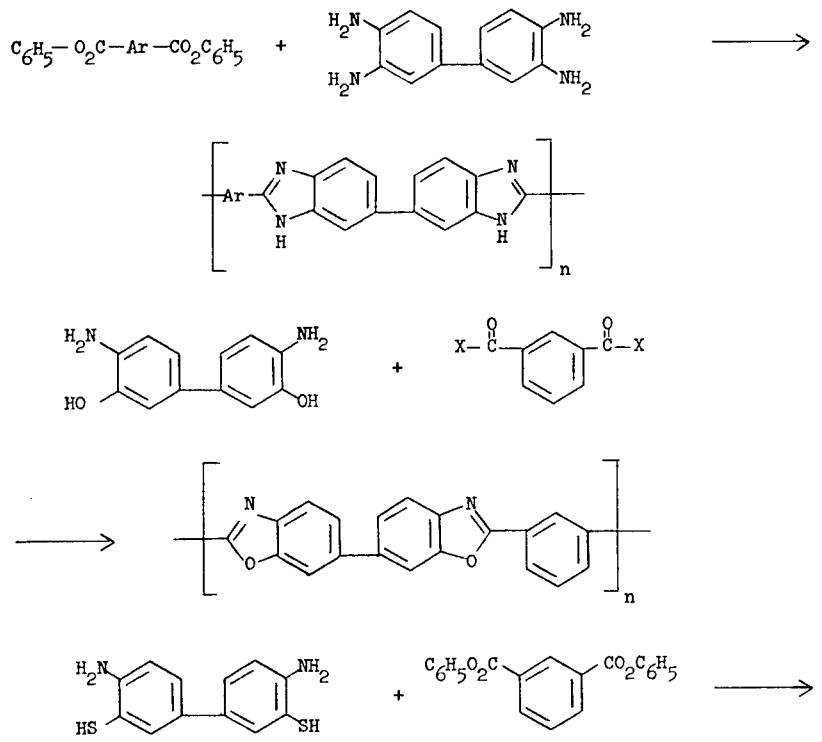

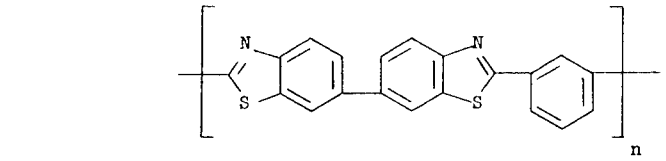

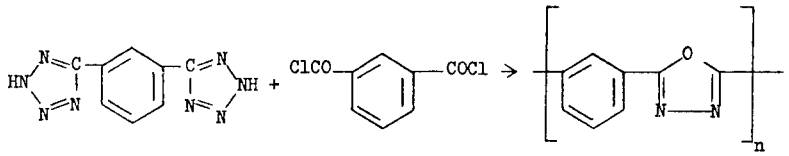

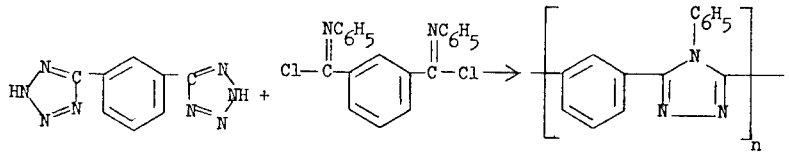

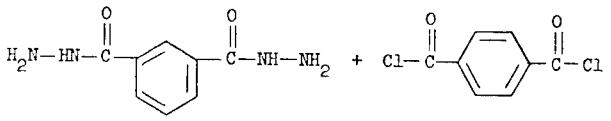

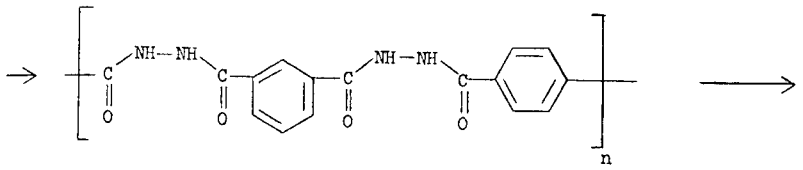

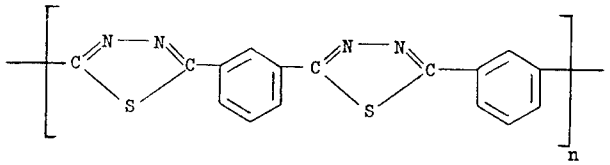

expensive and have not yet been produced in commercial quantities. These materials are all linear polymers with some solubility in organic solvents and sulfuric acid so that they can be fabricated into fibers.

The polypyrrolones [11] and polyquinoxalines [12] have been made into two-strand polymers and these show some increase in thermal stability over the linear types. Again, the problems are expense of raw materials and difficulty of fabrication. For example, the pyrrolone made by Van Deusen needs to be wet spun from concentrated sulfuric acid and drawn at about 500–525°C while still containing sulfuric acid as a plasticizer.

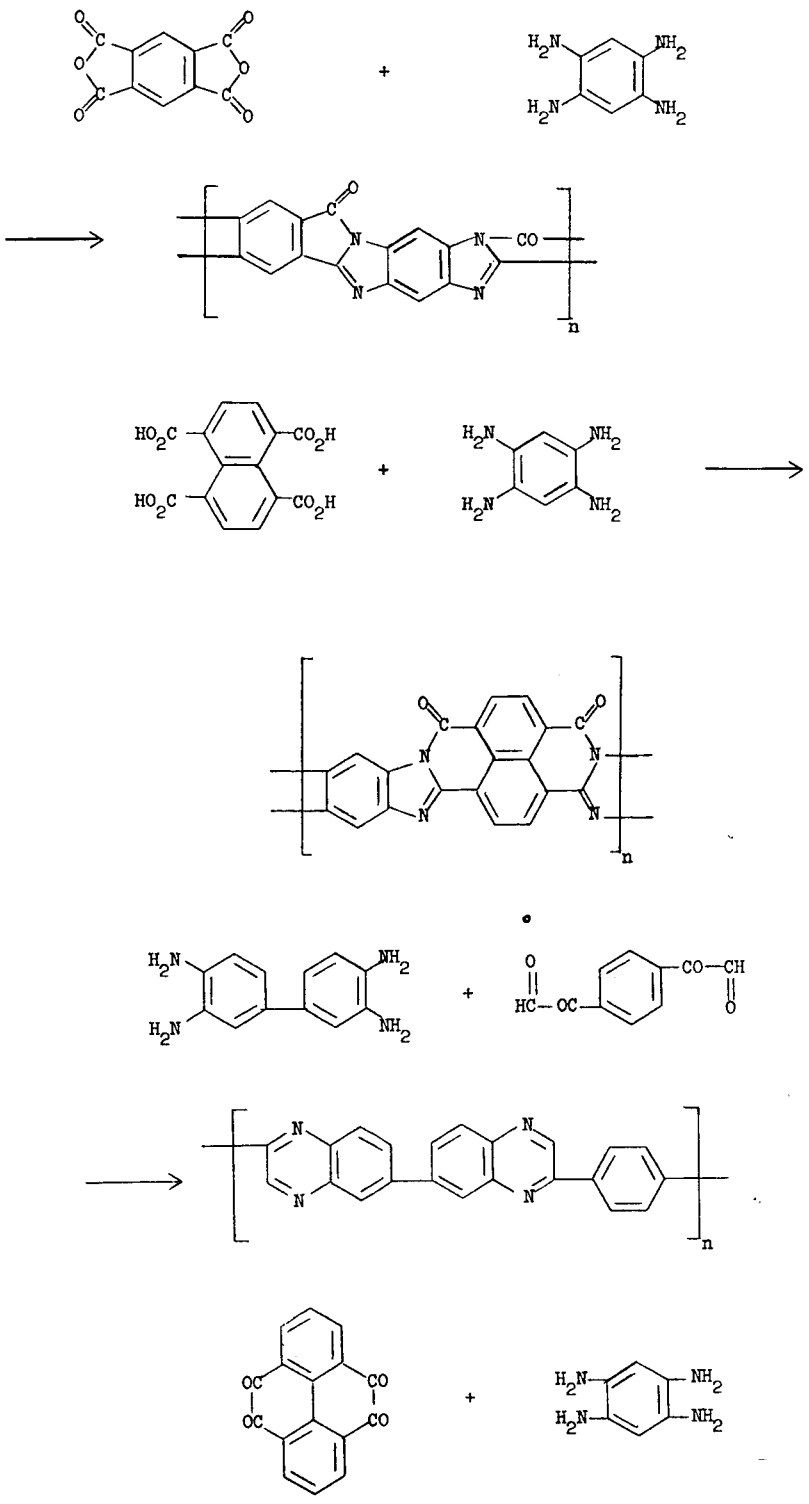

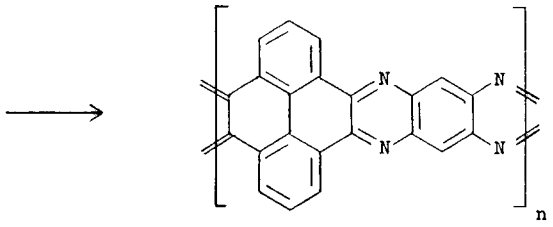

Ladder polyquinoxalines have been made by Stille and his students from aromatic tetraketones and tetraaminobenzene which show no break in TGA curve in air up to 460° and in nitrogen up to 683°C. These are again expensive materials and hard to fabricate.

Hirsch [13] has shown the advantage of low hydrogen content in the thermal and oxidative stability of polymers. He compared the polyimide made from pyromellitic dianhydride and diaminothiadiazole and the one from pyrazine 1,2,4,5-tetracarboxylic acid dianhydride and the same diamine. The latter was stable in air and nitrogen to 600°C, whereas the polyimide from pyromellitic dianhydride charred at 320°C in air.

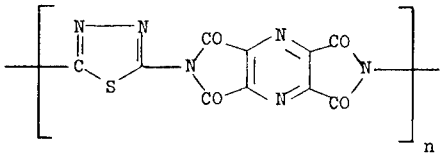

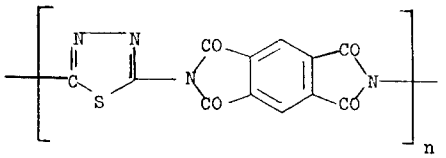

Brown [14] synthesized an interesting double chain siloxane polymer by the careful hydrolysis of phenyl trichlorosilane. This was at first quite stable, but it had a tendency to rearrange at high temperatures to a product which was less useful. Olin Chemicals [15] has announced a heat stable rubber called Dexsil which is a siloxane with a m-carborane unit in the chain. It is reported to be very heat stable, but it is a very expensive polymer which has not come into general use. The simpler siloxanes are not oxidatively stable above about 250°C.

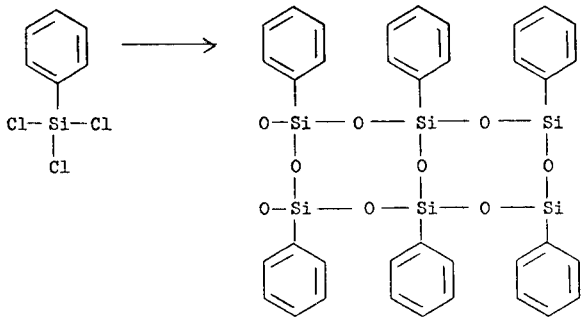

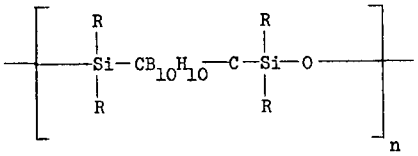

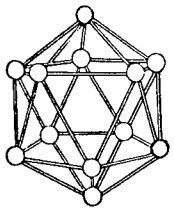

m-Carborane

Fluorinated ether molecules have been obtained which give good heat resistant oils, but they have not been obtained as high molecular weight polymers with good tensile strength.

In an attempt to solve the fabrication problem in the pyrrolones, we have condensed 1,2,5,6-tetraaminoanthraquinone with pyromellitic dianhydride and with 1,4,58-naphthalenetetetracarboxylic acid dianhydride [17] to give polymers which could be solubilized in aqueous DMAc or DMSO by reduction with alkaline sodium dithionite. The product from naphthalenetetracraboxylic acid dianhydride shows promise, but the preparation is difficult and erratic and needs much fuller study. But these polymers do show promise, although again they are very expensive at this stage of development.

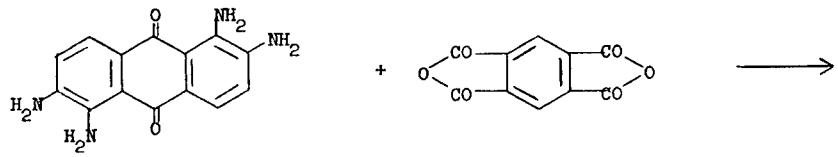

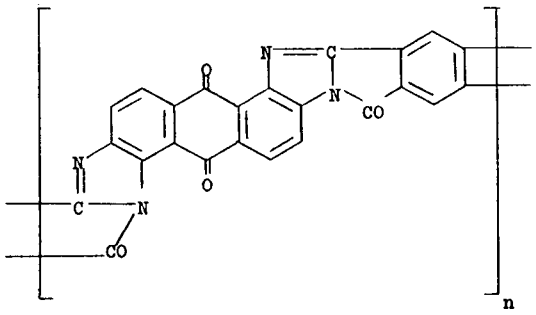

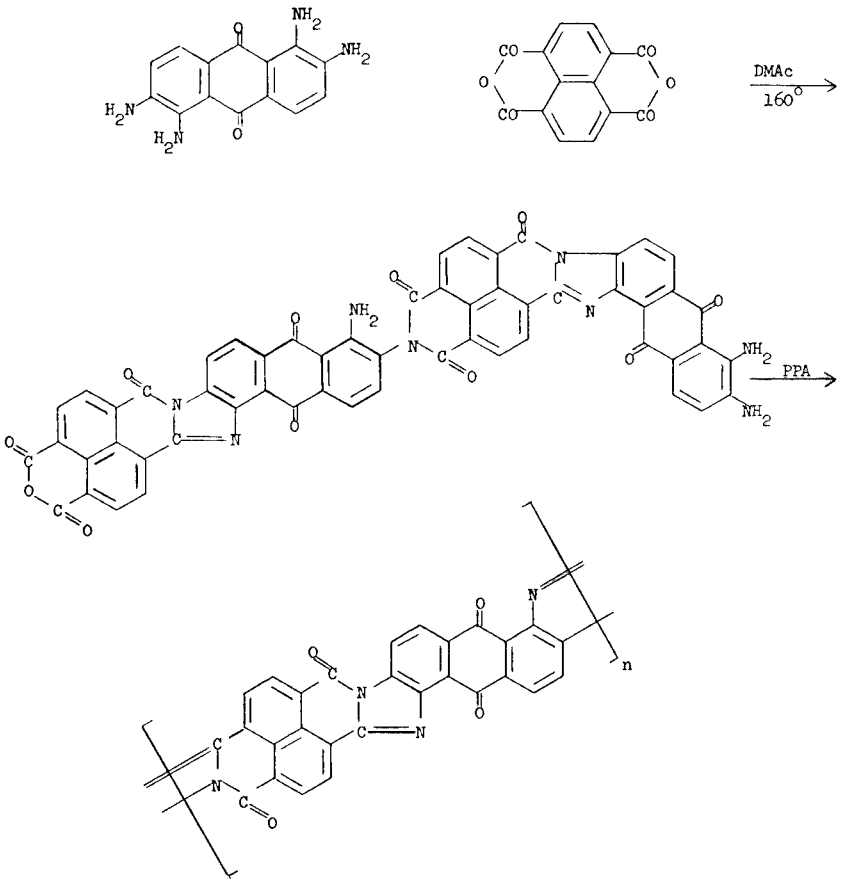

This does not exhaustively cover the entire field of synthetic work on high temperature polymers, but it does represent most of the types. There has not been the improvement in properties in the ladder structures that had been anticipated. This may well be due to the fact that there are sections in the polymer where ring closures have not been effected and the polymers are really not true double strand and the weakest link breaks first. Also, there are severe problems in building such condensation polymers to high molecular weight before crosslinking causes them to go intractable.

REFERENCES

[1] P. Kovacic and A. Kyriakis, *Tetra. Letters*, 467 (1962), *J. Am. Chem. Soc., 85*, 454 (1963); P. Kovacic and R. M. Lange, *J. Org. Chem., 28*, 968 (1963); P. Kovacic and F. W. Koch, *J. Org. Chem., 28*, 1864 (1963); P. Kovacic and J. Oziomek, *J. Org. Chem., 29*, 100 (1964); P. Kovacic, F. W. Koch and C. E. Stephan, *J. Polym. Sci., A, 2*, 1193 (1964); P. Kovacic, V. J. Marchionna and J. P. Kovacic, *J. Polym. Sci., A, 3*, 4297 (1965); P. Kovacic, J. T. Uchic and L. C. Hsu, Polymer Preprints, *Am. Chem. Soc., Div. of Polymer Chem., 8*, 31 (1967); C. S. Marvel and G. E. Hartzell, *J. Am. Chem.*

Soc., 81, 448 (1959); D. A. Frey, M. Hasegawa and C. S. Marvel, *J. Polym. Sci., A, 2*, 2057 (1963); G. L. LeFebvre and F. Dawans, *J. Polym. Sci., A, 2*, 3277 (1964); P. E. Cassidy, C. S. Marvel and S. Ray, *J. Polym. Sci., A, 3*, 1553 (1965).

[2] N. Bilow and L. J. Miller, *J. Macromol. Sci., A-3* (3), 501 (1969).

[3] C. E. Sroog, A. L. Endrey, S. V. Abramo, C. E. Berr, W. M. Edwards and K. L. Oliver, *J. Polym. Sci., A, 3* 1373 (1965); R. S. Irwin and W. Sweeny, *J. Polym. Sci., Part C, 19*, 41 (1967).

[4] J. Preston, *J. Polym. Sci., A-1, 4*, 529 (1966); F. Dobinson and J. Preston, *J. Polym. Sci., A-1, 4* 2093 (1966); J. Preston and W. B. Black, *J. Polym. Sci., B, 4*, 267 (1966); J. Preston and R. W. Smith, *J. Polym. Sci., B, 4*, 1033 (1966); J. Preston, R. W. Smith and C. J. Stehman, *J. Polym. Sci., Part C, 19*, 7 (1967); J. Preston and W. B. Black, *J. Polym. Sci., B, 3*, 845, 1033 (1965); *J. Polym. Sci., A-1, 5*, 2429 (1967); J. Preston, W. F. DeWinter and W. B. Black, *J. Polym. Sci., A-1, 7*, 283 (1969).

[5] H. Vogel and C. S. Marvel, *J. Polym. Sci., 50*, 511 (1961); K. C. Brinker and J. N. Robinson, U. S. Patent 2,895,948 (1959); H. Vogel and C. S. Marvel, *J. Polym. Sci., A, 1*, 1531 (1963); L. Plummer and C. S. Marvel, *J. Polym. Sci., A, 2*, 2559 (1964); R. T. Foster and C. S. Marvel, *J. Polym. Sci., A, 3*, 417 (1965); T. V. Lakshmi Narayan and C. S. Marvel, *J. Polym. Sci., A-1, 5*, 1113 (1967); V. V. Korshak, et al., *Bull. Acad. Sci., (USSR) Div. Chem. Sci. 1677*, 1859 (1963); *Vysokomol., Soedin., 6*, 901, 1251, 1394 (1964); Dokl. USSR, Chem. Sect., 149 195 (1963); *Bull. Acad. Sci. (USSR) Div. Chem. Sci., 1966*, 743 (1966); N. A. Adrova, M. M. Koton et al., *Dokl. USSR, Chem. Sec. 166*, 1 (1966); V. V. Korshak et al., *Vysokomol. Soedin*, 11A, 35 (1969); V. V. Korshak et al., *ibid, 11A*, 22 (1969); Y. Iwakura, K. Uno and Y. Imai, *J. Polym. Sci., A, 2*, 2605 (1964).

[6] C. J. Abshire and C. S. Marvel, *Macromol. Chem., 44-46*, 388 (1961); V. V. Korshak, E. S. Krongauz and A. L. Rusanov, *J. Polym. Sci., C., 16*, 2635 (1967).

[7] P. M. Hergenrother, W. Wrasidlo and H. H. Levine, *J. Polym. Sci., A, 3*, 1665 (1965); Teijin Ltd., Jap. pat. 19273; 11347 (1967); Y. Imai, I. Troka, et al., *Makromol. Chem. 83*, 167 (1964).

[8] T. Kubota and R. Nakanishi, *J. Polym. Sci., B, 2*, 655 (1964); Y. I. Braz, I. E. Kardash, et al., *Vysokomol. Soedin., 8*, 272 (1966); W. W. Moyer, Jr., C. Cole and T. Anyos, *J. Polym. Sci., A 3*, 2107 (1965); Y. Imai, K. Uno et al., *Makromol. Chem., 85*, 179 (1964); V. S. Yakubovich, N. N. Voznesenskaya et al., *Vysokomol. Soedin., 9*, 1973 (1967); Teijin Co. Ltd., Japanese Patent 19271 (1967).

[9] M. R. Lilyquist and J. R. Holsten, *Polym. Prepr., Am. Chem. Soc. Div-Polym-Chem.*, (2), 6 (1963); J. R. Holsten and M. R. Lilyquist, *J. Polym. Sci., A, 3*, 3905 (1965); J. R. Holsten, G. B. Butler and M. R. Lilyquist, French Pat. 1, 398, 146 (1965); M. R. Lilyquist and J. R. Holsten, *J. Polym. Sci., Part C, 19*, 77 (1967).

[10] A. H. Fraser and W. P. Fitzgerald, Jr., *J. Polym. Sci., Part C, 19, 95* (1967).

[11] F. Dawans and C. S. Marvel, *J. Polym. Sci., A, 3*, 3549 (1965); V. L. Bell and G. F. Pezdirtz, *Polym. Prepr. Am. Chem. Soc. Div. Polym. Chem., 6*, 747 (1965); *J. Polym. Sci., B, 3*, 977 (1965); J. G. Colson, R. H. Michel and R. M. Paufler, *J. Polym. Sci., A-1, 4*, 59 (1966); V. L. Bell and R. A. Jewell, *Polym. Prepr. Am. Chem. Soc. Div. Polym. Chem., 8* (1) 235 (1967); V. L. Bell and R. A. Jewell, *J. Polym. Sci., A-1, 5*, 3043 (1967); E. N. Teleshov and A. N. Pravednikov, *Dokl. Acad. Nauk., SSSR, 172*, (16) 1347 (1967); R. L. Van Deusen, *J. Polym. Sci., B, 4*, 211 (1966); R. L. Van Deusen, O. K. Goins and A. J. Sicree, *Polym. Preprints, Am. Chem. Soc. Div. Polym. Chem., 7*, (2) 528 (1966); W. H. Gloor, ibid, 819; A. A. Berlin, B. I. Liogon'kii, G. M. Shamroev and G. V. Belova, *Izv. Akad. Nauk. SSR, Ser. Khim, 5*, 945 (1966).

[12] J. K. Stille and J. R. Williamson, *J. Polym. Sci., B, 2*, 209 (1964); *J. Polym. Sci., A, 2*, 3867 (1964); G. P. deGaudemaris and B. J. Sillion, *J. Polym. Sci., B, 2*, 203 (1964); J. K. Stille and E. L. Mainen, *J. Polym. Sci., B, 4*, 39, 665 (1966); *Macromolecules, 1*, 36 (1968); J. K. Stille, E. L. Mainen, M. E. Freeburger and F. W. Harris, *Polym. Prepr. Am. Chem. Soc. Div. Polym. Chem., 8* (1), 244 (1967); J. K. Stille and M. E. Freeburger, *J. Polym. Sci., Part B, 5*, 989 (1967).

[13] S. S. Hirsch, *J. Polym. Sci., A-1, 7*, 15 (1969).
[14] J. F. Brown, Jr., *J. Polym. Sci., C, 1*, 83 (1963).
[15] K. O. Knollmueller, R. N. Scott, H. Kwasnik and J. F. Sieckhaus, *J. Polym. Sci., A-1, 9*, 1071 (1971).
[16] R. Pense and C. S. Marvel, *J. Polym. Sci., A-1, 8*, 3189 (1970).
[17] J. Szita, L. H. Brannigan and C. S. Marvel, *J. Polym. Sci., A-1, 9*, 691 (1971).

PHENYLQUINOXALINE COPOLYMERS X

P. M. HERGENROTHER

Materials Section, Aerospace Group,
The Boeing Company,
Seattle, Washington 98124

SYNOPSIS

Phenylquinoxaline homopolymers consisting of low, imtermediate, and high molecular weight versions were prepared from the reaction of 3,3′-diaminobenzidine (DAB)and 3,3′,4,-4′-tetraaminobenzophenone (TAB), each with *p*-bis(phenylglyoxalyl)benzene as solutions (18% solids content) in a 1:1 mixture of m-cresol and xylene. In addition, three random and three block copolymers were prepared from the reaction of various amounts of DAB and TAB with p-bis(phenylglyoxalyl)benzene. The copolymers were prepared with a distribution ratio of DAB and TAB of 3:1, 1:1, and 1:3. When stoichiometric quantities of reactants were used, metastable solutions of high molecular weight polymers ($\eta_{inh} > 2.0$ dl/g) were generally obtained. These solutions increased in viscosity and/or exhibited various degrees of gelation after stirring or standing for several days. Stable solutions of relatively high molecular weight polymers were obtained by stoichiometric imbalance. The preparation of PPQ in solution exhibits many features of an interfacial type polymerization. The properties of the homopolymers, copolymers, and a homopolymer blend are compared. The glass transition temperature (Tg) of the polymers vaired from 310 to 370°C. The thermaloxidative stability of PPQ films showed weight losses as low as 1.2% after aging in circulating air at 316°C (600°F) for 1100 hours. Certain films retained excellent flexibility after aging at 316°C in air for 631 hours. The homopolymers and copolymers underwent preliminary evaluation as laminating resins using a high modulus graphite fiber reinforcement. One polymer was selected on the basis of its overall performance and prepared in three separate batches (500 g solids) to demonstrate reproducibility. The polymer was thoroughly characterized and used in composite work. Preliminary mechanical properties of the composites from the 1:3 block copolymer are presented.

INTRODUCTION

The preparation of soluble high molecular weight polyphenylquinoxalines (PPQ) by the cyclopolycondensation of aromatic bis(o-diamines) with aromatic bisbenzils as shown in eq. 1 was first reported in 1967 [1]. These polymers were shown to exhibit good solubility and processability in high molecular weight form as well as excellent thermal oxida-

Applied Polymer Symposium No. 22, 57–76 (1973)

tive stability. As a result of their unique properties, a major effort has concentrated on the synthesis [2–4] and the thermal characterization [5–7] of PPQ. In addition, the potential of the PPQ for use as functional and structural resins in a high temperature environment has been demonstrated [8, 9]. The work reported herein concerns the preparation, characterization, and preliminary composite properties of a series of homopolymers and block and random type phenylquinoxaline copolymers. This work was performed primarily to determine if phenylquinoxaline copolymers exhibited any advantage over the homopolymers for use as functional or structural resins, especially as matrix material in combination with a high modulus graphite fiber reinforcement.

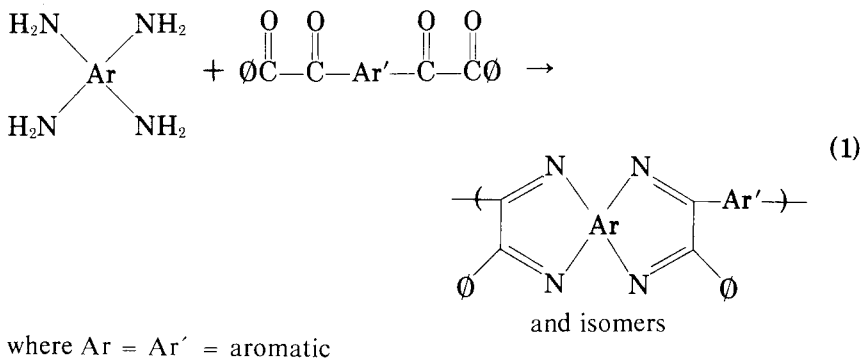

(1)

and isomers

where Ar = Ar′ = aromatic

From available information on more than thirty structurally different PPQ, two basic PPQ were selected for study in this program. At the time of selection, these PPQ represented the most promising phenylquinoxaline polymers for potential use as resin matrices in graphite composites for long term performance (e.g., 1000 hours) at 600°F (316°C) in air. These two basic PPQ were prepared from the reaction of p-bis(phenylglyoxalyl) benzene (p-BPGB) with 3,3′-diaminobenzidine (DAB) and with 3,3′,4,4′-tetraaminobenzophenone (TAB) to yield PPQ-I and PPQ-II respectively as shown in eq. 2.

Each homopolymer (PPQ-I and PPQ-II) was prepared in a low, intermediate, and high molecular weight version which corresponded to inherent viscosities (η_{inh}, 0.5% H_2SO_4 solution at 25°C) of < 1.0, 1.0 to 2.0, and > 2.0 dl/g respectively. Various molecular weight versions of the

TABLE I

Molar Amounts of Reactants for Copolymer Synthesis

Reactant			
p-BPGB	DAB	TAB	Polymer*
1.00	0.75	0.25	Random Co(3:1), Block Co(3:1)
1.00	0.50	0.50	Random Co(1:1), Block Co(1:1)
1.00	0.25	0.75	Random Co(1:3), Block Co(1:3)

* Ratio refers to PPQ-I: PPQ-II character.

homopolymers were prepared to determine if their processability, thermaloxidative stability, and mechanical performance differed.

In addition, three block type and three random type copolymers consisting of various degrees of PPQ–I and PPQ–II character were prepared using the stoichiometry as indicated in Table I.

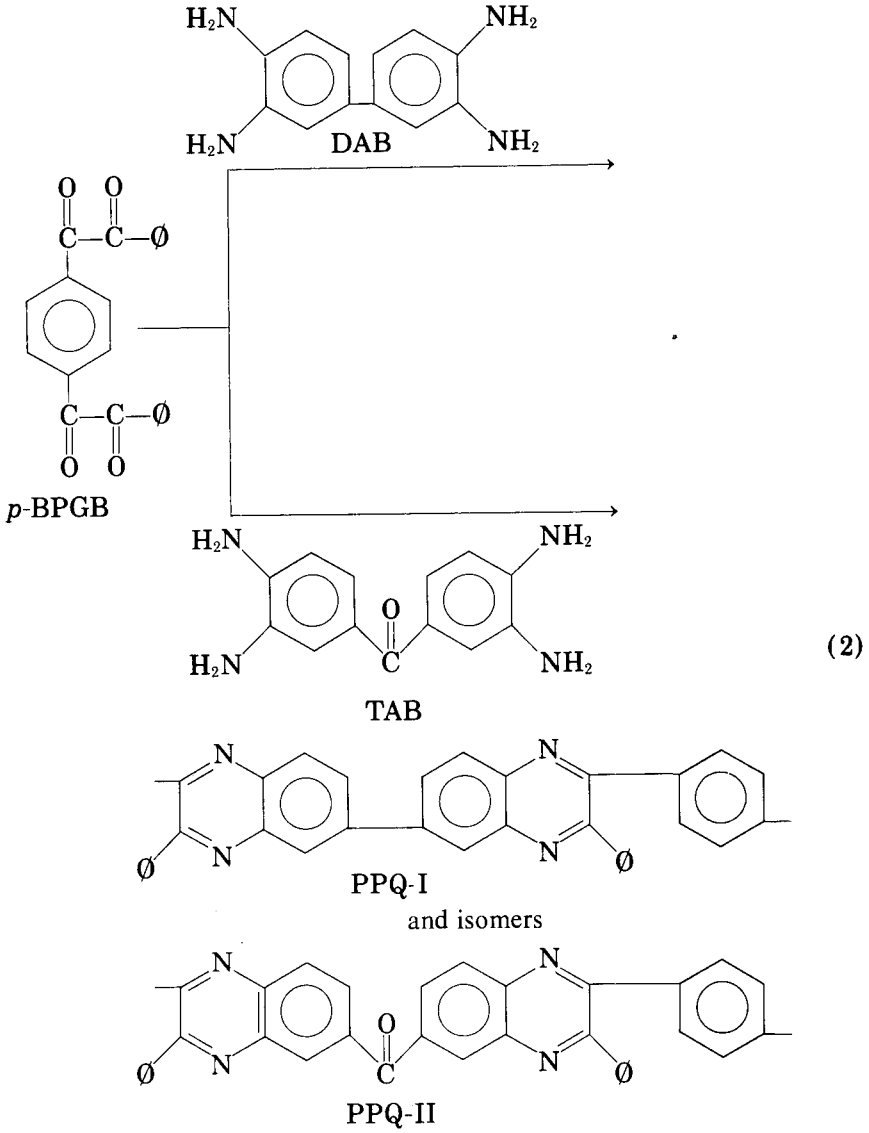

(2)

EXPERIMENTAL

Reactants

Para-bis(phenylglyoxalyl) benzene was prepared through a known route [3] as shown in eq. 3 and obtained in overall yield of 50.2% as yellow crystals, mp 124.5–126°C [lit mp 125–126°C [10]].

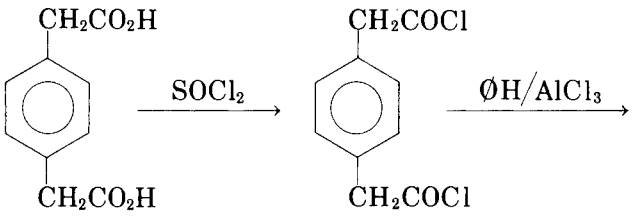

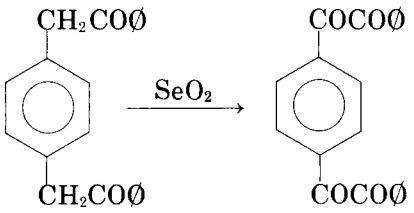

(3)

p-BPGB

3,3′-Diaminobenzidine, mp 174–176.5°C, was obtained commercially and recrystallized from deoxygenated water (150 g/liter) containing a pinch of sodium dithionite under nitrogen. The yellow solution was treated with charcoal, filtered, and cooled to provide light tan needles (105 g, 70% recovery), mp 176–177.5°C (lit mp 179–180°C [11]).

3,3′,4,4′-Tetraaminobenzophenone, mp 214–217.5°C, was obtained commercially and recrystallized from a mixture (1:2) of N, N-dimethylformamide and water (150 g/4.5 liters) under nitrogen. The yellow solution was treated with charcoal, filtered, and cooled to afford yellow needles (120 g, 80% recovery) mp 216–217.5°C (lit mp 217°C [12]).

Polymers

The homopolymers were prepared according to the following general procedure. Para-bis(phenylglyoxalyl) benzene as a fine powder was added during ~ 5 minutes to a stirred slurry of the tetraamine in a mixture of m-cresol and xylene (1:1, used 70% of the total volume of solvent). The remaining solvent was used to wash down the residual tetracarbonyl reactant and the reaction temperature maintained at < 35°C by cooling in a water bath. After the initial temperature surge (for DAB only), the reaction mixture was stirred at ambient temperature for 18 hours to provide a viscous solution. A small portion of the solution was poured slowly into methanol in a Waring blender to precipitate a fibrous yellow solid which was boiled twice in methanol and dried at 130°C in vacuo for 4 hours. Characterization of the solution and isolated polymer is given in Tables II and III.

The random copolymers were prepared following the same general procedure as described for the homopolymers except p-BPGB was added to a stirred slurry comprised of DAB and TAB according to the relative ratios given in Table I.

The block copolymers having a distribution ratio of PPQ–I to PPQ–II character as indicated in Table I were prepared by the following

TABLE II

Synthesis and Characterization of Preliminary Polyphenylquinoxalines

POLYMER NO.	POLYMER	STOICHIOMETRY[a] NH_2/CO	RX SCALE (MOLE)	CONC[b] % SOLIDS	SOL'N VISCOSITY,[c] CPS AFTER		η_{inh},[d] dl/g	UV SPECTRAL DATA[e]	
					3 DA	~74 DA		λ_{MAX}, Mμ	ε
1	HMW PPQ-I	1.00/1.00	0.01	20.0	GELLED	–	2.48	292	44,500
2	IMW PPQ-I	0.98/1.00	0.05	18.7	58,000	65,600	1.24	292	43,911
3	LMW PPQ-I	0.98/1.00	0.10	17.6	6,880	7,250	0.83	292	43,110
4	HMW PPQ-II	1.00/1.00	0.10	17.0	81,000	108,000	2.31	282	58,135
5	IMW PPQ-II	0.99/1.00	0.05	20.0	30,000	33,000	1.14	282	57,794
6	LMW PPQ-II	0.98/1.00	0.05	20.0	1,000	1,400	0.70	282	56,896
7	RaCo (3:1)	0.98/1.00	0.05	20.0	7,800	9,200	0.87	287	46,160
8	RaCo (1:1)	1.00/1.00	0.05	20.0	84,200	95,400	1.55	285	49,376
9	RaCo (1:3)	0.99/1.00	0.05	20.0	8,400	8,800	1.04	283	54,122
10	BICo (3:1)	1.00/1.00	0.05	13.4	107,000	119,400	1.89	287.5	44,739
11	BICo (1:1)	1.00/1.00	0.05	17.4	81,000	88,800	2.41	285	47,880
12	BICo (1:3)	1.00/1.00	0.05	15.5	24,000	27,200	1.92	283	52,099
13	1:1 MOLAR BLEND 2&5	–	–	–	–	–	1.18	285	49,724

[a] Molar amount of tetraamine to tetracarbonyl; solvent, 1:1 m-cresol and xylene.

[b] Concentration based upon weight of reactants and volume of solvent.

[c] Brookfield viscosity at 25°C.

[d] Inherent viscosity (0.5% H_2SO_4 at 25°C), polymer ppt in MeOH dried 130°C, in vacuo 4 hours.

[e] Ultraviolet spectrum determined in H_2SO_4; λ_{max} = wavelength of maximum absorption; ε = extinction coefficient (molar absorptivity).

TABLE III
Thermal Characterization of Preliminary Polyphenylquinoxalines

POLYMER NO.	PST[a] (°C)	Tg[b] (°C)	FILM THICKNESS (MILS)	WT LOSS (%)[c] AFTER TIME (hr) AT 316°C IN AIR			LIGHT TRANS (%) AFTER TIME (hr) AT 316°C IN AIR			FLEXIBILITY,[d] FAILURE AFTER TIME (hr) AT 316°C	WT LOSS (%)[c] AFTER TIME (hr) AT 371°C IN AIR				POLYMER FUSION AT TEMP (°F)[e] 1-GOOD 3-POOR 5-VERY LITTLE		
				25	1100	ACT WT LOSS	0	614	1100		25	~100	151	226	650(343°C)	700(371°C)	750(399°C)
1	>340	370	1.6	7.23	12.00	4.65	68	35	22	>259<330	6.9	37.1	–	–	5	5	3
2	395–41	350	1.3	7.49	12.12	4.63	67	36	20	>259<330	7.0	38.4	–	–	5	2	1
3	330–39	335	1.9	4.51	11.72	7.21	60	20	5	>187<259	5.7	34.3	–	–	2	1	1
4	300–10	325	1.9	8.37	13.43	5.06	65	35	–	>631<1100	10.1	15.1	–	46.6	2	1	2
5	300–08	314	2.6	7.20	9.67	2.47	67	37	20	>187<259	8.6	16.4	51.4	–	1	1	1
6	295–305	310	2.2	7.31	11.94	4.63	65	31	–	>187<259	8.9	18.1	–	51.3	1	4	5
7	325–35	337	2.4	7.04	16.69	9.67	70	22	–	>168<360	8.5	18.8	–	93.2	4	3	3

8	320-31	335	2.2	6.09	12.27	6.18	52	23	11	>614<1100	6.8	13.4	23.1	–	5	2	3
9	317-28	325	2.6	6.08	12.41	6.33	56	22	–	>168<360	8.5	16.3	–	82.0	2	1	2
10	326-38	352	2.3	9.97	17.83	7.86	59	6	–	>168<360	9.4	18.0	–	95.5	5	3	5
11	323-35	335	1.9	8.28	10.81	2.53	62	35	–	>631<1100	9.0	13.4	–	80.2	3	5	4
12	316-24	327	2.1	7.50	8.74	1.24	62	44	–	>631<1100	7.5	11.4	–	71.1	2	2	2
13	321-34	335	2.2	8.10	14.99	6.89	63	38	–	>631<1100	8.9	13.7	–	–	4	3	3

[a] Polymer softening temperature, determined on Fisher-Johns melting point apparatus with slight pressure.

[b] Glass transition temperature, determined by differential scanning calorimetry at ΔT = 20°C/min in N_2.

[c] Weight loss determined on films in circulating air.

[d] Flexibility measured by hard fingernail crease.

[e] Fusion test performed on powdered samples sandwiched between Al, placed in preheated press under pressure (200 psi).

TABLE IV
Thermal Characterization of Advanced Polyphenylquinoxalines

POLYMER NO.	Tg, °C		FILM THICKNESS (MIL)	WT LOSS (%) AFTER TIME (HR) AT 316°C IN AIR				LIGHT TRANS (%) AFTER TIME (HR) AT 316°C IN AIR			FLEXIBILITY, FAILURE AFTER TIME (hr) AT 316°C
	DSC[a]	DMRM[b]		25	403	1076	ACT WT LOSS	0	403	1076	
14	351	337	2.0	4.9	6.2	11.0	6.1	62	26	5	>136<403
15	350	–	–	–	–	–	–	–	–	–	–
16	318	290	3.8	7.4	8.4	11.9	4.5	59	15	4	>136<403
17	315	–	–	–	–	–	–	–	–	–	–
18	311	285	2.9	8.5	9.5	14.0	4.5	59	23	3	>136 <403
19	326	307	3.1	6.6	7.7	11.9	5.2	61	23	6	<136 >403
20	320	304	2.1	5.6	7.4	11.0	5.4	81	61	25	>377 <1076
21	318	303	2.7	6.1	7.2	11.2	5.1	79	58	24	>377 <1076
22	322	306	2.3	5.6	7.1	10.2	4.6	83	60	32	>377 <1076

[a] Differential scanning calorimetry, $\Delta T = 20°C/min$, N_2.

[b] Dynamic mechanical relaxation measurements using a Vibron Viscoelastomer (Model DDV-11), $\Delta T = 10°C/min$, N_2, Temperature reported is that of maximum dispersion peak at 110 cycles/sec.

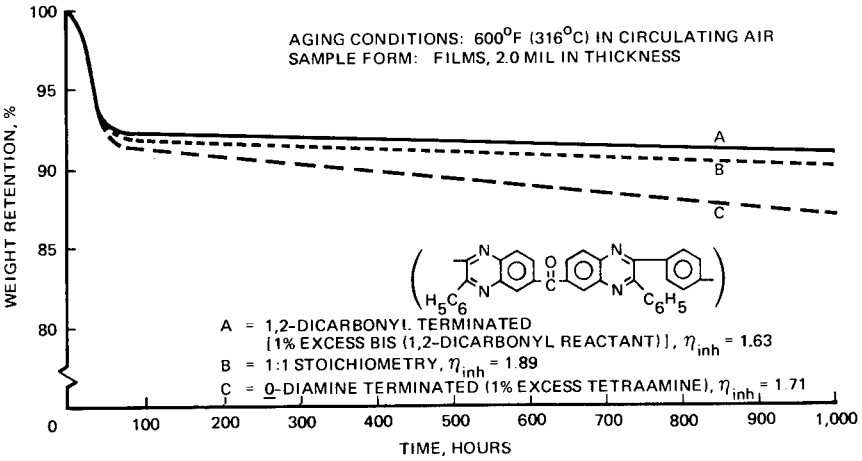

FIG. 1. Isothermal weight loss of polyphenylquinoxalines.

representative procedure. Para-bis(phenylglyoxalyl) benzene (10.271g, 0.030 mole) as a fine powder was added during 5 minutes to slurry of DAB (5.357 g, 0.025 mole) in a mixture of m-cresol and xylene (1:1, 40 ml). Additional solvent (12.5 ml) was used to wash down the residual tetracarbonyl reactant and the mixture stirred at ambient temperature to form a viscous orange solution.

In another flask, p-BPGB (6.847 g, 0.020 mole) as a fine powder was added to a slurry of TAB (6.057 g, 0.025 mole) in a 1:1 mixture of m-cresol and xylene (40 ml). Additional solvent (11.6 ml) was used to wash down the residual reactant and the mixture stirred at ambient temperature for 18 hours to form a viscous orange solution. The solution of PPQ–II oilgomer was then added slowly with vigorous stirring to the solution of the PPQ–I oligomer at ambient temperature. The viscosity increased and additional solvent which was used to wash out the PPQ–II oligomer's flask was added to reduce the solids content to 17.4%. Stirring was continued for 18 hours to provide a stable viscous orange solution of 1:1 block copolymer.

Films

Films were prepared from all of the polymer solutions by doctoring a portion of the solution onto a glass plate followed by drying overnight at ~70°C in air and then at ~130°C in vacuo for 4 hours. The yellow films were characterized as presented in Tables III and IV.

DISCUSSION

Preliminary Polymer Synthesis

The general procedure for polymer preparation involved the addition of the tetracarbonyl reactant as a fine powder during ~5 minutes to a slurry of the tetraamine in a 1:1 mixture of m-cresol and xylene at temperature

< 35°C. Preliminary polymer synthesis indicated that stoichiometric quantities of reactants on a 0.010 mole scale at 15 to 20% solids content (based upon weight of reactants and volume of solvent) generally gave very viscous to extremely viscous solutions and in some cases, gelation. The gelling phenomenon can be alleviated without any apparent detrimental effect upon the polymer by upsetting the stoichiometry of the reactants. The stoichiometry should be upset preferably in favor of the tetracarbonyl reactant since PPQ with amino end groups display poorer thermaloxidative stability (Fig. 1). As shown in Table II, when the stoichiometry was upset by 2% in favor of the tetracarbonyl reactant (Polymer No. 2, 3, 6, and 7), polymer of relatively high molecular weight was obtained (η_{inh} = 1.24 dl/g for Polymer No. 2). This was unexpected, since in condensation polymers from AA-BB type reactants, stoichiometric quantities of reactants are generally required to form high molecular weight polymers (excluding interfacial condensation). Similar to poly-as-triazines [13], this polycondensation exhibits many features of an interfacial polycondensation and as explained by Morgan [14], the rate of polymerization is faster than the rate of mixing or dissolution such that there may be temporary interfaces within which the polycondensation is proceeding independently of the two reactants in the complete system. The tetracarbonyl reactant is more soluble in the solvent mixture than the tetraamine. In some cases, the solution viscosity became extremely high prior to the formation of a complete solution. For example, the reaction of stoichiometric quantities of DAB and p-BPGB on a 0.1 mole scale in a 1:1 mixture of m-cresol and xylene at a solids content of 20% provided a viscous solution (Brookfield viscosity at 25°C = 50,000 cps) containing solid particles after stirring 0.5 hours. The solid particles were isolated and identified as unreacted DAB while the polymer was shown to be of substantially high molecular weight (η_{inh} = 2.4dl/g).

The random copolymers (polymers No. 7, 8 and 9, Table II) were prepared by adding p-BPGB to a slurry of the two tetraamines according to the stoichiometry given in Table I. Since DAB is more reactive with the tetracarbonyl compound than TAB, the random copolymers may contain a high degree of block character. The random copolymers were prepared by upsetting the stoichiometry from 0 to 2% in favor of the tetracarbonyl reactant to yield copolymers having Brookfield solution viscosities of 7,800, 8,400 and 84,200 centipoises and η_{inh} of 0.87, 1.04, and 1.55 dl/g respectively (see Table II). The solutions of the random copolymers appeared to be stable and exhibited no detectable gel structure even at exact stoichiometry (Polymer No. 8).

Block copolymer synthesis involved the preparation of low molecular weight forms (oligomers) of PPQ-I and PPQ-II. The stoichiometry was adjusted to yield the PPQ-II oligomer rich in amino groups while the PPQ-I oligomer was rich in carbonyl groups. The oligomeric solutions were blended by adding the PPQ-II oligomer to the other and the blend further reacted to provide block copolymers. The degree of PPQ-I and PPQ-II character was controlled by the relative amounts of each tetraamine used.

As indicated in Table I, a distribution ratio for PPQ-I and PPQ-II was 3:1, 1:1, and 1:3, respectively. The block copolymers were prepared using exact stoichiometry at 20% solids content. However, the solutions became extremely viscous after stirring for a few hours and were diluted to solids content of 13.4 to 17.4% (Polymers No. 10, 11, and 12, Table II).

Polymer Characterization

The solution viscosities as reported in Table II for eleven of the twelve polymers increased upon standing at ambient temperature over a period of ~74 days. Whereupon the solutions stabilized and exhibited no further increase in their viscosity after standing an additional 90 days. The high molecular weight version of PPQ-I (Polymer No. 1) gelled after stirring at ambient temperature for 6 hours. Although a stable solution of high molecular weight PPQ-I can be prepared at lower solids content (e.g., ~8%), it is desirable to use higher concentrations for prepreg preparation to reduce the number of coats to attain the desired resin content.

Ultraviolet spectroscopic characterization of the polymers in concentrated sulfuric acid showed the wavelength of maximum absorption (λ_{max}) for PPQ-I and PPQ-II to occur at 292 and 282 mμ respectively (Table II). The λ_{max} of the various copolymers and a 1:1 molar blend of PPQ-I and PPQ-II occurred between these two wavelengths. It appears as though the major contribution to the length of the conjugated system occurs primarily through the tetraamine portion of the molecule rather than through the tetracarbonyl portion, the phenylene moiety. Apparently the p-phenylene moiety and the phenyl group are forced out of the plane of the ring due to steric interaction and therefore unable to participate significantly in resonance. Although the sp^2 hybridized carbonyl group of the benzophenone portion of PPQ-II permits π bond overlap, this occurs to a lesser degree than in the biphenylene portion of PPQ-I. As a result, the λ_{max} for PPQ-I occurs 10mμ higher than PPQ-II.

The molar absorptivity (ϵ, molar extinction coefficient) of PPQ-II is greater than that of PPQ-I. For example, ϵ for high molecular weight versions of PPQ-I and PPQ-II are 44,550 and 58,135 respectively. The trend in the copolymers is as expected; as the amount of PPQ-II character increases, the λ_{max} decreases and ϵ becomes greater. The ultraviolet spectra for four PPQ are shown in Figures 2 and 3.

Thermal Characterization

The thermal properties of the various polymers are summarized in Table III. The polymer softening temperature (PST) was determined by applying spatula pressure to a powdered polymer sample sandwiched between cover slips which had been placed onto a preheated Fisher Johns Melting Point Apparatus. The temperature range where the opaque sample softened and became almost completely transparent was taken as the PST. Unfortu-

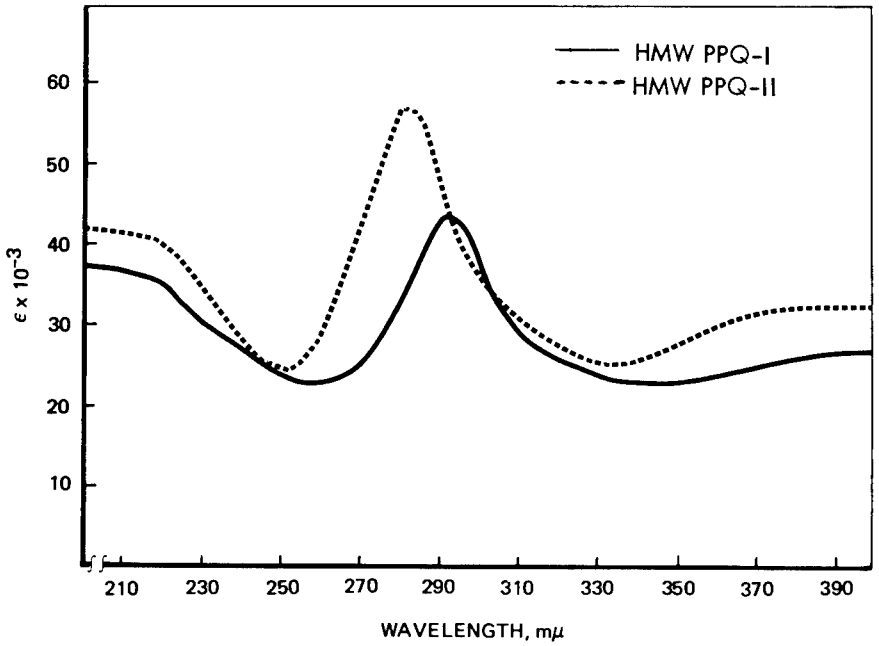

FIG. 2. Ultraviolet spectra of polyphenylquinoxalines in sulfuric acid.

nately, this method is crude and subject to variations due to several factors such as sample size, ΔT, and pressure. As a result, the PST of the low, intermediate, and high molecular versions of PPQ-I and PPQ-II failed to show pronounced differences.

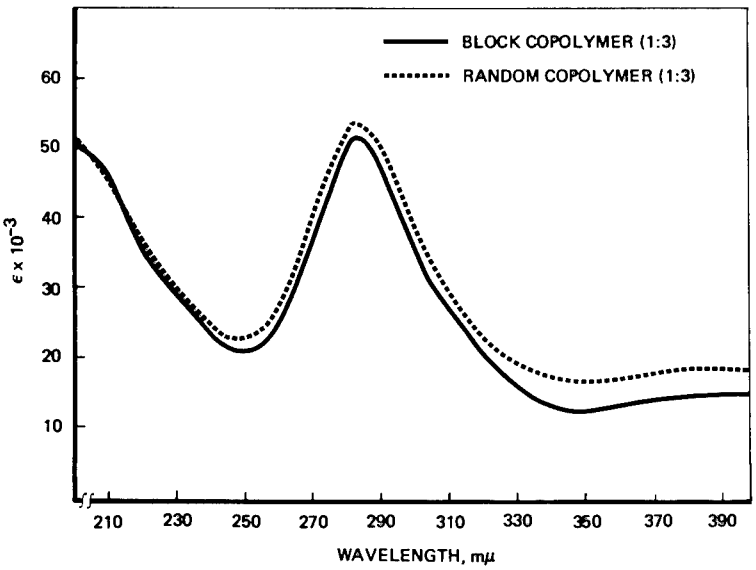

FIG. 3. Ultraviolet spectra of polyphenylquinoxalines in sulfuric acid.

The glass transition temperature (Tg) was determined by Differential Scanning Calorimetry (DSC) at a heating rate of 20°C/min in nitrogen. A typical DSC curve is shown in Figure 4 for a 1:3 block copolymer (Polymer No. 12). The sample was initially cycled to 400°C in an inert atmosphere and showed a broad endotherm at ~80°C which is attributed to the release of water and/or solvent. Upon a rerun, no initial endotherm was observed and the Tg was taken as the inflection point at the ΔT versus temperature curve.

The Tg of the various polymers corresponded well with what was expected. The Tg of high molecular weight PPQ-I (Polymer No. 1) was highest (370°C) and the Tg of low molecular weight PPQ-II (Polymer No. 6) was lowest (310°C) with the Tg's of the other forms of PPQ-I and II being in between. In addition, the Tg of the copolymers came out as anticipated. In the block copolymer series, the polymer (Polymer No. 10) containing the highest percent of the more rigid biphenylene moiety exhibited the highest Tg (352°C), while the polymer (Polymer No. 12) containing the highest degree of the flexible benzophenone moiety exhibited the lowest Tg (327°C). The polymer containing equal portions of biphenylene and benzophenone moieties exhibited a Tg of 335°C, in between the other two.

Since even low molecular weight versions of PPQ-I and PPQ-II were of sufficient molecular weight to provide tough, fingernail creaseable films, it was surprising to observe the wide spread in Tg (337°C to 370°C) for the various versions of PPQ-I. A curve of the apparent dependency of Tg on molecular weight (as indicated by η_{inh}) is shown in Figure 5 for PPQ-I. At η_{inh} of 2.2 dl/g the Tg for this particular polymer appears to level off.

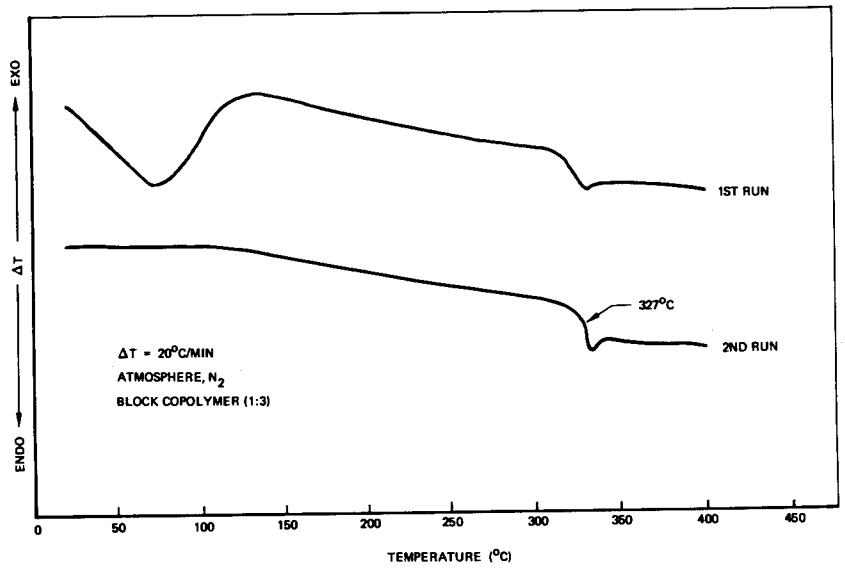

FIG. 4. Differential scanning calorimetry curve of the phenylquinoxaline block copolymer (1:3).

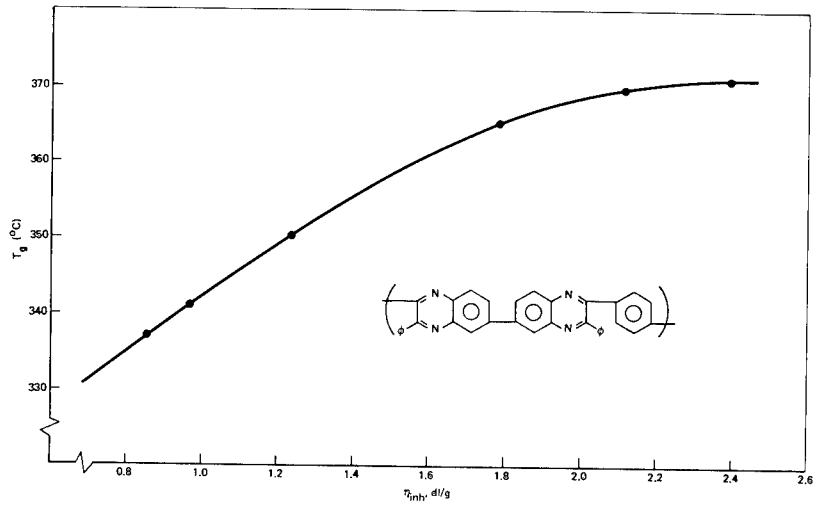

FIG. 5. Inherent viscosity versus T_g for PPQ–I.

The thermaloxidative stability of the polymers was determined by measuring the retention of weight, color, and flexibility of their film after isothermal aging in circulating air at 316°C (600°F) and at 371°C (700°F). The films were prepared by doctoring the polymer solution onto a glass plate followed by drying overnight at ~70°C in air and then at 130°C in vacuo for 4 hours. All of the polymers readily formed tough flexible transparent yellow films. The HMW PPQ-I film was cast just prior to the solution gelling. All of the films exhibited an initial weight loss after aging for 25 hours at 316°C and at 371°C which is attributed to the loss of residual solvent and water. After 1100 hours 316°C in circulating air, the actual weight loss on the films varied from a low of 1.24% for the block copolymer (1:3, Polymer No. 12) to a high of 9.67% for the (3:1) random copolymer (Polymer No. 7). The good thermaloxidative stability of the polymers is also reflected in the retention of film flexibility and color as indicated by % light transmission. Several of the polymers (Nos. 4, 8, 11 and 12) retained fingernail creaseability after more than 614 hours at 316°C in air.

At 371°C in circulating air, the block copolymer (1:3, Polymer No. 12) exhibited the highest weight retention, losing a total of 11.4% or an actual weight loss of 3.9% after 100 hours. None of the films exhibited good weight retention after 226 hours at 371°C in air.

The aging study was conducted on films rather than powders because the measurements (flexibility and color) are more meaningful than a simple weight loss determination which is about all the powder samples would have offered. The measurement of retention of some mechanical properties such as film flexibility, is a better means of ascertaining the potential use life of a polymer at elevated temperature. It is well known that a polymer (e.g., powder form) can undergo substantial thermaloxidative degradation

without exhibiting significant weight loss due to a number of factors such as oxygen uptake, molecular weights of the degradation products too high to volatilize, and/or crosslinking.

Powdered forms of each of the thirteen polymers were obtained in the following manner. A portion of the polymer solution was poured slowly into methanol in a Waring blender. The resulting fibrous yellow polymer was isolated and boiled for 0.5 hour twice in methanol followed by treatment in the blender after each wash. Drying was accomplished at 130°C in vacuo for 4 hours. At this stage, the yellow solids exhibit a total weight loss of ~0.2% as determined by heating at 350°C for 1 hour under argon. The yellow solid was pulverized in a Wig-L-Bug to particle size of ~60 mesh. Due to increased surface area and the environmental conditions, the powdered samples absorb atmospheric water as indicated in an increase in total weight loss of 1.5 to 2.0% after 1 hour at 350°C in argon. Polymer fusion tests were performed on powdered samples by sandwiching a small amount between aluminum and placing this in a preheated press under ~200 psi for 10 minutes. As shown in Table III, the degree of fusion (processability) was ranked numerically from 1 to 5, 1 representing good fusion where the polymer essentially melted in the center to form a tough translucent section while 5 represents poor fusion where no melting occurred but the powders have been pressed together. The intermediate molecular weight PPQ-II (Polymer No. 5) exhibited good fusion under the three different temperatures while the low molecular weight version exhibited poor fusion at the two higher temperatures (371 and 399°C). This is tentatively attributed to crosslinking inhibiting flow prior to the formation of a good fusion disc. As indicated in Table III, the polymers which exhibited the best fusion from each of the four groups of PPQ were low molecular weight PPQ-1 (No. 3), intermediate molecular weight PPQ-II (No. 5), random copolymer 1:3 (No. 9), and block copolymer 1:3 (No. 12). It was known that PPQ-II generally exhibits better processability than PPQ-I, hence it was not surprising to observe better fusion in those copolymers containing a higher degree of PPQ-II character.

Advanced Polymer Synthesis and Characterization

Based upon the thermaloxidative stability and processability of the polymer as summarized in Table III and also upon preliminary fiber wetting and flow tests, four polymers were selected for preliminary composite evaluation. These consist of LMW PPQ-I, IMW-PPQ-II, (1:3) random copolymer and (1:3) block copolymer. The four selected polymers were prepared on a larger scale as indicated in Table V. Although the solution of the polymers prepared on a larger scale (0.4 to 1.0 mole, 200 g to 500 g) failed to consistently agree with those prepared on a smaller scale (0.05 mole, 25g), the other properties (e.g., η_{inh} and UV data) agreed favorably.

The thermal properties of the polymer prepared on a larger scale are given in Table IV. The Tg's were determined by DSC and also by dynamic

TABLE V
Synthesis and Characterization of Advanced Polyphenylquinoxalines

POLYMER NO.	POLYMER	STOICHIOMETRY[a] NH_2/CO	RX SCALE (MOLE)	CONC,[a] % SOLIDS	SCL'N VISCOSITY, (CPS) AFTER[a]		η_{inh}, dl/g[a]	UV SPECTRAL DATA[a]	
					3 DA	11-14DA		λ_{MAX}	ϵ
14	LMW PPQ-I	0.97/1.00	0.4	17.1	4,300	4,400	0.78	292	43,785
15	LMW PPQ-I	0.98/1.00	0.24	18.0	7,000	–	0.95	–	–
16	IMW PPQ-II	0.985/1.00	0.24	20.0	5,000	5,700	1.05	282	57,814
17	IMW PPQ-II	0.985/1.00	0.2	20.0	4,300	–	1.03	–	–
18	RaCo (1:3)	0.985/1.00	0.4	20.0	1,750	1,800	0.78	283	52,713
19	BICo (1:3)	0.985/1.00	0.4	18.4	17,000	17,000	1.31	283	52,834
20	BICo (1:3)	0.985/1.00	0.4	18.6	22,150	23,000	1.46	283	49,759
21	BICo (1:3)	0.985/1.00	1.0	18.1	20,800	–	1.66	283	49,844
22	BICo (1:3)	0.985/1.00	1.0	18.3	21,400	–	1.61	283	49,963

[a] Previously defined in Table II.

mechanical relaxation measurements (DMRM) using a Vibron Viscoelastometer. Although the maximum dispersion peak temperature is lower than the Tg obtained by DSC, the trend is the same. A representative curve of the dynamic mechanical relaxation spectrum for the (1:3) block copolymer (Polymer No. 21) is shown in Figure 6. Film samples of the polymers exhibited good aging performance at 316°C in circulating air as shown by actual weight losses (neglecting initial weight loss due to solvent) of 4.5 to 6.1%. The retention of color and flexibility was less than that previously determined for similar polymers prepared on a smaller scale (see Table III, Polymers No. 3, 5, 9 and 10). However, this may be partially attributed to increased film thickness.

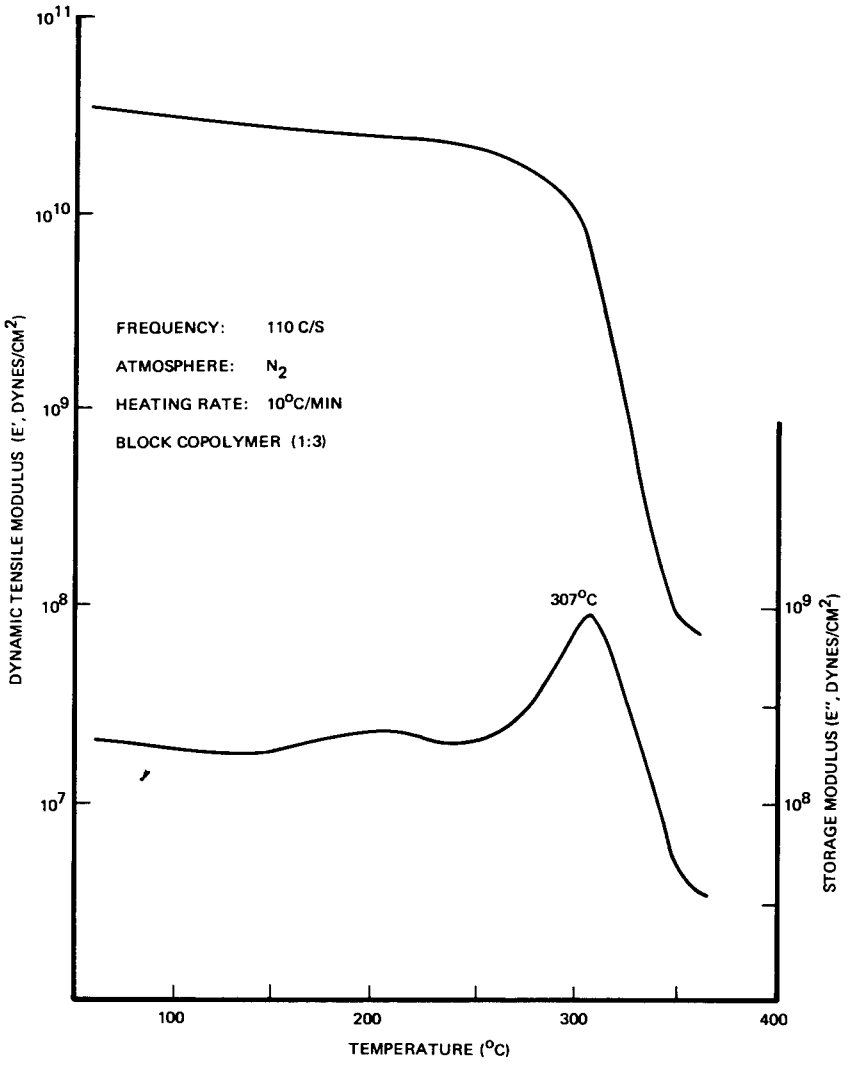

FIG. 6. Dynamic mechanical relaxation spectrum of a polyphenylquinoxaline.

TABLE VI
Unidirectional PPQ High Modulus Graphite (Hercules HM-S) Laminate Data[a,b]

Test Condition[c]	Tensile Strength[d] psi	Tensile Modulus psi x 10^6	Flexural Strength psi	Flexural Modulus psi x 10^6	Interlaminar Shear[d] Strength, psi
RT	101,500	24.4	120,800	19.6	4220
204°C after 100 hr at 204°C	100,300	20.6	117,700	16.1	5150
204°C after 1000 hr at 204°C	103,600	18.5	88,900	11.7	4060
316°C (600°F) after 10 min at 316°C	101,400	19.3	87,200	12.5	3110
316°C after 100 hr at 316°C	107,900	19.3	96,000	16.8	4550
316°C after 500 hr at 316°C	70,600	15.7	51,900	15.4	2780
316°C after 1000 hr at 316°C[e]	—	—	—	—	—

[a] All test results are the average of 10 specimens except for RT tensile strength results which are average of 5 specimens.
[b] Void content < 2%.
[c] Aged in circulating air (150 ml/min).
[d] Short beam shear.
[e] Excessive loss of matrix material during aging.

In general, good reproducibility was obtained in scaling up from 0.05 to 1.0 mole and also within four different batches of the same polymer prepared in a 0.4 to 1.0 mole scale (Table IV, Polymer No. 19 through 22).

Composite Properties

The four polymers in Tables IV and V underwent preliminary evaluation as resin matrices in unidirectional flat high modulus graphite fiber (Hercules HM-S) laminates. Based upon the results of this initial composite work, the 1:3 block copolymer was selected for more comprehensive composite study. The detailed results of the preliminary composite evaluation on the four polymers from Table IV as well as more advanced composite evaluation of the 1:3 block copolymer will be presented later [15].

The HM-S type high modulus graphite Yarn (E = 60 $\times$ 10^6 psi) was impregnated with the 1:3 block copolymer by solution coating and dried at 149°C (300°F) in air to a volatile content of $\sim$10%. The prepreg was unidirectionally laid up using bleeder cloths and steel shim stock and introduced into a preheated press at 336°C (636°F) $\sim$10°C above the Tg. After allowing for residual solvent removal, 200 psi was applied for 1 hour. The temperature was then increased at a rate of 3°C/min. to a final temperature of 454°C (850°F). The laminate (4'' $\times$ 12'' $\times$ 11 ply) was postcured for 1 hour at 454°C under 200 psi to provide the mechanical properties as reported in Table VI.

Since films of the 1:3 block copolymer used in the fabrication of these laminates exhibited low weight losses ($\sim$5%) after 1076 hours at 316°C in

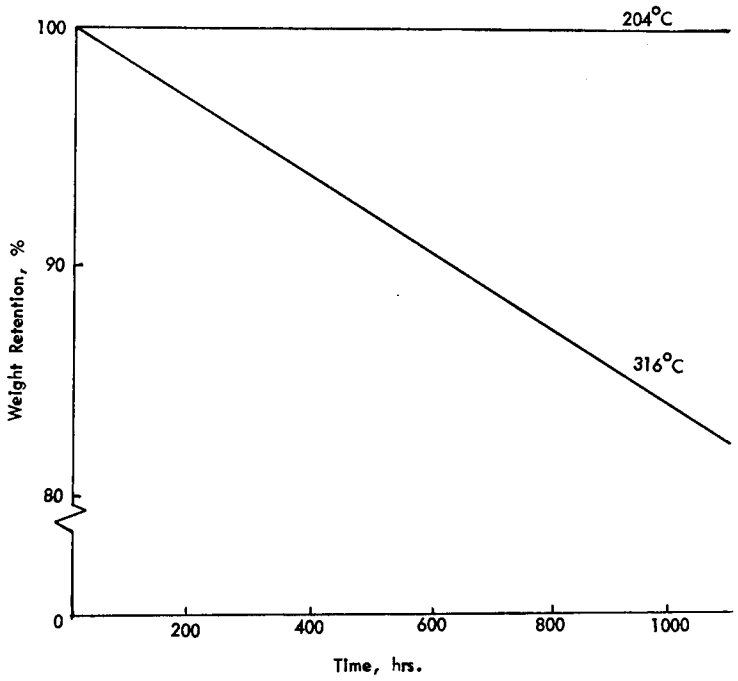

FIG. 7. Isothermal weight loss of laminates of phenylquinoxaline block copolymer (1:3).

air, it was surprising to observe such a high weight loss as shown in Figure 7 for the matrix resin in the laminates during aging under the same conditions (same oven, etc.).

Apparently the high cure and/or postcure temperature (454°C) initiated polymer degradation which then proceeded at a moderate rate upon aging the laminate specimens at 316°C in air.

The author gratefully acknowledges support of this work by the National Aeronautics and Space Administration (Contract NAS 3-15547), Lewis Research Center, Polymer Matrix Composite Section under Dr. Tito T. Serafini, with Dr. Peter Delvigs acting as Project Engineer. The composite work was performed by Mr. J. T. Hoggatt and Dr. J. G. Shdo.

REFERENCES

[1] P. M. Hergenrother and H. H. Levine, *J. Polym. Sci., A-1, 5*, 1453 (1967).
[2] P. M. Hergenrother, *J. Polym. Sci., A-1, 6*, 3170 (1968).
[3] W. Wrasidlo and J. M. Augl, *J. Polym. Sci., A-1, 7*, 3393 (1969); *J. Polym. Sci., Part B, 7*, 281 (1969).
[4] W. J. Wrasidlo and J. M. Augl, *Macromolecules 3* (5), 544 (1970).
[5] W. Wrasidlo, *J. Polym. Sci., A-1, 8*, 1107 (1970).
[6] W. Wrasidlo, *J. Polym. Sci., A-2, 9*, 1603 (1971).
[7] J. M. Augl, *J. Polym. Sci., A-1, 10*, 2403 (1972).
[8] P. M. Hergenrother, *J. Macromol. Sci.—Revs. Macromol. Chem. C6* (1), 1 (1971).
[9] P. M. Hergenrother *SAMPE 3* (1), 1 (1971).

[10] J. Schmitt, P. Comoy, J. Boitar and M. Suguet, *Bull. Soc. Chim. France* 636 (1956).
[11] H. Vogel and C. S. Marvel, *J. Polymer Sci., 50*, 511 (1961).
[12] P. J. Montagne, *Ber., 48*, 1034 (1915).
[13] P. M. Hergenrother, *Polym. Prepr. Am. Chem. Soc. Div. Polym. Chem. 13* (2), 930 (1972); *J. Macromol. Sci., Chem. A7(3)*, 573 (1973).
[14] P. W. Morgan, *Condensation Polymers*, Interscience Pub. Inc., New York, 1965, p. 125.
[15] J. T. Hoggatt and J. G. Shdo, to be presented at the *Nat'l. SAMPE Meeting* in Los Angeles, Calif. April 1973.

AFR

Paper + book while book both good.

A74-22106 **The preparation and properties of high performance polyimide composites.** H. D. Stenzenberger (Technochemie GmbH, Heidelberg, West Germany). In: Polymeric materials for unusual service conditions; Proceedings of the Conference, Moffett Field, Calif., November 29-December 1, 1972. (A74-22101 08-18) New York, Wiley-Interscience, 1973, p. 77-88. Research sponsored by the Bundesministerium für Bildung und Wissenschaft.

A new approach to the preparation of polyimide binders, based on the idea of using low-melting monomeric bismaleimides that can be polymerized to thermally stable high-crosslinked polyimides is outlined. It is shown that low-melting bismaleimide resin can be used for the preparation of high-performance filament-wound high-temperature composites. The ease of processing is the principal advantage of the resin system; it is usable not only for filament winding but also for prepreging and pultrusion operations. V.P.

A74-22109 **A new engineering material for advanced design concepts.** G. H. Kalb, R. W. Quarles, Jr., and R. S. Graff (Du Pont de Nemours and Co., Inc., Wilmington, Del.). In: Polymeric materials for unusual service conditions; Proceedings of the Conference, Moffett Field, Calif., November 29-December 1, 1972. (A74-22101 08-18) New York, Wiley-Interscience, 1973, p. 127-142.

ECD-006 perfluoroelastomer is a new high performance elastomer based on the copolymerization of tetrafluoroethylene, perfluoro(methyl vinyl ether) and a third monomer (a perfluorovinyl ether grouping with an active cure site monomer). This material, when cross-linked, gives vulcanizates with outstanding chemical and fluid resistance and high temperature oxidative resistance. In many cases this elastomer may be used to replace either metal or plastic parts, but a direct shape replacement very often is not satisfactory. Instead, the design must be modified. Some areas of application for ECD-006 parts are indicated. (Author)

A74-22110 **Block copolymer elastomers from polysiloxanes and high temperature resistant segments.** M. Matzner, A. Noshay, L. M. Robeson, C. N. Merriam, R. Barclay, Jr., and J. E. McGrath (Union Carbide Corp., Bound Brook, N.J.). In: Polymeric materials for unusual service conditions; Proceedings of the Conference, Moffett Field, Calif., November 29-December 1, 1972. (A74-22101 08-18) New York, Wiley-Interscience, 1973, p. 143-156. 33 refs.

Several types of silicone containing block copolymer elastomers have been prepared. A general synthetic method which involves the coupling of hydroxyl-terminated organic hard blocks with amino-terminated siloxanes was utilized to synthesize the materials. Both aromatic polyesters and polyethers as well as cycloaliphatic polycarbonates were incorporated into the novel elastomers. The latter displayed excellent thermal oxidative and hydrolytic stability combined with good mechanical properties. Outstanding ultraviolet stability was observed for the transparent elastomers containing the cycloaliphatic polycarbonate. T.M.

A74-22111 * **Recent advances in elastomer service-life prediction.** R. F. Landel, R. F. Fedors, and J. Moacanin (California Institute of Technology, Jet Propulsion Laboratory, Pasadena, Calif.). In: Polymeric materials for unusual service conditions; Proceedings of the Conference, Moffett Field, Calif., November 29-December 1, 1972. (A74-22101 08-18) New York, Wiley-Interscience, 1973, p. 157-168. 15 refs. Contract No. NAS7-100.

The mechanical properties of an elastomer, including rupture and its time dependence, are defined uniquely by a tensile property surface in normalized stress-strain-time coordinates. In practice, the property surface is determined from short-time constant strain-rate uniaxial tests. By using the time reduction properties of both temperature and cross-link density, an effective time scale of over ten decades of log time can be covered. Changes in cross-link density, filler content, or swelling do not affect the limits of the property surface when plotted in logarithmic coordinates but merely shift their positions. The shape, however, may be modified in certain cases. The service life of an elastomer in the absence of aging reactions can be estimated from the property surface and expected in-use conditions such as strains (static or dynamic). T.M.

A74-22116 **Ultrathin membranes for treatment of waste effluents by reverse osmosis.** L. T. Rozelle, J. E. Cadotte, B. R. Nelson, and C. V. Kopp (North Star Research and Development Institute, Minneapolis, Minn.). In: Polymeric materials for unusual service conditions; Proceedings of the Conference, Moffett Field, Calif., November 29-December 1, 1972. (A74-22101 08-18) New York, Wiley-Interscience, 1973, p. 223-239. 19 refs. Research supported by the U.S. Environmental Protection Agency.

Properties and fabrication techniques are reviewed for the main types of ultrathin (500 to 6000 A) polymer membranes, originally developed for reverse osmosis water desalination processes. Four were selected for testing their potential use in sewage and industrial waste treatment: cellulose acetate o-propyl sulfonic acid (CAOPSA), beta-glucan dimethylamino ethyl ether, cellulose acetate methyl sulfonate, and a new nonpolysaccharide membrane called NS-1. A schematic diagram is given of the osmosis test loop and the dynamic flat test cell used. In the sewage test, measurements were made of the average water flux; the drop of water flux in time due to fouling; and rejection of organic carbon, ammonia nitrogen, and suspended and dissolved solids. The industrial test measured rejection of nickel, iron, copper, zinc, and chromic acid solutions at different driving pressures and pH levels. In both tests, CAOPSA performed best. A third test showed NS-1 membranes effective in treating high-alkaline metal cyanide rinse waters. P.T.H.

A74-22117 **Reverse osmosis membranes formed by plasma polymerization of organic compounds.** H. Yasuda (Research Triangle Institute, Research Triangle Park, N.C.). In: Polymeric materials for unusual service conditions; Proceedings of the Conference, Moffett Field, Calif., November 29-December 1, 1972. (A74-22101 08-18) New York, Wiley-Interscience, 1973, p. 241-253. 28 refs. U.S. Office of Saline Water Contract No. 14-30-2658.

The technique of plasmapolymerization (of organic compounds) by an electrodeless (inductive coupling) glow discharge is applied to the preparation of a composite reverse osmosis membrane. The membrane consists of an ultrathin semipermeable membrane deposited from plasma of organic compounds onto a porous substrate. The technique makes it possible to deposit semipermeable membrane onto porous substrates of various shape and of various materials. It is shown that reverse osmosis membranes of glow discharge polymers are characterized by a steady increase of salt rejection and water flux with time of reverse osmosis run, and by excellent performance at high salt concentrations and under high pressures. V.P.

A74-22201 # **A comparison of adsorption and boundary lubricant failure.** H. A. Spikes and A. Cameron (Imperial College of Science and Technology, London, England). *Royal Society (London), Proceedings, Series A*, vol. 336, no. 1607, Feb. 19, 1974, p. 407-419. 25 refs.

A comparison has been made between the reversible adsorption and the friction-reducing properties of long-chain fatty amines on stainless steel. This has shown that adsorption and lubricant failure depend on concentration of amine and temperature in a similar way. Breakdown of lubrication may therefore be associated with reversible desorption of amines from steel surfaces. Measurement of the adsorption properties of the fatty amines indicates a lowering of the isosteric heat of adsorption at low temperatures, which may result from 'pre-freezing' of the hydrocarbon solvent. (Author)

A74-22226 # **Mechanical interaction of fiber and matrix during the deformation of composite metal materials (K voprosu o mekhanicheskom vzaimodeistvii volokon i matritsy pri deformirovanii metallicheskikh kompozitsionnykh materialov).** A. S. Obchinskii, I. M. Kop'ev, and Iu. E. Busalov (Akademiia Nauk SSSR, Institut Metallurgii, Moscow, USSR). *Problemy Prochnosti*, vol. 5, Dec. 1973, p. 3-8. 7 refs. In Russian.

Theoretical analysis of the stresses arising at the fiber-matrix interface during the deformation of metallic composites with elastic fiber and plastic matrix. The variations of such stresses are determined as functions of axial deformation, the mechanical properties of the matrix, and the volume proportion of fiber. It is also found that the stresses at the fiber-matrix interface amount to only some tenths of that of the yield point and cannot, according to current theories, affect noticeably the strength of fiber. V.Z.

A74-22236 # **Breakdown kinetics in reinforced metals under cyclic loads (Kinetika razrusheniia armirovannogo metalla pri tsiklicheskikh nagruzkakh).** V. V. Ostashev (Leningradskii Politekhnicheskii Institut, Leningrad, USSR). *Problemy Prochnosti*, vol. 5, Dec. 1973, p. 113, 114. 5 refs. In Russian.

Experiments were carried out in a microscopic study of the development of fatigue cracks in flat reinforced-steel specimens with

THE PREPARATION AND PROPERTIES OF HIGH PERFORMANCE POLYIMIDE COMPOSITES

HORST D. STENZENBERGER

Technochemie GmbH,
Verfahrenstechnik,
Heidelberg, West Germany

SYNOPSIS

Under the sponsorship of the German Ministery of Science, represented by the German "Gesellschaft für Weltraumforschung," the polymer group of Technochemie discovered a new technical approach for processible polyimides. The idea was to utilize low melting monomeric bismaleimides that can be polymerized to thermally stable high crosslinked polyimides without the evaluation of by-products. Low melting bismaleimides should make it possible to work them up in the molten stage by a filament winding process.

For the intended filament winding process it was necessary to know the properties, polymerization conditions and the viscosimetric behavior of the molten bismaleimides or bismaleimid systems. It was found that bismaleimides and systems begin to polymerize just above their melting points, indicated by a rapid increase in the melt viscosity. Differential enthalpic analysis showed that the polymerization seems to go by a first order reaction. It was therefore possible to obtain values of the activation energy by a plot of log k against the reciprocal of the absolute temperature in the usual way. On the basis of this knowledge two low melting resin formulations were evaluated which were used for preparing and testing unidirectional carbon fiber-laminates. The laminates were fabricated by the intended filament winding process, and basic properties including flexural, shear, and impact strength of the composites at elevated temperatures are determined. Also the long-term creep behavior under flexural load was examined.

INTRODUCTION

The essential and only partly solved problem which has confronted those who are working in high temperature high performance composites has been the difficulty to develop binders or binder systems which combine ease of processing, good high temperature, physical properties, and retention after thermal aging at elevated temperatures and high stress levels. The most important requirement for a binder from the commercial point of view is materials which can be processed under low pressure and temperatures up to 400°F. This is demanded by the industry which employ equipment and tooling designed for the use with epoxies and phenolics.

The past decade has born out many novel polymer systems with outstanding mechanical properties at elevated temperatures. The most ex-

Applied Polymer Symposium No. 22, 77–88 (1973)

tensive investigated class are the polyimides and a variety of them has been commercialized. In general at the movement there are available two types of polyimide-binders. The first are made from aromatic dianhydrides and aromatic diamines using the polyamic-acid-precurser route. These binder types result in composites having a significant level of voids, which comes about as a consequence of the volatiles which are evolved during the final cure step. In these types of binders very poor properties are achieved if the final cure step is completed prior to the application of pressure. The second group are imide oligomers or bisimide monomers containing unsaturated aliphatic end groups that can be polymerized through these double bonds without the evolution of byproducts. Using such prepolymers, composites containing a very low void content can be produced.

It is the purpose of this paper to describe a new technical approach for a processible polyimide binder system based on low melting bismaleimides. The idea was to use a system that can be worked up in the molten stage by a filament winding process without using a solvent for the fiber impregnation step to overcome many of the deficiencies which have been found to exist in current high temperature binder systems. The following properties are of special interest to a suitable resin system:

1. Melting temperature	Impregnation temperature
2. Viscosity of melt	Wettability
3. Viscosity time function	Pot life
4. Mechanical property profile	High temperature property retention
5. Thermooxidative stability	Application temperature.

Low melting bismaleimides are preferred for the filament winding process to make low impregnation temperatures possible. The viscosity of the molten resin should be low to secure a good fiber coating. Of major interest is the viscosity-time function at or above the melting temperature; the increase of viscosity vis time should be low to secure a definite resin pick-up to guarantee an unique fiber-resin distribution in the cured filamentary wound application.

BISMALEIMIDES

Preparation and Polymerization

Processes for the preparation of bismaleimides are well known [1, 2]. The process starts from diamines and maleic acid anhydride, followed by a cyclodehydration step of the resulting bismaleamic acid. Using acetic acid anhydride as a cyclodehydration agent, high yields in bismaleimides are produced. Aromatic types are preferably made in DMF as a solvent without the isolation of the bismaleamic acid. Cyclodehydration is catalyzed by sodium or potassium acetate [2].

Bismaleimides possess two double bounds, which are highly electron poor because of the two flanking imide carbonyl groups. Therefore,

bismaleimide compounds can be involved in a self-polymerization reaction effected by a simple heating resulting in highly crosslinked polybismaleimides.

To study the properties and polymerization behavior we prepared a variety of bismaleimides listed in Table I. It can be seen that types containing long chain aliphatic diamines give the lowest melting points and very low melting viscosities, while the aromatic ones are high melting. Only the 4,-'4'-bismaleimido-diphenyl-methane is low melting. For the filament winding process we formulated a very low melting type (H 353) which can be used for fiber impregnation at 125°C having a starting viscosity of about 100 centistokes. This resin system contains 85% by weight of aromatic bismaleimides and additives to prevent recrystallisation when cooling. Table I contains also the decomposition temperatures of the corresponding polybismaleimides determined by thermogravimetric analysis (N_2, 10°C/min). It is surprising that the aliphatic types give very high decomposition temperatures, but, as was to be expected, the thermooxidative stability is poor, indicated by high isothermal weight loss at 260°C in air. Therefore, they can not be used for a high temperature resin formulation.

Polymerization

It is a property of bismaleimides that they begin to polymerize just above their melting points indicated by an rapide increase of the viscosity. The polymerization velocity is a function of the polymerization temperature and

TABLE I
Properties of Bismaleimides and Polybismaleimides

Bisimid	Melting point (°C)	Viskosity[a] cSt/Temp. °C	TGA-break[b] °C	Stability[c]
1,6-Bismaleimido-hexan	137-138	13.2/140	420	3.20
1,8-Bismaleimido-octane	118-119	18.0/120	430	3.30
1,10-Bismaleimido-decane	111-113	14.5/120	440	3.10
1,12-Bismaleimido-dodekan	110-112	13.7/120	455	3.20
2,2,4-Trimethyl-hexamethylen-bis-maleimid	70-130	15.5/130	432	1.90
1,3-Bismaleimido-benzene	198-201	-	475	0.60
1,4-Bismaleimido-benzene	> 300	-	485	0.30
2,4-Bismaleimido-toluene	172-174	47.0/175	501	0.10
4,4'-Bismaleimido-diphenylmethane	154-156	28.0/160	495	1.40
4,4'-Bismaleimido-diphenylether	180-181	-	488	1.10
H 353	70-125	105-110/125	475	1.54

[a] Determined using method of Ubbelohde.
[b] TGA-heating rate 10°C/min, N_2.
[c] Weight loss after 100 hours at 260°C (500 F) in air.

TABLE II
Values of Rate Constants for the Polymerisation of Bismaleimides

Temp.; (°C)	Temp.; (°K)	1,12-Bismaleimido-dodecane k, sec^{-1}	1,6-Bismaleimido-hexane k, sec^{-1}	4,4'-Bismaleimido-diphenylmethane k, sec^{-1}	Resin H 353 k, sec^{-1}
220	493			$6.20 \cdot 10^{-4}$	
230	503			$1.91 \cdot 10^{-3}$	
235	508		$2.20 \cdot 10^{-3}$		
240	513	$2.77 \cdot 10^{-3}$		$2.99 \cdot 10^{-3}$	
245	518		$4.01 \cdot 10^{-3}$		
250	523	$3.97 \cdot 10^{-3}$		$5.56 \cdot 10^{-3}$	$1.86 \cdot 10^{-3}$
255	528		$6.28 \cdot 10^{-3}$		
260	533	$5.27 \cdot 10^{-3}$		$9.55 \cdot 10^{-3}$	$3.25 \cdot 10^{-3}$
265	538		$1.055 \cdot 10^{-2}$		
270	543	$7.12 \cdot 10^{-3}$		$1.57 \cdot 10^{-3}$	$5.44 \cdot 10^{-3}$
275	548		$1.744 \cdot 10^{-2}$		
280	553	$1.01 \cdot 10^{-2}$		$1.97 \cdot 10^{-2}$	$9.06 \cdot 10^{-3}$
285	558		$1.965 \cdot 10^{-2}$		
290	563	$1.39 \cdot 10^{-2}$			$1.42 \cdot 10^{-2}$
300	573				$1.92 \cdot 10^{-2}$
E_A (Kcal/Mol)		18.40	30.2	28.7	29.5

the nature of the diamine used for the preparation of the special bismaleimide compound. The polymerization is an exothermic reaction, therefore, the differential enthalpic curves can be used to calculate the thermal kinetic data and activation energies.

Using the method of K. E. J. Barrett [3], we calculated the reaction rates and activation energies for the polymerization of three bismaleimides and

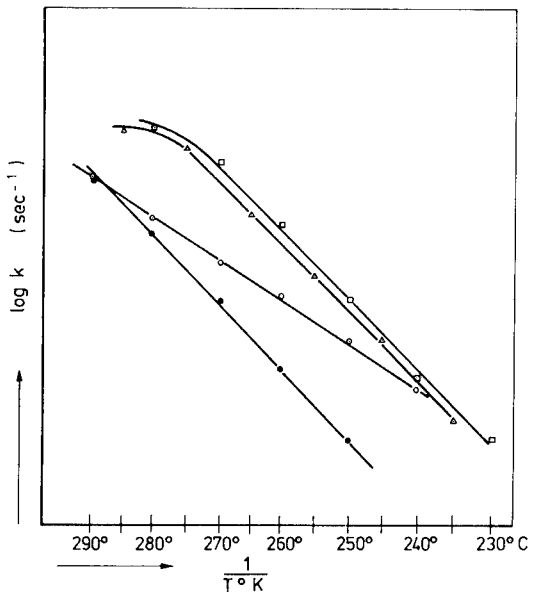

FIG. 1. Arrhenius plot for polymerization of bismaleimides at constant heating rate (20°C/min); ○ is 1,12-Bismaleimidododecane; △ is 1,6-Bismaleimidohexane; □ is 4,4'-Bismaleimidodiphenylmethane; ● is Resin H 353.

the resin formulation H 353. The values are listed in Table II, and Figure 1 shows the Arrhenius plots for the polymerization reaction indicating straight lines for all four bismaleimides over a wide temperature range. This serves as a diagnosis for a first order reaction which was accepted for the calculation of the rate values. From the differential enthalpic curves it can be seen that the polymerization can be accomplished by heating at temperatures of about 200–250°C. Tests applied have demonstrated that bismaleimides and the binder system H 353 can be cured by isothermal heating to 200–250°C for 3 to 5 hours. Postcuring at 200–250°C to get maximum mechanical properties is recommended.

H 353 UNIDIRECTIONAL LAMINATES

Materials

Fibers

Glass-fiber laminates were made using commercial available E-glass-fiber rowings with two different sizings (K 43-amino-silane, S 22/558 methacrylsilane). Carbon fiber laminates were prepared using Morganites high modulus (HM, Modmor I) and high strength (HS, Modmor II S) types.

Resins

Laminates were fabricated using the resin formulation H 353 having the following properties:

Melting temperature	70–125°C
Impregnation temperature	125°C
Viscosity of melt	105–110 centistrokes at 125°C
after 1 hour at 125°C	125–130 centistrokes at 125°C
after 2 hours at 125°C	145–150 centistrokes at 125°C
after 3 hours at 125°C	165–175 centistrokes at 125°C
after 4 hours at 125°C	200–205 centistrokes at 125°C
Curing temperature	205–240°C,
Curing time	5–3 hours
Postcuring	15 hours/210°C
Loss on curing	0.005 g/cm^2 of free surface
Density of cured resin	1.37 g/cm^3

For comparison unidirectional laminates were prepared using the Epoxy-Novolac resin, Rütpox 0302/MNA/DMP 30 (Rütag) and Kerimid 601 (Rhone Poulenc). Kerimid 601 laminates were made from prepregs produced with NMP (N-methylpyrolidon) as a solvent.

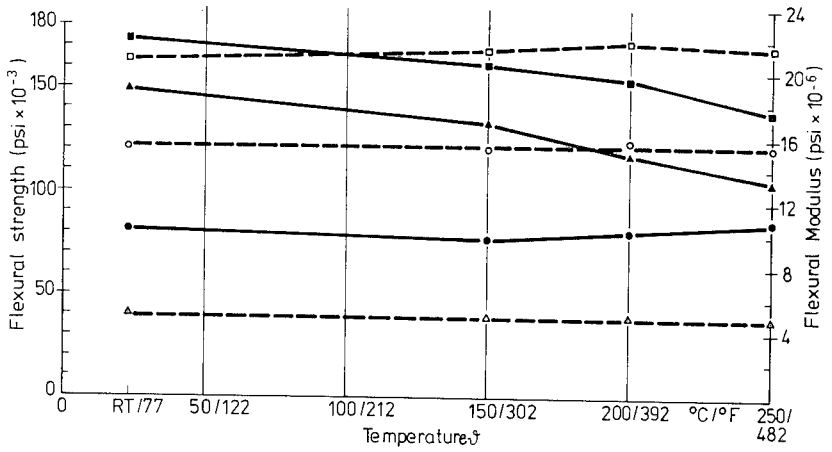

FIG. 2. Flexural strength and modulus of uni-H 353-Laminates. Flexural strength: ■, Modmor II S (HS), 56 v/o; ●, Modmor I (HM), 39 v/o; and ▲, E-Glass, 52.3 v/o. Flexural Modulus: □, Modmor II s (HS), 56 v/o; ○, Modmor I (HM), 39 v/o; △, E-Glass, 52. 3 v/o.

Laminate Preparation

Unidirectional H 353 laminates for the determination of mechanical properties including flexural, shear, and impact strength and also the long-term creep behavior under high stress levels were fabricated using the intended filament winding process. The impregnation bath was heated by oil to 125°C to keep the resin liquid during the filament winding process. The preimpregnated fibers were wound over a card winder which was formed as a positive open end mould. The card winder was heted to 150°C to keep the resin liquid during the lay-up of the fibers. The mould was closed by steel platens to squeeze off the excess resin and to get an uniform thickness of the flat panels. Curing was done at 210°C for four hours and postcured for 15 hours at 220°C, and then cut to the desired dimensions. The thickness of the laminates were 3 mm for the flexural samples and 4 mm for the shear and impact specimens.

MECHANICAL PROPERTIES

The mechanical properties of unidirectional laminates made from carbon and glass fibers are given in Tables III, IV, and V. Table III gives the flexural strength and modulus of uni-H 353 laminates determined at RT, 150, 200, and 250°C. The values were determined in 3-point bending using a span to depth ratio of 33:1, indicating a high property retention at 250°C when compared with the room temperature values. The loss of flexural strength at 250°C is about 30% for glass-fiber laminates and only 18% for the Modmor II S-laminates. The modulus change for Modmor I and glass can be negligated while the modulus values for Modmor II S-laminates

TABLE III

Flexural Properties of H 353 Uni-laminates

Fiber	Fiber loading v/o	Temperature °C/°F	Flexural strength[a] psi 10^{-3}	Retention %	Flexural Modulus psi 10^{-6}	Retention %
Modmor I (HM)	39.5	RT/ 77	79.5	100	15.7	100
		150 /302	75.6	95.1	15.1	96.2
		200 /392	80.5	101	15.5	98.7
		250 /482	85.6	107.5	15.3	97.5
Modmor II s (HS)	56	RT/ 77	173.1	100	19.0	100
		100 /302	162.5	94	21.60	113.7
		200 /392	155.6	90	22.15	116.5
		250 /482	142.2	82.2	21.85	115.0
E-Glass	52.3	RT/ 77	149.3	100	5.19	100
		180 /300	139.4	93.4	5.12	98.6
		200 /392	119.6	80.4	5.23	100.7
		250 /482	104.0	70.0	4.94	95.2

[a] Three point bending: Span to depth ratio 33:1.

TABLE IV

Shear Properties of H 353 Uni-laminates

Fiber	Fiber loading v/o	Shear strength[a] psi RT/77°F	150°C/302°F	200°C/392°F	250°C/482°F
Modmor I (HM)	39.5	4280[b]	4300[b]	4100[b]	4250[b]
Modmor II s (HS)	56.0	10650	7970	6980	6690
E-Glass - K43 (Aminosilan finish)	52.3	9880	7110	6400	5830
E-Glass - S 22/558 (Methacrylsilan)	66.0	11030	9600	7460	6960

[a] Short beam shear: span to depth ratio 5:1.
[b] Scissors shear test.

TABLE V

Impact Properties of H 353 Unilaminates.

Fiber	Fiber loading v/o	Impact resistance[a] (lb. ft /inch^2) RT/77°F	150°C/302°F	200°C/392°F	250°C/482°F
Modmor I (HM)	54.5	11.85	11.20	11.00	9.91
Modmor II s (HS)	54.4	35.40	42.20	44.15	42.20
E-Glass (S 22/558)	59.0	112.1	98.3	92.7	92.7

[a] Unnotched specimen DIN 53453 (sample size No. 2).

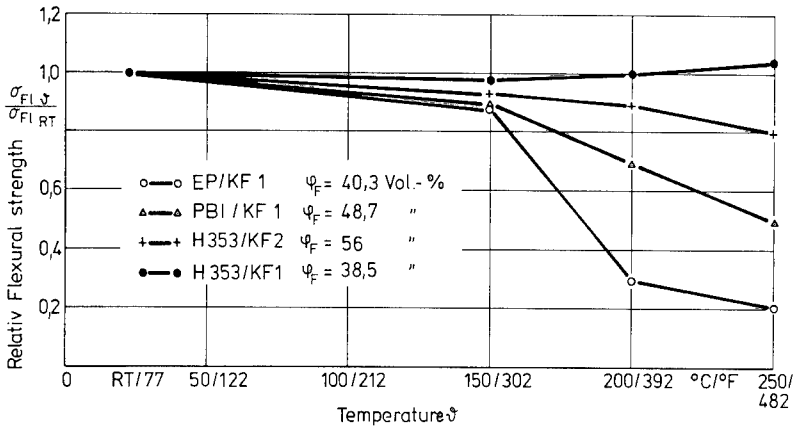

FIG. 3. Relative flexural strength $\delta_{FL\theta}$ /δ_{FL} RT of uni-Carbon fiber laminates: O, Rütapox 0302/Modmor I is 40.3 vol.; Δ, Kermid 601/Modmor I is 48.7 vol%; +, H 353/Modmor IIs is 56.0 vol%; and ●, H 353/Modmor I is 38.5 vol%.

increase with increase of temperature. For comparison, Figure 3 gives the relative flexural strength ($\delta_{FL\theta}/\delta_{FL_{KT}}$) for carbon fiber laminates with different resin systems (Kerimid 601, Rütapox 0302). As can be seen, the H 353 laminates show the best property retention up to 250°C for the three resin types taken into consideration.

In Table IV are listed the shear values for H 353 uni-laminates. The shear strength was determined using laminates having a thickness of 4 mm at a span to depth ratio of 5. Only the values for Modmor I (HM) with the

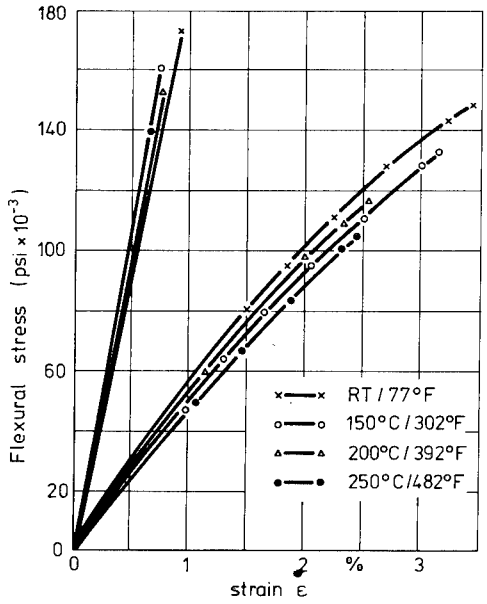

FIG. 4. Stress–strain curves of uni-H 353-laminates: —Modmor IIs is 56 vol.%; - -E-Glass is 52 vol.%.

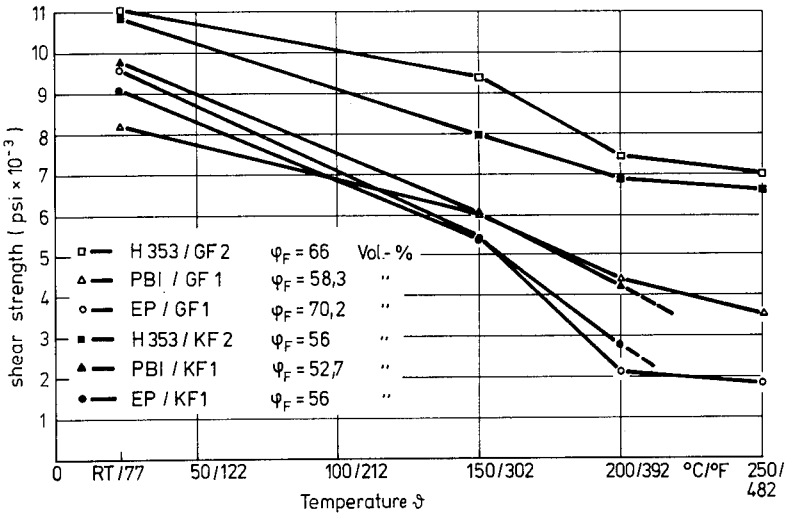

FIG. 5. Shear strength of uni-Carbon and glass fiber laminates. GF is glass fiber; KF1 is Modmor I; KF2 is Modmor IIs; EP is Rütapox 0.302; and PBI is Kerimid 601.

low fiber loading of 39.5% were determined by the scissors shear test because these samples did not lead to a real shear failure when tested using the short beam shear test. It can be seen from the values for the glass fiber laminates that the shear strength is influenced by the fiber sizing. The S 22/558 (Methacrylsilane) finish gives higher values than the Aminosilane (K 43) sizing. Very high shear values are also possible using Modmor II S. The property loss up to 250°C is about 35% compared to the room temperature value. The comparative values for Kerimid 601 and Rütapox can be taken from Figure 5.

In Table V are listed the impact values for unnotched H 353 unilaminates according to DIN 53453. These values and the comparitive values for Kerimid 601 and Rütapox 0302 which can be taken from Figure 6 indicate that the impact strength is merely influenced by the fiber type.

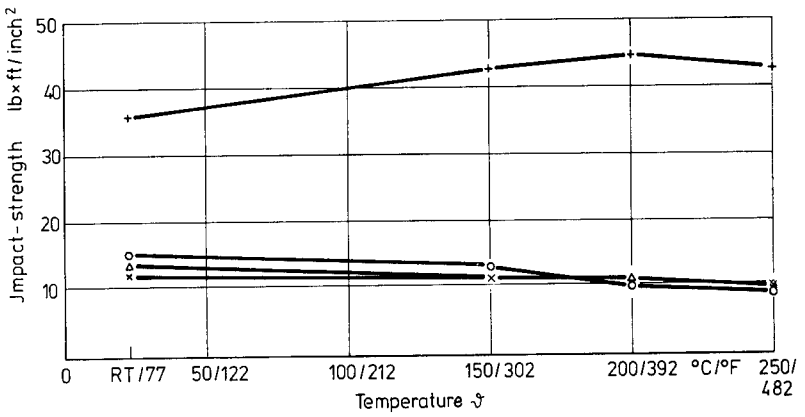

FIG. 6. Impact-strength of uni-Carbon fiber laminates: +, H 353/Modmor IIs is 54.4 vol.%; ×, H 353/Modmor I is 54.5 vol.%; Δ, Kerimid 601/Modmor I is 52.0 vol.%; and O, Rütapox/Modmor I is 49.0 vol.%.

Modmor I laminates for all three resin types give nearly the same values up to 250°C. They are low compared with Modmor II S and glass but this comes about as a consequence of the brittleness of the high modulus fiber. Modmor II S gives higher impact values according to the lower fiber modulus and the higher elongation to break. The impact values of glass fiber laminates are much higher, but Figure 6 shows that only a little property loss up to 250°C for the H 353 laminates exist.

CREEP RESISTANCE OF UNI-H 353-CARBON FIBER LAMINATES

For the determination of the application temperature of H 353 laminates under high stress levels in air, the flexural creep curves were investigated. To get maximum resin dependence, laminates with a low fiber loading (39 V/O) were tested (H 353/Modmor I laminates, ultimate flexural strength 80.000 psi). Figure 8 represents the creep curves at room temperature and 200°C. Figure 8 indicates that at room temperature no creep of the laminate occurs at high stress levels (50 and 60% ultimate). At 200°C, only a small increase of the fiber strain of the outermost extended layer was found. Flexural samples tested after a 1000 hours heat exposure at 200°C under a flexural stress of 60 o/o of the ultimate effected no change in flexural properties. At 250°C (Figure 9) in air the laminates showed an increased creep after 300 hours at stress levels of 20, 30, and 40% of ultimate, while under higher stress levels (50, 60% of ultimate) this increased creep occured after 100 hours. The figures showed that the carbon fiber laminates made of H 353 can be used at high stress levels and temperatures up to 250°C.

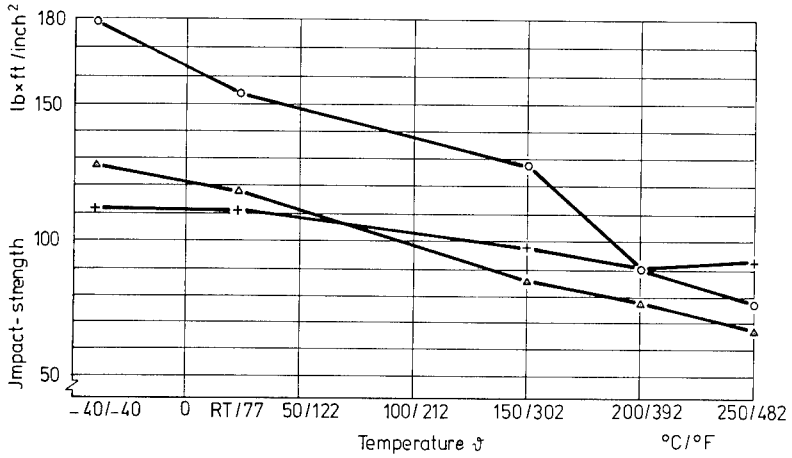

FIG. 7. Impact strength of uni-Glass-fiber laminates: O, Rütapox/E-Glass is 70.0 vol.%; Δ, Kerimid 601/E-Glass is 60.5 vol.%; +, H 353/E-Glass is 59.0 vol.%.

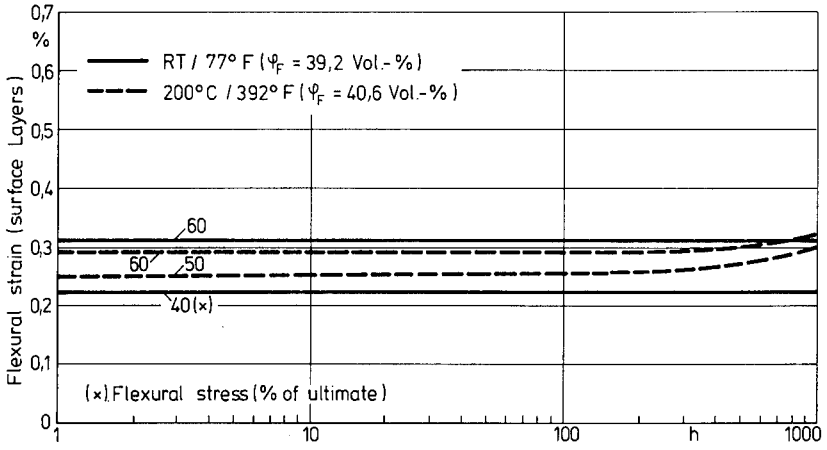

FIG. 8. Flexural creep-curves of uni-H 353/Modmor I (39.2–40.6 vol.%)-laminates at room-temperature and 200°C.

SUMMARY

The experimental low melting bismaleimide resin system (H 353) can be used for the fabrication of high performance filamentary wound high temperature composites as was shown by the properties of unidirectional laminates up to 250°C. The tensile properties are under investigation, also laminate with PRD–49 III are in test. The advantage of the resin system lies in the easy processability. It is usable not only for filament winding but also for prepreging and pulltrusion operations.

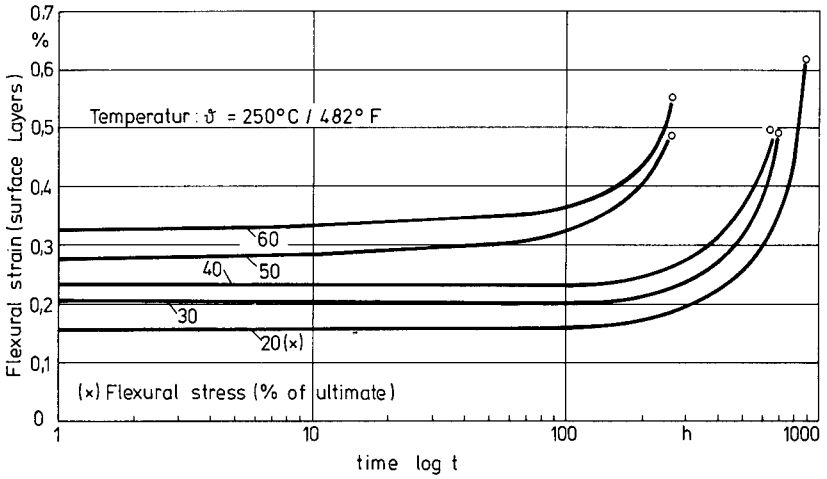

FIG. 9. Flexural creep-curves of uni-H 353/Modmor I (39.2–40.6%)-laminates at 250°C.

This development was made under a development contract sponsered by the German Ministry of Science. We also thank Mr. A. v. Harnier (IKV-Aachen) for the determination of laminate properties.

REFERENCES

[1] Y. R. Elliot, Ed., *Macromolecular Syntheses*, Vol. 2, John Wiley Sons, Inc., 1966, P. 111.
[2] USP 3 127 414 (March 31, 1964).
[3] K. E. J. Barrett *J. Appl. Polym. Sci., 11*, 1617 (1970).

A REVIEW OF PROCESSABLE HIGH TEMPERATURE RESISTANT ADDITION-TYPE LAMINATING RESINS

TITO T. SERAFINI and PETER DELVIGS

Lewis Research Center,
National Aeronautics and Space Administration,
Cleveland, Ohio 44135

SYNOPSIS

An important finding that resulted from research that was conducted to develop improved ablative resins was the discovery of a novel approach to synthesize processable high temperature resistant polymers. Low molecular weight polyimide prepolymers end-capped with norbornene groups were polymerized into thermo-oxidatively stable modified polyimides without the evolution of void producing volatile materials.

This paper reviews basic studies that were performed using model compounds to elucidate the polymerization mechanism of the so-called addition-type polyimides. The fabrication and properties of polyimide/graphite fiber composites using A-type polyimide prepolymer as the matrix are described. An alternate method for preparing processable A-type polyimides by means of in situ polymerization of monomeric reactants on the fiber reinforcement is also described. Polyimide/graphite fiber composite performance at elevated temperatures is presented for A-type polyimides.

INTRODUCTION

In order to synthesize polymers capable of withstanding temperatures of about 600°F for extended periods of time, it is necessary to incorporate thermo-oxidatively stable aromatic and/or heterocyclic structural units in the polymer molecular structure. Until recently, all thermally stable polymers were synthesized by condensation reactions. These polymers can be referred to as C-type polymers. There are a number of disadvantages associated with the use of C-type polymers as matrix resins for fiber reinforced composites. The primary disadvantage is conversion of the polymer into an intractable state prior to the complete elimination of void-producing volatile materials.

Under NASA sponsorship, TRW, Inc. developed an approach to prepare processable thermally stable polyimides, known as A-type polyimides, which cure by an addition reaction [1]. This approach utilizes low molecular weight amide-acid prepolymers end capped with reactive

Applied Polymer Symposium No. 22, 89–100 (1973)

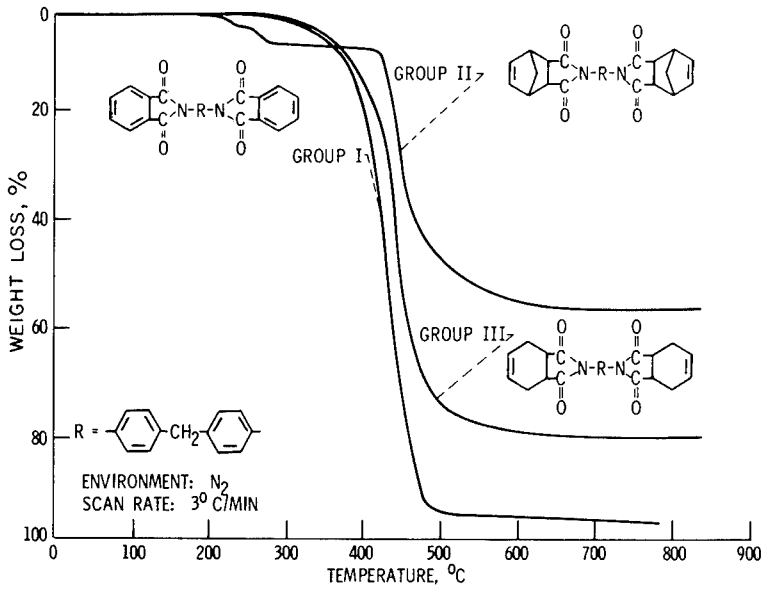

FIG. 1. Thermograms of model bisimides [1].

norbornene rings that polymerize into thermo-oxidatively stable polyimides without evolution of by-products. A method was developed in our laboratory to fabricate A-type polyimide/fiber composites using a technique of in-situ polymerization of monomers [2].

This report reviews composites fabrication and characterization studies that were conducted using the prepolymer or in situ polymerized A-type polyimides.

AMIDE-ACID PREPOLYMER

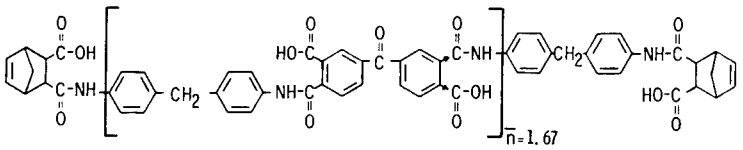

IMIDIZED PREPOLYMER

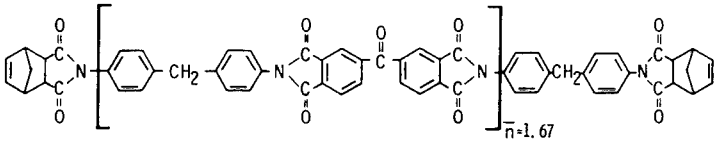

FIG. 2. P13N prepolymers.

DISCUSSION

Studies performed under NASA sponsorship to develop improved ablative resins were reported by Burns et al. [1]. These investigators concluded that the polymers best able to withstand the combustion environment of fluorine containing propellants were polymers whose molecular structure contained a multiplicity of aromatic groups. Their studies with model compounds such as those shown in Figure 1 to determine the temperatures required for thermally induced aromatization led to the discovery of what are known today as addition-type (A-type) polyimides. It can be seen in Figure 1 that the Group II bis-imide capped with the partially unsaturated bridged structure gave a higher weight retention than either Group 1 (completely aromatic) or Group III (partially unsaturated) model compounds. The inflections in the thermogravimetric analysis (TGA) curve between 200° and 300°C for the Group II model compounds, compared to the smooth curves for model compounds in Groups I and III, led them to conclude that macromolecules were formed during the heating of the Group II model compounds. They referred to the polymerization process as pyrolytic polymerization. They immediately realized the significance of this finding and their continued research culminated in the development of the A-type polyimide known as P13N. This processable polyimide met with considerable acceptance by the plastics industry. The structures of the amide-acid and imidized prepolymers of P13N are shown in Figure 2. P13N is available from the Ciba-Geigy Corporation which acquired license to the material from TRW, Inc.

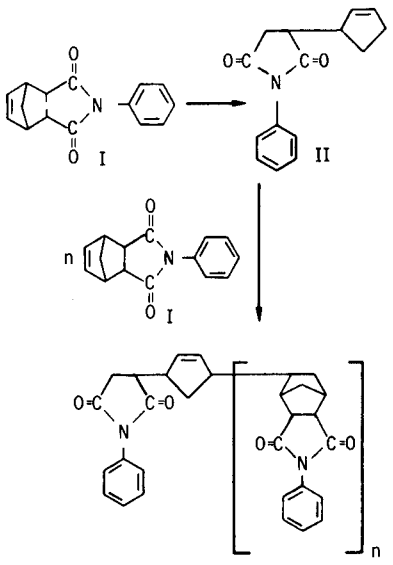

FIG. 3. Pyrolytic polymerization reaction mechanism [4].

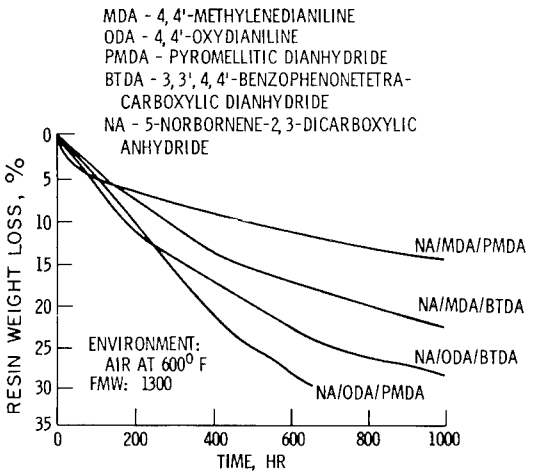

FIG. 4. Weight loss of A-type polyimides [3].

Under subsequent NASA sponsored programs [3, 4], studies were performed to develop A-type polyimides having improved thermo-oxidative stability (TOS) at 600°F for use as laminating resins. Some studies were also performed during these programs to elucidate the mechanisms of the reactions leading to the formation of macromolecules. Pyrolysis studies were conducted with the model compound I, N-phenyl-5-norbornene-2,3-dicarboximide (Fig. 3) under vacuum, pressure or pressure/catalyst environments. It was concluded that essentially the same polymer structure results from pyrolysis in any of the environments [4]. It should be pointed out that low molecular weight oligomers instead of high molecular weight polymer resulted from the pyrolysis of the model compound. The postulated reaction mechanism is shown in Figure 3. The first step involves a reverse Diels-Alder reaction which leads to the formation of cyclopentadiene and N-phenylmaleimide, which immediately co-react to form adduct II. It was further postulated that the adduct initiates homopolymerization of the norbornene species I. The various environments only seem to affect the degree of polymerization. TGA analysis of residues produced at pyrolysis temperatures in the range of 271° to 350°C indicated the optimum pyrolytic polymerization temperature to be 316°C.

Figure 4 shows the results from isothermal-gravimetric analysis (ITGA) in air at 600°F of various A-type polyimides [3]. The label given on each curve identifies the reactants that were used to synthesize prepolymers which were subsequently cured to cross-linked polyimides. The stoichiometry of the reactants was selected to prepare prepolymers having an average formulated molecular weight (FMW) of 1300. It is clear from the results presented in Figure 4 that the use of ODA with either BTDA or PMDA resulted in A-type polyimides exhibiting lower TOS than the use of MDA. The most significant finding was that the polymers made from

NA/MDA/PMDA prepolymer exhibited higher TOS than any of the other A-type polyimides including P13N (curve labeled NA/MDA/BTDA in Fig. 4).

Composite fabrication studies with the NA/MDA/PMDA prepolymers showed that it was necessary to adjust the stoichiometry of the reactants to yield prepolymers having an average FMW of 1000. This prepolymer became known as P10P. The reduction in the FMW was necessary for adequate resin flow. Properties of composites made from the P10P prepolymer and Hercules HTS graphite fibers are shown in Figure 5 as a function of exposure time in air at 500° and 600°F [5]. The mechanical property results presented in Figure 5 clearly show excellent retention of properties at 500°F for 1000 hours. In contrast, at 600°F after 600 hours of exposure the composites retained approximately 30% of their room temperature values. It was suggested [5] that some of the composite property degradation at 600°F could be attributed to oxidative degradation of the HTS graphite fiber.

Another approach to prepare A-type polyimides was developed in our laboratories [2]. Our approach eliminates the need for prepolymer synthesis and circumvents some of the shortcomings of A-type amide–acid prepolymers. The method involves the use of ester–acids rather than anhydrides, thereby preventing the formation of prepolymers at room temperature. A solution containing a diamine and the ester–acids is used to impregnate the reinforcing fibers. In situ polymerization of the monomer reactants (PMR) occurs upon heating the impregnated fibers. Figure 6 shows the structures of the various ester–acids used in the study reported in Reference 2. Figure 7 shows the variation of solution viscosity with time for

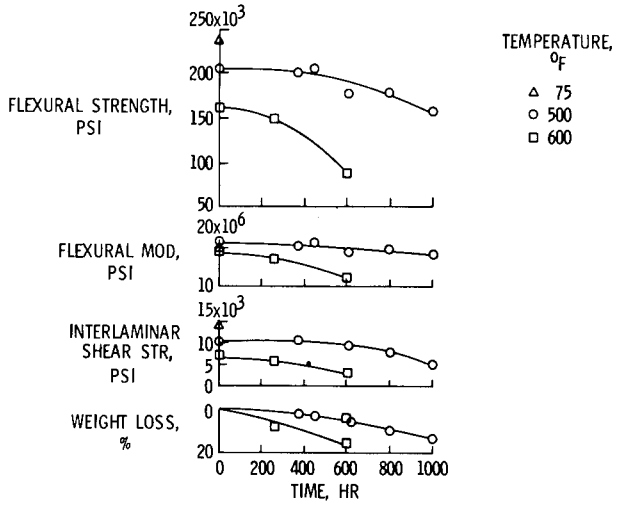

FIG. 5. Properties of HTS/P10P composites as function of time at temperature [5].

STRUCTURE	NAME	ABBREVIATION
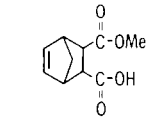	MONOMETHYL ESTER OF 5-NORBORNENE-2, 3-DICARBOXYLIC ACID	NE
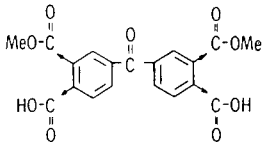	DIMETHYL ESTER OF 3, 3', 4, 4'-BENZOPHENONETETRACARBOXYLIC ACID	BTDE
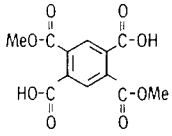	2, 5-DICARBOMETHOXYTEREPHTHALIC ACID	PMDE

FIG. 6. Structures of ester-acids.

monomer and prepolymer solutions. Monomer solution A referred to in Figure 7 has the same stoichiometry as the amide–acid prepolymer P10P. Figure 7 shows the following: (1) monomer solutions exhibit considerably less viscosity variation than prepolymer solutions and (2) monomer solutions have a much lower viscosity. Their lower viscosity enhances fiber wetting and also permits the use of solutions having higher solids contents. In contrast to amide–acid prepolymers which require the use of high boiling aprotic solvents, such as N,N-dimethylformamide, low boiling alcohols, e.g., methanol, can be used as solvents for monomer solutions.

The variation of composite interlaminar shear strength with exposure time in air at 600°F for HTS graphite composites made from either a

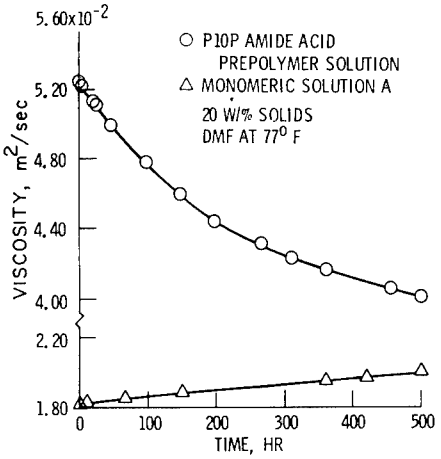

FIG. 7. Viscosity changes of P10P amide acid and monomeric solution A [2].

monomer or prepolymer solution is shown in Figure 8. It can be seen that the interlaminar shear strength retention of the PMR/HTS fiber composites was essentially identical to the interlaminar shear strength retention of the P10P/HTS fiber composites. Comparison of other properties, such as flexural strength, served to establish the utility of the PMR approach. In fact, a composite made from a NE/MDA/BTDE solution in which the stoichiometry had been selected to yield a prepolymer having an average FMW of 1500 exhibited 9.5% weight loss after 600 hours in air at 600°F [2]. Under identical conditions a P10P/HTS composite lost approximately 18%.

Studies conducted to establish the validity of the aforesaid finding and to improve the TOS of PMR A-type polyimides are reported in Reference 6. In the earlier work using the PMR approach the diamines used in the prepreg solutions were either MDA or TDA [2]. Six additional diamines were used in a composite screening study reported in Reference 6. Their structures are shown in Figure 9.

The chemical composition and some properties of 11 various 1/2 by 2-1/2 inch composites are summarized in Table I. The stoichiometry of the reactants was governed by the desired number of imide rings or by the desired percentage of alicyclic content. FMW is considered to be the average molecular weight of the imidized prepolymer that could have been formed if amide-acid prepolymers had been synthesized. For any given monomer combination, the molar ratio of 5-norbornene-2, 3-dicarboxylic acid monomethyl ester/diamine/tetracarboxylic acid dimethyl ester was $2/(n + 1)/n$. The composite processing conditions used throughout this investigation were essentially those which had been optimized for amide acid prepolymer solutions [3].

Samples 1 to 5 are chemically similar to the commercially available P13N resin. All of them, however, have a lower alicyclic content than P13N. Samples 1 to 3 possessed a combination of unusually high ther-

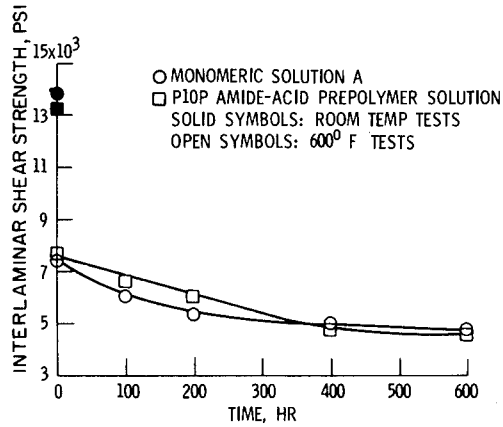

FIG. 8. Interlaminar shear strength of polyimide/HTS graphite fiber composites [2].

STRUCTURE	NAME	ABBREVIATIONS
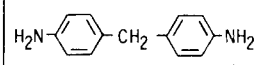	4, 4'-METHYLENEDIANILINE	MDA
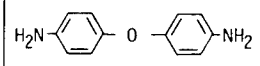	4, 4'-OXYDIANILINE	ODA
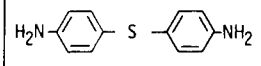	4, 4'-THIODIANILINE	TDA
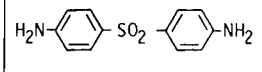	4, 4'-SULFONYLDIANILINE	SDA
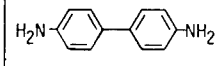	BENZIDINE	BZD
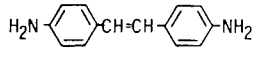	4, 4'-DIAMINOSTILBENE	DAS
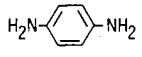	p-PHENYLENEDIAMINE	PPDA
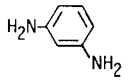	m-PHENYLENEDIAMINE	MPDA

FIG. 9. Structures of diamines.

TABLE I
Properties of Polyimide/HTS Graphite Fiber Composites

Sample number	Monomeric solution composition	n	FMW	Laminate properties: Interlaminar shear (75° F), ksi	Laminate properties: Interlaminar shear (600° F), ksi	Composite weight loss, percent[a]
1	NE/MDA/BTDE	2.087	1500	15.3	6.0	9.5
2		2.603	1750	14.4	5.5	9.8
3		2.913	1900	15.0	5.1	10.0
4		3.120	2000	9.8	4.6	11.4
5		5.186	3000	8.2	5.1	28.0
6	NE/MDA/PMDE	1.342	1000	10.8	6.2	17.6
7	NE/MDA/PMDE	1.868	1200	12.3	6.2	17.9
8	NE/MDA/PMDE	2.658	1500	6.1	2.9	20.8
9	NE/MDA/(1BTDE:1PMDE)	2.338	1500	14.3	6.2	10.6
10	NE/MDA/(1BTDE:1PMDE)	2.917	1750	13.6	5.5	8.6
11	NE/MDA/(1BTDE:1PMDE)	3.264	1900	12.6	4.5	10.9

[a] After 600 hr in air at 600°F.

mooxidative stability and high initial interlaminar shear at room temperature. The results from a more detailed study of their mechanical properties after exposure at 600°F will be described later.

Sample 6 has a composition equivalent to that of P10P prepolymer. Its properties were shown to be virtually identical with those of composites made from P10P. Samples 7 and 8 have the same chemical composition as sample 6, but differ in stoichiometry.

The monomer combination used in samples 9 to 11 was selected to investigate the effect of increasing the number of imide linkages over that in the corresponding samples 1 to 3 while maintaining a constant alicyclic content. For example, sample 9 has the same alicyclic content as sample 1, but a higher number of imide linkages. The higher number of imide linkages is achieved by partial substitution of PMDE for BTDE. Theoretically this should give a correspondingly higher thermooxidative stability. Actually, the results indicate that the thermooxidative stability of samples 9 to 11 is approximately equivalent to that of samples 1 to 3.

Results from the screening study with diamines other than MDA showed that the incorporation of these diamines did not improve composite properties. In some instances, for example with PPDA, BZD and DAS, the composites were poorly consolidated and could not be tested.

Based on the results of the screening study and detailed investigation of samples 1 to 3, 7 and 9 the monomer system which displayed the best overall balance of processability and thermo-mechanical properties was NE/MDA/BTDE in which n has a value of 2.087 (sample 1, FMW = 1500). Some results of the studies conducted with monomer systems having FMW's of 1500, 1750, 1900 and 1000 (samples 1, 2, 3 and 6, Table I) are presented in Figure 10. The range of interlaminar shear strength values is 13800 to 17800 psi. These values are somewhat higher than those previously reported [5] for A-type polyimide/HTS fiber composites. There is a considerable drop in the interlaminar shear strength when the composites are tested at 600°F, to as low as 5000 psi. There was a greater decrease for

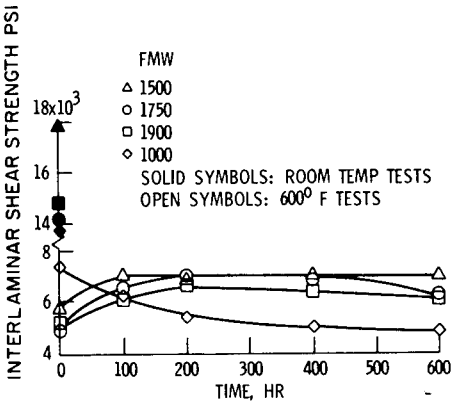

FIG. 10. Interlaminar shear strength of polyimide/HTS graphite fiber composites [6].

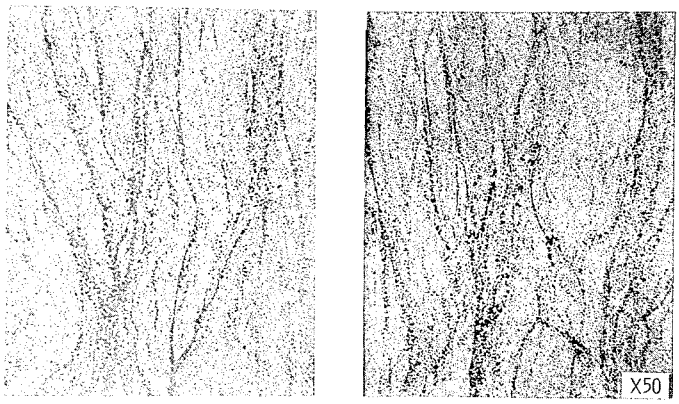

FIG. 11. Polyimide/HTS graphite fiber composites before and after exposure in air at 600°F for 600 hours [6].

samples 1 to 3 for sample 6. The inerlaminar shear strength decrease for sample 6 is nearly identical to that reported by Hanson and Serafini [6].

It appears that composite samples 1 to 3 underwent a postcure on exposure in air at 600°F, since the interlaminar shear stregnth increased during exposure, whereas that of sample 6 decreased with time. The important fact to note is that the interlaminar shear strength of samples 1 to 3 remained nearly constant from 100 to 600 hours. The strength after 600 hours for samples 1 to 3 averaged approximately 6500 psi. The data for samples 1 to 3 represent the best interlaminar shear retention for A-type polyimide/HTS fiber composites reported to date. The interlaminar shear strength of sample 1 increased to 7000 psi after 200 hours of exposure and remained constant up to 600 hours of exposure.

Photomicrographs of a cross section of composite sample 1, before and

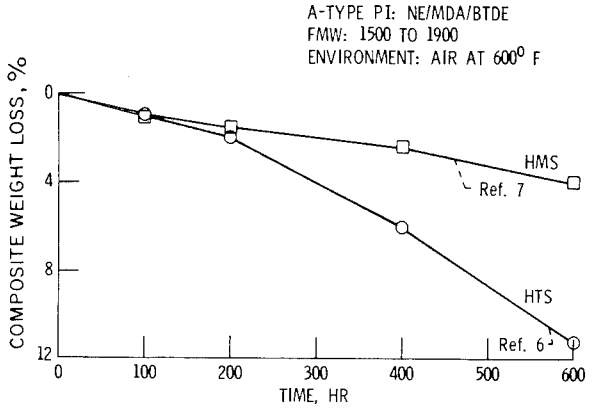

FIG. 12. Weight loss of A-type polyimide/graphite fiber composites.

after exposure, are shown in Figure 11. There is no evidence of voids in the composite as a result of fabrication. After exposure at 600°F for 600 hours, the composite shows an extremely small number of voids. This indicates that the original void-free composite was very resistant to oxidative degradation that might occur by a diffusion mechanism. Any degradation that did occur, took place on the surface of the composite. The absence of internal voids after exposure also indicates that the composite is very resistant to thermal decomposition.

Under NASA sponsorship, TRW, Inc. is using the PMR approach to develop high temperature resistant polyimide/graphite fiber air breathing engine components, such as blades and vanes. The monomer system being investigated is NE/MDA/BTDE at FMW's in the range of 1500 to 1900. Figure 12 shows the average weight loss of HMS graphite fiber composites exposed at 600°F in air [7]. Also shown on the figure is the weight loss of composites fabricated with HTS fiber [6]. It can be seen that the HMS composites exhibited excellent weight retention (~96%). The greater weight loss of the HTS composite can be attributed to the lower thermo-oxidative stability of the HTS fiber [5]. The point that can be made is that the investigators of Reference 7 were able to fabricate thermo-oxidatively stable composites using the in situ PMR approach with little or no difficulty. Figure 13 is a flow chart of the PMR approach for the fabrication of high performance resin/fiber composites. We have been able to use the PMR approach for the fabrication of polyphenylquinoxaline/graphite fiber composites. These studies will be described in a forthcoming publication. The PMR approach as outlined in Figure 13 is considerably less complex than composites fabrication processes which utilize conventional prepreg fabrication techniques. In addition to the advantages discussed previously, such as low viscosity, high solids content solutions etc., the PMR approach eliminates the problems associated with packaging, shipping and storage of prepreg. The PMR approach also should ultimately lead to overall cost savings.

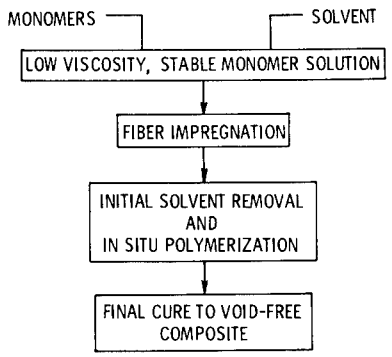

FIG. 13. Approach for preparation of resin/fiber composites using in situ polymerization of monomer reactants.

We view the PMR approach as an approach which should permit the utilization of a number of polymers which have demonstrated outstanding high temperature TOS but could not be used as matrix resins because of the intractability inherent in their polymer structure.

CONCLUSIONS

Modification of the molecular structure of aromatic polyimide precursors by incorporating norbornene end groups is an excellent approach to achieve processable thermally stable polyimides for use as matrix resins in fiber reinforced composites. Preparation of A-type polyimide/fiber composites using a technique of in situ polymerization is a powerful approach which should be applicable to a variety of high-temperature polymers. The in situ polymerization approach offers a number of advantages to the composites fabricator, such as the use of low boiling, nontoxic solvents, and simplified materials handling logistics.

REFERENCES

[1] E. A. Burns, H. R. Lubowitz, and J. F. Jones, "Investigation of Resin Systems for Improved Ablative Materials", TRW-05937-6019-RO-00, NASA CR-72460, TRW Systems Group, October 1968.

[2] T. T. Serafini, P. Delvigs, and G. R. Lightsey, *J. Appl. Polym. Sci. 16*, 905 (1972).

[3] E. A. Burns, R. D. Jones, R. W. Vaughan, and W. P. Kendrick, "Thermally Stable Laminating Resins", TRW-11926-6013-RO-00, NASA CR-72633, TRW Systems Group, January 1970.

[4] R. J. Jones, R. W. Vaughan, and E. A. Burns, "Thermally Stable Laminating Resins", TRW-16402-6012-RO-00, NASA CR-72984, TRW Systems Group, February 1972.

[5] M. P. Hanson and T. T. Serafini, "Effects of Thermal and Environmental Exposure on the Mechanical Properties of Graphite/Polyimide Composites", NASA TN D-6604, December 1971.

[6] P. Delvigs, T. T. Serafini, and G. R. Lightsey, "Addition-Type Polyimides from Solutions of Monomeric Reactants", NASA TN D-6877, August 1972.

[7] Unpublished results from NASA Contract NAS 3-15829.

ADAMANTANE EPOXIES—THEIR SYNTHESIS AND VISCOELASTIC BEHAVIOR

GEORGE F. PEZDIRTZ

NASA-Langley Research Center,
Hampton, Virginia 23365

and

VINCENZO GUIDOTTI

Montecatini Edison, S.p.A.,
Milan, Italy

SYNOPSIS

Interest in the chemistry of adamantane and its derivatives [1, 2] has continued to increase with the increasing availability of these compounds from petroleum feed stocks. In recent years adamantane and biadamantane derivatives have been used in the synthesis of a variety of polymers including polyamides [3, 4], polyethers and polyesters [4], epoxy novolacs and polycarbonates [5].

This paper is concerned with the effect of structure of three epoxies on their thermomechanical and thermoxidative properties. The three structures differ in the central portion of the bis-phenol moiety of the epoxy by substituting (1) adamantane, and (2) biadamantane, for (3) the isopropylidene group (Epon 828).

Torsional Braid Analysis [6–22] was used to study the thermomechanical behavior and curing conditions of the resins. The diglycidyl ethers were synthesized from epichlorohydrin and adamantane, biadamantane, or isopropylidene bis-phenols [5]. The epoxy equivalent for the adamantane derivative (ABD) was 238 (theory 219); however, the biadamantane derivative (BABD) had a much higher value of 694 versus 283 from theory. The high value may be due to the longer reaction time and poor solubility of the biadamantane diphenol [5]. The diglycidyl ether of bis-phenol A (Epon 828) had an epoxy equivalent of 185–192 as obtained from Shell Chemical Co.

Curing conditions were determined by observing the response of the relative rigidity of the resin during Torsional Braid Analysis (TBA) under isothermal conditions in nitrogen. For all resins, solvent removal and initial reactions were carried out by heating the resin deposited on the glass braid for 1 hour at 120°C and 2 hours at 150°C. The Epon 828 was post-cured at 165°C and the relative rigidity increased asymptotically to a limiting value after 13 hours at temperature, at which time curing was considered complete. Under identical conditions the ABD resin did not show a leveling of its relative rigidity which, instead, continued to increase for more than 20 hours of heating. When the post-curing temperature was raised to 200°C the ABD resin's relative rigidity did reach a limiting value, i.e., curing was complete. The BABD resin required a curing temperature of 250°C for the relative rigidity to reach its limiting value in 18 hours. Completion of post-cure was further evidenced by the disappearance of the infrared band of the epoxy group at 10.9 microns.

Applied Polymer Symposium No. 22, 101–102 (1973)

The maximum damping index for the cured resins were: 180°C for the Epon 828, 220°C for the ABD resin, and 230°C for the BABD resin. This increase in the maximum damping index is considered to be due to the increased chain rigidity which results from the increased rigidity of the adamantane groups over that of the isopropylidene groups.

Thermogravimetric analysis of the three resins was also studied with the result that the two resins based on adamantane and biadamantane gave a higher percent char yield at 400°C than the Epon 828. The initial break in the TGA curves for the ABD occurred at about 390°C in air compared to about 340°C for the Epon 828.

REFERENCES

[1] R. C. Fort and P. R. Schleyer, *Chem. Rev., 64*, 277 (1964).
[2] V. V. Sevost'yanova, M. M. Krayushkin, and A. G. Yurchenko, *Russ. Chem. Rev., 39*, 817 (1970).
[3] Sun Oil Co., Italian Pat. 823,540 (1968).
[4] Du Pont de Nemours, U.S. Pat. 3,342,880 (1967).
[5] B. J. Burreson and H. H. Levine, *J. Polym. Sci.*, Chem. Ed., *11*, 215 (1973).
[6] J. K. Gillham and A. F. Lewis, *Nature, 195*, 1199 (1962).
[7] A. F. Lewis and J. K. Gillham, *J. Appl. Polym. Sci., 6*, 422 (1962).
[8] J. K. Gillham, *Science, 139*, 494 (1963).
[9] J. K. Gillham and A. F. Lewis, Polym. Prepr., Amer. Chem. Soc., Div. Polym. Chem., 4, 531 (1963).
[10] A. F. Lewis and J. K. Gillham, *J. Appl. Polym. Sci., 7*, 685 (1963).
[11] J. K. Gillham and A. F. Lewis, *J. Appl. Polym. Sci., 7*, 2293 (1963).
[12] J. K. Gillham and A. F. Lewis, *J. Polym. Sci., C, 6*, 125 (1964).
[13] A. Adicoff and A. A. Yukelson, *J. Appl. Polym. Sci., 10*, 159 (1966).
[14] J. K. Gillham, *Appl. Polym., 2*, 45 (1966).
[15] J. K. Gillham and R. F. Schwenker, Jr., *Appl. Polym. Symp., 2*, 59 (1966).
[16] A. Adicoff and A. A. Yukelson, *J. Appl. Polym. Sci., 12*, 1959 (1968).
[17] J. K. Gillham and M. Roller, Paper presented at 29th Antec of SPE, Washington, D.C., May 10–13, 1971.
[18] R. E. Coulehan, Paper presented at 29th Antec of SPE, Washington, D.C., May 10–13, 1971.
[19] A. F. Lewis and G. J. Pietsch, Paper presented at 29th Antec of SPE, Washington, D.C., May 10–13, 1971.
[20] J. K. Gillham, Paper presented at 29th Antec of SPE, Washington, D. C., May 10–13, 1971.
[21] B. L. Williams, Paper presented at 29th Antec of SPE, Washintton, D.C., May 10–13, 1971.
[22] J. R. Martin and J. K. Gillham, Paper presented at 29th Antec of SPE, Washington, D.C., May 10–13, 1971.

HIGH-TEMPERATURE FLUOROSILICONE ELASTOMERS

OGDEN R. PIERCE and YUNG K. KIM

Advanced Research Department,
Dow Corning Corporation,
Midland, Michigan 48640

SYNOPSIS

The following types of fluorosilicone polymers are described in regard to their preparation and properties:

$$-(CF_3CH_2CH_2SiMeO)-_n \qquad -(ZCF_2CF_2CH_2CH_2SiMeO)-_n$$

$Z = Br, CCl_3$

$$-\left(\begin{matrix} R' \\ | \\ SiCH_2CH_2 \end{matrix}\overline{\mathcal{Z}}\begin{matrix} CH_2CH_2Si \\ | \\ R \end{matrix}\begin{matrix} R' \\ | \\ O \end{matrix}\right)-_n$$

$R = R' = CH_3, CF_3CH_2CH_2$

$\overline{\mathcal{Z}}$ = perfluoroalkylene, perfluoroalkylene Oxide

The polymer, $-(CF_3CH_2CH_2SiMeO)-_n$, exhibits good solvent resistance, thermal and oxidative stability, and is commercially available in the form of rubbers, sealants, and fluids. The other polymers are in the research stage. The halogen containing polymers, $-(ZCF_2CF_2CH_2CH_2SiMeO)-$, showed good fire-retardant properties, and the hybrid type, $\left(\begin{matrix} R' \\ | \\ SiCH_2CH_2ZCH_2CH_2Si \\ | \\ R \end{matrix}\begin{matrix} R' \\ | \\ O \end{matrix}\right)-_n$, has demonstrated much improved stability especially under confined heating conditions.

INTRODUCTION

The role of fluorine and the carbon–fluorine bond in achieving a high degree of solvent resistance and stability is well known in organic polymer systems. Only recently has the combination of these properties been demonstrated in silicone polymers by similar means, the incorporation of fluorine into polyalkylsiloxane systems. Before describing the preparation and properties of fluorosilicones, a brief consideration of pertinent structural factors is presented.

The first consideration is the choice of the carbon–fluorine bond rather than the silicon-fluorine bond. The latter, while of high thermal stability, is

Applied Polymer Symposium No. 22, 103–125 (1973)

subject to hydrolysis, thereby restricting its usefulness. The second consideration then becomes the location of the fluorine relative to silicon in the alkyl substituent. Due to the great electronegativity and strong inductive effect of fluorine, the position alpha to silicon, such as $CF_3Si\equiv$, suffers a major disadvantage, hydrolytic cleavage of the SiC bond. In addition, thermal rearrangement is possible with the formation of SiF bonds as:

$$CF_3Si\equiv \xrightarrow{\Delta} [CF_2] + n\,[SiF].$$

This appears to be similar to the alpha elimination mechanism proposed for one mode of carbene formation.

The position beta to silicone, CF_3CH_2Si, also suffers the same disadvantages, namely hydrolytic instability and easy thermal rearrangement. In the latter, the side chain is eliminated as an olefin.

$$CF_3CH_2Si\equiv \xrightarrow{\Delta} CF_2{=}CH_2 + [\equiv SiF]$$

Consequently, the gamma position, $CF_3CH_2CH_2$, was the obvious choice for maximum stability and ease of preparation. Of course, positions beyond gamma are also suitable, but another factor, oxidation of the CH bonds in the alkyl group, becomes the limiting factor. From these facts, the polymer chosen ititially was $[CF_3CH_2CH_2SiMeO]_n$, since it demonstrated excellent solvent resistance and stability.

More recently, the problem of reversion resistance of the poly(fluoroalkyl)siloxanes became crucial, and the hybrid fluorosilicone, derived from a combination of the $(CF_3CH_2CH_2)MeSiO$ unit and a fluorocarbon segment, both in the polymer backbone, was prepared to gain stability in confined heat applications. While only in the research stage, the hybrids exhibit outstanding solvent and reversion resistance from preliminary evaluation studies conducted in our laboratories.

For general reading in the field of synthetic organic fluorine chemistry and fluorosilicone polymers, References 1–5 are suggested.

POLY(TRIFLUOROPROPYL)METHYLSILOXANE

Monomer Preparation

The compound, $CF_3CH_2CH_2SiMeCl_2$, is the principal starting point for the fluorosilicone polymer system. This is prepared as follows:

$$CCl_3CH{=}CH_2$$
$$\text{cat.}\downarrow \text{HF}$$
$$CF_3CH{=}CH_2$$
$$\text{init.}\ \big|\ MeSiHCl_2$$
$$\downarrow$$
$$CF_3CH_2CH_2SiMeCl_2$$

The desired chlorosilane is purified by distillation and then converted to a cyclotrisiloxane as follows:

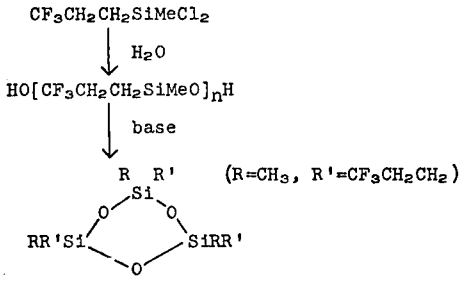

The cyclic siloxane is purified by distillation and serves as the monomer for polymer synthesis.

Polymer Preparation

Preparation of fluorosilicone polymers from the cyclic trimer is best accomplished by base catalysis at elevated temperatures. The system involves the equilibria as illustrated, cyclic trimer ⇄ polymer ⇄ cyclic tetramer, with the equilibrium position at about 90% cyclic tetramer. Consequently, the polymerization reaction must be stopped before equilibrium is reached as contrasted to most silicone examples. Careful control of the reaction time and temperature is essential for good yields of high purity polymer.

In general, the commercial production yields polymers of a DP of about 6000 which are suitable for most rubber applications. By the proper choice of conditions and the use of endblocking agents, lower molecular weight polymers can be made for sealant and fluid applications.

TABLE I

Physical Properties of Silastic® LS Rubber

Oven cured 8 hours at 200C (392F)	
Durometer Hardness, Shore A Scale	50 ± 5
Tensile Strength, psi	1250
Elongation, percent	500
Tear Strength, (Die B) pounds per inch	265
Tear Strength, (Die B) pounds per inch at 100C (212F)	165
Compression Set, percent	
after 22 hrs. at 150C (302F)	20
after 22 hrs. at 177C (350F)	35
Brittle Point, degrees	−66C (−87F)
Stiffening Temperature,[a] degrees	−55C (−67F)
Resistance to ASTM Reference Fuel B, after 70 hrs. at 25C (77F)	
Durometer Change, points	−10
Volume Change, percent	+22

[a] Temperature at which Young's Modulus reaches 10,000 psi.

TABLE II

Typical Oil and Fuel Resistance (Tested according to ASTM D 471)

	Immersion Conditions	Shore A Durometer Change, pts.	Percent Volume Change
ASTM No. 1 Oil	70 hr. at 150C (302F)	Nil	Nil
ASTM No. 3 Oil	70 hr. at 150C (302F)	Nil	+4
ASTM Reference Fuel B	70 hr. at 25C (77F)	−10	+22
Jet Fuel, Jp-4	70 hr. at 25C (77F)	−6	+10
MIL-H-5606 (Univis J-43)	70 hr. at 57C (135F)	−4	+8
MIL-L-7808 (Turbo Oil No. 15)	70 hr. at 150C (302F)	−12	+8
Di-2-ethylhexyl-sebacate with 0.5% phenothiozene	48 hr. at 150C (302F)	−7	+9

Properties of Fluorosilicone Rubber

The stock is prepared by combining a reinforcing filler, usually a silica, with a peroxide vulcanizing agent and various additives for heat stability. It may be readily processed by milling, calendering, extruding, or molding. Typical properties are listed in Table I. One of the outstanding features of fluorosilicones is their solvent resistance as shown in Table II.

The effect of oven aging at elevated temperatures is shown in Table III. Finally, thermogravimetric analysis of the catalyst-free, unvulcanized gum indicates the good thermal and oxidative stability of the polymer system (Table IV).

An interesting comparison can be made between fluorosilicone and fluorocarbon elastomers. Both materials exhibit exceptional resistance to fuels and solvents and both are capable of use over a wide temperature range. However, while fluorocarbon elastomers perform better at room temperature, the advantage is quickly lost under service conditions. A series of evaluations conducted in our laboratories demonstrate that at

TABLE III

Effects of Heat Aging

		Samples Aged for:		
Property	Control	70/100C (212F)	70/150C (302F)	70/200C (392F)
Durometer, Shore A	52	53	53	54
Tensile, psi	1250	1260	1260	1100
Elongation, percent	500	470	450	400
Tear, Die "B", ppi	265	260	210	175

TABLE IV

T.G.A. (10°C/min.) $(CF_3CH_2CH_2SiO)_n$ Gum
CH_3

Temperature (°C)		
10% Wt. Loss	25% Wt. Loss	50% Wt. Loss
385° (air)	405° (air)	415° (air)
415° (N_2)	430° (N_2)	445° (N_2)

temperature extremes the fluorosilicone rubber shows less property changes than the fluorocarbon elastomer. A summary of test results follows:

A hardness stability measurement was conducted using samples of 70 durometer at room temperature. Above room temperature the fluorosilicone retained most of its hardness while the fluorocarbon softened rapidly. Below room temperature the fluorocarbon rubber hardened rapidly while the fluorosilicone was much less effected (Figure 1). These results illustrate the greater flexibility of the polysiloxane polymer backbone as compared to the relatively stiff fluorocarbon polymer chain.

Figure 2 illustrates the fact that the tensile retention of Silastic® LS Rubber at elevated temperatures is superior to that of a fluorocarbon rubber. In addition, it can be seen from Figure 3 that the fluorosilicone rubber retains most of its tensile strength over a one year period at 392°F. At higher temperatures (450°F–500°F) the fluorocarbon elastomer is superior, which is most likely attributable to chain scission and depolymerization of the silicone.

One of the common drawbacks of silicone rubber is the relatively low tear strength, which is also true in the case of fluorocarbon elastomers. Silastic® LS Rubber, when specially compounded, can achieve superior tear strengths and retain much of this advantage as compared to a fluorocarbon (see Table V).

Tensile modulus, the unit load required to produce a particular elongation, is illustrated in Figure 4 as a function of temperature at 100% elongation. The fluorocarbon, while initially higher, loses much of its modulus as compared to the fluorosilicone. The steep slope of the curve indicates the

TABLE V

Tear Strength Stability

Tear Die B	Temperature °F		
	Room	300	400
Fluorocarbon (FC)	150	40	25
Fluorosilicone (FS)	100	35	20
Hi-Strength Fluorosilicone	265	105	100

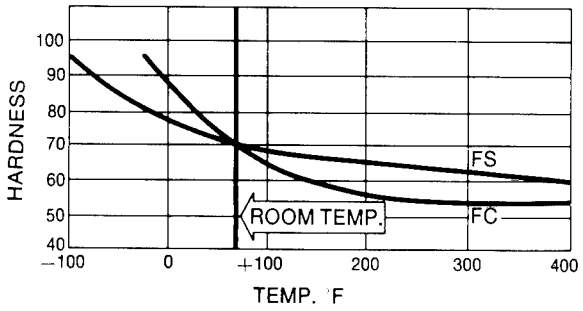

FIG. 1. Comparison of hardness at various temperatures.

thermal variability and short temperature range capability of the fluorocarbon rubber.

Finally, the chain flexibility of the fluorosilicone is clearly demonstrated by measurement of the TR–10 value (100% elongated samples were frozen in the elongated state than warmed until they had retracted to 10% of their original deflection). The fluorosilicone rubber gave a TR–10 of −75°F while the fluorocarbon elastomer was 0°F.

Properties of Fluorosilicone Sealants

Formulation of a low molecular weight polymer with appropriate fillers, chain extenders, crosslinking agents, and catalysts gives a low viscosity stock with excellent extrusion characteristics which will cure at room temperature (termed an RTV system). Vulcanization results from the interaction of reactive groups in the polymer chain with a crosslinking agent. One type of curing mechanism requires moisture in the air to react with an alkoxy or acetoxy group to produce the crosslink. This reaction liberates alcohol or acetic acid and such sealants are used where the by-products do not interfere with the application. A second method of curing depends on the reaction of a vinyl group with a silicon hydride and liberates no volatile products. Use of this type sealant lends itself to thick section applications.

Typical properties of fluorosilicone sealants in comparison with a typical dimethylsiloxane based sealant are given in Table VI. Here we see that the

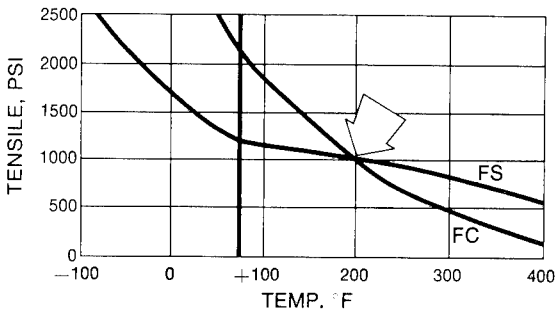

FIG. 2. Comparison of tensile at various temperatures.

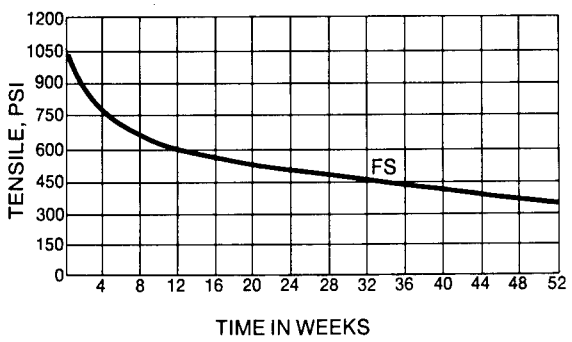

FIG. 3. Tensile of a fluorosilicone which has been heat-aged at 392°F for indicated lengths of time.

fluorosilicone sealants can be designed to have equivalent physical properties to the conventional dimethylsiloxane materials.

The superior solvent resistance of fluorosilicoe rubber is also evident in the sealants (Table VII).

Because of these unique properties, the trifluoropropylmethylsiloxane sealants have found extensive use in both subsonic and supersonic aircraft construction. In these applications, the sealant must withstand temperature extremes from −70 to 450°F and continuous contact with aircraft fuel.

The primary applications for the fluorosilicone sealants on aircraft are as filleting sealants for the integral fuel tanks built into the wings and as noncurable channel sealants. They also are used on ground support fuel handling systems and in areas of the aircraft where solvents are used for cleaning and wash-down procedures.

Perhaps the most outstanding characteristic of the sealants is their resistance to degradation at elevated temperatures in fuels. Table VIII shows the fuel resistance as a function of time and temperature and clearly indicates the stability of the polymer system. At even higher temperature (Figures 5 and 6) both the tensile and elongation retention are excellent. At the present time, the fluorosilicone sealants are prime candidates for the fuel tank seals of the future advanced supersonic aircraft, and are currently used in several types of military aircraft.

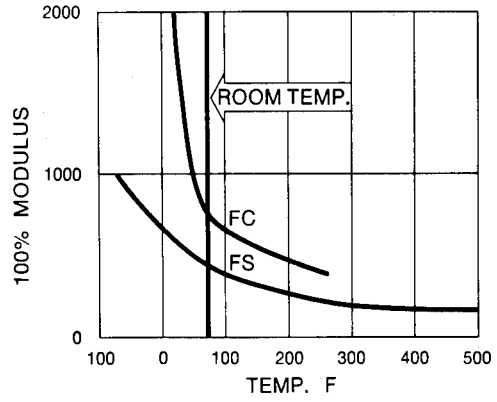

FIG. 4. Tensile modulus stability at operating temperatures.

TABLE VI

Properties of Silicone Sealants

	After 7 Days at 25°C	
	Me_2	TFP-Me
Durometer	40	42
Tensile Strength, psi	775	550
Elongation, %	850	500
Tear Strength, psi	115	70
Brittle Point, °F	−85	−70
Lap Shear Strength, psi	375	550
Peel Strength, psi	85	100

In summary, fluorosilicone elastomers show excellent solvent resistance, thermal and oxidative stability, and outstanding low temperature flexibility. They are superior in many respects to the fluorocarbon elastomers but fall short of them at temperatures above 450°F. In one respect, both fluorosilicone and conventional dimethylsilicone polymers are at a disadvantage at high temperatures in confined areas. Depolymerization (reversion) can occur with resultant deterioration of the physical properties.

FIRE-RETARDANT FLUOROSILICONES

While fluorosilicone elastomers possess excellent solvent resistance, thermal and oxidative stability, and outstanding low temperature flexibility, they are as flammable as are most silicone elastomers. In some instances, flammable polymers can be rendered fire-retardant by the incorporation of additives. However, the structural modification of the fluorosi-

TABLE VII

Solvent Resistance of Fluorosilicone Sealants
(72 hrs. at room temperature)

	Percent Swell	Durometer Change
ASTM No. 1 Oil	0	+6
10 W-30 Oil	0	+4
Methyl Alcohol	0	+6
VM & P Naptha	1	+4
Ethylene Glycol	1	+8
Perchloroethylene	3	+3
Gasoline	4	+1
Toluene	6	0
Methyl Chloride	14	−4
Chlorothene	14	−5
Ethyl Acetone	43	>−10
Acetone	51	>−10

licone elastomer system was investigated to achieve fire-retardant properties. This approach led to the preparation of halofluorosilicone polymer of the structure, $-(-ZCF_2CF_2CH_2CH_2SiMeO-)-_n$, Z=Br or CCl_3 and the polymer systems were found to have good fire-retardant properties.

Monomer Preparation

The desired halofluoroolefins were prepared as shown below:

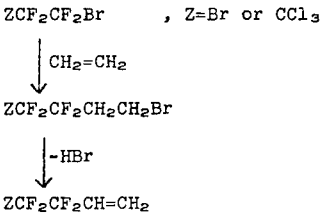

Chloroplatinic acid catalyzed addition of methyldichlorosilane to the olefin gave $ZCF_2CF_2CH_2CH_2MeCl_2$, from which cyclic trimer, $(BrCF_2CF_2CH_2CH_2SiMeO)_3$, was prepared as follows:

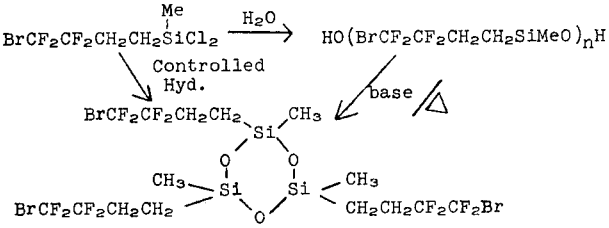

The above described chlorosilanes and the cyclic siloxane are used as the monomers for polymer preparation.

Preparation and Preliminary Evaluation of Polymers

The fluid polymers end-blocked with vinyl as well as hydroxy groups were prepared using the cyclic trimer as shown below:

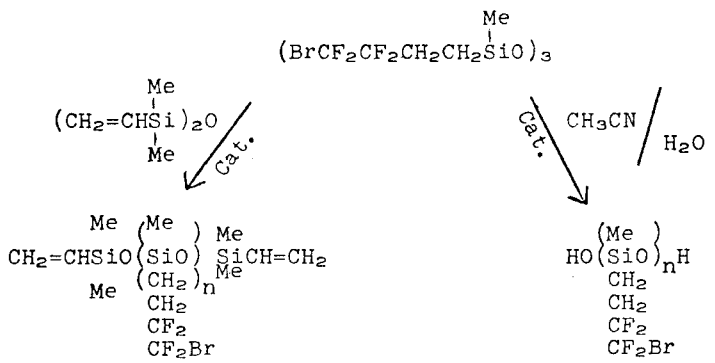

TABLE VIII

Fuel Resistance of Fluorosilicone Sealants (in N_2)

		JP-4 at 250°F		JP-4 at 450°F	
	Original	4 wks.	8 wks.	4 wks.	8 wks
Durometer, Shore A	42	32	33	38	33
Tensile Strength, psi	550	495	530	600	540
Elongation, %	500	420	310	265	270

The compounded and cured polymer does not support flame and the limited oxygen index (LOI) for the polymer was found to be 33.7%.

The hydroxy end-blocked fluid polymer $HO(CCl_3CF_2CF_2CH_2CH_2SiMeO)_nH$, derived from the controlled hydrolysis of $CCl_3CF_2CF_2CH_2CH_2SiMeCl_2$, was end-blocked with $—SiMe_3$ to give a fluid having good lubrication properties (Table IX). Condensation of the diol, $HO(CCl_3CF_2CF_2CH_2CH_2SiMeO)H$, gave a polymeric material which would not support combustion.

FLUOROSILICONE-FLUOROCARBON HYBRID SYSTEMS

The need for reversion resistance at elevated temperatures prompted an investigation into the preparation of polymers of the type $(SiCh_2CH_2\text{-}(CF_2)xCH_2CH_2SiO)_n$ ($R = CH_3$, $R' = CF_3CH_2CH_2$) x = 1–10, in which the backbone consisted essentially of fluorocarbon units connected by a

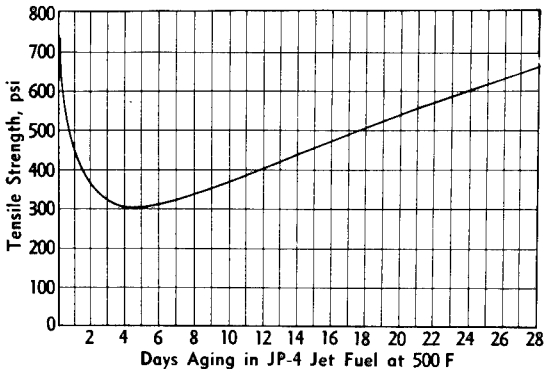

FIG. 5. Tensile strength of fluorosilicone sealant exposed to jet fuel at 500°F in pressure bomb.

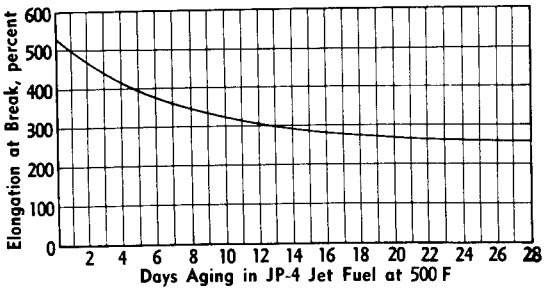

FIG. 6. Elongation of fluorosilicone sealant exposed to jet at 500°F in pressure bomb.

disiloxane linkage. It was believed that structures of this type would show improved reversion resistance while retaining the other excellent properties of the fluorosilicones. It was recognized that some sacrifice of low temperature flexibility would be necessary.

Monomer Preparation

The monomers were prepared by the following reaction sequence (Scheme I) [6]:

Scheme I

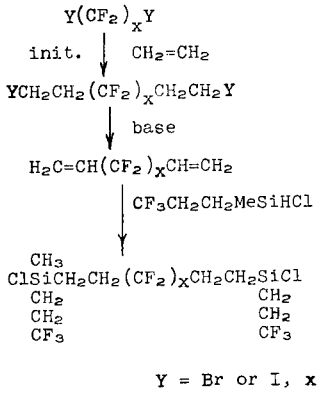

Y = Br or I, x = 1-10

The investigation of the addition of $CH_2{=}CH_2$ to $Y(CF_2)_xY$ to form $YCH_2CH_2(CF_2)_xCH_2CH_2Y$ was initiated with commercially available $BrCF_2CF_2Br$ (I). Although seemingly a straight forward reaction, the free radical catalyzed addition of $CH_2{=}CH_2$ to dibromide I resulted in the

TABLE IX

Shell 4-Ball Test
1,200 R.P.M. for ½ hr. at 167°F—Steel on Al.

Load	Scar Dia.	F. Ave.
10 Kg	0.32 mm	0.1207

TABLE X
Reaction of $CH_2=CH_2$ With $BrCF_2CF_2Br$

Run	Mole of $BrCF_2CF_2Br$	Rx Press $CH_2=CH_2$ psi	Catalyst	Rx Time (hr)	Rx Temp (°C)	% Conv. of $BrCF_2CF_2Br$, glc (isolation)	% Yield, glc (isolation) II[a]	III[b]	IV[c]
1	1.42	85	DTBP	25	120	16	57		
2	1.42	150	DTBP	27	120	67	51	28	8
3	1.42	120	DTBP	25	120	68 (73)	64 (59)	19 (18)	8 (6)
4	1.42	80	DTBP	72	120	75 (89)	68 (46)	9	9 (6)
5	0.62	120	None	25	120	N. R.			
6[d]	7.04	115	DTBP	17	135	58	87	4	5

[a] $BrCH_2CH_2CF_2CF_2Br$
[b] $Br(CH_2)_4CF_2CF_2Br$
[c] $BrCH_2CH_2CF_2CF_2CH_2CH_2Br$
[d] About 5 mole % catalyst and a 2-liter stainless steel stirring pressure reactor were used.

formation of 1:1 adduct, $BrCH_2CH_2CF_2CF_2Br$ (II), in high yield and no more than a trace amount of the desired 1:1:1 diadduct, $BrCH_2CH_2CF_2CF_2CH_2CH_2Br$ (IV) (Scheme II). The results of several examples

Scheme II

$$\underset{\text{I}}{BrCF_2CF_2Br} + CH_2=CH_2 \xrightarrow[\text{conv.}]{\sim 67\%} \underset{\text{II}}{BrCF_2CF_2CH_2CH_2Br} \sim 65\%$$

$$\underset{\text{III}}{BrCF_2CF_2(CH_2)_4Br} \sim 15\%$$

$$\underset{\text{IV}}{BrCH_2CH_2CF_2CF_2CH_2CH_2Br} \sim 8\%$$

of this addition reaction are shown in Table X. After several unsuccessful attempts to prepare the desired diadduct IV in quantity directly from dibromide I, the addition reaction of $CH_2=CH_2$ to adduct II was investigated. The reaction of $CH_2=CH_2$ with adduct II should occur preferentially at the $BrCF_2-$ group rather than at the $BrCH_2-$ end. Therefore, if the reaction of $CH_2=CH_2$ with adduct II occurs the predominant product would be the desired diadduct IV.

The results of several examples of the free radical catalyzed addition of $CH_2=CH_2$ to adduct II are summarized in Table XI. As these data show, only an average of about 17% conversion of adduct II was realized, and approximately 19% of this was the desired diadduct IV. The remainder of the product consisted of about 10% of diadduct III, $BrCH_2CH_2CF_2CF_2(CH_2)_4Br$ (V), and several unidentified products. All of the above experimental results clearly indicate that the addition reaction of $CH_2=CH_2$ to dibromide I or adduct II cannot be employed as a practical method for the production of diadduct IV. Similar low conversion was obtained in the addition of $CH_2=CH_2$ to CF_2Br_2 (VI) and $BrCF_2CH_2CH_2Br$ (VII). The free radical catalyzed addition of $CH_2=CH_2$ to dibromide VI gave adduct VII in high yield, but the addition of $CH_2=CH_2$ to adduct VII under free radical catalysis resulted in only about a 5% conversion of adduct VII, in which $BrCH_2CH_2CF_2CH_2CH_2Br$ (VIII) amounted to about 46%.

After unsuccessful attempts to obtain diadduct IV and VIII in quantity from the addition of $CH_2{=}CH_2$ to adducts II and VII, respectively, our effort was directed toward the investigation of the addition of $CH_2{=}CH_2$ to $Br(CF_2)_6Br$ (IX). The addition of $CH_2{=}CH_2$ to dibromide IX was conducted under 50–60 psi of constant $CH_2{=}CH_2$ pressure at 130–140°C. The results (average and isolated yield) of this addition reaction are shown in Scheme III.

Scheme III

$$Br(CF_2)_6Br + CH_2{=}CH_2 \xrightarrow[73\%\ \text{conv.}]{\text{DTBP}} \begin{cases} Br(CF_2)_6CH_2CH_2Br & 63\% \\ \text{X} & \\ BrCH_2CH_2(CF_2)_6CH_2CH_2Br & 18\% \\ \text{XI} & \\ \text{Other Telomers} & \end{cases}$$

$$X + CH_2{=}CH_2 \xrightarrow[69\%\ \text{conv.}]{\text{DTBP}} \begin{cases} \text{XI} & 60\% \\ BrCH_2CH_2(CF_2)_6(CH_2)_4Br & 18\% \\ \text{XII (presumed)} & \end{cases}$$

The addition of $CH_2{=}CH_2$ to dibromide IX was found to proceed smoothly giving rise to 1:1 adduct X, 1:1:1 adduct XI, and other telomers. The further addition of $CH_2{=}CH_2$ to adduct X gave the desired diadduct XI without difficulty. Dehydrobromination of diadduct XI yielded $CH_2{=}CH(CF_2)_6CH{=}CH_2$ (XIII) in high yield. Although the exact nature of the failure to form a reasonable yield of diadducts IV and VIII is not clear at present, the successful formation of diadduct XI from the addition of $CH_2{=}CH_2$ to dibromide IX or adduct X indicates the importance of the chain length of α,ω-dibromoperfluoroalkanes for the formation of α,ω-diethylene addition products.

In contrast to the results of the addition of $CH_2{=}CH_2$ to dibromide I, it has been reported that thermal addition of $CH_2{=}CH_2$ to ICF_2CF_2I (XIV)

TABLE XI
Reaction of $CH_2{=}CH_2$ With $BrCF_2CF_2CH_2CH_2Br$

Run	Mole of $BrCF_2CF_2CH_2CH_2Br$	Rx Press $CH_2{=}CH_2$ psi	Catalyst[a]	Rx Time (hr)	Rx Temp (°C)	% Conv. of $BrCF_2CF_2CH_2CH_2Br$ glc (isolation)	% Yield, glc (isolation) IV[b]	III[c,d]	V[e]
1	0.694	110	Bz_2O_2	20	70	14 (26)	20 (1)	18	40 (16)
2	0.694	180	DTBP	44	110	23	19	8	33
3	0.347	120	DTBP	25	110	23	38	7	4
4	0.347	100	DTBP	13	140	15	13	Trace	
5[f]	0.246	60	DTBP	46	120	9	5	Trace	5
6[g]	0.4			85	65	N.R.			

[a] About 3 mole %.

[b] $BrCH_2CH_2CF_2CF_2CH_2CH_2Br$.

[c] $Br(CH_2)_4CF_2CF_2Br$.

[d] Since this was identified by glc retention time only, the identification is not considered to be positive.

[e] $Br(CH_2)_4CF_2CF_2CH_2CH_2Br$.

[f] 0.8 g of $NaHCO_3$ added.

[g] Ultraviolet induced reaction bubbling $CH_2{=}CH_2$ into the telogen.

TABLE XII
H_2PTCl_6 Catalyzed Addition of Silane XVIIb to Dienes[a]

Diene	Yield (%) Rear. Monoadduct (XXIV) A	B	Diadduct A	B	Diadduct/Rear. Monoad. A	B
XVIb	9	9	74	86	8.2	9.6
XVIc	19	29	75	43	4.0	1.5
XIII	20 33		71 51		3.6 1.5	
XVId	11 22	24	78 72	63	7.1 3.3	2.8

[a] Gas chromatographic analysis.

A. Diene was added to silane containing catalyst (H_2PtCl_6) at 100–110°C.

B. Silane was introduced to diene containing catalyst (H_2PtCl_6) at 100–110°C except XVIb, (~70°C).

gave rise to 1:1:1 adduct, $ICH_2CH_2CF_2CF_2CH_2CH_2I$ (XV), in high yield [10]. However the free radical catalyzed addition of $CH_2{=}CH_2$ to diiodide XIV gives no adduct and generally results in almost quantitative recovery of starting material. The required α,ω-divinylperfluoroalkanes (XVI) were therefore prepared from α,ω-diiodoperfluoroalkanes following the reported method with the exception of XVIa which was obtained according to the method of Henne and DeWitt [11].

$$CH_2{=}CH(CF_2)_xCH{=}CH_2$$

XVI a x = 1
b x = 2
c x = 4
d x = 8
e x = 10

The addition of ≡SiH to the dienes XVIa–e and XIII was successfully effected either by chloroplatinic acid or di-*t*-butyl peroxide catalysis (Scheme IV). However, the chloroplatinic acid catalyzed addition $CF_3CH_2CH_2(CH_3)SiHCl$ (XVIIb) to the dienes XVIb–d and XIII gives rise to the corresponding rearranged monoaddition products XXIVa–d in addition to the diadducts XIXb–XXIIb, respectively (Scheme V).

Scheme IV

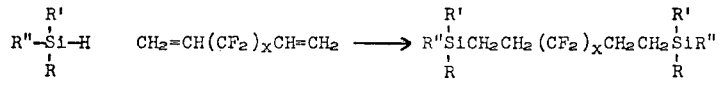

XVIIa, R=R'=CH_3, R"=Cl
b, R=CH_3-, R'=$CF_3CH_2CH_2$-, R"=Cl
c, R=R'=$CF_3CH_2CH_2$-, R"=Cl
d, R=CH_3-, R'=$C_4F_9CH_2CH_2$-, R"=Cl
e, R=CH_3-, R'=R"=Cl
f, R=R'=R"=Cl
g, R=CH_3-, R'=$CF_3CH_2CH_2$-, R"=H
h, R=$CF_3CH_2CH_2$-, R'=R"=H

XVIIIb, x = 1
XIXb, x = 2
XXb, x = 4
XXIa-h, x = 6
XXIIb, x = 8
XXIIIb, x = 10

Scheme V

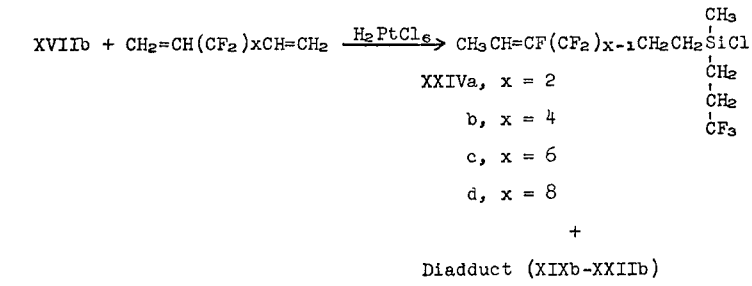

The yield of the rearranged monoadduct XXIV and the diadduct (XIXb–XXIIb); and the ratio of the diadduct to the rearranged monoadduct XXIV are summarized in Table XII.

These results are unexpected and quite interesting. Although the addition of ≡SiH to a variety of olefins including dienes, functional olefins, and polyfluoroolefins, such as CF_2=CF_2 and CH_2=CF_2 has been abundantly documented, little work in the addition of ≡SiH to vinylperfluoroalkanes, especially α,ω-di(vinyl)perfluoroalkanes, has been reported. As the data in the Table XII show, the formation of the rearranged monoadduct XXIV is quite significant, and the ratio of the diadduct to the rearranged monoadduct XXIV could not always be reproduced. These nonreproducible results appear to suggest that the reaction is heterogeneous in most cases. The ratio of the diadduct to the rearranged monoadduct XXIV was found to be unaffected by subjecting the reaction mixture, that already completed, to the conditions of its formation. Similarly, the chloroplatinic acid catalyzed addition of silane XVIIa to diene XIII gave a 29% yield of CH_3CH=$CF(CF_2)_5CH_2CH_2Si(CH_3)_2Cl$ (XXV) and a 51% yield of diadduct XXIa.

Scheme VI

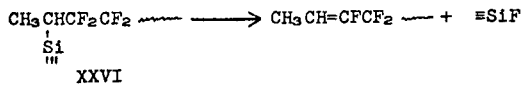

Although the rearranged monoadduct XXIV may possibly be formed by a reverse addition followed by decomposition of the adduct XXVI as shown in Scheme VI, it is difficult to conceive that such an ≡SiF elimination would occur under relatively mild conditions of the reaction (100–110°C) or during the isolation of the rearranged monoadduct XXIV (< 100°C). In fact, polyfluoroalkylsilicon compounds similar to adduct XXVI are reported to be reasonably stable [12]. On the basis of the mechanism advanced for the chloroplatinic acid catalyzed addition of organosilicon hydrides to hydrocarbon olefins [13] the rearranged monoadduct XXIV appears to have been formed by the decomposition of a reversely oriented Pt-olefin or Pt-diene complex without actual formation of the reverse adduct XXVI. No attempt has been made to detect the rearranged diene, CH_3CH=$CF(CF_2)_yCF$=$CHCH_3$ (XXVII) which might have been formed to some extent. Although exact mechanistic aspects of the formation of the rearranged monoadduct XXIV are uncertain at the present time, platinum or its derivative indeed causes the formation of the rearranged monoadduct XXIV. This conclusion is based on the observation that the peroxide

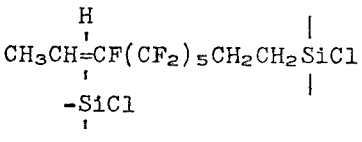

XXVIII

catalyzed addition of the silane XVIIb to the dienes XIII, XVIb, XVId, and XVIe yielded the desired diadducts XXIb, XIXb, XXIIb, and XXIIIb, respectively, in high yield without the formation of the rearranged monoadduct XXIV in an appreciable quantity (less than 3% if any). Since no reaction was observed between the silane XVIIb and the rearranged monoadduct XXIVc under the conditions of free radical reaction, the possibility of the formation of a non-separable rearranged diadduct of the type XXVIII under the free radical conditions was ruled out. The similar free radical catalyzed addition of the silanes XVIId–h to the diene XIII, respectively, offered the diadducts XXId–h in high yield without any complication.

Synthesis of Homopolymers

Aqueous sodium bicarbonate hydrolysis of the monomer chlorosilane, $ClSiCH_2CH_2(CF_2)_xCH_2CH_2SiCl$ (R′ and R), in ether as the solvent followed by tetramethylguanidine trifluoroacetic acid catalyzed bulk polymerization yielded a high consistency elastomeric gum XXIX without any difficulty (Scheme VII).

Scheme VII

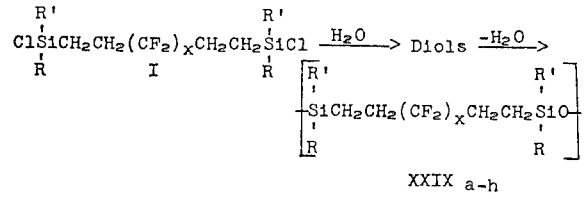

XXIX a-h

XXIX a, x = 1
b, x = 2
c, x = 4
d, x = 6
e, x = 8
f, x = 10
} R′ = CH_3, R=$CF_3CH_2CH_2$

g, x = 6, R′ = R′ $CF_3CH_2CH_2$

h, x = 6, R′ = R = CH_3.

No evidence of cyclization of the diols was observed during polymerization. Although no attempt was made to isolate the monomer diol the infrared, the elemental, and the gas chromatographic analyses and

molecular weight determination suggest that the hydrolyzate is composed of mostly monomer diol. When the hydrolyzate was allowed to stand at room temperature for several days, the viscosity of the hydrolyzate increased slowly indicating a partial condensation.

When a low molecular weight liquid polymer XXIXd was prepared by stopping the polymerization prior to its completion and keeping it at room temperature, the liquid polymer turned into a high consistency elastomer within a few hours even though the water of condensation was not removed. The water formed from the condensation stayed with the polymer in a dispersed form. Therefore, the removal of water by mechanical means during the condensation-polymerization was proven to be a non-critical factor for the formation of the polymer of the Type XXIX. In contrast to polysiloxanes, such as dimethylpolysiloxane [7] and methyl (3,3,3-trifluoropropyl)polysiloxane [2], the catalyst (tetramethylguanidine-CF_3COOH) does not appear to affect the stability of the polymers of Type XXIX. Polymer XXIXd containing the catalyst was dissolved in isopropyl acetate, and the solution was kept in open air at room temperature for several days to evaporate the solvent. After the evaporation of the solvent, the resulting polymer did not show any apparent loss of molecular weight. Therefore, all evidence obtained to date indicates that polymer XXIX does not suffer from reversion by water and/or catalyst like polysiloxanes do. The fact is that no appreciable amount of volatile reversion product was observed by heating polymer XXIXd at 270°C in the presence of potassium hydroxide under a high vacuum. Under these conditions, dimethylpolysiloxane as well as methyl(3,3,3-trifluoropropyl)polysiloxane gives rise to volatile reversion products almost quantitatively [7d].

The degree of polymerization of the elastomeric gum, determined by membrane osmometry, was found to be about 30–160 depending upon the purity of monomer. For the vulcanization of the high consistency elastomers, vinyl crosslinking sites were introduced in the polymer either by cohydrolysis of the monomer chlorosilane and alkyl(vinyl)dichlorosilane or by reacting the hydrolyzate (diol) of the monomer chlorosilane with alkyl(vinyl)dichlorosilane followed by tetramethylguanidinetrifluoroacetic acid catalyzed polymerization.

Synthesis of Block Copolymers

Two block copolymers of the structure XXX and XXXI were synthesized. The synthetic route for the preparation of XXX and XXXI is

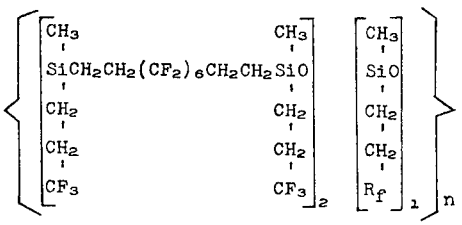

XXX a, $R_f = CF_3-$
b, $R_f = C_4F_9-$

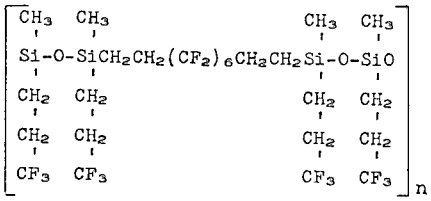

XXXI

shown in Scheme VIII. The copolymer XXX was obtained as a high consistency elastomeric gum having a molecular weight of ca. 70,000. The vinyl crosslinking sites were again introduced in the copolymer by the cohydrolysis technique described for homopolymers. Because of the slightly impure state of XXXII, the copolymer XXXI was not a gum but a very viscous fluid.

Scheme VIII

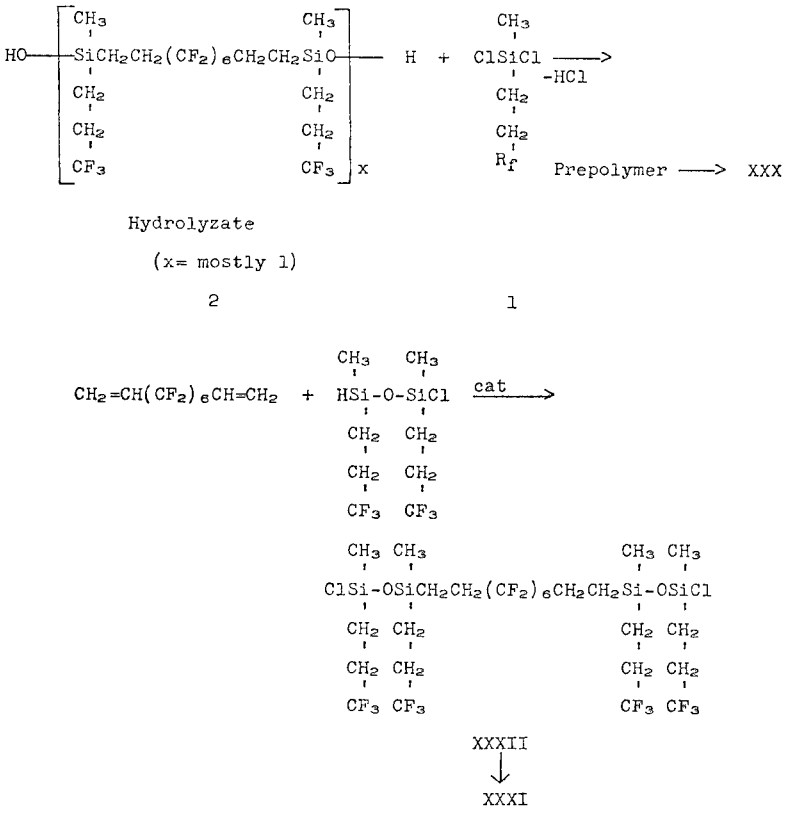

Evaluation of Polymers

Polymer XXIX was found by x-ray diffraction to be non-crystalline amorphous material. The high consistency elastomers were compounded with reinforcing silica and an organic peroxide, then vulcanized in the conventional manner [8, 9].

Scheme IX

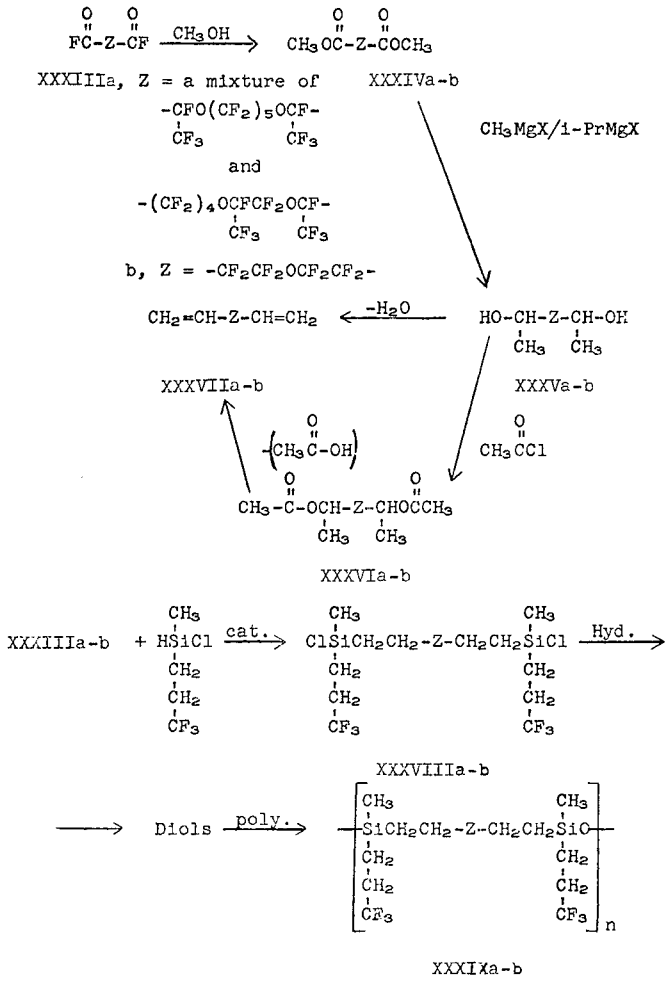

Some of their physical properties and evaluation results are summarized in Table XIII. Poly (3,3,3-trifluoropropyl)methysiloxane was selected for the purpose of comparison. As the data in Table XIII shows, the polymers, with the possible exception of XXIXa, have superior thermal stability with greatly improved reversion resistance compared to polydialkylsiloxanes. Polymer XXIXa appears to suffer from thermooxidation, which is not too surprising because the polymer backbone contains the least possible number of fluorocarbon segments. It is quite interesting to observe that copolymer XXX also has an improved thermal stability and does not suffer from reversion as much as polydialkylsiloxanes do. Therefore, it appears that copolymerization is an apprach to improving the low temperature properties. In fact, the improvement of low temperature-properties by copolymerization was demonstrated with copolymer XXXI even though the improved thermal stability of XXXI has not been demonstrated as of yet. The solvent resistance of the hybrid polymers is comparable to poly(3,-

TABEL XIII
High Consistency Rubbers

Polymer		XXIXa	XXIXb	XXIXc	XXIXd	XXIXe	XXIXf	XXIXg	XXIXh	XXXa	XXXb	XXXI	LS[e]
M.W.[a]		8,000	13,000	16,000	100,000					70,000			800,000
Sp. G.		1.40	1.45	1.54	1.59	1.63	1.69						1.40
T_g[b] (°C)		-38	-27	-25	-24	-28	-11			-29	-30	-43	
Original, post cured at 200°C/ 8 hr	Durometer	54	62	54	58	68	69			53	60		45
	Tensile Strength, psi	1127	1789	1117	2548	1650	2000			1610	1250		1500
	Elongation, %	180	300	225	300	453	500			230	330		350
% Volume Swell[c]	Methylisobutyl Ketone	260	254	261	285	325	270	243	346	255			290
	Toluene	22	77	56	31	44	43	15	158	28			17
	Heptane	11	16	9	13	36	26		111	4			10
After 24 hr at 250°C in Air	Durometer	97	62	56	65	68	65			60			42
	Tensile Strength, psi	407	1008	1373	2333	1784	1167			1450			470
	Elongation, %	0	200	240	260	300				220			260
	% Wt Loss	46.2	2.7	2.5	2.2	3.1	2.3			1.6			1.1
After 24 hr[d] at 250 C in sealed glass container	Durometer	42	46	43	54					62	55		20
	Tensile Strength, psi	346	843	823	1355					495	460		50
	Elongation, %	195	300	290	300					140	220		100

[a] M.W. was difficult to obtain because of the insolubility of the polymer in common organic solvent. M.W. was determined either by vapor pressure or membrane osmometry.

[b] Determined by differential scanning calorimetry.

[c] Seventy-two hours immersion at room temperature.

[d] Test for reversion resistance.

[e] Poly(3,3,3-trifluoropropyl)methylsiloxane.

TABLE XIV
Pyrolysis of the Branched Fluoroether-Diacetate XXXVIa

Run	Temp. (°C)	N_2 (cc/min)	Relative Percentages[a] Unidentified By-Products	Unidentified By-Products	Diene	Unidentified By-Products	Mono-Acetate[b]	Unidentified By-Products	Diacetate	Unidentified By-Products
1	600	400	—	52.3	9.3	1.5	20.1	1.6	7.0	8.2
2	500	400	21.6	26.7	18.3	11.3	13.2	2.7	3.1	3.1
3	500	400	—	33.9	23.3	14.4	16.8	3.4	4.1	4.1
4	480	400	0.6	←	2.6	→	3.3	17.6	73.1	2.8
5[c]	515	400	18.0	10.1	17.1	5.6	25.2	4.4	18.5	1.1
6[d]	515	400	—	—	6.4	6.2	44.9	7.7	34.8	—
7[d]	515	350	13.1	17.2	30.4	10.5	20.0	3.4	5.0	0.4

[a] G.L.P.C. analysis; increasing in retention time from left to right; acetic acid was not included.

[b] Presumed to be the monoacetate, $CH_2{=}CH\text{-Fluoroether-}\underset{\displaystyle CH_3}{\underset{|}{CH}}\text{—O—}\overset{\displaystyle O}{\overset{\|}{C}}\text{—}CH_3$

[c] Products and by-products of Run 4 used as starting material.

[d] Residue from preceding run after removal of volatiles used as starting material.

3,3-tri-fluoropropyl)methylsiloxane and appears to be independent of the length of fluorocarbon chain in the polymer backbone.

Fluorosilicone–Fluoroether Hybrid Systems

As shown in the preceding section, the polymers based on fluorosilicone–fluorocarbon were found to possess superior thermal stability with greatly improved reversion resistance as compared to polydialkylsiloxanes. However, the low temperature properties were inferior to that of polydialkylsiloxanes although they were quite adequate for most applications. Therefore, it was decided to seek improvement of the low temperature properties while retaining the high temperature reversion and fuel resistance exhibited by the polymer based on fluorosilicone–fluorocarbon.

TABLE XV
Pyrolysis of the Fluoroether–Diacetate XXXVIb

Packing (g)	Temp. (°C)	Nitrogen (cc/min))	Weight % Recovered (bp > 25°C)	Relative Percentages[a] HOAc	Diene	Monoacetate[b]	Diacetate
89	610	400	72.12	11.23	6.56	17.27	31.44
89	610	300	69.33	16.28	12.40	19.71	26.58
134	610	250	49.67	30.36	34.35	4.17	5.69
134	610	275	48.67	31.82	37.50	4.55	2.13
134	610	325	23.50	30.27	41.57	5.96	1.78
134	610	400	57.89	33.92	31.58	8.77	2.19

[a] G.L.P.C. analysis; increasing in retention time from left to right.

[b] Presumed to be the monoacetate, $CH_2{=}CHCF_2CF_2OCF_2CF_2\underset{|}{C}HCH_3$

TABLE XVI
Thermal Gravimetric Analysis (17°/min)

	10% Wt. Loss, °C		50% Wt. Loss, °C	
Polymer	Air	Nitrogen	Air	Nitrogen
XXXIXa [a]	390	415	430	455
XXXIXb	380	440	460	500

[a] Partially vulcanized sample with 25 parts of silica filler.

Of the various possible modifications of the fluorosilicone–fluorocarbon hybrid polymer for improvement of the low temperature properties, including the copolymerization approaches mentioned in the preceding section, fluoroethers were chosen for substitution of the fluorocarbon segment, thus resulting in fluorosilicone–fluoroether hybrid polymers.

Preparation of Monomers and Polymers

The synthetic route for preparation of fluorosilicone–fluoroether hybrid polymer system is shown in Scheme IX.

The conversion of the methyl ester XXXIV to the secondary diol XXXV was successfully effected in one step by the known mixed Grignard route [14]. The isolated yield of the diol XXXV was an average of 70% for XXXVa and 35% for XXXVb. The diol XXXVb was found to be difficult to obtain in pure form. The dehydration of the diol XXXV was quite difficult as expected. The dehydration of the diol XXXV with phosphorous pentoxide gave the diene XXXVII in ca. 10% yield. The preparation of the diene XXXVII by pyrolysis of the diacetate XXXVI was found to be equally poor in the case of XXXVIIa (ca. 5% yeild of XXXVIIa). However, the diene XXXVIIb could be obtained in a moderate yield (ca. 20% yield) by the pyrolysis approach. The major by-products in the pyrolysis were low boiling materials. The results and conditions of the pyrolysis of XXXVI are summarized in Tables XIV and XV.

The method of preparation of the fluorosilicone–fluoroether hybrid polymer XXXIX is identical to the procedure described in the preceding section for the fluorosilicone–fluorocarbon hybrid polymers as shown in Scheme IX. The results of thermal gravimetric analysis of polymer XXXIX indicate the good thermal and oxidative stability of the polymer

TABLE XVII
Glass Transition Temperature of Polymer VIII

Polymer	Tg (°C)[a]
XXXIX	-47
XXXIXb	-39

[a] Determined by differential scanning calorimetry.

system (Table XVI). The glass transition temperature of polymer XXXIX is shown in Table XVII and the low temperature properties as expected are an improvement over that of the fluorosilicone–fluorocarbon hybrid polymers.

The authors wish to express their appreciation to the Elastomers and Coatings Branch, Non-Metallic Materials Division, Air Force Materials Laboratory for supporting this work in part under Contract No. F33615-69-C-1301.

REFERENCES

[1] O. R. Pierce, *J. Appl. Polym. Sci., 14*, 7 (1970).
[2] O. R. Pierce et al., Ind. Eng. Chem., *52*, pp. 783 (1960).
[3] K. E. Polmanteer, *J. Elastoplastics, 2*, 165 (1970).
[4] P. Tarrant, *Fluorine Chem. Rev.*, Marcel Dekker, Inc., N.Y., (a series of volumes).
[5] W. A. Sheppard and C. M. Shorts, *Organic Florine Chemistry*; W. A. Benjamin, Suc., N. Y. (1969).
[6] Y. K. Kim, O. R. Pierce, A. G. Smith, and W. X. Bajzer, *J. Fluorine Chem., 1*, 203 (1971).
[7] a. M. Kucera, J. Lanikova, and M. Jelinek, *J. Polym. Sci., 53*, 301 (1961); b. M. Kucera, J. Jelinek, J. Lanikova, and K. Vesely, *J. Polym. Sci., 53*, 311 (1961); c. R. L. Merker, M. J. Scott, and G. G. Haberland, *J. Polym. Sci., A2*, 31 (1964); d. M. J. Hunter, J. F. Hyde, E. L. Warrick, and H. J. Fletcher, *J. Am. Chem. Soc., 68*, 667 (1964).
[8] W. Noll, *Chemistry and Technology of Silicones*, Academic Press, N. Y., 1968, pp. 392–409, and references cited therein.
[9] E. D. Brown (to Dow Corning Corporation), Can. Patent No. 586,871 (1959).
[10] a. N. O. Brace, U. S. Patent No. 3,016,407 (1962); b. I. L. Knunyants, S. P. Khrlakyan, Yu. V. Zeifman, and V. V. Shokina, *Izr. Akad. Nauk USSR, Ser. Khim.* 384 (1964).
[11] A. L. Henne and E. G. DeWitt, *J. Am. Chem. Soc., 70*, 1548 (1948).
[12] a. A. M. Geyer and R. N. Haszeldine, *J. Chem., Soc., 3925 (1967). b. W. I. Bevan, R. N. Haszeldine, and J. C. Young. Chem. and Ind.*, 789 (1961).
[13] a. J. W. Ryan and J. L. Speier, *J. Am. Chem. Soc., 86*, 895 (1964). b. A. J. Chalk and J. F. Harrod, *J. Am. Chem. Soc., 87*, 16 (1965).
[14] O. R. Pierce et al., *J. Am. Chem. Soc., 75*, 6324 (1953).

A NEW ENGINEERING MATERIAL FOR ADVANCED DESIGN CONCEPTS

GEORGE H. KALB, RICHARD W. QUARLES, JR., and RALPH S. GRAFF

Elastomer Chemicals Department,
E. I. Du Pont de Nemours & Company, Inc.,
Wilmington, Delaware 19898

SYNOPSIS

ECD-006 perfluoroelastomer is a new high performance elastomer based on the copolymerization of tetrafluoroethylene, perfluoro(methyl vinyl ether) and a third monomer (a perfluorovinyl ether grouping with an active cure site monomer). This material, when cross-linked, gives vulcanizates with outstanding chemical and fluid resistance and high temperature oxidative resistance. In many cases this elastomer may be used to replace either metal or plastic parts, but a direct shape replacement very often is not satisfactory. Instead, the design must be modified. Some areas of application for ECD-006 parts are indicated.

INTRODUCTION

Polytetrafluoroethylenes are well known for their outstanding resistance to thermal oxidative degradation and their outstanding solvent and chemical resistance. This stability, when compared with hydrocarbon polymers such as polyethylene, is due in a large measure to the greater stability of the carbon-to-fluorine bond as compared with the carbon-to-hydrogen bond. Because similar stability and inertness would be a tremendous virtue in an elastomer, this laboratory and many other laboratories have sought for elastic materials in which hydrogen is replaced by fluorine. Examples in which part of the hydrogen is replaced by fluorine are the commercial high performance elastomers, Fluorel® and Viton®. These rubbers exhibit much superior resistance to chemical and oxidative thermal attack and solvent swelling when compared with the parent hydrocarbon polymers. However, since they still contain a large proportion of hydrogen, on a molar basis, they are subject to chemical attack and their performance at 450–500°F (232–260°C) is not outstanding. As a consequence, a major goal has been to prepare a completely fluorinated elastomer to more closely approximate the chemical inertness of polytetrafluoroethylene.

Applied Polymer Symposium No. 22, 127–142 (1973)

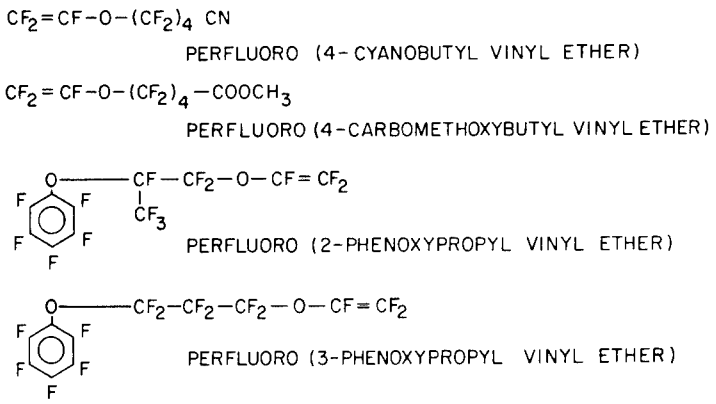

FIG. 1. Comonomers for introduction of crosslink sites.

EARLY INVESTIGATIONS

The obvious starting point was to begin with tetrafluoroethylene and to modify the polymer by the addition of a comonomer which would break up crystallinity and the chain regularity to yield a rubbery material. In order to obtain rubbery properties, it was necessary to copolymerize not just a few percent, buta significant quantity of one or more other monomers. It is known that the polymerization rates of higher homologs of tetrafluoroethylene—for example hexafluoropropylene—are much lower than tetrafluoroethylene in the preferred aqueous polymerization systems so that it is practically impossible to incorporate sufficient quantities of a higher perfluoro homolog to attain rubbery properties. Therefore, a search was initiated for a structure which would copolymerize more readily. After investigating a number of other comonomers, it was found that perfluorovinyl ethers copolymerize easily with tetrafluoroethylene and when present in the 20–50 mole % range give elastomeric compositions which are thermally stable and chemically resistant. The preferred second monomer is the simplest member of the series, namely, perfluoro(methyl vinyl ether).

Polymerization is carried out under pressure in an aqueous medium using redox or thermal persulfate initiation. The polymer is rubbery and is characterized by excellent chemical and thermal stability. For example, on

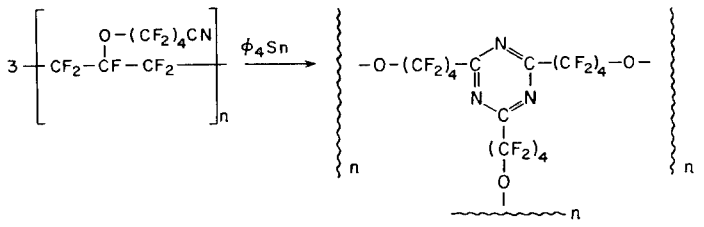

FIG. 2. Crosslinking of polymer through the nitrile group.

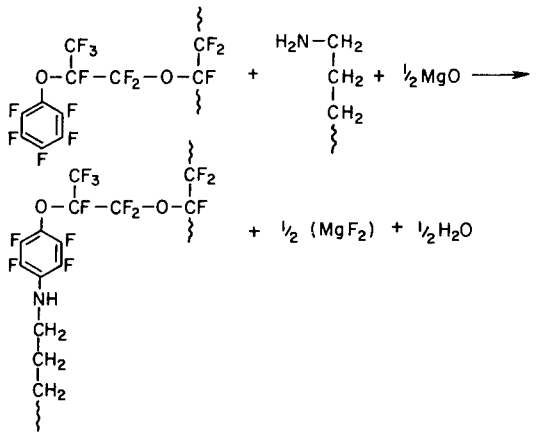

FIG. 3. Diamine curing of phenoxy-containing polymer.

heat aging in an air circulating oven at 316°C for a week, a slab loses only 5–7% of its weight, (mostly low molecular weight polymeric material and moisture) and over an additional month under these conditions only a few more percent. During this treatment, the polymer loses its slight haze and becomes clear and white.

This dipolymer is, however, a thermoplastic and a crosslinked network (vulcanization) is required for true elastomeric properties, especially at elevated temperatures. The tetrafluoroethylene–perfluoro(methyl vinyl ether) dipolymer was found to be a chemically inert and extremely solvent resistant elastomeric material—in fact it was so unreactive that it could not be suitably crosslinked. This led to a search for a third monomer, to be copolymerized, which would provide a site for chemical crosslinking. Studies again indicated that the best route was to synthesize a perfluorovinyl ether with a site built into the perfluorinated group opposite the vinyl grouping because even long chain vinyl ethers copolymerized readily, allowing varied and controlled amounts of the third monomer to be incorporated. One of the main requirements was that the functional group would not affect the polymerization reaction, which is particularly susceptible to

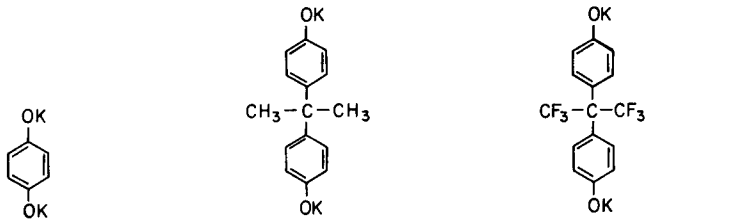

FIG. 4. Curing of perfluorophenoxy-containing polymer aromatic nucleophiles.

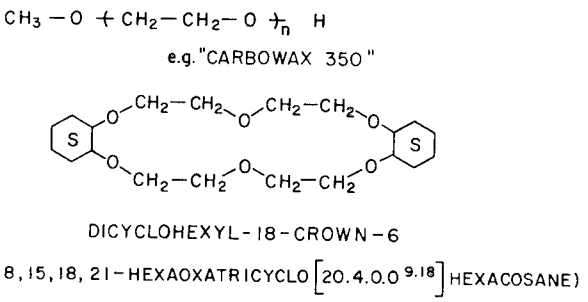

FIG. 5. Accelerators for perfluoroelastomer curing.

chain transfer. Other requirements were that the crosslink had to be chemically and thermally inert and finally it had to be amenable to the standard methods of rubber processing such as milling, molding and calendering and then be activated to complete vulcanization by raising the temperature.

VULCANIZATION SITES AND VULCANIZATION

The generalized structure of the comonomers investigated was CF_2 = CF—O—R_f X where X was —COOR, —CN, or —OC_6F_5 and R_f was perfluoroalkyl or perfluoroalkyl ether groups. Figure 1 lists the four major

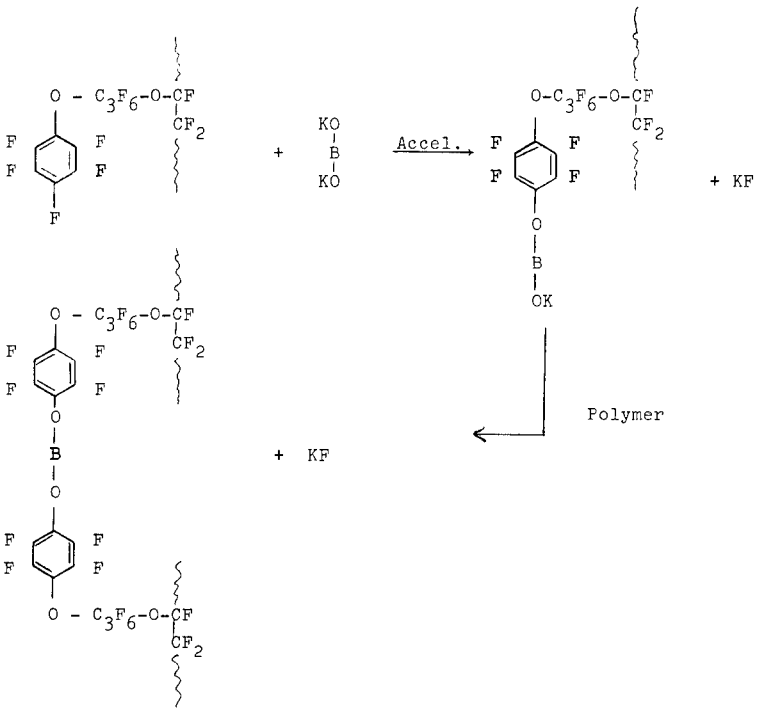

FIG. 6. Curing reaction of perfluoroelastomer (nucleophilic substitution).

TABLE I
Vulcanizate Properties

Original Physical Properties	20 phr SAF	10 phr SAF	Gum
Durometer at 75°F (Shore A)	89	78- 82	55-65
Stress/Strain at 75°F			
M_{100} (psi)	1350	1200-1800	500-1000
T_B (psi)	2720	2200-2900	1400-2500
E_B (%)	160	120-160	150-190
Compression Set - ASTM D-395 Method B			
70 h/121°C (250°F)	23		
70 h/288°C (550°F)	45		
70 h/204°C		28-50	25-35
Clash-Berg Stiffness Test ASTM D-1043 (at 10,000 psi torsional modulus)	+28°F	+30- +34	
Brittle Temperature	-38°F		
Retraction Temperature ASTM D-1329			
T-10	+30°F		
T-50	+46°F		
Tear (pli) ASTM D-470	13	14-20	11-18
Compression Deflection psi			
15%	580		
25%	1160		

candidate comonomers investigated. All of these monomers incorporate readily. There were some differences in vulcanizate properties depending on the strength of the crosslink but there is little effect on the chemical or solvent resistance because only 0.3–2.0 mole % of the third monomer is required for an adequate number of crosslink sites.

These different functional groups require different crosslinking agents. For example, polymer containing perfluoro(4-carbomethoxybutyl vinyl ether) may be crosslinked by ester interchanger with a glycol or by reaction with a diamine.

TABLE II
Vulcanizate Properties at Elevated Temperatures

	Black Stock		
	20 phr SAF	10 phr SAF	Gum Stock
S/S at 75°F (ambient)			
M_{100}	1350	700	900
T_B	2720	2400	1630
E_B	160	130	120
S/S at 212°F (100°C)			
T_B	740 (250°F)	450	380
E_B	90	160	60
% Tensile Set		5	3
S/S at 400°F (204°C)			
T_B	375	220	
E_B	90	70	
% Set	-	0	

TABLE III
Effect of Temperature on S/S
Black Stock

Temperature (F°)	(C°)	Elongation Rate (%/min)	M_{100} (psi)	T_B (psi)	E_B (%)	Tensile Set (%)
-85[a]	-65	100	-	8420	13	-
-50[a]	-46	100	-	7280	42	-
-50[a]	-46	500	-	3860	4	-
75	24	100	1125	3150	190	9
250	121	100	-	740	90	-
400	204	100	-	375	90	-

[a] Experiments carried out in methanol.

On the other hand, polymer containing pendent nitrile groups by copolymerization of perfluoro(4-cyano-butyl vinyl ether) may be vulcanized using tetraphenyl tin or silver oxide catalysts. It is known that perfluoroalkyl triazines are formed from perfluoroalkyl nitriles so that it would be expected that the crosslinking reaction would proceed as illustrated in Figure 2. Infrared examination does show the disappearance of the —C—N aborption. However, perfluorotriazines have a characteristic strong absorption in the 6.40–6.45 μ region and, although these polymers did crosslink as expected, the characteristic triazine infrared band was not found. Catalysts remain in the rubber but do not affect polymer properties. Another cure site grouping is the perfluorophenoxy group. It is known that the fluorine on the carbon in the para position from the oxygens is more labile than the other fluorine atoms and this activity is employed in crosslinking.

One technique used to crosslink the polymer containing the perfluorophenoxy moiety is to react it with a derivative of hexamethylene diamine in the presence of an acid acceptor such as magnesium oxide. Equations for the reaction are shown on Figure 3. Magnesium fluoride remains in the elastomer.

TABLE IV
Compression Set Data at Elevated Temperatures[a]
10 PHR SAF Block Stock[b]

	Perfluoroelastomer	
	Pellets	O-Rings[c]
70 hrs / RT	34	—
70 hrs / 250°F	32	25
70 hrs / 400°F	34	37
70 hrs / 450°F	34	43
70 hrs / 500°F	41	40
70 hrs / 550°F	49	62

[a] Method B, ASTM D-395-55, 25% deflection.
[b] Cure: 30 min at 350°F plus 5 days oven at 550°F.
[c] Nominal 1′ I.D. and 0.139′ cross-section.

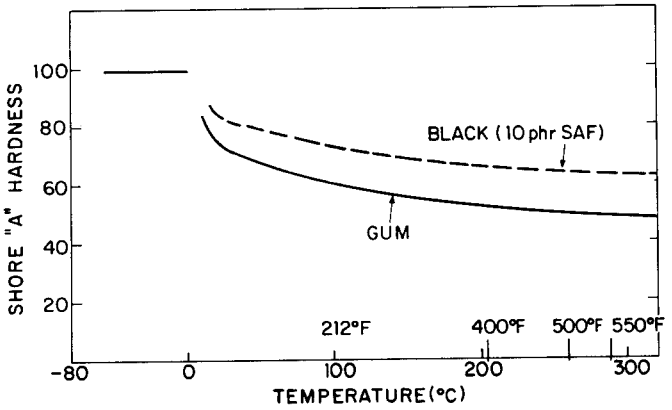

FIG. 7. Effect of temperature on shore hardness (ECO-006).

Another successful technique worked out for crosslinking the phenoxy-containing polymer employed aromatic bisnucleophiles. Bisnucleophiles from hydroquone or from bisphenol A types, as shown in Figure 4, crosslink the polymer. However, these reactions require accelerators to be effective. Effective accelerators are "carbowax" 350 and dicyclohexane-18-crown-6 (Fig. 5). An overall formulation of the reaction is shown in Figure 6. In this vulcanization method potassium fluoride remains in the polymer.

So much for the chemical background of the perfluoroelastomer. It is obvious that these elastomers are based on monomers having difficult and costly syntheses. However, both the monomer and polymer synthesis have been successfully scaled up from laboratory scale to a market development facility.

PHYSICAL PROPERTIES

Many of the physical and chemical properties are grossly identical even though different third monomers are used for crosslinking sites. Therefore,

TABLE V
Permeability of ECD-006

MATERIAL	TEST	TEMP °C	PERMEABILITY cc /cm^2 sec atm	DIFFUSIVITY cm^2/sec	SOLUBILITY cc /cm^3 atm
ECD-006-	BENZENE VAPOR	150	4.9×10^{-6}	1.6×10^{-6}	3
	ISOOCTANE	150	1.51×10^{-6}	6.83×10^{-7}	2.22×10^{-2}
	JET FUEL II	30	$0.5 \times 10^{-11(1)}$		
	JET FUEL II	150	$2.88 \times 10^{-8(2)}$		
	O_2	32	9.6×10^{-8}	3.8×10^{-7}	0.25
	N_2	30	2.6×10^{-8}	1.8×10^{-7}	0.14

TABLE VI
Dielectric Properties of Gum perfluoroelastomer

	ELASTOMER[a]	TFE[b]
DIELECTRIC CONSTANT "E"	2.8–3.2	2.1
DISSIPATION FACTOR "D" (50% RH, 73°F)	1×10^{-3}	3×10^{-4}
D.C. RESISTIVITY "ρ"	10^{18} ohm-cm	10^{18}
DIELECTRIC STRENGTH (BREAKDOWN)	>2000 volts/mil	400

[a] Gum stock-vulcanized.
[b] Plastics World (1965).

much of the following data applies to ECD–006 perfluoro elastomer irrespective of the crosslink site selected.

Table I shows selected vulcanizate data obtained on gum, 10 phr and 20 phr SAF black stock. The 20 phr data are given for a single, typical stock, whereas data for 10 phr black and gum stock show ranges which depend on the particular polymer compound. It is interesting that the room tem-

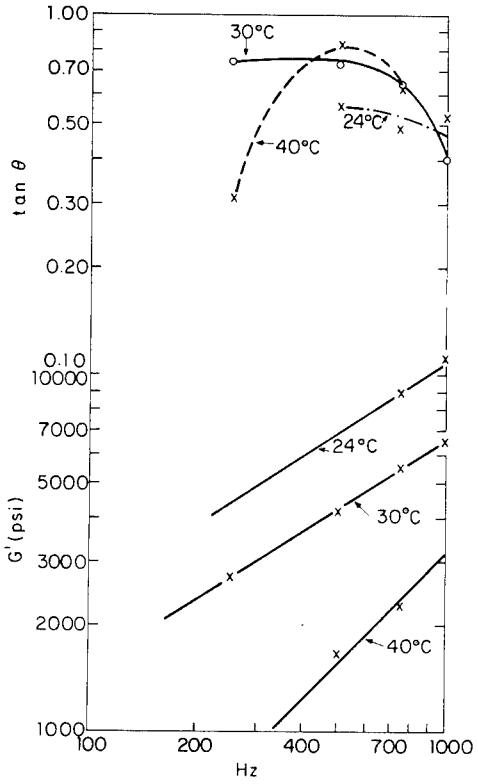

FIG. 8. Dynamic modulus vs frequency (ECD–006).

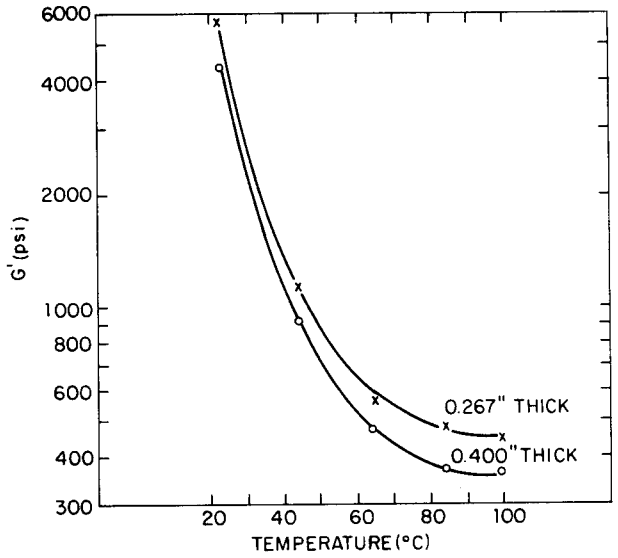

FIG. 9. Dynamic modulus vs temperature (ECD-006).

perature values are similar to those obtained on the commercial fluoroelastomers.

In the tables, data are given for black loaded vulcanizates but other reinforcing agents such as asbestos, titania, and silica may also be used. However, SAF black is the most effective agent studied to date. Stocks

TABLE VII
Miscellaneous Engineering Data

Density	
10 phr SAF black vulcanizate	2.02
Gum vulcanizate	2.01
Linear Coefficient of Thermal Expansion:	
Over the range of 25-200°C using the equation of the form $T = T_0 + \alpha T_0 \Delta T$	
$\alpha = 1.9 \times 10^{-4}$	
Specific Heat (Differential Scanning Calorimetry)	
ECD-006 gum vulcanizate	
C_p (50°C) = 0.226 cal/g	
C_p (100°C) = 0.233 cal/g	
C_p (150°C) = 0.252 cal/g	
Refractive Index	
$n_D^{25} = 1.3500$	

TABLE VIII
Chemical Fluid Resistance of ECD-006 Black Stock Organic compounds

	Temperature (F°)	Temperature (C°)	Time Days	Rating
HYDROCARBONS				
Aviation Gas	111	45	100	A
Kerosene	111	45	100	A
Jet Fuel (JP-5)	75	24	7	A
Cyclo-Hexane	75	24	600	A
Benzene	75	24	7	A
Toluene	75	24	600	A
ALCOHOLS				
2B Alcohol	75	24	7	A
Butanol	111	45	100	A
Methanol	111	45	100	A
n-Hexanol	111	45	100	A
Ethylene glycol	111	45	100	A
ESTERS				
Butyl acetate	111	45	100	A
Vinyl acetate	111	45	100	A
Dioctylphthalate	111	45	100	A
ANHYDRIDES				
Acetic	111	45	100	A
	75	24	7	A
KETONES				
Acetone	75	24	7	A
MEK	111	45	100	A
Isofuranone	111	45	100	A
NITRILES				
Acetonitrile	111	45	100	A

may also be plasticized with a limited group of compatible agents. These include perfluorinated oils and greases. The effects on vulcanizate properites are similar to those observed on plasticizing other elastomers.

Vulcanizate properties of the perfluoroelastomers at elevated temperatures show similar decreasing trends as do the fluoroelastomers, and at 400°F both the perfluoroelastomer and the fluoroelastomers approach the fluorosilicone values (Table II). However these losses in properties can be compensated for by correct design.

The next table, Table III, gives values for a single SAF black compound over the range of -65°C to 204°C. The brittle point temperature is -38°C. However, the polymer does not get really stiff and boardy below this temperature. . . rather it resembles a highly plasticized plastic. In fact a gum stock was tested as a valve seat in a quick opening valve for liquid oxygen service and it operated successfully. Returning to the values shown in Table III, studies at −50°F were carried out at two different extension rates. Even at 500%/min reasonable tensile and elongation values were obtained.

Another indication of the high performance characteristic is its flat resistance to compression set over the range of room temperature to 500°F. Only above 500°F does the set increase rapidly. It is well known that compression set values will vary depending on the compound. The data shown in Table IV represents a single compound.

Like other rubbers, ECD-006 vulcanizates become softer at higher temperatures. Figure 7 shows the variation from room temperature to 550°F. Over this range the hardness drops by some 25 points with the gum showing a greater drop than black. When parts are designed to be utilized at elevated temperatures, this property must be taken into account.

ECD-006 shows relatively low permeability to a number of solvents and gases. This may be attributed to the low solubility of most classes of materials in the polymer. Table V tabulates these data.

The electrical properties of the perfluoroelastomer are also of considerable interest because its potential use in many environments hostile to most other rubbers and plastics. Table VI gives comparative data for a gum vulcanizate and poly TFE. There is a great similarity between the perfluoroelastomer and poly TFE except that the dielectric strength (breakdown potential) is some 5 times that of poly TFE. This is a real advantage for the ECD-006 perfluoroelastomer when it is used as an insulator.

Figures 8 and 9 show dynamic modulus results obtained on an ECD-006 black stock using a Lockheed Test Fixture. The values obtained are quite similar to the fluoroelastomers taking into account differences in T_G. The perfluoroelastomer would be selected for use as a dampening agent at low temperatures where $\tan \theta = 0.5$ or as an isolating mount at high temperatures, not because of any outstanding dynamic properties, but rather because of its resistance to the particular service atmosphere.

Miscellaneous data of potential importance in design work is given in Table VII. Like the fluoroelastomers, the density is high—just above 2.0 for both black and gum stock. Another interesting property is its coefficient of linear expansion. For a gum stock it is 1.9×10^{-4} within about $\pm$ 10% (190×10^{-6}). For reference, metals usually run in the range of 10–20 $\times 10^{-6}$ and quartz about 2×10^{-6}. Thus, the perfluoroelastomer has a coefficient of thermal expansion about an order-of-magnitude greater than metals and about two orders of magnitude higher than quartz. The next item on Table VII is the specific heat. This was determined on a Du Pont #900 Differential Scanning Calorimeter. The final item is the refractive index of raw stock. As anticipated for fluorinated polymers it is low. . . 1.3500.

These data complete the studies on physical properties. Let us now turn to some of the chemical and fluid resistant properties of ECD-006.

FLUID AND CHEMICAL RESISTANCE

The next several tables indicate how closely ECD-006 perfluoroelastomer approaches the solvent resistance of poly TFE. For simplicity

TABLE IX
Chemical Fluid Resistance of ECD-006 Black Stock Organic Compounds

	Temperature (F°)	Temperature (C°)	Time (Days)	Rating
AMINES				
Ethylene Diamine	111	45	100	C
Pyridine	75	24	7	A
Monoethanolamine	111	45	100	A
ACIDS				
Glacial Acetic	111	45	100	C
10% Glacial Acetic	111	45	100	C
Formic Acid	111	45	100	C
2-ethyl hexanoic	111	45	100	A
ALDEHYDES				
Butyraldehyde	111	45	100	C
Formaldehyde	111	45	100	C
Glyoxal (40%)	111	45	100	A
MISCELLANEOUS ORGANIC				
Freon 113	75	24	10	C
CCl_4	111	45	100	B
Ethylene dichloride	111	45	100	A
Butyl cellosolve	111	45	100	A
THF	75	24	600	A
Nitrobenzene	75	24	600	A

TABLE X
ECD-006 Industrial and Proprietary Materials Resistance to Attack

	Temperature (F°C)	(C°)	Time (Days)	Wt. Increase %	Retention T_B PSI	E_B(%)	Rating
JP-5 Jet Fuel	75°	24	7	0	100	100	A
Jet Fuel Type II	600	316	3	4.6			A
Skydrol	300	149	7	9.8 (vol.)			A
Anderol	400	204	7	31 (vol.)			B+

the effects of fluids on ECD-006 under the conditions indicated has been categorized as follows:

A. No effect
B. Slight effect—practically no loss in physical characteristics, slight swelling
C. Moderate swelling, but polymer is still integral.

Table VIII lists fluids which appear to have no effect on ECD-006. These include hydrocarbons, alcohols, esters, anhydrides, lactones and nitriles.

The next table, Table IX, lists some fluids which do swell ECD-006. As indicated, some of the amines cause difficulty, as do some of the lower acids. Among the aldehydes, butyraldehyde, and formaldehyde swell ECD-006. Among the miscellaneous group, halogenated organics have slight to no effect, but the Freons swell ECD-006. Of particular interest is the resistance of the perfluoroelastomer to butyl cellosolve, tetrahydrofuran, and nitrobenzene, all of which are important commercial solvents.

Among industrial materials, the perfluoroelastomer shows a high degree of fluid resistance to materials of interest to the aircraft industry even at

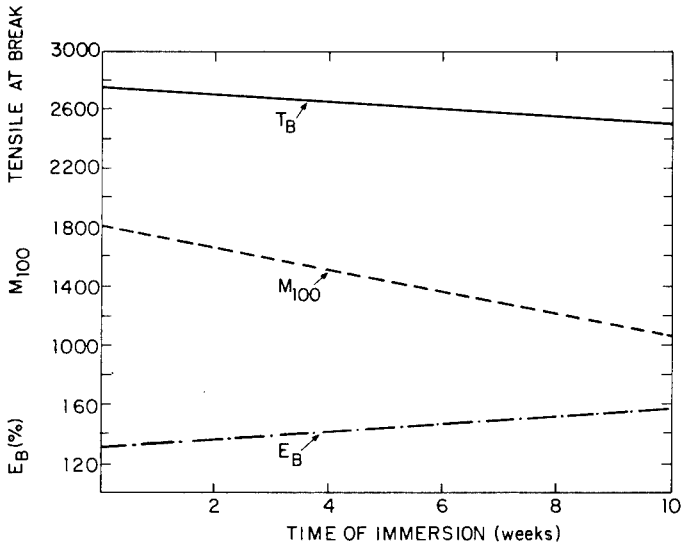

FIG. 10. Effect of immersion in boiling jet fuel (10 PHR SAF black stock) (ECD-006).

TABLE XI
Chemical fluid Resistance of ECD-006 Black Stock Inorganic compounds

	Temperature (F°)	(C°)	Time (Days)	Rating	
INORGANIC ACIDS					
HNO_3 (70%)	158	70	7	A	Gum Stock
HNO_3 (90% Fum.)	75	24	10	B	Gum Stock
HNO_3 (10%)	111	45	100	B	Gum Stock
H_2SO_4 (conc.)	75	24	10	A	
INORGANIC BASES					
NaOH (46%)	75	24	7	A	
NH_4OH(35%)	111	45	100	A	
Hydrazine Hydrate	75	24	10	A	
MISCELLANEOUS					
$TiCl_4$	75	111	2	A	

elevated temperatures (Table X and Figure 10). Resistance to the hydraulic fluids Skydrol and Anderol is good. In jet fuel ECD-006 black vulcanizates showed only a 10% drop in tensile at break, a 20% increase in elongation at break, and about a 40% drop in modulus in boiling jet fuel (200–210°C, 400°F) over a 10 week period. Furthermore, when the fluid was concentrated, there was no evidence of fluorocarbon residues in the fuel as indicated by infrared absorption measurements.

ECD-006 shows high resistance to attack by bases at the temperatures investigated (Table XI). Concentrated sulfuric acid had little effect—but nitric acid showed some acitivity even towards the gum stock (which is more resistant to oxidizers than black stock). Metal halogen compounds, such as titanium tetrachloride, have little effect. Furthermore, recent experience in laboratory has indicated that a plasticized gum stock makes an excellent syringe stopper for diethylaluminum chloride and triethyl aluminum in hexane solution. In addition to being inert towards these corrosive substances, the gum stock exhibits the property of resealing after being punctured with a syringe needle.

TABLE XII
Unusual Test Conditions (Black Stock)

Exposure				Form	Results
$H_2O/CO_2/CH_4$	1 week	20,000 psig	650°F (343°C)	Slab	Swelled
$H_2S/CH_4/CO_2$	1 week	20,000 psig	300-400°F (149-204°C)	Slab	Swelled
Air/Water	2 hrs	20,000 psig	650°F (343°C)	O-ring	Sealed-leaked on cooling
Prototype Oil Well	2 hrs	20,000 psig	500°F (260°C)	Elect. boot	Sealed
30% Oleum	471 hrs		180°F (82°C)	Slab	Swell - 10% on X-section modulus unchanged
Air	156 hrs	26 KV Pulses, 0.75 sec. apart	625°F (329°C)	Ign. cable	Dielectric breakdown

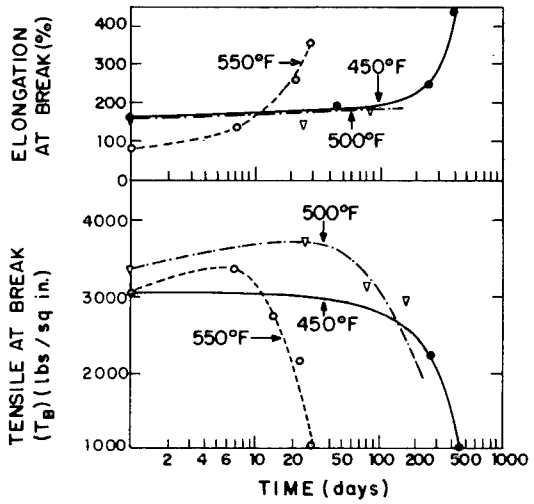

FIG. 11. Effect of heat aging at various temperatures on s/s of black stork.

ECD-006 has been exposed to some quite unusual conditions and these are listed in Table XII. In most cases there are no known competitive rubbers physically capable of withstanding these conditions.

The first three experiments were run on test samples to simulate conditions met in deep oil well drilling applications-20,000 ft or deeper. Under these conditions, the test specimens were only slightly swollen and as a result were judged to be useful. Therefore, we have in production for deep oil well use prototype electrical boots where both electrical resistance and sealing characteristics are required. It seems likely that ECD-006 will find use in this application.

In 30% oleum at 180°F, a slab of black stock was swollen 10% on cross section, but the part remained integral and was functional.

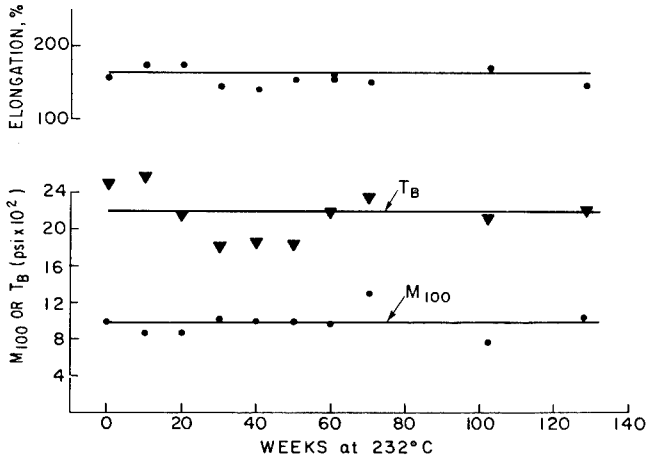

FIG. 12. Heat aging effect of block perfluoroelastomer vulcanizates (232°C (450°F) 30 mm Hg of moist air).

The last example is a test ignition cable subjected to the conditions indicated. The part functioned for 156 hours and then like almost all insulating materials the insulation broke down catastrophically. There are few if any rubber insulating materials capable of withstanding such conditions.

Figure 11 shows heat aging performance data on black stock exposed in an air circulating oven at 450°, 500 and 550°F. Shown here are the best data obtained to date. Variations in the polymer and in curing change these values. However, ECD–006 must be synthesized and compounded for various uses requiring properties other than just thermal resistance, and as a consequence the heat aging characteristics may vary.

In considering market areas for ECD–006, high performance aircraft appeared to require some of the properties the perfluoroelastomer had to offer. Accordingly, it was tested under conditions which simulate supersonic operation at 60,000 ft. altitude where the air pressure is about 30 mm of Hg and temperatures of 450°F were postulated. As Figure12 indicates there was little change in properties after some 135 weeks of exposure of the elastomer to these conditions.

STATUS OF THE DEVELOPMENT

Current commercial production includes septa used in a liquid chromatograph built and marketed by the Du Pont Instrument Products Division. In addition, parts of various shapes and sizes are being fabricated and test marketed for evaluation by interested customers. In many instances, requests have been made to replace a part made from plastic, metal, or perhaps another elastomer. Usually, it is found that a direct shape substitution of ECD–006 is not satisfactory. Rather, a cooperative study must be made with the design engineer to develop a suitable part to meet requirements and in many cases, this requires new engineering design concepts.

SAFETY NOTES

1. Many of the perfluorinated monomers and their intermediates are highly toxic and should be handled in well ventilated areas by competent investigators.
2. Certain of the cure ingredients and accelerators mentioned are toxic to animals. The effect on humans is not known and is still under investigation. Based on our current knowledge extreme care should be taken to prevent ingestion, skin contact, or contact with the eyes.
3. The polymerization work reported herein requires compression of tetrafluoroethylene—perfluoro-(methyl vinyl ether) mixtures. This operation is considered potentially hazardous and should be carried out only in adequately barricaded areas.

The authors wish to acknowledge the contributions of the following coworkers to the information reported herein: Dr. A. L. Barney; Dr. J. E. Barry; Dr. D. E. Blair; Dr. A. F. Brizzolara; Dr. H. K. Frensdorff; Dr. R. J. Harder; Dr. W. J. Keller; Dr. A. A. Khan; Dr. M. J. Maskornick; Dr. D. B. Pattison; Dr. H. J. Stinger; Dr. N. M. van Gulick; and Mr. H. O. Wolf.

REFERENCES

[1] A. L. Barney, W. J. Keller, N. van Gulick, *J. Polym. Sci. A-1, 8*, 1091–1098 (1970).

[2] A. L. Barney, G. H. Kalb, and A. A. Khan, *Rubber Chem. Tech. 44* (3), 660–667 (1971).

[3] G. H. Kalb, A. A. Khan, R. W. Quarles, Jr., and A. L. Barney; *Polym. Prep. Amer. Chem. Soc. Div. Polym. Chem. 13* (1), 490 (April, 1972).

BLOCK COPOLYMER ELASTOMERS FROM POLYSILOXANES AND HIGH TEMPERATURE RESISTANT SEGMENTS

M. MATZNER, A. NOSHAY, L. M. ROBESON,
C. N. MERRIAM, R. BARCLAY, JR., and J. E. McGRATH

Research and Development Department,
Union Carbide Corporation,
Chemicals and Plastics,
Bound Brook, New Jersey 08805

SYNOPSIS

The reaction of well-characterized hydroxyl terminated aromatic polyethers, polyesters, or cycloaliphatic polycarbonates with dimethylamino terminated polydimethylsiloxane oligomers in chloroaromatic solvents yielded ideally alternating $-(A-B-)_n$ elastomeric block copolymers. The reaction proceeded at high rates in those cases where aromatic hydroxyls were the terminal groups. The rate of block copolymer formation was considerably slower with the less acidic and more sterically hindered cycloaliphatic hydroxyl functions.

The novel elastomers showed excellent mechanical properties; the latter were superior to those of cross-linked silicone gums and silica filled compositions. The dynamic mechanical behavior indicated the formation of 2-phase systems at relatively low oligomer molecular weight which undoubtedly reflects the high degree of incompatibility of the segments. Thermogravimetric analysis of the elastomers showed that they possessed good thermal stability both in nitrogen and in air. Best results were observed for the poly(aryl ether)-based copolymers. The cycloaliphatic polycarbonate derived elastomers are the least stable and begin to lose weight in air at ~290°C. Further studies established that the elastomers possess good thermal oxidative stability and retain their initial properties after prolonged aging at 150–170°C. The copolymers containing aromatic moieties did not show exceptional ultraviolet stability; however, those materials that incorporated the cycloaliphatic polycarbonate blocks displayed outstanding ultraviolet behavior as evidenced by the retention of properties after extended RS Sun Lamp accelerated aging. All of the elastomers possessed remarkable hydrolytic stability which is believed to be closely related to their two-phase character. The oxygen permeability of the copolymers was high and approached that of silicone rubbers.

INTRODUCTION

Block copolymers based on polydimethyl siloxane (1) are candidates of choice for elastomers possessing excellent properties both at high and low temperatures. Indeed, polydimethylsiloxane (1) has a glass transition temperature of −123°C [1] and a melting point of −55°C. Thus good characteristics at low temperatures are expected. Moreover, (1) shows good

Applied Polymer Symposium No. 22, 143–156 (1973)

TABLE I
Siloxane Containing Block Copolymer Elastomers

No.	Hard Segment[a]	Oligomer Molecular Weight		Block Copolymer	
		Hard	Soft	% Siloxane	RV
1	Poly(aryl ether) (6)	5,200	5,100	50	0.85
2	"	5,200	9,700	66	0.91
3	"	6,500	24,000	78	1.30
4	Poly(aryl ester) (8)	2,000	2,000	50	0.75
5	"	3,000	5,400	65	0.64
6	Poly(aryl ester) (9)	2,800	4,600	62	0.59
7	Poly(aryl ester) (10)	2,100	2,000	50	0.83
8	"	2,100	4,700	68	0.62
9	Polycarbonate (11)	6,400	7,500	54	1.17
10	"	8,000	9,700	53	0.84

[a] See equation V in text for structures.

stability at elevated temperatures [2–4]. If one were to prepare a block copolymer incorporating polydimethylsiloxane and an appropriately chosen

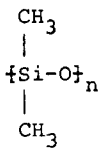

(I)

(1)

hard block, one would obtain a material with unique properties. Due to the presence of the hard phase dispersed in the rubbery matrix, the ultimate mechanical behavior should be vastly superior to the very weak silicone gums or even silica filled compositions [5, 6].

Block copolymers based on polydimethylsiloxanes have been prepared. Polystyrene-based copolymers possessing both the A—B—A and $-(-A-B-)_n$ structures have been reported [7–11]. Mechanical properties were good. However, due to the low glass transition temperature, Tg of the polystyrene, the upper temperature capability of the soft segment was not fully utilized. A similar situation probably exists with the recently prepared methyl methacrylate counterparts [12, 13]. Some enhancement in high temperature properties was realized in the case of α-methylstyrene multiblock systems [14].

Potentially higher Tg materials would be expected if the hard blocks were of the condensation polymer type. Copolymers derived from bisphenol A polycarbonate and polydimethylsiloxane were prepared and investigated in detail at the General Electric Company [15–19]. Unfortunately, the hard segments of most of these interesting materials possessed molecular weights in the lower range at which the glass transition was below 100°C.

Since 1965 an extensive investigation of silicone block copolymers has been in progress in our laboratories. Thermoplastic elastomers based on heat and/or light resistant hard blocks were prepared. A novel method for the synthesis of perfectly alternating $-(-A-B-)-_n$ polymers was developed. Sufficiently long hard segments were utilized in order to ensure phase separation and a transition behavior approaching the ultimate for a given system.

This paper describes the properties obtained with five different rigid blocks.

PREPARATION

The preparation of the silicone elastomers was conducted using the general scheme shown in equation II. The subject reaction is very facile; the

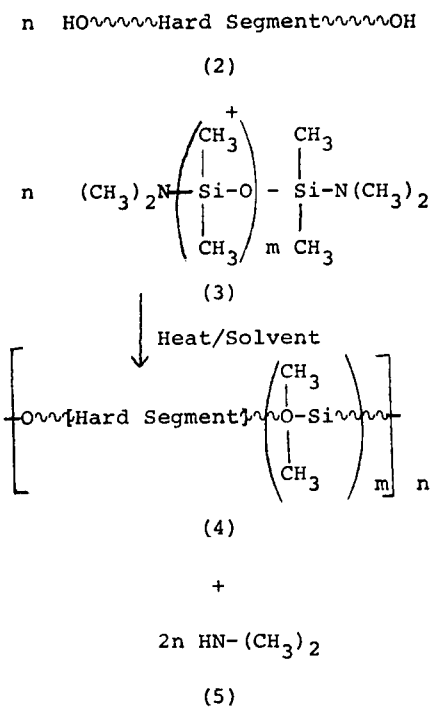

(II)

only by-product formed is the volatile dimethylamine which is easily removed from the reaction mixture. The polymer can be isolated in the usual manner, e.g., coagulation or devolatilization. The reaction was found to proceed in ether-type solvents such as THF or in chlorinated aromatics. The latter yield higher rates and are preferred [20–22]. Phenolic hydroxyls have shown greater reactivity than aliphatic hydroxyls. For example, a bisphenol A terminated polyaryl ether oligomer (6) of a number average

TABLE II
Mechanical Properties of the Siloxane Containing Block copolymer Elastomers at Room Temperature [1, 2]

No.	Weight % Siloxane	Tensile Modulus psi	100% Modulus psi	300% Modulus psi	Tensile Strength psi	Elongation at Break,%
1	50	35,000	1,800	2,500	3,300	410
2	66	1,200	575	1,000	1,300	435
3	78	100	101	400	1,030	995
4[a]	50	40,000	1,200	-	1,900	210
5	65	2,900	900	1,500	1,800	475
6	62	12,000	1,300	-	1,325	115
7	50	70,000	2,300	3,300	3,600	350
8	68	2,300	1,120	-	1,500	190
9[a]	54	7,000	750	1,700	2,100	360
10	53	30,000	1,300	2,300	2,300	300

[a] Compression molded at 270°C. All other test specimens were films cast from chloroform.

molecular weight of 5000 (Dp $\simeq$ 12) when reacted with a dimethylamino

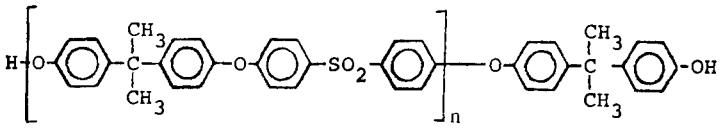

(III)

(6)

terminated polydimethylsiloxane oligomer of a similar $\overline{M}n$ in chlorobenzene solvent at 70°C gave high polymer within minutes [20]. On the other hand, analogous reaction utilizing a hydroxy-capped poly (α-methylstyrene) (7) oligomer required a much higher temperature and longer time in order to proceed to completion [14]. Clearly, since the oligomers contain

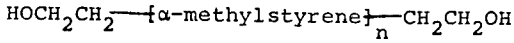

(IV)

(7)

mutually reactive groups, ideally alternating copolymers are obtained. It is, of course, essential that the molecular weights of the oligomers be known with precision. Appropriate characterization methods (e.g., potentiometric titrations and vapor pressure osmometry) were developed.

The following hard segments were utilized for the work described in this paper.

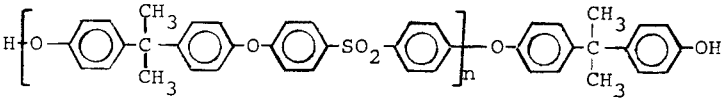

(6)

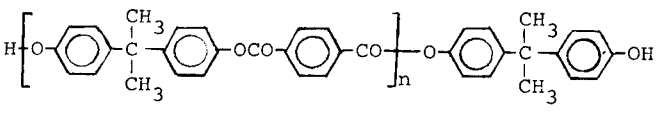

(V)

(8)

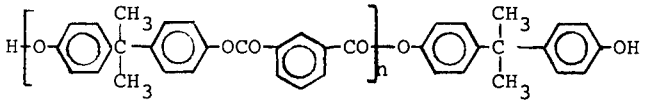

(9)

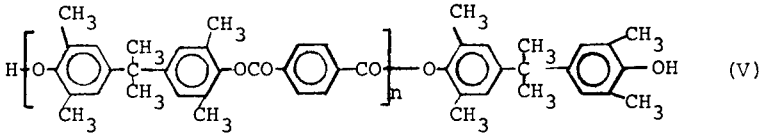

(V)

(10)

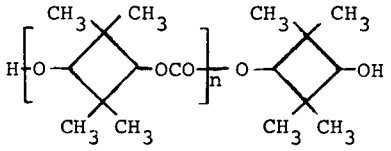

(11)

EXPERIMENTAL

Oligomers

The preparation of (6) is described elsewhere [20]. The hard segments (8), (9), and (10) were prepared by the non-catalyzed high-temperature polycondensation [23] in refluxing 1,2,4 trichlorobenzene of the bisphenol with the appropriate phthaloyl chloride. Bisphenol A was high purity Union Carbide grade recrystallized from toluene, mp = 157°C; the tetramethyl bisphenol A was prepared as described by Curtis et al. [24], mp = 166°C after recrystallization from benzene. Iso-and terephthaloyl chlorides were purchased from Matheson, Coleman and Bell and recrystallized from hexane prior to use; their respective melting points were 43–44°C and 82–84°C. The preparation of oligomer (11) entailed the synthesis of 2,2,4,4-tetramethylcyclobutane-1,3-diol dichloroformate (13) followed by its condensation with the diol (12) as shown in equation (VI).

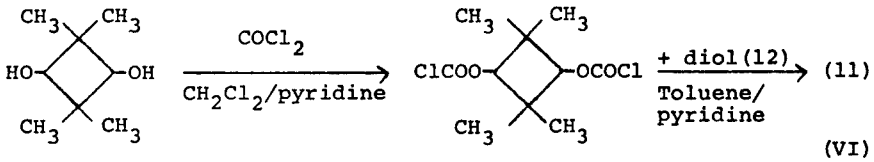

(12) (13) (VI)

Details of the preparation can be found in a recent patent [25].The molecular weights of the hard segments were regulated by employing a calculated excess of the dihydroxy reactant and were within the range of 2,000–10,000.

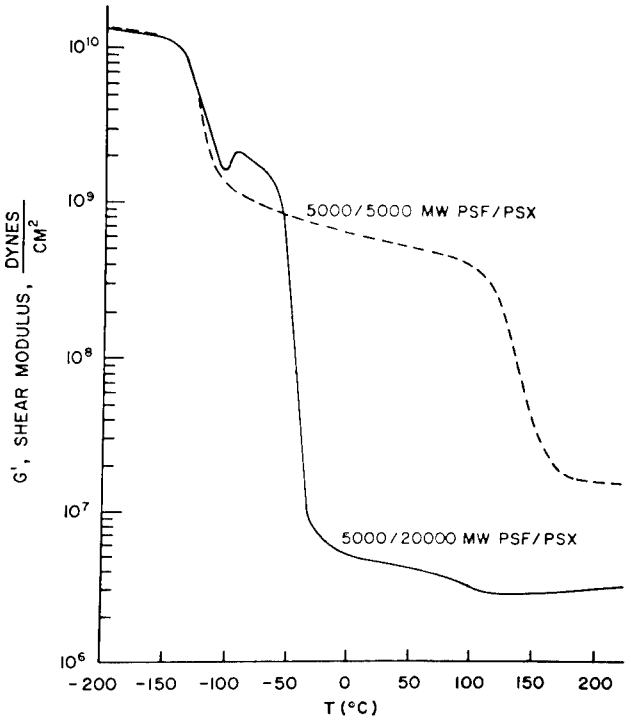

FIG. 1. Shear modulus curves for two different polysulfone–polydimethylsiloxane block copolymers.

The siloxane oligomers that were used were received from Union Carbide Silicones Division and had molecular weights also in the range given above.

Block Copolymers

All of the block copolymers derived from the polyaryl ethers and esters were synthesized in chlorobenzene as described previously [20–22, 26]. The preparation of the cyclo-aliphatic polycarbonate-polysiloxane analog required more stringent conditions and/or longer reaction times due to the presence of the sterically hindered and less acidic hydroxyl function. For preparative details, see reference [25].

Polymer Characterization and Properties

All polymers were characterized by determining their reduced specific viscosity (RV) in $CHCl_3$ at 25°C at a concentration of 0.2g/100ml. In a number of cases, silicone contents were determined by elemental analysis

(Galbraith Laboratories). The percent of Si determined was usually in good agreement with that calculated from the reactant charge. Gel permeation chromatography (Waters Instrument, THF solvent) was utilized to demonstrate that the presence of unreacted oligomers in the final polymers was negligible.

The properties discussed in this paper were obtained by well-known techniques. An Instron was used to determine the tensile strength and elongation. Dynamic-mechanical behavior was studied with a torsion pendulum at approximately 3 cycles/second to 0.1 cycles/second. Thermogravimetric analysis was performed using a Perkin Elmer thermogravimetric analyzer at 10°C/minute in air and in nitrogen. Additional information was obtained by differential scanning calorimetry (Perkin Elmer DSC 1B) at 10°C/minute. UV stability was determined by exposure to an R.S. sunlamp. Heat stability was studied on film samples suspended in a circulating air oven. Permeability to oxygen was measured as described in ASTM D-1434-66.

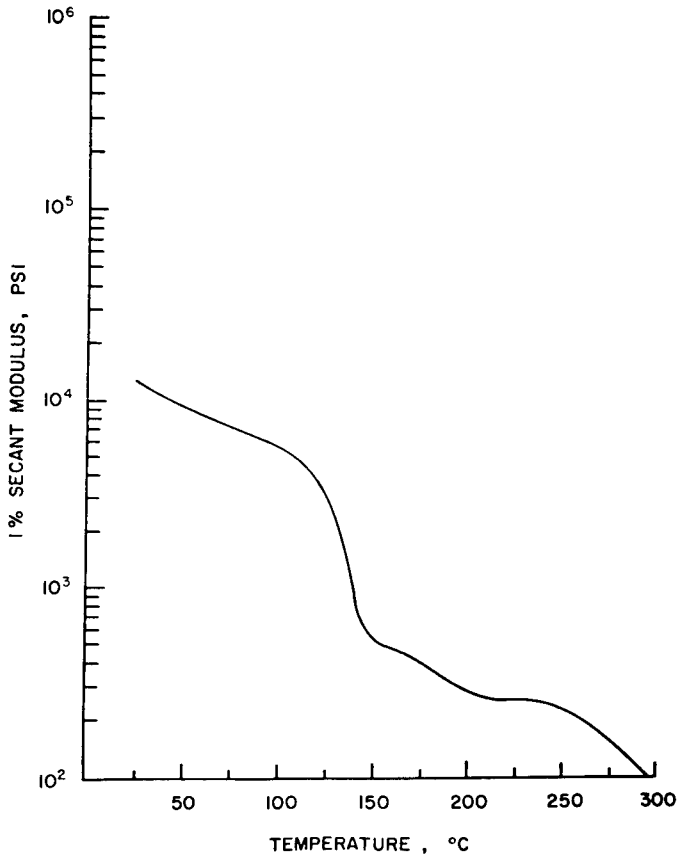

FIG. 2. Modulus-temperature relationship for a bisphenol A-terephthalate-polydimethylsiloxane block copolymer. Block molecular weights are 3,000 and 5,400.

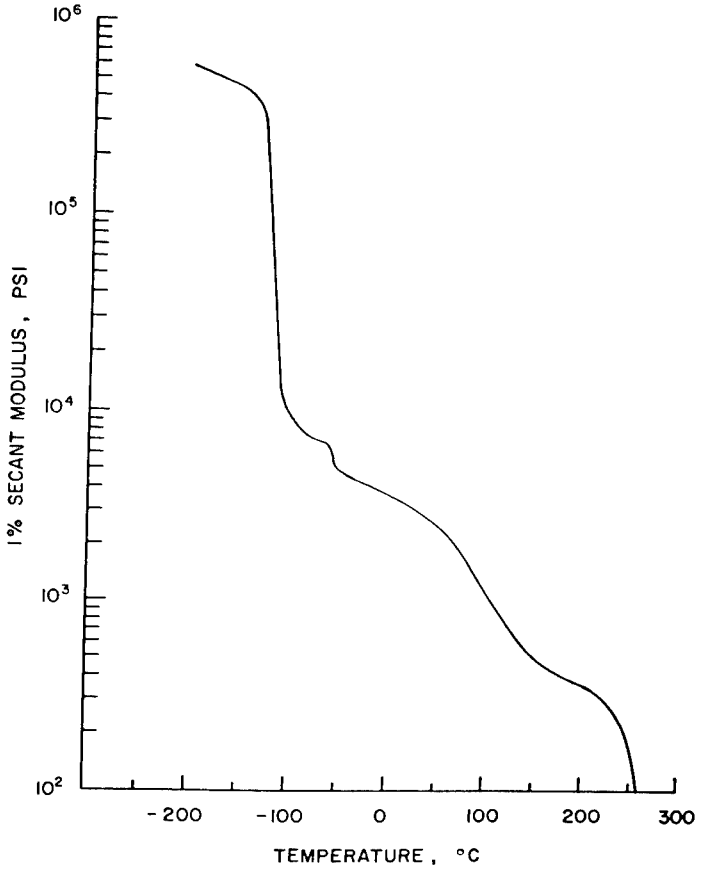

FIG. 3. Modulus–temperature relationship for a bisphenol A–isophthalate-polydimethylsiloxane block copolymer. Block molecular weights are 2,800 and 4,600.

DISCUSSION

The silicone based thermoplastic elastomers which are the subject of this paper are summarized in Table I. All of the polymers yielded transparent cast or molded films. Transparency was retained after annealing at elevated temperatures.

The mechanical properties of the polymers 1–10 are listed in Table II. The data shows that very good elastomeric response was realized in most of the cases. Note that silicone rubbers are generally very weak materials [5, 6]; thus, one sees the improvement in toughness that can be achieved via incorporation of the glassy or crystalline hard microdomains into a siloxane matrix. Stress–relaxation data for polymer [3] was obtained at 20% elongation. The relaxation time at 100°C was calculated to be 1×10^9 seconds which indicates the presence of a stable physical network in agreement with theoretical considerations [27–30]. Variation in 1% tensile modulus at ~50% siloxane content reflects the subtle changes in phase continuity that

can be observed with cast films in these systems [31]. On the other hand, no such dramatic changes in modulus are observed at higher elongations which is probably due to the disruption of the molecular order on extension.

The dynamic mechanical behavior of the polymers is shown in Figures 1–6. Due to the high degree of incompatibility of the soft and hard segments, a two-phase microstructure is developed at relatively low block molecular weight. The phenomenon is illustrated in Figure 1. It can be seen that at a molecular weight as low as 5,000, the block copolymer displays an upper Tg of 160°C which is the expected value for the poly (aryl ether) of that chain length [31].

The development of crystallinity was observed with the polyesters 5 and 6, and the polycarbonates 9 and 10. All transitions, including the crystalline melting points of both the hard and the soft segments, were noted. Moreover, DSC measurements have also confirmed the presence of crystallinity in polymers 9 and 10. The high damping and the temperature interval between transitions (Fig. 6) are very unusual and will be discussed in depth in a forthcoming paper.

Thermogravimetric analysis was carried out in air and in nitrogen on polymers 1, 5, 7, and 10. Based on the temperature at which weight loss

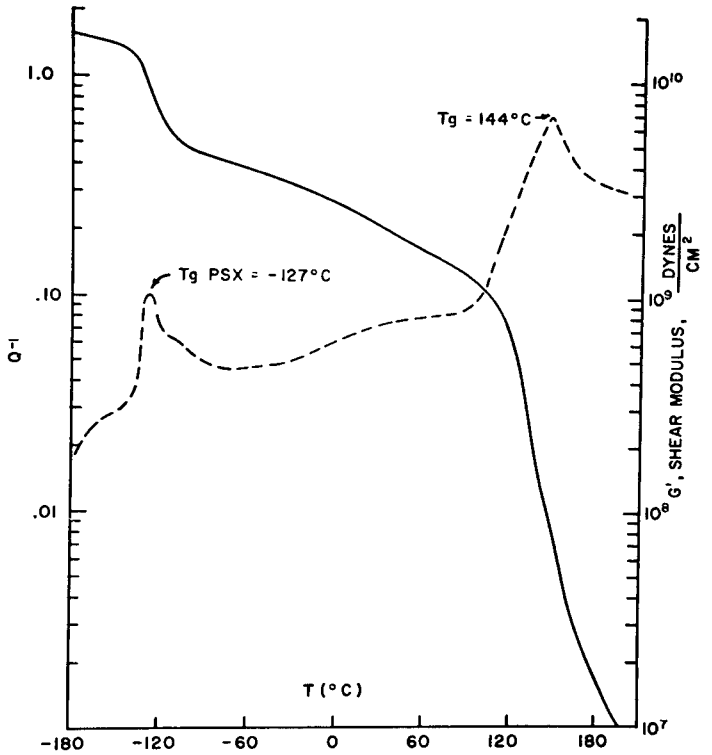

FIG. 4. Dynamic mechanical behavior of a tetramethyl bisphenol A–terephthalate–polydimethylsiloxane block copolymer. Block molecular weights are both 2,000.

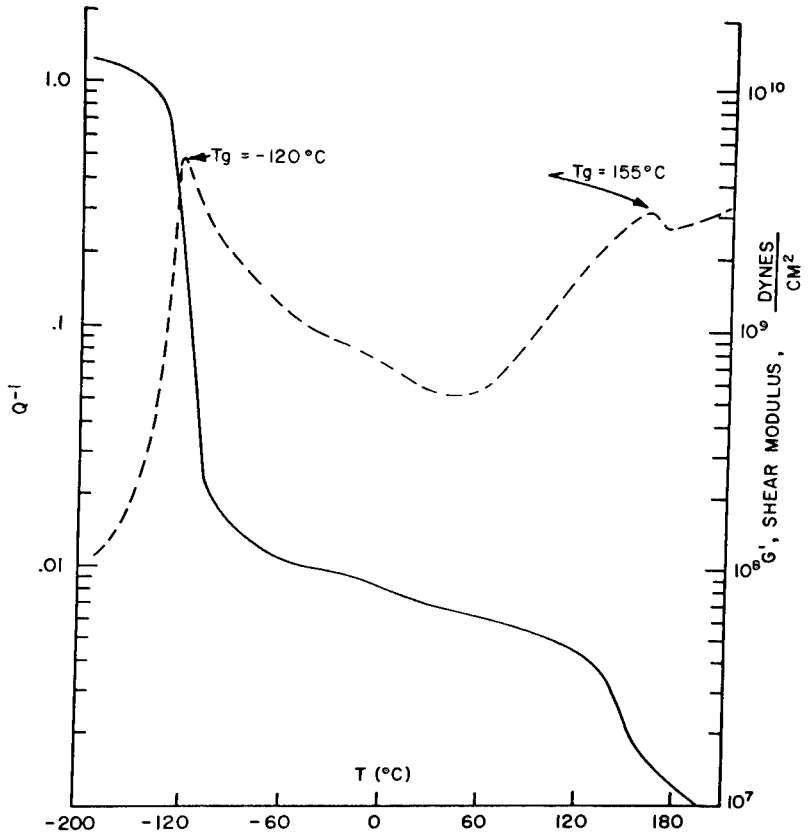

FIG. 5. Dynamic mechanical behavior of a tetramethyl bisphenol A–terephthalate–polydimethylsiloxane block copolymer. Block molecular weights are 2,000 and 5,000.

started, the stability in nitrogen (Fig. 7) decreased in the following order: poly(aryl ether) > poly(bisphenol A terephthalate) $\simeq$ poly(tetramethyl bisphenol A terephthalate) > poly(tetramethylcyclobutylene carbonate).

The same order prevailed when the copolymres were heated in air (Fig. 8) except that the material containing poly(bisphenol A terephthalate) had better thermal-oxidative stability than the one containing the poly(tetramethyl bisphenol A terephthalate). The latter finding suggests the potential utility of this methylated bisphenol in those instances where crosslinking by peroxides or irradiation might be desired. Polymers prepared from unsubstituted bisphenols are quite resistant to these treatments [32].

Thermal aging studies in air showed that materials 1–3 retained their properties for more than 1000 hours at 170°C. Even the "less stable" elastomers [9] and [10] still retained at least 80% of their initial tensile strength and 90% of their initial elongation after 1000 hours at 150°C.

Another important criterion in elastomers for extreme environments is their stability to ultraviolet light. This is especially important if one wishes to retain transparency (e.g., avoid the use of pigments such as carbon black, etc.). Our data has confirmed the expectation that the copolymers

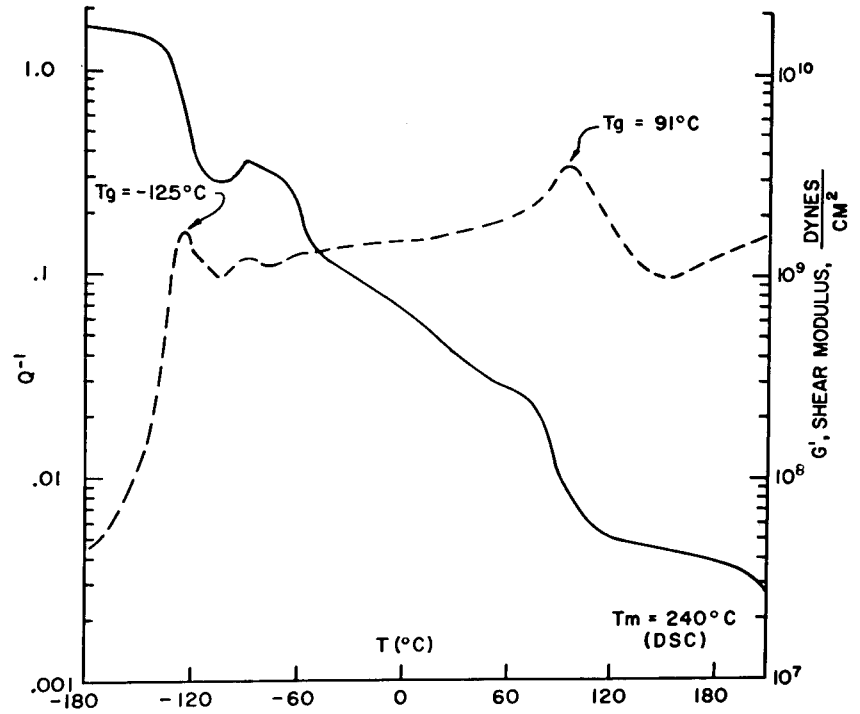

FIG. 6. Dynamic mechanical behavior of a cycloaliphatic polycarbonate–polydimethylsiloxane block copolymer. Block molecular weights are 8,000 and 10,000.

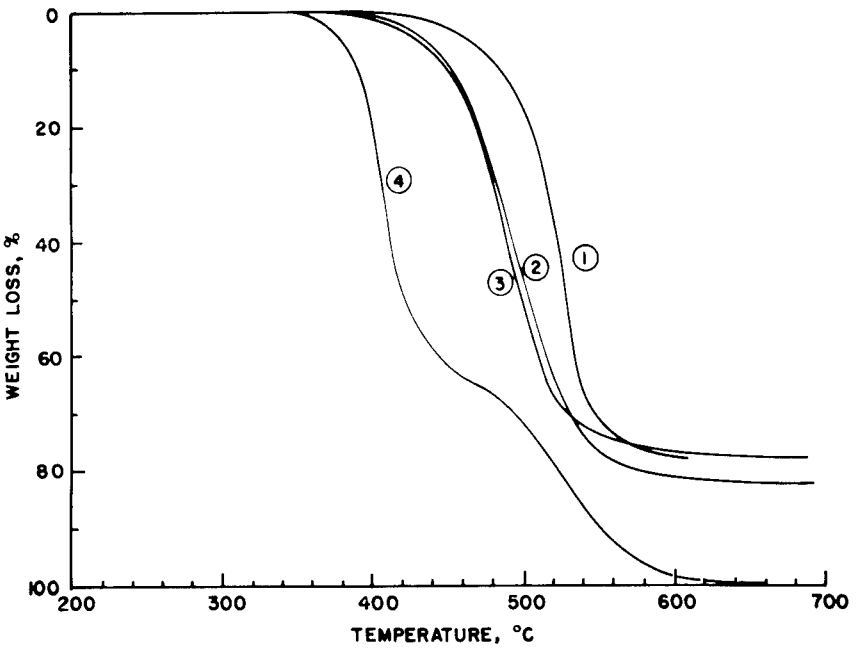

FIG. 7. Thermal stability of siloxane block copolymers in nitrogen (10°C/minute): 1, polysulfone–polydimethylsiloxane; 2, poly (bisphenol A terephthalate)–polydimethylsiloxane; 3, poly(tetramethyl bisphenol A terephthalate)–polydimethylsiloxane; and 4, cycloaliphatic polycarbonate–polymethylsiloxane.

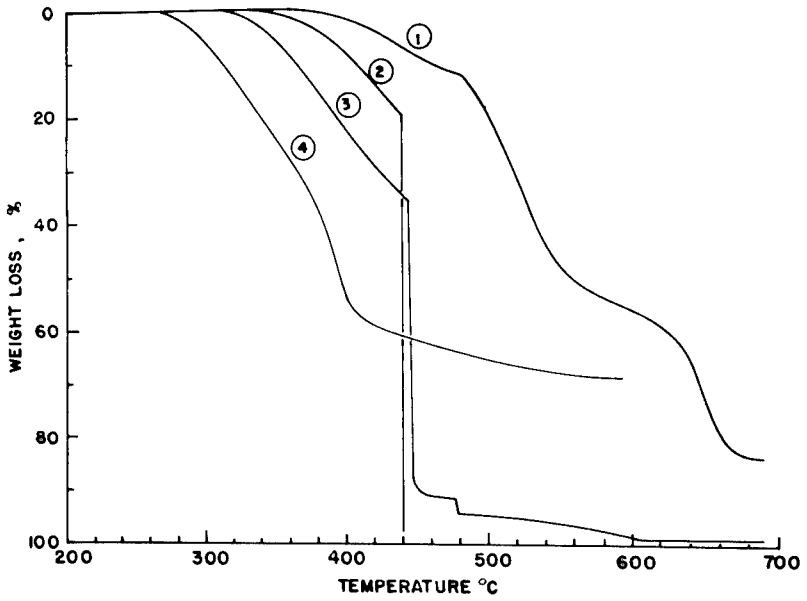

FIG. 8. Thermal and oxidative stability of siloxane block copolymers in air (10°C/minute): 1, polysulfone–polydimethylsiloxane; 2, poly (bisphenol A terephthalate)–polydimethylsiloxane; 3, poly(tetramethyl bisphenol A terephthalate)–polydimethylsiloxane; 4, cycloaliphatic polycarbonate–polymethyl–siloxane.

containing the aromatic moieties had only limited usefulness in this regard. However, the cycloaliphatic polycarbonates 9 and 10 indicated excellent performance in accelerated testing. For example, after eight weeks under the R.S. sunlamp, the tensile strength actually increased by 15% while elongation at break was unchanged.

All of the elastomers examined showed remarkable hydrolytic stability even after prolonged (four to eight weeks) treatment in boiling water. This is surprising in view of the generally accepted idea that silicon–oxygen–carbon linkages are hydrolytically unstable [2, 33]. It is our view that the phenomenon must be closely related to the steric hindrance of

TABLE III
Oxygen Permeability of the Siloxane Containing Block Copolymer Elastomers

No.[a]	% Siloxane	Oxygen Permeability cc(STP/cm-sec -cm Hg)
Silicone Rubber Control	-	5.0×10^{-8}
1	50	2.1×10^{-8}
2	66	2.6×10^{-8}
3	78	4.4×10^{-8}
9	54	2.1×10^{-8}

[a] See Table I for structures.

the Si—O—C bond and to the two-phase character of the polymers in question.

Oxygen permeability was also of interest and was measured on several samples. The data are listed in Table III.

A detailed discussion of the parameters relating oxygen permeability to micromorphology in silicone block copolymers has been recently developed [31].

CONCLUSIONS

Several types of silicone containing block copolymer elastomers have been prepared. A general synthetic method which involves the coupling of hydroxyl-terminated organic hard blocks with amino-terminated siloxanes was utilized to synthesize the materials. Both aromatic polyesters and polyethers as well as cycloaliphatic polycarbonates were incorporated into the novel elastomers. The latter displayed excellent thermal oxidative and hydrolytic stability combined with good mechanical properties. Outstanding ultraviolet stability was observed for the transparent elastomers containing the cycloaliphatic polycarbonate.

The authors would like to thank Dr. B. L. Joesten for the thermogravimetric analysis results and Dr. M. T. Shaw for the Stress-relaxation measurements.

REFERENCES

[1] R. F. Boyer, *Rubber Reviews, 36*, 1303 (1963); R. F. Boyer, "Changements de Phases," p. 383, published by Soc. de Chimie Physique, Paris, 1952.
[2] F. M. Lewis, *Rubber Reviews, 35*, 1222 (1962).
[3] S. B. Hamilton, Jr., "Silicone Technology", Applied Polymer Symposia No. 14, Interscience, (1970).
[4] H. K. Lichtenwalner and M. N. Sprung, "Encyclopedia of Polymer Technology," Vol. 12, 464 (1970).
[5] E. R. Bartholomew, G. R. Eykamp, and W. E. Gibbs, *Rubber Reviews, 32*, 1587 (1959).
[6] D. K. Thomas and B. B. Moore, *Polymer, 13*, 109 (1972).
[7] J. C. Saam, D. J. Gordon, and S. Lindsey, *Macromolecules, 3*, 1 (1970).
[8] J. W. Dean, *J. Polym. Sci., Part. B*, 8, 677 (1970).
[9] W. G. Davies and D. P. Jones, I and EC Prod. *Res. Develop. 10*, 168 (1971).
[10] J. C. Saam and F. W. G. Fearon, I and EC Prod. *Res. Develop., 10*, 10 (1971).
[11] M. J. Owen and T. C. Kendrick, *Macromolecules, 3*, 458 (1970).
[12] P. C. Juliano, U.S. 3,663,650 (to General Electric), May 16, 1972.
[13] P. C. Juliano, D. E. Floryan, R. W. Hand, and D. D. Karttunen, 19th Sagamore Conference on Block and Graft Copolymers, September 5-8, 1972; to be published by Syracuse University Press.
[14] A. Noshay, M. Matzner, G. Karoly, and G. B. Stampa, *Polym. Prepr., 13*, No. 1, 292, (1972).
[15] R. P. Kambour, p. 263 in "Block Polymers", S. L. Aggarwal, Ed., Plenum Press, (1970).
[16] H. A. Vaughn, *J. Polym. Sci., Part B, 7*, 569 (1969).
[17] D. G. LeGrand, *J. Polym. Sci., Part B, 7*, 579 (1969).

[18] R. P. Kambour, *J. Polym. Sci., Part B, 7*, 573 (1969).
[19] D. G. LeGrand, *Trans. Soc. Rheol., 15*, 541 (1971).
[20] A. Noshay, M. Matzner and C. N. Merriam, *J. Polym. Sci., A-1, 9*, 3147 (1971).
[21] A. Noshay, M. Matzner and C. N. Merriam, *Polym. Prepr. Am. Chem. Soc. Div. Polym. Chem. 12*, No. 1, 247 (1971).
[22] A. Noshay and M. Matzner, U.S. 3,539,657 (to Union Carbide) November 10, 1970.
[23] H. G. Weyland, C. A. M. Hoefs, K. Yutema and W. J. Mys, *Europ. Polym. J., 6*, 1339 (1970).
[24] R. F. Curtis, *J. Chem. Soc.*, 415 (1968).
[25] M. Matzner and A. Noshay, U.S. 3,579,607, May 18, 1971.
[26] M. Matzner, A. Noshay and R. Barclay, Jr., Canadian Patent No. 864,020 (to Union Carbide), February 16, 1971.
[27] M. Morton, J. E. McGrath and P. C. Juliano, *J. Polym. Sci., Part C*, No. 26, 99 (1969).
[28] "Block Copolymers", edited by J. Moacanin, G. Holden and N. W. Tschoegl, *J. Polymer Sci., Part C*, No. 26, (1969).
[29] "Block Copolymers", edited by S. L. Aggarwal, Plenum Press, (1970).
[30] M. Morton, "Styrene-Diene Block Copolymers", *Encyclopedia of Polymer Technology*, Vol. 15, 508 (1971).
[31] L. M. Robeson, A. Noshay, M. Matzner and C. N. Merriam, *Die Angewandte Makromolekulare Chemie, 29/30*, 47 (1973).
[32] A. R. Lyons, M. C. Symons and J. K. Yandell, *Makromol. Chem., 157*, 103 (1972).
[33] K. D. Steffen, *Angew. Makromol. Chem., 24*, 21 (1972).

RECENT ADVANCES IN ELASTOMER SERVICE-LIFE PREDICTION*

R. F. LANDEL, R. F. FEDORS, and J. MOACANIN

Jet Propulsion Laboratory,
California Institute of Technology,
Pasadena, California 91103

SYNOPSIS

The mechanical properties of an elastomer, including rupture and its time dependence, are defined uniquely by a "tensile property surface" in normalized stress–strain–time coordinates. In practice, the "property surface" is determined from short time constant strain-rate uniaxial tests. By using the time reduction properties of both temperature and crosslink density, an effective time scale of over ten decades of log time can be covered. Changes in crosslink density, filler content, or swelling do not affect the limits of the "property surface" when plotted in logarithmic coordinates but merely shift their positions. The shape, however, may be modified in certain cases.

The service life of an elastomer in the absence of aging reactions can be estimated from the "property surface," especially its limits, along with the knowledge of expected in-use conditions such as strains (static or dynamic).

When an elastomer experiences aging reactions, some of the parameters will change with time in a manner determined by the kinetics of the aging reactions. Consequently, the position of the "property surface" will shift with time. The parameters which are of primary interest are crosslink density and the extent of plasticization (sol fraction, swelling, etc.). This means that the performance of an elastomer can be anticipated from the knowledge of the kinetics of changes of very few parameters.

INTRODUCTION

The mechanical properties of an amorphous elastomer including rupture and its time dependence are uniquely defined by what we call a tensile property surface—a surface in normalized stress–strain–time coordinates [1]. Therefore, we shall first describe what a tensile property surface is, what this surface means in terms of rupture behavior, and how it depends on things like chain concentration (or, if you will, crosslink density), on the amount of filler and on the concentration of plasticizer. We will tend to restrict our remarks to the effects of chain concentration, for we have

* This paper presents the results of one phase of research carried out at the Jet Propulsion Laboratory, California Institute of Technology, under Contract No. NAS7-100, sponsored by the National Aeronautics and Space Administration.

Applied Polymer Symposium No. 22, 157–168 (1973)

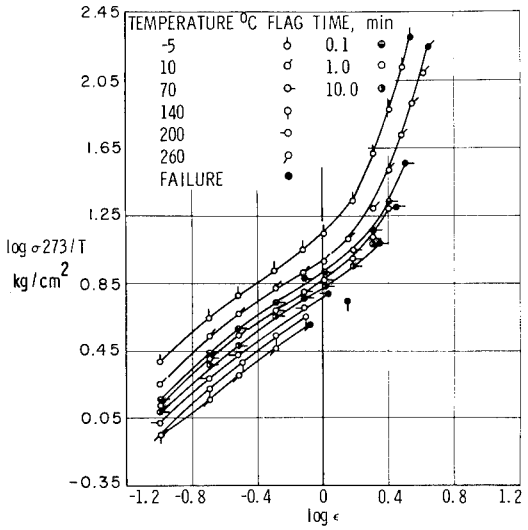

FIG. 1. Stress-strain curves, plotted logarithmically, for a Viton elastomer [1].

done more work in this area than on the other two factors—filler content and plasticizer. Nevertheless, we are confident that the effect of these two variables will follow the lines which we will indicate in this paper. After describing what a tensile property surface is, we would like to show that this is a universal surface. That is, it is independent of the type of elastomer that you have—whether hydrocarbon or fluorocarbon, whether it contains only C—C or C—C plus C—O or C—N bonds, or even if it contains no C—C bonds at all as in siloxane polymers. It is applicable to any elastomer. It depends only on the fact that one has a network. Finally, we will indicate some important consequences of this universality—especially those relevant to aging and service life prediction.

DISCUSSION

What do we mean by a tensile property surface? As indicated above, this refers to the mechanical properties as a function of stress, of strain, and of time, although by time here we shall mean temperature-reduced time. If we

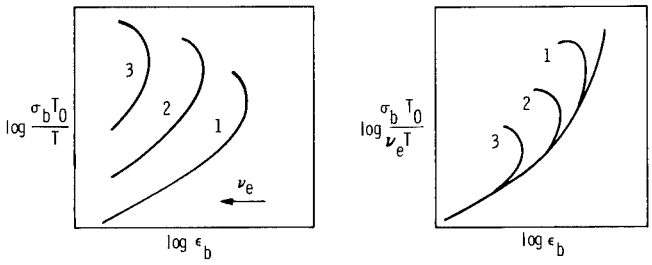

FIG. 2. Failure envelopes, schematic, for an elastomer at three crosslink densities before and after reduction or normalization of the breaking stress to unit chain concentration. T_o/T represents the usual temperature correction factor and the ρ_o/ρ term has been omitted.

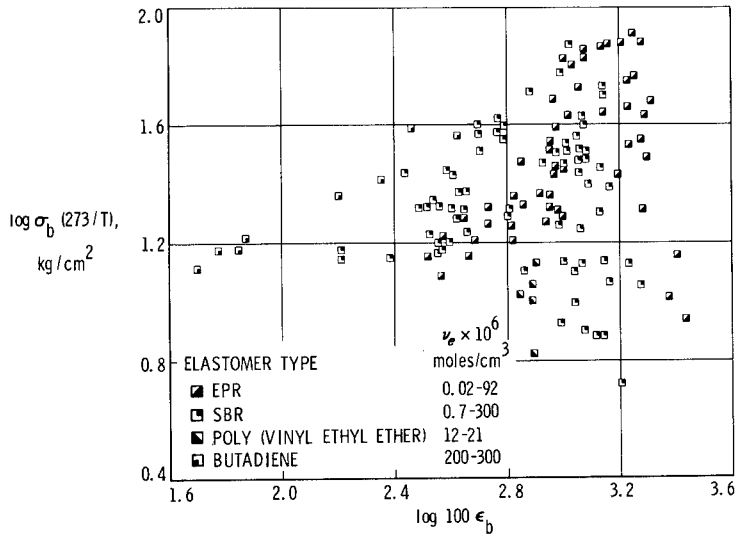

FIG. 3. Rupture data at various strain rates and temperatures for four elastomers plotted as failure envelopes [5].

examine the mechanical properties, in this case the uniaxial stress-strain curves, as shown in Figure 1, we will obtain for any given elastomer a set of curves such as this, progressively displaced upward as the temperature is lowered. The terminal points on each of these stress–strain curves represent rupture. The envelope of all these failure points is called the failure envelope, a concept introduced a number of years ago by Thor Smith [2]. It will play an important role in examining the response. These stress-strain curves illustrate (primarily) the effect of changing the temperature at one strain rate. However, if we changed the strain rate at a given temperature,

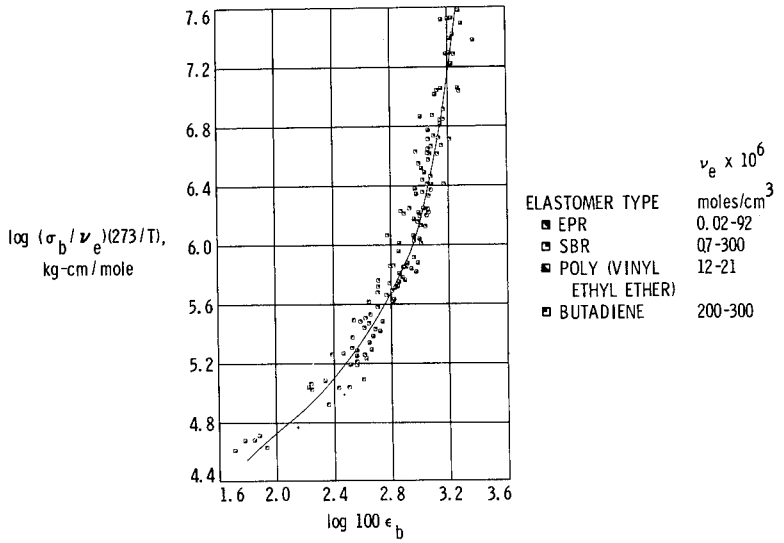

FIG. 4. Data of Figure 3 converted to reduced failure envelope [5].

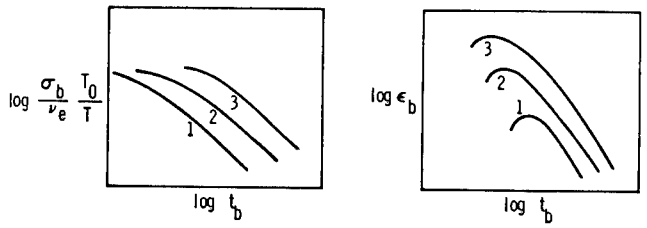

FIG. 5. Time dependence of the reduced breaking stress and of the breaking strain, schematic.

we would observe the same type of response with the curves now being displaced upward by an increase in test speed. If time were displayed on a third axis, a three-dimensional surface would result, hence the name "tensile property surface". Now we can ask ourselves, what should we expect to happen to the response if we lower the crosslink density or chain concentration? If we consider the stress-strain response *at the highest temperature* (Fig. 1), the stress at a very low value of the strain is proportional to the modulus. And we know that as the chain concentration decreases, the modulus will decrease. Therefore, we should expect the stress-strain curve to fall to a lower value. In the low temperature region, however, we are going toward the rubber-to-glass transition zone. It is known that the modulus in the transition zone is relatively insensitive to chain concentration [3, 4]. And we should expect these points to remain more or less fixed. If we consider only the failure envelope, the effects of the chain concentration are shown explicitly in Figure 2a for three different chain concentrations. Now it turns out from theoretical considerations that we should expect to find the breaking stress at a fixed value of the breaking strain to be directly proportional to the number of chains, in the high temperature region.* This is qualitatively understandable—the more chains you have in the network, the harder it is to break it. And so we proposed a number of years ago [1] that one could obtain a *reduced* failure envelope, as indicated in Figure 2b; that is, normalization of the breaking stress to unit chain concentration, by dividing by ν_e, should produce a set of curves which superpose in the manner indicated. We can illustrate this reduced failure envelope concept in the next two figures, in the first of which (Fig. 3) we will show the breaking stress as a function of breaking strain for four different elastomers, crosslinked to different extents. Here, contrary to expectation, one sees that there is no failure envelope, such as indicated in Figure 1, or even a common pattern of response, and there is no order, one might conclude that the concept of the envelope itself is something of a myth. However, note that there is quite a range of chain concentrations and, according to what we said above, we should normalize these data to a consistent value of ν_e, and more specifically to unit chain concentration. When we do this we find the results illustrated in Figure 4. Now the buckshot

* In the usual experiment at a fixed strain rate and temperature, however, both σ_b and ϵ_b change with ν_e and so σ_b is not proportional to ν_e, but passes through a maximum as it increases.

pattern *has* been reduced to a master curve. Moreover, the line drawn through these data is the reduced master curve obtained from tests in which the test speed or the test temperature were varied at constant chain concentration. The important point to note is that all of these different elastomer types give the same reduced failure envelope. Indeed, what is plotted here is the breaking stress *per chain* as a function of the breaking strain. And because this curve is independent of the chemical structure, we conclude that the breaking stress per chain is a unique, universal curve, dependent not at all on the chemical structure of the material, but only on the fact that the material is a network polymer. We shall not dwell on this important conclusion, but rather reemphasize the fact that in order to treat the effect on the stress-strain response of changing chain concentration, the stress should first be normalized to unit chain concentration.

But what about the effect of changing chain concentration on the time scale? This can be illustrated in Figure 5 where we show schematically both the breaking stress as a function of time and breaking strain as a function of time, again for three different chain concentrations. Notice that the reduction of the stress to unit chain concentration has no counterpart in the strain coordinate. Moreover, there is still a residual effect of chain concentration which shows up as a displacement of these curves along the time scale. Unfortunately, there is no molecular theory to guide one in accounting for this effect. On the other hand, it has been noted by Plazek [6] that a similar displacement along the time scale is found in the properties measured at very small strains (in the linear viscoelastic range). Specifically, he and Chasset and Thirion [7] have found that both compliance [6] and stress relaxation curves [7] can be transposed horizontally to superpose to a master curve. They call the time scale shift factor a_x, in analogy with the temperature time scale shift factor, a_T. Figure 6 indicates schematically what would happen in applying an a_x factor. The normalized breaking stress curves are all brought together to form a single curve, whereas only the high temperature portions of the breaking strain curves are superposed. It is known from other work, however, that the maximum value of the breaking strain is related to the square root of the chain concentration, [8–11] and so we should not expect a simple translation only along the time scale to lead to complete superposition. For our purposes,

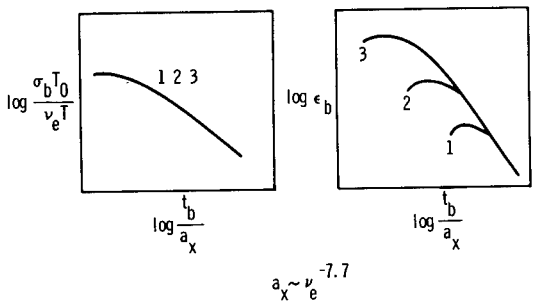

FIG. 6. Curves of Figure 5 after translation along the time scale by a factor a_x.

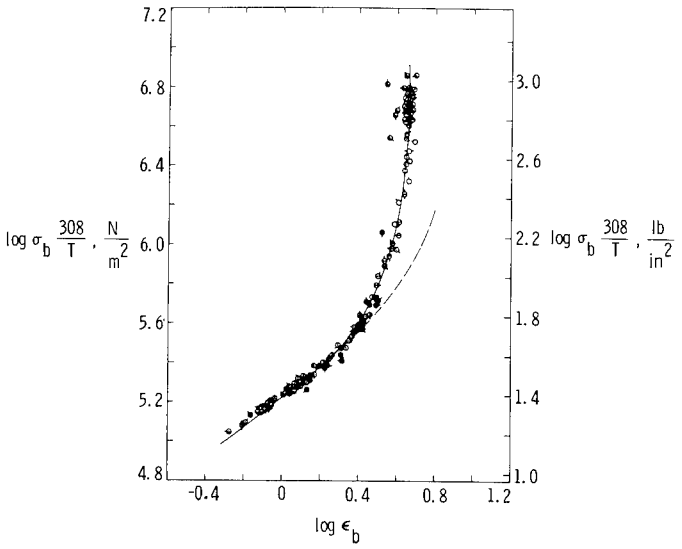

FIG. 7. Comparison of the predicted and the experimentally observed failure envelope for a methyl-trifluoropropyl siloxane elastomer.

however, we wish to concentrate on the superposed or master envelope of breaking strain against reduced time. Furthermore, we wish to point out the extreme dependence of a_x on chain concentration, namely, that it varies as the reciprocal 7.7 power of the chain concentration. [12]. This indicates an enormous sensitivity of break time to chain concentration. For example, for given strain conditions a decrease in the chain concentration by a factor of about two will shift these curves towards longer time and lead to

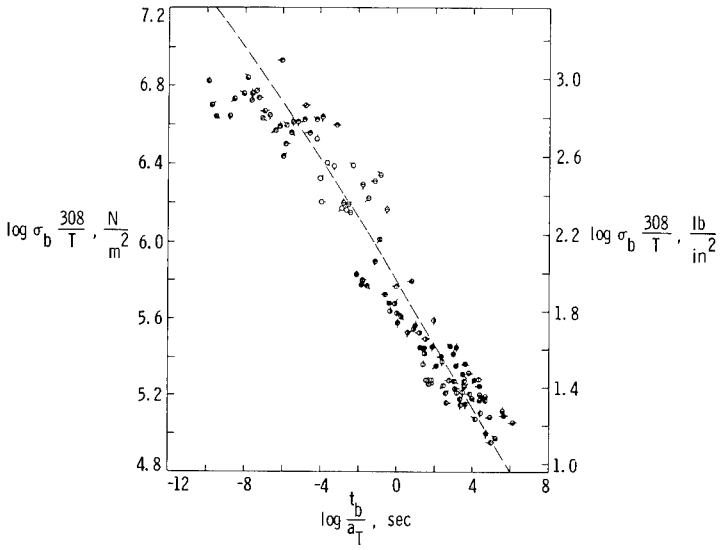

FIG. 8. Comparison of the predicted and experimental σ_b versus t_b response for the elastomer of Figure 7.

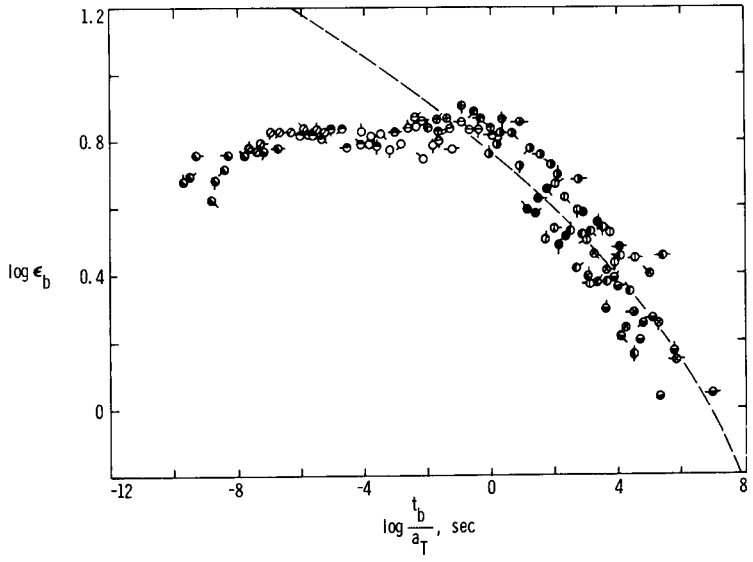

FIG. 9. Comparison of the predicted and experimental ϵ_b versus t_b response for the elastomer of Figure 7.

an increase in lifetime by a factor of roughly 250. These curves are, of course, schematic, drawn to indicate the principle involved. Let us now examine some actual failure data, for a fluorosilicone elastomer [13], and let us consider plots in all three coordinate systems: stress versus strain, stress versus time, and strain versus time. The first of these (Fig. 7) is the failure envelope. The dashed line shows the mean reduced curve for all other elastomers. One can see the divergence of the two curves in the low temperature/high rate region as was indicated schematically earlier, in Figure 3. One should particularly note the lack of scatter in this plot and contrast that with time-to-break data as illustrated by stress-at-break plotted against time-to-break in Figure 8. Such scatter is characteristic of all breaking time response measurements. The width of this scatter band measured horizontally represents the statistical fluctuation to be expected

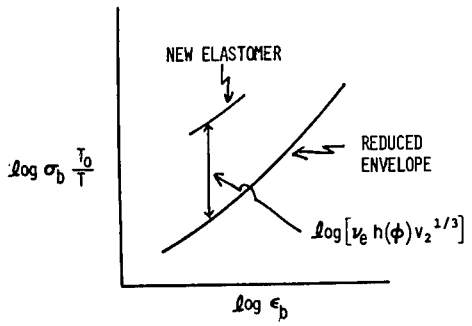

FIG. 10. Comparison of the response of a new elastomer with the master curve for the failure envelope.

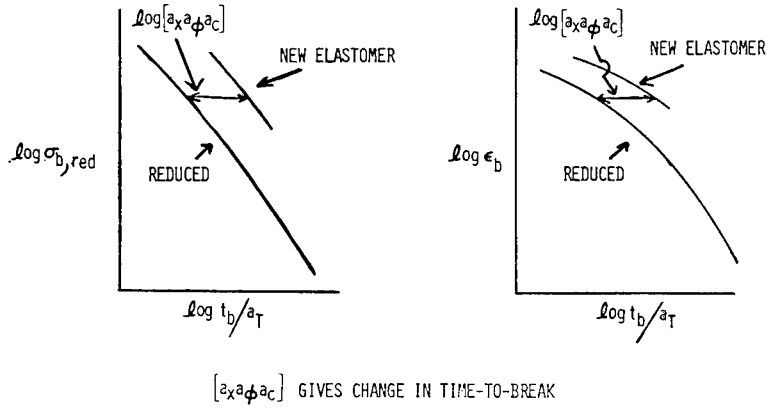

FIG. 11. Comparison of the break-time response of a new elastomer with the master curves.

in the break times measured at constant stress. Again, the dashed line is a master curve drawn from the composite results obtained with a variety of other elastomers. It is important to note that the shapes are identical within experimental error. The breaking strain versus time plot, Figure 9, also shows a master curve based on the results for a variety of other elastomers. The divergence between this and the experimental data, previously shown schematically in Figure 6, is analogous to that seen in Figure 7. The important point to note again is that in the region to the right of the maximum all elastomers give the same response. The dashed lines indicate a universal response, that is, a response which is independent of the nature of the polymer. All amorphous rubbers in this characteristic part of the time or temperature scale exhibit identically the same response. This statement is true not only for varied chain structure and chain concentration, but it also holds for varying plasticizers and filler content.

Having illustrated what is meant by the tensile property surface and how this surface is affected or moved around in stress–strain–time space by parameters such as change in crosslink density, how can we use this information? What good is it other than simply a way of economically representing data? One important consequence is that it should now be possible to determine properties of a new elastomer with far fewer tests, and hence to evaluate the response of such a new polymer far more economically. In principle, a single point determination of breaking stress and breaking strain should enable us to estimate the response over wide, wide ranges in time, temperature, or crosslink density. In fact, because of the statistical scatter one must make a number of tests and evaluate both the time dependence and the failure envelope in a limited range at a single crosslink density. Having done so, these results can now be compared with the master curves as indicated in Figures 10 and 11. In Figure 10, the vertical separation of the two curves reflects contributions from chain concentration, as indicated previously, but it can include contributions from filler, $h(\phi)$, or from plasticizer as well. In the latter case, the

contribution should be $v_2^{1/3}$ where v_2 is the volume fraction of rubber present. In Figure 11, the reduced breaking stresses are first calculated and then the separation along the time scale reflects the contributions due to chain concentration, a_x; to filler, a_ϕ; or to the concentration of plasticizer, a_c. Moreover, if the experimental data lies in the proper region on the time scale, the same horizontal shift factor should be found for both σ_b and ϵ_b data. The resulting curves (master superposed on experiment) can then be used to estimate the breaking response over much wider test conditions, thus providing a simple, speedy way to assess the new material.

A second important consequence or way of using the knowledge of how the tensile property surface is moved around, especially by the a_x shift, is to extend the time scale by changing ν_e just as we now extend it by raising the temperature. Raising the temperature has its limitations—we can only go to the point where degradation sets in. Now, however, there is a way of avoiding this limitation and extending the results to an otherwise inacessible time scale.

It is interesting to compare the extent of the shift caused by a raise in temperature with that produced by change in ν_e. For example, in a dimethyl siloxane specimen we investigated, the highest temperature we could work at was 160°C. At this temperature the reduced time scale for response at 35°C goes to about 20 years. To find the response at still longer times, it is only necessary to lower ν_e by a factor of two to extend the time scale by a factor of 250. To cause the same time-scale extension by raising the temperature would have required a 115° temperature rise to 274°, and since we were already operating close to the degradation limit in this sample, this would clearly have been impossible.

A third way of using the tensile property surface and its dependence on simple parameters is to investigate fatigue behavior. Fatigue can be carried

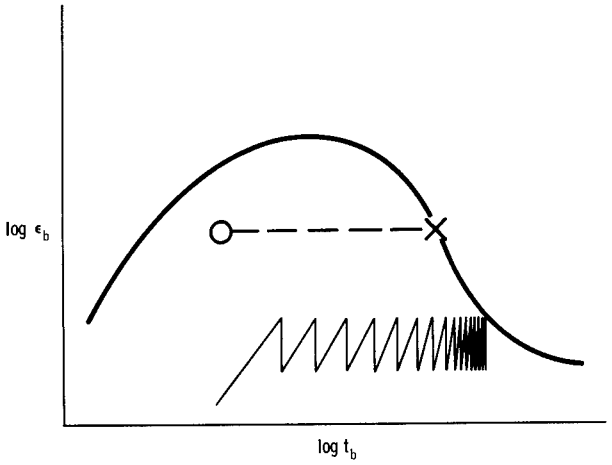

FIG. 12. Schematic representation of the breaking time as measured in constant strain rate tests (solid line) compared with the course of a fixed strain (dashed line) or a dynamic strain (sawtoothed line) fatigue test.

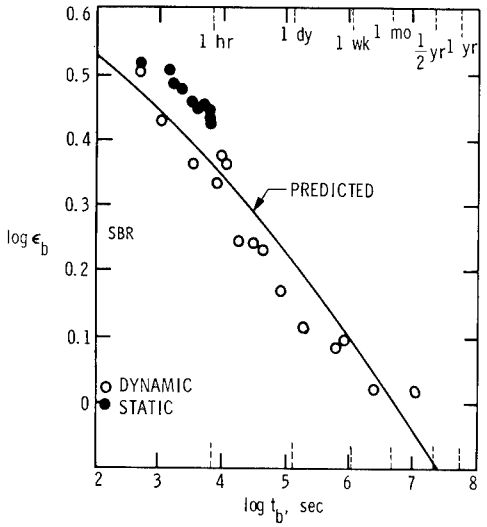

FIG. 13. Comparison of fatigue life of an SBR rubber with that predicted from short term, high temperature constant strain rate tests on entirely different samples [13].

out either under dynamic or static conditions and with varying stress or varying strain. We will illustrate the behavior with strain-at-break data. In Figure 12 the solid curve sketches the results for constant strain rate tensile tests. If the sample is strained to the point indicated by the circle, however, one could hold the strain fixed and as time passes one would traverse the horizontal line, and as the point x is approached, one could ask whether the sample should be expected to break. Conversely, the sample might be loaded under dynamic conditions, giving a resulting strain-time history somewhat as indicated by the sawtooth bar at the bottom of the sketch. Again, will the specimen break sooner or later than the time indicated by the solid line? It turns out that the failure times in the static fatigue tests carried out at fixed stress or strain are the same as those found in constant strain rate tests, within statistical scatter. The dynamic fatigue experiments can give rise to the same lifetime. In some cases, however, lifetime will be a

TABLE I
Ultimate Property Normalization Parameters

	$\sigma_b \frac{T_0}{T}$	ϵ_b	t_b/a_T
CROSSLINK DENSITY	ν_e	1	a_x
FILLER	$h(\phi)$	1	a_ϕ
PLASTICIZER (AND/OR SOL FRACTION)	$v_2^{1/3}$	1	a_c

function of the number of cycles instead of the total elapsed time, as would be indicated by Figure 12. (This may depend on where the initial point, i.e., the circle, is located with reference to the maximum in the solid curve.) Thus, for dimethyl siloxane, the fatigue behavior is related to the number of cycles of strain to which the sample is subjected [14] whereas for SBR, as shown in Figure 13, the dynamic and static results are in rather good agreement with each other and the curve predicted on the basis of the constant strain rate experiments describes the dynamic lifetimes extremely well [15].

Hence, it appears possible to estimate service life at time scales previously impossible to obtain.

To recap, Table I shows how data is to be treated in the normalization procedure discussed here. It can be seen that changes in crosslink density, filler, plasticizers, etc. will cause (primarily) a change in the σ_b scale without affecting ϵ_b. The latter statement is evidently only an approximation for ϵ_b, although it will hold for the long time behavior which we are interested in here. Similarly, a change in these parameters will cause a shift along the time scale.* Of these, only a_x has been extensively investigated, though it can be expected from the results of small strain dynamic studies that a_ϕ should depend on the nature of the filler, i.e., there would be a stronger shift factor from a highly reinforcing black than there would be from non-reinforcing glass beads.

However, all that has been said so far has presumed that there has been no degradation at long times. When this occurs additional effects on the behavior should be expected. However, the major effects of such degradation can now be either anticipated or investigated economically. For when an elastomer ages, some of the parameters will change with time in a manner determined by the course of the aging reactions. Consequently, the position of the "property surface" will shift with time. The parameters which are of primary interest are crosslink density and the extent of plasticization (sol fraction, swelling, effect on T_g, etc.). This means that the performance of an elastomer can be anticipated from the knowledge of kinetics of changes in only very few parameters. It should not be necessary to make extensive surveys of the effect of degradation on properties and lifetime. Rather, one should concentrate on the kinetics of the rate of chain scission or crosslinking or on the rate of sol production. Then a knowledge of the behavior of these more basic parameters would enable one to predict (or at least estimate to an order of magnitude) the major consequences of such aging reactions. Hence, rather than striking out blindly and making measurements to observe what will happen, one can now anticipate the key problem areas for his application and concentrate the necessary experimental program of measuring physical properties only in these critical areas, with a consequent much smaller expenditure of time and money.

* This is not to say that, for example, σ_b is proportional to ν_e or that ϵ_b is independent of ν_e. Rather, these are the factors which reduce data to a consistent basis for comparison.

REFERENCES

[1] R. F. Landel and R. F. Fedors, *Fracture Processes in Polymeric Solids, Phenomena and Theory*, B. Rosen, Ed., John Wiley & Sons, New York, 1964, Chapter 3B

[2] T. L. Smith, *J. Polym. Sci., A-1*, 3597 (1963).

[3] J. D. Ferry, *Viscoelastic Properties of Polymers*, John Wiley & Sons, New York, 1970.

[4] A. Tobolsky, *Properties and Structure of Polymers*, John Wiley & sons, New York, 1960.

[5] R. F. Fedors and R. F. Landel, *Proc. First Int. Conf. on Fracture,* T. Yokobori, T. Kawasaki, and J. L. Swedlow, Eds., Vol. 2, 1965, p. 1247.

[6] D. J. Plazek, *J. Polymer Sci., A-2, 4*, 745 (1966).

[7] R. Chasset and P. Thirion, *Physics of Non-crystalline Solids*, J. Prins, Ed., N. Holland Pub., Amsterdam, 1965, p. 345.

[8] R. F. Fedors and R. F. Landel, *Space Programs Summary, 37-37, Vol. 4*, Jet Propulsion Laboratory, Pasadena, California, Feb., 1966,p. 139.

[9] T. L. Smith, *Proc. of the Fourth Int. Congress on Rheol.*, E. H. Lee, Ed., Interscience Pub., New York, 1965, part 2, p. 525.

[10] F. Bueche, B. J. Kinzig, and C. J. Coven, *J. Polym. Sci., Polym. Lett., 3*, 399 (1965).

[11] J. Furukawa, A. Nishioka, and T. Kotani, *J. Polym. Sci., Polym. Lett., 8*, 25 (1970).

[12] R. F. Fedors, and R. F. Landel, *Space Program Summaries, 37-58, Vol 3*, Jet Propulsion Laboratory, Pasadena, California, Aug., 1969, p. 180.

[13] R. F. Fedors and R. F. Landel, unpublished results.

[14] J. Moacanin, E. F. Cuddihy, and R. F. Fedors, unpublished results.

[15] R. F. Landel and R. F. Fedors, *Mechanical Behavior of Materials, Vol. 3*, Soc. of Materials Science, Japan, 1972.

THE EFFECT OF DILUTE FLUORINE ON CERTAIN FLUOROPOLYMERS*†

DANIEL W. BROWN, ROLAND E. FLORIN and LEO A. WALL**

Polymer Chemistry Section,
Institute for Materials Research,
National Bureau of Standards,
Washington, D.C. 20234

SYNOPSIS

Various fluoropolymers were exposed to 5% fluorine in helium at 25°C and one atmosphere. About 10–100% as many fluorine molecules were charged as monomer units in each polymer. Certain polymers degraded as shown by decreases in their intrinsic viscosities. Degrading polymers had the structures

$\begin{pmatrix} CH_2CF \\ CF_3 \end{pmatrix}$, $\begin{pmatrix} CH_2CF \\ CF_3 \end{pmatrix}\begin{pmatrix} C_2F_4 \end{pmatrix}$ (1:4), $\begin{pmatrix} CHFCH \\ CF_3 \end{pmatrix}$, $\begin{pmatrix} CH_2CH \\ C_3F_7 \end{pmatrix}$, $\begin{pmatrix} CF_2CF{=}CFCF \\ CF_3 \end{pmatrix}$,

and

$$\begin{pmatrix} CF_3 \\ CH_2C \\ CF_3 \end{pmatrix}\begin{pmatrix} C_2F_4 \end{pmatrix} \text{ (1:4).}$$

The intrinsic viscosity of polyperfluoropropene was not changed. Other polymers cross-linked, as shown by formation of gel. These had the structures

$\begin{pmatrix} CH_2CH \\ CF_3 \end{pmatrix}$, $\begin{pmatrix} CH_2CH \\ CF_3 \end{pmatrix}\begin{pmatrix} C_2F_4 \end{pmatrix}$ (1:2), $\begin{pmatrix} CH_2CH \\ C_3F_7 \end{pmatrix}\begin{pmatrix} C_2F_4 \end{pmatrix}$ (1:3), $\begin{pmatrix} CH_2CH \\ C_6F_5 \end{pmatrix}$, $\begin{pmatrix} CF_2CF \\ C_6H_5 \end{pmatrix}$

and

$$\begin{pmatrix} CF_2CF \\ C_6F_5 \end{pmatrix}$$

In homopolymers the greater the hydrogen content the more likely the polymer was to crosslink, suggesting that crosslinking proceeds via abstraction of hydrogen atoms. However, an increased content of tetrafluoroethylene in copolymers also was associated with greater crosslinking or reduced degradation. Viton and a copolymer of 3,3,3-trifluoropropene gave highly crosslinked materials. The vulcanizates of Viton are quite resistive to stress relaxation at 250°C in air. Those of the trifluoropropene copolymer are very unstable.

* Supported in part by the Army Research Office, Durham.
† Contribution of the National Bureau of Standards, not subject to copyright.
** Deceased September 19, 1972.

Applied Polymer Symposium No. 22, 169–180 (1973)

INTRODUCTION

Exposure of polymers to dilute elemental fluorine generates radicals that may be observed by electron spin resonance [1,2]. Usually the spectra can be attributed to peroxy radicals and also to radicals on carbon probably having hyperfine interaction with fluorine. it is uncertain whether the oxygen of the peroxy radicals comes from the container or is that present as a contaminant in the fluorine. The radicals may react in various ways so the polymer is usually crosslinked or degraded. In this work the predominant process at 25°C was determined for several fluoropolymers. More detailed studies were made with a two to one copolymer of tetrafluoroethylene and 3,3,3-trifluoropropene and with a commercial fluoropolymer. Vulcanizates of these two polymers were subjected to thermogravimetric analysis and stress relaxation.

Others have treated polymers with fluorine [3–5]; generally large amounts were used and considerable replacement of hydrogen and addition to aromatic groups occurred. In our work, usually relatively little fluorine was used, since the intent was to affect the polymer without changing its constitution appreciably.

EXPERIMENTAL

Most of the polymers were prepared in radiation-induced polymerizations at high pressure [6]. Copolymer compositions were calculated from carbon contents determined in combustion analyses. Polymers obtained commercially were Viton*, the four to one copolymer of vinylidene fluoride and hexafluoropropene, and Kel F Elastomer 3700, the commercial 3.5 to 1 copolymer of vinylidene fluoride and chlorotrifluoroethylene. A sodium fluoride trap, fluorine pressure regulator, and cylinders of mixed fluorine and helium containing 5% of the former were purchased.

Polymers were hot pressed into films of desired thickness. Strips weighing 0.02–0.2 g were exposed to the fluorine mixture in batch or flow reactors. The apparatus as it finally evolved is shown in Figure 1. Copper is used except as noted. The fluorine mixture flows over sodium fluoride to eliminate residual hydrogen fluoride. It is then passed through a stainless steel U tube, which may contain polymer, to a cold trap that condenses any hydrogen fluoride formed. From there the gases flow over hot sodium bromide in a glass tube which forms bromine from the remaining fluorine [7]. It then enters a glass cold trap having glass-Teflon valves in which the bromine condenses. The helium volume is then measured by displacing water. The fluorine charged was calculated from this volume. The amount of

* Certain commercial materials are identified in this paper in order to adequately specify the experimental procedure. In no case does such identification imply that the material identified is necessarily the best available for the purpose. Viton and Teflon are trade names of E. I. duPont de Nemours & Co. and Kel F Elastomer is a trade name of Minnesota Mining & Manufacturing, Co.

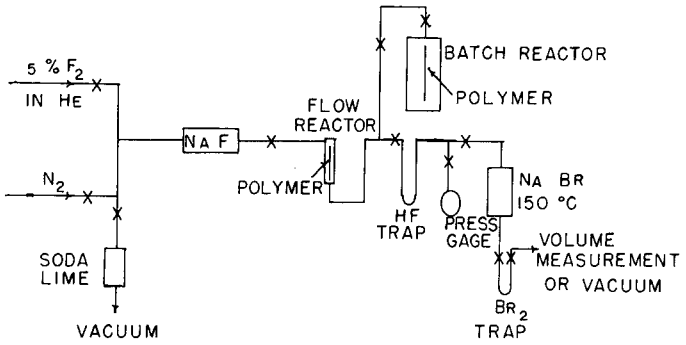

FIG. 1. Fluorination apparatus.

hydrogen fluoride was calculated from the pressure that developed on warming its trap to 25°C. The pressure in this trap was always below 10 cm, Hg, thus avoiding serious effects due to association. The bromine trap was warmed to room temperature and weighed to determine the bromine collected.

A 300-cc stainless steel batch reactor was often used instead of the U tube. After insertion of the polymer, it was evacuated and charged with the

TABLE I
Crosslinking of Polymers by Exposure to F_2[a]

Polymer	C_2F_4 mol %	Sol wt %	Swelling Ratio[b] Swollen wt/dry wt.	T_g[c] °C
CH_2CH CF_3	0	93	—	27
$(CH_2CH)(C_2F_4)$ CF_3	53	46	55	15
$(CH_2CH)(C_2F_4)$ CF_3	64	4.9	11.5	10
$(CH_2CH)(C_2F_4)$ C_3F_7	76	97	12	28
CH_2CH C_6F_5	0	63	95	105
CF_2CF C_6F_5	0	95	20	194
CF_2CF C_6H_5	0	70[d]	—	202
Viton	0	42	22	-50
Kel F Elastomer	0	51[e]	31[e]	—

[a] Polymer films 0.025–0.1 mm thick exposed for 20 hours at 25°C to 5 mole % F_2 in He. F_2 charged to reactor was 10 mole % of monomer units in polymer.

[b] In C_6F_6 at 25°C except as indicated.

[c] Determined by differential scanning calorimetry.

[d] In C_6H_6.

[e] In $C_2H_5COCH_3$.

TABLE II
Degradation of Polymers by Exposure to F_2 [a,b]

Polymer	C_2F_4 mol %	$[\eta]_0$[b] dl/g	$[\eta]$[b] dl/g	T_g[c] °C
$CH_2CF(CF_3)$	0	4.28	2.52	42
$(CH_2CF(CF_3))(C_2F_4)$	79	4.04	3.89	7
$CHFCH(CF_3)$	0	0.23	0.20	85
$CH_2CHC_3F_7$	0	0.63	0.43	58
$(CH_2C(CF_3)CF_3)(C_2F_4)$	80	2.62	2.16	50

[a] Polymer films 0.025–0.1 mm thick exposed for 20 hours at 25°C to 5 mole % F_2 in He.
[b] F_2 charged was 10 mole % of monomer units in polymer.
[c] In C_6F_6 at 29.8°C.
[d] By differential scanning calorimetry.

fluorine mixture to the desired pressure. At the end of the reaction it was vented to and finally evacuated through the traps. In our early runs, both reactors were used without the analytical system. For reactions above ambient temperature, the U tube was heated in water and the batch reactor detached and put in an oven.

The fluorine measuring capability was tested twice by passing mixture at 30cc/min through the system in the absence of polymer. Assuming that the nominal content of 5% fluorine is accurate, 3.7×10^{-4} mol fluorine was used in each case. The first passage generated 3.3×10^{-4} mole bromine and and 0.4×10^{-4} mole hydrogen fluoride. The second passage generated 3.8×10^{-4} mole bromine and 0.4×10^{-4} mole hydrogen fluoride. Apparently this method of measuring fluorine appears to have an uncertainty of about 10%. Probably the hydrogen fluoride formed in reaction between fluorine and hydroxyl groups on the walls.

TABLE III
Effect of 5% Fluorine on Polymers of Perfluoropropene and Perfluoropenta-1,3-diene

Polymer	$(CF_2CF(CF_3))$	$(CF_2CFCFCF(CF_3))$	
Conditions	Flowing Gas	Flowing Gas F_2: non Units = 3:1	Batch Reactor[a]
$[\eta]_0$, dl/g	0.38	0.68	0.68
$[\eta]$, dl/g	0.38	0.22	0.14
Wt. gain, %	0	8[b]	8[b]
Infra Red[c]	No peaks, 1500 -2000cm^{-1}	1710 cm^{-1} peak disappears 1770 cm^{-1} peak appears	

[a] Three months at 25°C.
[b] Saturation would give 18% gain.
[c] Ten percent solution in FC 75. Polymer scraped from outside of specimen.

Dry nitrogen was passed through the system when it was not in use. After a few operations the fluorine tank valve and pressure regulator did not shut completely. However, the needle valves provided with the regulator worked well and generally the system was well behaved. No evidence of vigorous reaction was found with any fluoropolymer. However, when the mixture was passed rapidly through a polyethylene tube, melting and charring were observed [1].

Hexafluorobenzene was generally used in determining the intrinsic viscosities, sol contents, and swelling ratios, as before [8]. Benzene and methyl ethyl ketone were used with poly α,β,β-trifluorostyrene and Kel F elastomer respectively, because neither polymer is soluble in hexafluorobenzene. The apparatus for stress relaxation has been described [9].

RESULTS

Before the analytical train was constructed, samples of several polymers were exposed simultaneously in the batch reactor. The initial fluorine concentration was 2×10^{-3} M/liter and the weights of polymer were

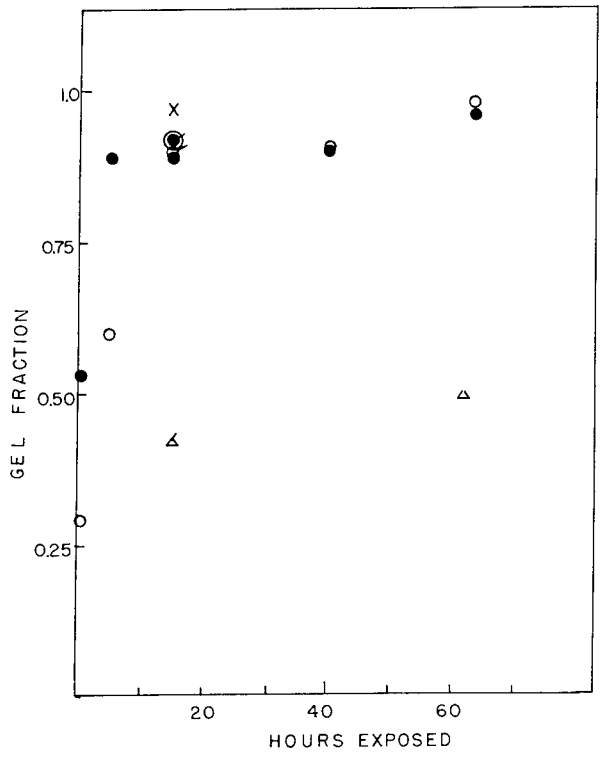

FIG. 2. Gel contents of fluorine-treated Viton. Temp = 25°C, $[F_2] = 3 \times 10^{3}$M/liter; ● is 0.002 in.; ○ is 0.006 in.; and △ is 0.036 in. Temp = 25°C, $[F_2] = 8 \times 10^{-3}$M/liter; ◐ is 0.002 in.; ◑ is 0.006 in.; and ◭ is 0.036 in. Temp = 100°C, Initial $[F_2] = 8 \times 10^{-3}$M/liter; × is 0.006 in.

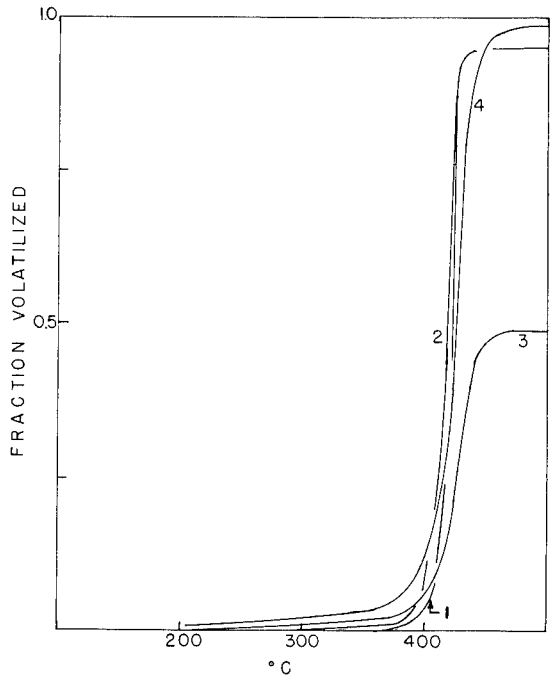

FIG. 3. Thermogravimetric analysis of Viton in vacuum. (1) Untreated; (2) F_2-treated; (3) Viton O-ring (4) O-Ring scaled for nonvolatiles.

chosen so that there were about ten times as many monomer units as fluorine molecules in the vessel. After 20 hours, the polymers were re-weighed, no changes being found, and then immersed in solvent. Those polymers which had crosslinked are listed in Table I along with their glass temperatures, Tg, sol contents, and weight swelling ratios. Gamma radiation also crosslinks these polymers. Table II lists the polymers that were degraded along with their Tg's and the initial $[\eta]_0$ and final $[\eta]$, intrinsic viscosities. Gamma radiation crosslinks the first two and degrades the next two polymers.

Since most of the degrading polymers have Tg's above 25°C, some were exposed at 100°C to see if increased mobility would permit crosslinking. This could increase degradation also if scissions follow H-atom abstraction. The first and second polymers listed in Table II crosslinked very lightly and the fourth polymer degraded. Our supply of the other two polymers was exhausted before the high temperature run was made.

Polymers of perfluoropropene and of perfluoropenta-1,3-diene were treated with relatively large amounts of fluorine at 25°C. Results are in Table III. The intrinsic viscosity of polyperfluoropropene was not affected not was its infrared spectrum changed. A spin resonance spectrum of the type described above was observed, indicating that some reaction occurred [2]. The polymer of the perfluoropenta-1,3-diene, which is thought to have the structure $\left(CF_2CF = CF—\underset{CF_3}{CF}\right)$, was degraded by fluorine. It gained

considerable weight and lost the infrared absorption band at 1710cm^{-1} characteristic of internal unsaturation, Also, a new band appeared at 1770 cm^{-1}; compounds containing carboxylic acid groups absorb in this region. Absorption due to acid fluoride groups occurs at 1890 cm^{-1}. None was observed before or after exposure.

In Table IV are results obtained by treating Viton with dilute fluorine for various times. In each case one fourth as many fluorine molecules were charged as monomer units in the polymer. If it substitutes for hydrogen, forming hydrogen fluoride, a 6% gain in polymer weight would be observed. The amounts of bromine and hydrogen fluoride collected are expressed in the unit molecules collected per monomer unit in the polymer. The gel fractions listed were used to calculate the approximate fraction of crosslinked monomer units from the theory of random crosslinking [10], assuming that no scissions occurred, that the initial weight average degree of polymerization was 10^4 [11], and that a most probable distribution was initially present. Weight swelling ratios are listed also. The bromine formed varies erratically; in one instance 85% of the fluorine was still present after 64 hours.

Since no weight gains were found (a 1% gain would have been detected) and since the fraction of crosslinked monomer units is trifling our conclusion is that the bulk of the fluorine that disappeared reacted with the reactor. The hydrogen fluoride formed also must come mostly from the reactor, since otherwise the amounts formed would have resulted in de-

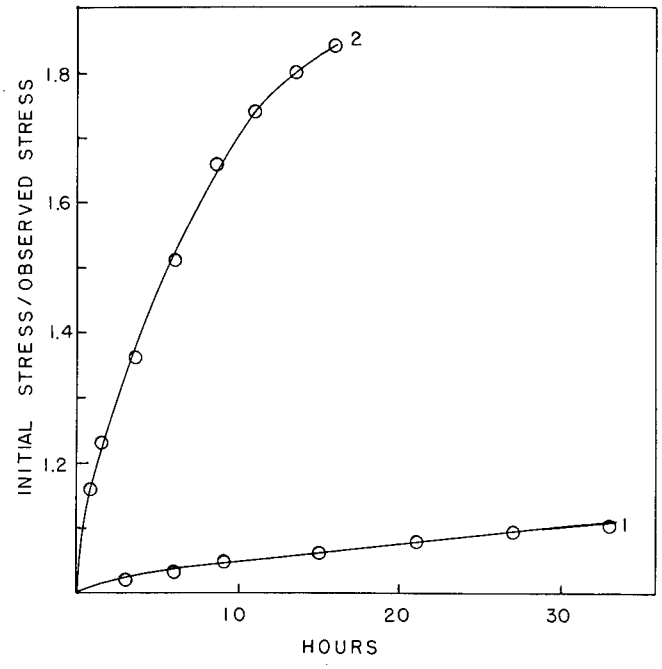

FIG. 4. Stress relaxation of F_2-treated Viton (0.006-in. thick) in air at 250°C. Curve 1: 64-hr sample; Table IV; and 18% elongation. Curve 2: 15-hr sample; Table IV; and 71% elongation.

TABLE IV
Effect of 5% Fluorine on Viton at 25°C

Time Hours	Br_2 Molecule/Monomer Unit	HF	Gel Fraction	X-Linked Units Fraction X 10^4	SR[b]
5	0.25	0.02	0.60	2	14
15	0.15	0.06	0.92	4.8	5.5
40	0.12	0.08	0.90	5.5	5.1
64	0.22	lost	0.98	12	4.3

[a] Initial $[F_2] = 3.3 \times 10^{-3}$ M/liter, molecules F_2/monomer unit = 0.25. Sample thickness = 0.006 in.

[b] Weight swelling ratio in C_6F_6.

tectable gains in polymer weight. The hydrogen fluoride formed is large when the bromine formed is small, indicating that varying amounts of moisture account for the erratic behavior.

If little fluorine reacts with the polymer, the total weight of the latter in a well passivated reactor is unimportant. Significant variables are exposure time, fluorine concentration, and thickness. In Figure 2 is shown the variation of gel fraction with exposure time for Viton samples of different thicknesses. At 5 hours, a 0.002-in. thick piece has more gel than a 0.006-in. piece. Between 15 and 64 hours, the gel contents are similar for these thicknesses. Pieces 0.035-in. thick have less gel even at 63 hours. In 15 hours, a 2.5 fold difference in fluorine concentration has little effect on gel contents at thicknesses of 0.002 and 0.006 in. Pieces 0.006 in. thick form more gel in 15 hours at 100°C than at 25°C. The gel formed had a swelling ratio of 13, whereas gels formed at 25°C in 15 hours and swelling ratios of 5.5–7.7.

Figure 3 shows results of thermogravimetric analyses in vacuum performed on untreated Viton, fluorine-treated Viton, and a portion of a

TABLE V
Effect of 5% Fluorine at 25°C a 2:1
Copolymer of Tetrafluoroethylene and 3,3,3-Trifluoropropene

Time Hours	Thick 10^3(In)	$[F_2]$ 10^3(M/l)	Gel Fraction	SR[a]
20	4	2	0.95	12
18[b]	4	2	0.96	5.9
15	4	8	0.88	13
15	6	8	0.86	16
175[c,d]	6	8	0.71	16
15[d,e]	6	2	0.71	16

[a] Weight swelling ratio in C_6F_6 at 25°C.

[b] Mixture flowing at 600 cc/hr.

[c] Previous sample, exposed an additional 160 hours.

[d] 2% weight gain.

[e] 75°C.

cured Viton O-ring. Untreated and fluorine-treated Viton give curves 1 and 2 respectively. Curve 3, for the O-ring, is low due to the presence of fillers. Curve 4, scaled to allow for this, initially shows more volatilization than curves for the other materials.

Figure 4 shows relaxation of Viton at constant length in air at 250°C using the 15- and 64-hour samples in Table IV (curves 1 and 2 respectively). Initial fractions of elastically effective crosslinked monomer units, calculated form the theory of rubber elasticity [9], are 1.2 and 8.5×10^{-3} respectively. The ratio of the initial to the instantaneous stress is plotted versus time. Permanent set was measured after removal of the stress. Expressed as the fraction of the strain retained one hour after removal of the stress, values were 0.24 for 18% elongation and 0.39 for 71% elongation.

A 2:1 copolymer of tetrafluoroethylene and 3,3,3-trifluoropropene was treated with fluorine. It consumed little fluorine. Results are in Table V. Gel with a smaller swelling ratio was formed when a flow system was used. A four-fold higher fluorine concentration resulted in low gel fractions being formed in batch reactor. Prolonged reexposure of a gelled sample actually reduced the gel content. Exposure at 75°C gave a lower gel content than a similar one at 25°C.

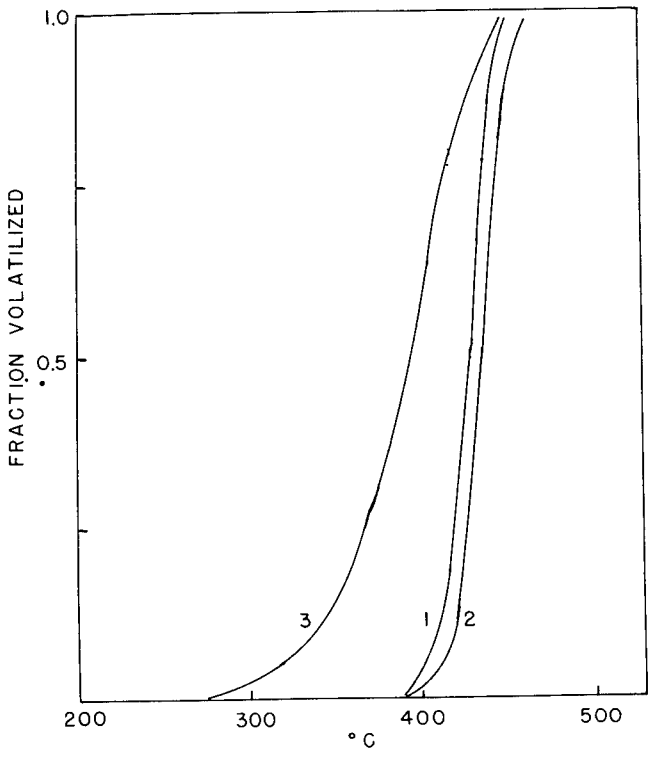

FIG. 5. Thermogravimetric Analysis of 2:1 C_2F_4 — CH_2CHCF_3 copolymer in vacuum. (1) Untreated; (2) F_2 treated; (3) not treated but irradiated.

In Figure 5 are thermogravimetric analyses of untreated polymer, fluorine-formed gel, and radiation-formed gel. The fluorine-formed gel is much more stable than the radiation-formed gel.

Attempts were made to do stress relaxation in air at 250°C with this fluorine-treated polymer. Characteristically it failed within five minutes by flowing under its own weight. Reextraction of the "aged" polymer indicated that the network was practically gone, i.e., the sol content approached 100%. The contrast with the irradiated polymer is extreme, since at 250°C only about 50% of the stress disappeared in one hour [9].

DISCUSSION

Since the reacting gas must enter the polymer it is worth considering the effect of diffusion on reaction. The time required for simple diffusion of a gas into an unreactive flat slab to within 10% of saturation is [12]:

$$t = \frac{l^2}{4D}$$

where t is the time in seconds, l is the thickness in cm, and D is the diffusion coefficient in cm^2/sec. As no value of D for fluorine in polymers is known to us a value, 8×10^{-7} cm^2/sec [13], found for nitrogen in polyisobutylene was used. Most of our quantitative work was done with rubbery polymers 0.002- and 0.006-in. thick. For these t is calculated to be 8 and 70 sec respectively; for pieces 0.036-in. thick, t is about 0.75 hour. Since fluorine reacts irreversibly there is no saturation value. Instead, steady state concentrations of dissolved fluorine will be approached more slowly than given above; the larger the rate constants for consumption of fluorine, the slower will be the approach to the steady state. The fluorine concentration will decrease toward the center of the specimen in the steady state. Differences between surface and center concentrations will be greater for more rapid reaction of fluorine and thicker samples.

In Figure 2 one can see that gel fractions for 0.002- and 0.006-in. thick pieces of Viton are different at 40 min and 5 hr, but very similar between 15 hr and 64 hr. This implies that steady concentrations of fluorine for both are achieved in times less than 15 hr and are rather similar. For pieces 0.036-in. thick differences in gel fractions are rather small for 15- and 64-hr exposures. This may imply that the rate constants for fluorine consumption are large enough to keep the fluorine concentration in the center much less than that in the outside layer. This will probably prevent attainment of high crosslink densities in thick specimens unless much fluorine enters the polymer.

How reaction starts is uncertain but probably most of the fluorine consumed by the polymer disappears by the sequence:

$$F + RH \xrightarrow{k_1} HF + R \qquad (1)$$

$$R + F_2 \xrightarrow{k_2} RF + F \qquad (2)$$

Here F and RH represent fluorine atoms and polymer molecules respectively. R and F_2 represent radicals and fluorine molecules respectively. Crosslinking presumably occurs much less rapidly than fluorine is consumed. The reaction probably involves combination of radicals:

$$2\,R \rightarrow \times \text{ link} \tag{3}$$

Some combining radicals may be the peroxy type, since these appear in spin resonance spectra.

Degradation reactions are quite speculative. The polymeric radicals formed in reaction (1) may scission

$$R_n \rightarrow P_m + R_{n-m} \tag{1a}$$

Possibly the heat released in reaction (2) can cause scission of adjacent carbon–carbon bonds.

Greater amounts of hydrogen in the polymer will yield greater numbers of radicals and so favor crosslinking provided there is some mobility of radicals. Mobility conferred by reduction of T_g may explain the beneficial effect of tetrafluoroethylene in aiding crosslinking.

The difference between the stabilities of vulcanizates of Viton and the trifluoropropene copolymer is interesting. We speculate that abstraction of the tertiary hydrogen in the latter is preferred. When the resulting tertiary radicals combine, crosslink of low stability forms. With Viton, only secondary hydrogens are present. The crosslinks formed by combination of secondary radicals are apparently stable. That more stable networks were formed from the trifluoropropene copolymer by gamma radiation implies to us that radiation is less selective than fluorine, and that crosslinks form by reactions of secondary as well as tertiary radicals.

The two Viton samples differed by a factor of seven in the density of crosslinked monomer units (using the elastic theory calculation). The lightly crosslinked sample lost stress about 13 times as rapidly as the other. Random scission in both samples would have resulted in a seven-fold higher decay for the former sample [14]. The difference may be accounted for by the greater extension used with the less crosslinked sample.

REFERENCES

[1] R. E. Florin and L. A. Wall, *J. Chem. Phys. 57*, 1971 (1972).

[2] R. E. Florin and L. A. Wall, Paper presented at the 164th National Meeting, Am. Chem. Soc., New York, N.Y., Aug.–Sept., 1972.

[3] J. L. Margrave and R. L. Lagow, *Chem. Eng. News, 48*, 40–41 (Jan. 12, 1970).

[4] H. Schonhorn and R. H. Hansen, *J. Appl. Polym. Sci. 12*, 1231 (1968).

[5] H. Shinohara, M. Iwasaki, and S. Tsujimura, *J. Polym. Sci. A-1, 10*, 2129 (1972).

[6] L. A. Wall, *Fluoropolymers*, Wiley Interscience, New York, 1972, p. 127.

[7] L. K. Nash, *Anal. Chem., 21*, 980 (1949).

[8] D. W. Brown and L. A. Wall, *J. Polym. Sci. A-1, 6*, 1367 (1968).

[9] D. W. Brown and L. A. Wall, *J. Polym. Sci., Polym. Chem. Ed. 10*, 2967 (1972).

[10] A. Charlesby, *Atomic Radiation and Polymers*, Pergamon Press, New York, 1960, p. 143.
[11] T. Yoshida, R. E. Florin, and L. A. Wall, *J. Polym. Sci. A, 3*, 1685 (1965).
[12] J. Crank, *The Mathematics of Diffusion*, Clarendon Press, Oxford, 1956, p. 55.
[13] S. Prager, *J. Phys. Chem. 61*, 178 (1957).
[14] A. V. Tobolsky, *Properties and Structure of Polymers*, John Wiley & Sons, New York, 1960, p. 233.

FIRE HAZARDS OF POLYMERIC MATERIALS

JOSEPH E. CLARK

National Bureau of Standards,
Washington, D.C. 20234

SYNOPSIS

The wide usefulness of polymers is being recognized in the market for clothing, interior furnishings and building materials. The advantages of these products are sometimes offset by disadvantages inherent in the use of combustible organic materials. The fire hazards of these materials depend on their exposure, ignition, spread of flame, smoke and toxic gas production, and difficulty of extinguishment. Actions which can be taken to reduce the loss from these fire hazards include mandatory and voluntary standards, education of product designers as well as the public, building codes with increased emphasis on life safety, and specialized extinguishment techniques.

INTRODUCTION

To provide a rational basis for an approach to fire problems of polymeric materials, consider the basic chain-of-events which lead to fire loss:

a. the *exposure* of ignitable material to an ignition source (e.g., the exposure of paper in a waste basket to a discarded match);
b. the *ignition* of the material (e.g., the paper catches fire),
c. the *spread of fire* (e.g., the waste basket fire spreads up the draperies); and then
d. the *fire loss* (e.g., destruction of the waste basket, draperies, other room contents, and perhaps the entire building).

This view of the basic chain of events: exposure, ignition, fire spread, and fire loss, is useful to understand and attack the causes of human loss and property damage from fire.

DISCUSSION

To minimize fire loss we must interrupt this chain-of-events. Therefore, a broad effort to solve this problem would have the following major elements:

Applied Polymer Symposium No. 22, 181–183 (1973)

a. Fire prevention,
b. Fire control, and
c. Fire suppression,

with the foundation activities of:

d. Research,
e. Accident information and data

The foundation of this approach lies in understanding real world fire problems through analysis of fire accidents as well as researching fire to understand why and how fire hazards exist. These foundation activities provide a sound basis for outputs to building fire codes, fabric flammability standards, and test methods for plastics flammability.

FIRE PREVENTION

As recently pointed out by the National Commission of Fire Prevention and Control, fire prevention is a prime area in which to expect a major impact in saving human lives and property. Thus, considerable effort should be put into increasing public awareness of fire hazards, into encouraging the fire services to assist homeowners in voluntary inspections and similar fire protection activities, into exploring new designs for common ignition sources such as kitchen ranges, matches, and lighters, and into providing the technical basis for test methods and standards on the flammability of polymeric materials.

We should note that the clothing flammability standards set by the Secretary of Commerce for children's sleepwear are expected to have a significant impact in saving lives of children threatened by fire. Likewise, standards on large carpets, small rugs, mattresses, blankets, and upholstered furniture should have a very significant impact on building fire loss as well as on human loss.

FIRE CONTROL

The control of fires can be accomplished through reduction of fire loads in buildings, through early detection and suppression of fire, and through minimization of smoke and fire movement in burning buildings. A representative picture is needed of fire loads in residences, office buildings, hospitals, and schools. Once the nature of these fire loads has been determined, we should be better able to design buildings that resist the spread of fire.

In the category of automatic fire control, smoke and toxic gas detectors are most important. Many commercial detectors could be improved by simple design changes to ensure smoke and gas access to the detecting element. Performance criteria are needed for residential detectors, and new approaches are needed to early detection of fire, as well as to measuring unique fire signatures so that we can reduce false alarms.

In addition, improved design criteria and flammability tests are needed for building materials and systems leading to improved building standards for fire-safe buildings.

FIRE SUPPRESSION

Improved protective clothing and equipment for firefighters are needed. There are some surprising inadequacies which might help account for the hundreds of firefighters' lives lost and the very high rate of firefighter injuries each year. Most firemen's protective coats are flammable; many are not as fire-safe as children's sleepwear under the new Commerce flammability standard. Some helmets melt when exposed to moderate heat which firemen could otherwise harmlessly withstand; clearly a melting helmet is not a very good protective "hard hat".

RESEARCH

We need to define important fire problems in which new knowledge in science and technology can make a contribution to saving lives. Investigation of the chemistry and physics of combustion should point the way to improved fire retardant materials and improved fire extinguishers. The exploration of the dynamics of the fire situation may lead us to a fire knowledge of the best location for fire detectors. Presently, we do not really know how many fire detectors are needed in a building or their optimum location.

ACCIDENT INFORMATION AND DATA

The accident data on which we should base our priorities and monitor our progress must be solidly founded. The accident information must also be quite detailed so that its analysis can clearly indicate the critical causes of fires that need to be attacked. A national fire loss data system is urgently needed. A good example of the value of such a system is found in FFACTS, the Flammable Fabrics Accident Case and Testing System, which now guides development of Federal fabric flammability standards.

CONCLUSION

New polymeric materials can safely make their way into our everyday lives if their potential flammability haxards are understood and planned for.

MODELING TECHNIQUES FOR PREDICTION OF FIRES

J. DE RIS

Factory Mutual Research,
Norwood, Massachusetts 02062

SYNOPSIS

This paper reviews the state-of-the-art of fire modeling. Two modeling techniques are discussed—Froude (or Atmospheric) Modeling and Pressure Modeling. The advantage of Froude modeling is the ready availability of suitable experimental facilities, whereas the advantage of pressure modeling is its accuracy and generality. Froude modeling, which maintains the balance of buoyancy and inertial forces, can successfully model many fully turbulent flows including steady and certain transient fires, provided viscous effects do not become important. On the other hand, pressure modeling, which maintains the balance of buoyancy, inertial, and viscous forces by an increase in ambient pressure, models both laminar and turbulent fires including essentially all transient phenomena. However, pressure modeling does require the availability of a suitable pressure vessel.

Both these modeling techniques are now well enough advanced to answer a wide variety of pressing applied research problems facing the fire protection community.

INTRODUCTION

There is much current interest in fire modeling techniques for the practical evaluation of potential fire hazards. This interest is a natural consequence of: (1) the rising national concern with consumer and safety problems; (2) recent advances in our basic understanding of fire phenomena suggesting new modeling techniques; (3) the success of modeling work currently in progress; (4) appreciation of the technological advances made possible by modeling in other technical fields; and finally and perhaps most important, (5) the realization that full scale fire tests are much too combersome and expensive for analyzing the wide variety of potential fire hazards. Fire modeling should also prove helpful for the perennial problem of developing quantitative relationships between potential fire hazards and standard materials flammability rating test results.

The principal virtue of full scale tests is their faithful simulation of actual fire hazards. However, their high cost severely limits the number of tests which can be performed in any given research program—often leaving considerable doubt as to the general validity of the research conclusions. Full scale tests, being intrinsically hazardous, are also quite difficult to instrument, measure and observe in detail.

Applied Polymer Symposium No. 22, 185–193 (1973)

The principal virtue of model tests is their ease and economy. This allows one to perform numerous related tests while developing rather general conclusions. The convenient scale of model tests also eases problems of instrumentation, measurement and detailed observation. However one's confidence in conclusions based on modeling tests is predicated on one's confidence in the modeling techniques employed. This issue of establishing confidence is the principal challenge facing scientists developing fire modeling techniques. While full scale fire tests could be used to corroborate conclusions drawn from modeling studies, firm confidence ultimately must be based on a knowledge of the basic scaling laws governing fire behavior.

Currently two fire modeling techniques are being developed by FMRC with NSF support. One technique, pressure modeling, takes advantage of the fact that small scale fires at high pressure simulate large scale fires at ordinary atmospheric conditions. The other technique, Froude (or Atmospheric) Modeling, takes advantage of the fact that large scale fires are principally controlled by turbulent free convection which can, in many cases, be modeled by maintaining the same Froude number for both model and full scale situations. Both modeling techniques are based on the fundamental conception that fires can be regarded as diffusion flames and therefore follow fluid dynamic scaling laws. The above two techniques, being the most advanced, are the central topic of this paper.

FROUDE MODELING OF FIRES

Turbulent free convective flows are governed by buoyancy forces, inertial forces and viscous forces. These three types of forces can not be simultaneously modeled by simply reducing the scale of an experiment. However for fully turbulent flows viscous effects are usually unimportant except possibly near flow boundaries. These viscous forces can also be unimportant even near flow boundaries if the boundaries are sufficiently rough. For example it is well known that the friction loss and heat transfer for fully turbulent flows in rough pipes is independent of Reynolds number (i.e. independent of viscosity).

Froude modeling takes advantage of this simplification by preserving the Froude number (i.e., the ratio of buoyancy to inertial forces) while reducing the scale of the experiment but preserving its geometry. Of course such a scale reduction has its limits; for example Alpert [1] has shown that for fires (or heat sources) beneath smooth ceilings less than two feet high the viscous effects can noticeably distort the flow patterns as compared to equivalent room sized flows.

Froude modeling already has been used in a number of practical applications involving studies on smoke and heat movement in enclosures. For example: (1) the recent British [2, 3] studies on smoke movements in mine tunnels and urban malls, as well as (2) Heskestad's [4] recently completed study to determine the optimum size of air pollution (smoke removal)

equipment for FMRC's large test facility. This latter study also included the modeling of sprinkler spray patterns and their induced flow. Froude modeling will also shortly be used by FMRC in a HUD supported project on the optimum location of fire detectors in high rise residences.

The above applications all involve the modeling of heat and smoke convection after their production by a fire. Such fluid dynamic modeling is achieved by preserving the ratio of the dynamic pressure head, ρu^2, associated with the gas motion to the gravitational pressure head $\Delta\rho g l$ which induces the free convection motion; that is, one preserves the Froude number $Fr = \rho u^2/(\Delta\rho g l)$, where ρ is the gas density, $\Delta\rho$ is the characteristic density change as a result of heating, u is the gas velocity either driven by forced or free convection, g is the acceleration of gravity, and l is a characteristic length scale. Under faithful modeling conditions the gas temperatures should also be preserved implying that the density ratios $\rho/\Delta\rho$ are identical at equivalent points of the model and full scale situations. To preserve the Froude number $(u^2/gl)(\rho/\Delta\rho)$ one must therefore maintain $u \sim l^{1/2}$, that is, maintain velocities proportional to the square root of the scale. This relationship provides a clear recipe for the scaling of externally controlled forced convection drafts. However, fires almost always involve free-convective velocities which are induced by the fire's heat output, $\dot{Q}$, which has units of [thermal energy/time]. To find the appropriate scaling for $\dot{Q}$, one can consider the free convection induced by a heat source of magnitude $\dot{Q}$, in the absence of forced convection. In this case the heat flux carried away by the fluid is

$$\dot{Q} = \rho C_p \Delta T\, (\pi d^2/4) u$$

where d is an effective plume diameter at the same position above the source where one also evaluates the mean temperature rise of the gas $\Delta T = T - T_\infty$, and the mean velocity u. The specific heat C_p is regarded here as being constant. For a perfect gas $\rho\Delta T = \rho T - \rho T_\infty = T_\infty(\rho_\infty - \rho) = T_\infty \Delta\rho$, so that

$$\dot{Q} = C_p T_\infty \Delta\rho\, (\pi d^2/4) u$$

where T_∞ and ρ_∞ are the ambient temperature and density respectively. Substituting this into the Froude number $Fr = (u^2/gl)(\rho/\Delta\rho)$ for the velocity u, one has after a little manipulation.

$$\frac{\dot{Q}}{\rho_\infty C_p T_\infty} g^{-1/2} l^{-5/2} = \frac{\pi}{4}\left(\frac{d}{l}\right)^2 \left(\frac{\rho}{\rho_\infty}\right)\left(\frac{\Delta\rho}{\rho}\right)^{3/2} Fr^{1/2}$$

All the right hand quantities are preserved for Froude modeling so that one must scale $\dot{Q}$ with the five halves power of the length scale, $l^{5/2}$.

In summary, the Froude modeling of turbulent free convective flows can be achieved by: (1) preserving the geometry; (2) scaling externally controlled velocities $\sim l^{1/2}$; and (3) scaling free convection heat sources $\dot{Q} \sim l^{5/2}$. The modeling scheme reproduces the temperature distribution and provides an accurate simulation of the overall flow patterns provided the model scale is sufficiently large to mask any viscous effects.

It appears that Froude modeling can be extended to include certain fire phenomena as well—especially those processes involving turbulent diffusion flames not dominated by viscous effects. For example, it is well known that (fully) turbulent flame heights for given fuels are well correlated by the 2/5 power of the fuel supply rate [5, 6]. This is consistant with Froude modeling which has $l \sim \dot{Q}^{2/5}$. In certain cases, the fire burning rate itself can be Froude modeled. For example, Gross [7] and Block [8] showed that the burning rate of densely packed cribs (i.e., cross piles of wooden sticks) is proportional to the air supply rate entering the crib bottom. This air supply rate being independent of the Reynolds number (i.e., insensitive to viscosity) can be Froude modeled, resulting in a burning rate $\dot{Q} \sim l^{5/2}$. Similarly Kim, de Ris and Kroesser [9] showed the turbulent burning rate inside tubes of Plexiglas is proportional to $l^{5/2}$ provided the tube length to diameter ratio exceeds 10.

We are further encouraged when we consider the radiant output from turbulent flames, which is known to be approximately proportional to the burning rate [7, 10, 11]; thereby preserving the ratio of radiant energy transfer to convective heat transfer. The radiation from solid surfaces does not quite scale properly, since such radiation, being controlled solely by the surface emissivity and temperature, remains essentially independent of scale rather than increasing with $l^{1/2}$ as the convective and flame radiative heat fluxes do. This lack of scaling for solid surfaces should have little effect on the reported crib and Plexiglas tube burning rates, since in these cases the solid radiation is immediately recaptured by facing fuel surfaces making the solid radiation essentially irrelevant to the burning process.

The above Froude modeling concepts are currently being tested by Heskestad [12] and Croce at FMRC with NSF support. The experiments involve the burning of cribs in various sized enclosures each of which models the same residential room with walls made of gypsum board.

Before becoming too optimistic about Froude modeling, one should be aware of some of its, as yet, unsolved problems. As anticipated Froude modeling encounters difficulties when viscous effects become important, as they are, for example, in the exterior burning of smooth surfaces. The convective heat transfer from flames adjacent to smooth fuel surfaces tends to be independent of scale rather than increasing as $l^{1/2}$ as demanded by Froude modeling [13]. This difficulty with the burning of smooth surfaces may not be a problem for rough surfaces. Further basic research on this question is required.

Problems also arise when one considers transient processes such as fire spread. The various characteristic transient times can follow different scaling laws. For example, the characteristic time, τ_g, for gas to move between two characteristic points varies as $l/u \sim l^{1/2}$ as one might expect. On the other hand, solid-phase times scale differently. For example, the time τ_s, required by a thermally thick fuel element to reach its vaporization temperature, T_s in response to a steady heat flux $\dot{q}''$ per unit area is governed by the relation $\dot{q}''\tau_s \simeq \rho_s C_{ps}(T_{vap} - T_\infty)\delta_s$, where δ_s is the effective depth of heat penetration into the solid. This distance δ_s is also con-

trolled by the conduction relation $\dot{q}'' \simeq \lambda_s(T_s - T_\infty)/(2\delta_s)$, where λ_s is the solid thermal conductivity. Eliminating δ_s between these two relations one has

$$\tau_s \simeq \rho_s C_{ps} \lambda_s (T_s - T_\infty)^2/(2\dot{q}''^2)$$

which scales as l^{-1} since $\dot{q}'' \sim l^{1/2}$. We note here also that the depth of heat penetration δ_s at the characteristic time τ_s, scales with $(\dot{q}'')^{-1}$ or $l^{-1/2}$, which means that the thermal penetration depth δ_s decreases as l increases (at the same scaled times)!!

In itself, the difference in scaling for τ_s and τ_g is usually considered unimportant, since typically $\tau_g \ll \tau_s$, permitting one to treat the gasphase fire processes as quasi-steady. A problem does arise, however, when one wants to model the transient response or fire spread over a fuel array having both thermally thin and thermally thick solids.[a] As is noted above, the thermal penetration depths δ_s scales with $l^{-1/2}$ forcing one to scale *all* the solid thicknesses with $l^{-1/2}$ to achieve a similar time scaling for both thin and thick solids. This means that one must actually increase the thickness of fuel elements as one reduces the model scale. Such a scaling recipe will soon encounter practical difficulties for significant changes in length scales.

Many of these viscous and transient problems encountered by Froude modeling can be avoided when one considers particular modeling applications for which the complete generality of possible fire situations is not necessarily required. For example, in a study on the nature and causes of room flashover, one might be satisfied with model tests involving only thermally thick fuel elements whose response times, as is shown above, all scale with l^{-1}

PRESSURE MODELING

It has recently been recognized that laboratory scale fires at high ambient pressures can more precisely model full scale fires under standard atmospheric conditions. The theory of pressure modeling and its experimental corroboration have both been discussed in considerable detail elsewhere [14]. Here we shall review only its principal features.

Being based on fundamental combustion principles, pressure modeling avoids most of the complications encountered by Froude modeling. For example, the same scaling laws apply to both laminar and turbulent flows—resulting in both a more general and more precise modeling technique. In addition, the transient response times of both thermally thin and thick fuel elements follow the same scaling relations—permitting the generalized modeling of fire growth and spread. Although the fundamental laws of flame radiation are still unknown, we find experimentally that the

[a] By the words "thermally thin solid" we mean that the solid is sufficiently thin to have approximately uniform temperature across its thickness; whereas by the words "thermally thick solid" we mean that its surface temperature responds as if it were infinitely thick.

radiant output from fully turbulent flames remains proportional to their rate of combustion—regardless of pressure—implying that the radiant heat fluxes from turbulent flames remain proportional to the convective heat fluxes. The only significant inaccuracies of pressure modeling appear to be: (1) the solid surface radiation which probably does not increase strongly enough with pressure; and (2) finite gas-phase chemical kinetic effects which are presumably disproportionately speeded up at high pressure. This latter inaccuracy is probably of little practical consequence because finite gas-phase chemical kinetic effects are rarely important in large scale fires. It appears then that the principal drawback in using pressure modeling is the availability of a suitable pressure vessel. This drawback can be overcome; for example FMRC is in the process of acquiring a pressure vessel with its auxiliary equipment at a cost about equal to the cost of two or three full scale fire tests.

The remaining part of this section provides a brief derivation of the most important scaling relationships involved in pressure modeling. A more detailed and rigorous discussion is given by de Ris, Kanury, and Yuen [14].

The scaling laws for pressure modeling can be obtained from the several dimensionless groups governing fire behavior. For accurate modeling, each of these groups must be identical for both the model and full scale situations.

(1) Consider first the Grashof number which relates buoyancy ($\Delta\rho g l$) and inertial (ρu^2) forces to viscous forces ($\mu u/l$),

$$\mathrm{Gr} = \frac{\rho u^2 \cdot \Delta\rho g l}{(\mu u/l)^2} = \frac{g}{\mu^2}\left(\frac{\Delta\rho}{\rho}\right)\rho^2 l^3$$

where μ is the dynamic viscosity which is independent of pressure. Since temperatures are preserved in pressure modeling $\Delta\rho/\rho$ is also independent of pressure. This means that to maintain Gr invariant both the model and full scale situations must have the same value of $\rho^2 l^3$. That is, the model length scale must decrease with the minus two-thirds power of pressure, $l \sim p^{-2/3}$.

(2) To model the effects of forced drafts on a fire, one considers the Reynolds number which relates inertial forces (ρu^2) to viscous forces ($\mu u/l$).

$$\mathrm{Re} = \rho u^2/(\mu u/l) = \rho u l/\mu$$

Since the gas density ρ is proportional to the pressure while l is proportional to $p^{-2/3}$, the Reynolds number is held invariant by scaling the externally controlled velocities, $u \sim p^{-1/3}$. If one models both the Grashof number and Reynolds number, one automatically models the Froude number, since

$$\mathrm{Fr} = \rho u^2/\Delta\rho g l = \mathrm{Re}^2/\mathrm{Gr}$$

Of course, for such a modeled flow, even in the absence of externally driven velocities, the various dependent flow velocities will all scale as $u \sim p^{-1/3}$.

(3) Gas-phase transient processes, such as flow accelerations (whether externally driven or not), can be described in terms of a gas-phase Fourier number

$$\mathrm{Fo_g} = \lambda_g \tau_g / \rho C_p l^2$$

where τ_g is the characteristic gas-phase time of interest and λ_g is the gas-phase thermal conductivity which is independent of pressure. If all independent dimensionless groups are preserved, that is, if the flow is modeled, $\mathrm{Fo_g}$ will also be preserved, implying $\tau_g \sim \rho l^2 \sim p^{-1/3}$. This time τ_g could, for example, represent the time required for the gas to move between two points a distance l apart, which also suggests the scaling $\tau_g \sim l/u \sim p^{-2/3}/p^{-1/3} \sim p^{-1/3}$ similar to the Fourier prediction.

(4) Solid-phase transient processes, such as fuel burn-out or fire spread etc., can be described in terms of a solid-phase Fourier number

$$\mathrm{Fo_s} = \lambda_s \tau_s / \rho_s C_{ps} l^2$$

where $\lambda_s/\rho_s C_{ps}$ is the solid-phase thermal diffusivity (which is independent of pressure) and τ_s is the solid-phase transient time of interest. Preservation of $\mathrm{Fo_s}$ implies that $\tau_s \sim l^2 \sim p^{-4/3}$. We immediately see that the gas phase and solid-phase transient times follow different scaling laws. In practice this discrepancy is unimportant in most fire situations, since gas-phase times are typically several orders of magnitude less than solid-phase times.

This scaling of solid-phase times applies to both thermally thick and thin solids with the presumption that all solid dimensions are scaled as $l \sim p^{-2/3}$.

It is interesting to inquire how these scaling laws apply to flame spread rates. In fact, one can use them to predict the pressure dependence of these spread rates. Consider two points on a fuel element a distance l apart. The time, τ_s, required for the flame to spread from one point to the other should be governed by the solid-phase scaling laws. The corresponding solid-phase spread rate, $V_s = l/\tau_s$ should scale as $p^{-2/3}/p^{-4/3} = p^{2/3}$. It has been experimentally established [15] that spread rates over thermally thick solids are proportional to the two thirds power of pressure; thereby confirming our prediction.

(5) Heat and mass transfer rates can be described in terms of a Nusselt number

$$\mathrm{Nu} = \frac{hl}{\lambda_g} = \frac{\dot{q}'' l}{\Delta T \lambda_g}$$

or its equivalent $\dot{m}'' l/\mu$ for mass transfer rates, $\dot{m}''$, per unit area. Both these dimensionless numbers, being dependent parameters, should be preserved if all the other independent groups are preserved. Thus, we expect to have $\dot{q}'' \sim l^{-1} \sim p^{2/3}$ and $\dot{m}'' \sim l^{-1} \sim p^{2/3}$. These scaling relations have been experimentally verified [14].

(6) These pressure modeling concepts are based on the fundamental hypothesis that fires can be regarded as diffusion flames. That is, the gaseous burning rates are governed by the time required for the fuel and oxidant to come together rather than the time required for them to react after coming together. The rather excellent agreement of modeling theory and experiment supports this hypothesis. In view of this, we conclude that the burning rates of various solid fuels are influenced primarily through their chemical thermodynamic properties rather than their gas-phase chemical kinetic properties. Since the various chemical thermodynamic properties remain essentially independent of pressure, one expects a reasonably precise modeling of the gas phase temperatures at each point of the flow. In addition, since activation energies associated with the vaporization of solids are typically quite large, one anticipates only slight changes in surface vaporization temperature for the relatively large changes in vaporization rates required by the modeling procedure. In summary, the combustion chemistry, at least in so far as it influences burning rates, should be modeled provided one uses the same fuel and oxidant in both the model and full scale situations.

CONCLUSIONS

1. The states-of-the-art for both Froude modeling and pressure modeling are rapidly advancing.
2. The advantage of Froude modeling is the ready availability of suitable experimental facilities, whereas the advantage of pressure modeling is its accuracy and generality.
3. Both these modeling techniques are now well enough advanced to answer a wide variety of pressing practical problems facing the fire protection community.
4. While the value of each of these modeling techniques is now well established, we should continue to look for and explore other modeling techniques which have other advantages.
5. It should be recognized that all such modeling techniques have their conceptual origins in previous basic research studies.

REFERENCES

[1] R. L. Alpert, "Fire Induced Turbulent Ceiling-Jet," FMRC Tech. Rept. 19722-2, Factory Mutual Research Corp., 1971.

[2] A. J. M. Heselden and P. L. Hinkley, "Smoke Travel in Shopping Malls. Experiments in Cooperation with Glasgow Fire Brigade, Part 1," Joint Fire Research Organization, Fire Research Note 832/1970.

[3] P. L. Hinkley, "The Flow of Hot Gases Along an Enclosed Shopping Mall—A Tentative Theory," Joint Fire Research Organization, Fire Research Note 807/1970.

[4] G. Heskestad, "Preliminary Report—Model Study for the Determination of Gas Venting Geometry and Capacity of Air Pollution Control System at Factory Mutual

Research Center," FMRC Serial No. 20581, Report RC 72-7-31, Factory Mutual Research Corp., 1972.

[5] P. H. Thomas, "The Size of Flames from Natural Fires," *Ninth Symposium on Combustion*, Academic Press, New York, N.Y., 1963, pp. 844–859.

[6] F. R. Steward, "Prediction of the Height of Turbulent Diffusion Buoyant Flames," *Combust. Sci. Technol., 2*, 203 (1970).

[7] D. Gross, *J. Res. Natl. Bur. Standards, 66C*, 99 (1962).

[8] J. A. Block, "A Theoretical and Experimental Study of Non-Propagating Free-Burning Fires," *Thirteenth Symposium (International) on Combustion*, The Combustion Institute, Pittsburgh, 1971, pp. 971–978.

[9] J. S. Kim, J. de Ris, and F. W. Kroesser, "The Burning of Two Vertical Parallel Plates," FMRC Tech. Rept. 19720–5, Factory Mutual Research Corp., 1972.

[10] D. A. Burgess, J. Grumer, and A. Strasser, *Fire Research Abstracts and Reviews, 3*, 177 (1961).

[11] T. Yumoto, "An Experimental Study of Heat Radiation from Oil Tank Fires," Report of the Fire Res. Inst. of Japan, No. 33 (1971).

[12] G. Heskestad, "Modeling of Enclosure Fires," *Fourteenth Symposium (International) on Combustion*, The Combustion Institute, Pittsburgh, 1973.

[13] L. Orloff and J. de Ris, "Some Effects of Orientation on Turbulent Burning of Fuel Surfaces," Abstract, 1972 Meeting of the Eastern Section of the Combustion Institute, Princeton, N.J.

[14] J. de Ris, A. M. Kanury, and M. C. Yuen, "Pressure Modeling of Fires," *Fourteenth Symposium (International) on Combustion*, The Combustion Institute, Pittsburgh, 1973.

[15] F. A. Lastrina, R. S. Magee, and R. F. McAlevy III, "Flame Spread over Fuel Beds: Solid Phase Energy Considerations," *Thirteenth Symposium (International) on Combustion*, The Combustion Institute, Pittsburgh, 1971.

TOXICOLOGICAL AND ENVIRONMENTAL FACTORS INVOLVED IN THE SELECTION OF DECABROMODIPHENYL OXIDE AS A FIRE RETARDANT CHEMICAL

J. M. NORRIS, J. W. EHRMANTRAUT, C. L. GIBBONS, R. J. KOCIBA, B. A. SCHWETZ, J. Q. ROSE, C. G. HUMISTON, G. L. JEWETT, W. B. CRUMMETT, P. J. GEHRING, J. B. TIRSELL, and J. S. BROSIER

The Dow Chemical Company, Midland, Michigan 48640

SYNOPSIS

The growing need for fire resistant polymers has stimulated development of new compounds for use as fire retardant additives. Their toxicological and environmental properties are a major factor in determining suitability for large-scale use. Both decabromodiphenyl oxide (DBDPO) and octabromobiphenyl (OBBP) perform well as fire retardant additives for thermoplastics. They both have low acute oral toxicity and low skin absorption toxicity. They are neither primary skin irritants or skin sensitizers, and are only mildly irritating to the eyes. A 30-day dietary feeding study in rats established 8 mg DBDPO/kg/day as an unequivocal no-effect level and 80 mg/kg/day as a marginal effect level. A no-effect level was not established for OBBP in a comparative study. Two-year studies on rats providing 0.1 mg DBDPO/kg/day in the diet revealed bromine concentration in the liver plateaued within 30 days while the concentration in adipose tissue slowly increased. With OBBP the bromine concentration in the liver and adipose tissue increased steadily and rapidly with no attainment of a plateau during 180 days of the study. Neither compound produced an accumulation of bromine in other tissues. After administration of ^{14}C DBDPO, all ^{14}C activity was eliminated via the feces within 2 days. After administration of ^{14}C OBBP, 62% was eliminated with a half-life of less than 24 hours; the half-life for the remainder was greater than 16 days. In teratology studies, 10, 100, or 1000 mg DBDPO/kg/day had no effect in rats.

Environmental testing performed on DBDPO and OBBP include fish bioconcentration, photolytic degradation, sewage decomposition, leaching from plastics, and thermal decomposition products.

INTRODUCTION

A growing recognition of the huge annual toll taken by fire is resulting in more stringent flammability requirements for synthetic polymers in a variety of applications. Because of economic constraints and the need to produce flame resistant polymers without total replacement of existing manufacturing processes, increased flame resistance is generally achieved

Applied Polymer Symposium No. 22, 195–219 (1973)

by incorporation of a fire retardant chemical in the finished product. This chemical is usually based on bromine, chlorine, phosphorus, or nitrogen and may either be chemically reacted or physically blended into the product. Since polymer systems differ markedly in both flammability characteristics and physical properties, selection of a suitable flame retardant depends on a variety of factors that severely limits the number of acceptable materials.

A general class of synthetic polymers that require flame retardancy because of their use in electrical and high temperature applications, but pose severe problems in selecting a suitable flame retardant are the high performance thermoplastic resins such as thermoplastic polyesters, polyphenylene oxides, and acrylonitrile–butadiene–styrene (ABS) terpolymers. Some of the most important criteria for an acceptable flame retardant in these applications are:

1. It must be as effective as possible to minimize both cost and effect on polymer properties. Use levels may range up to 15% by weight.
2. It must have sufficient stability to withstand conditions encountered during polymer processing and use. Processing conditions (blending, extrusion, and molding) often involve temperatures exceeding 300°C. The flame retardant must tolerate these conditions without degradation or volatilazation. Also, attention must be given to hydrolytic stability and oxidative degradation, particularly under extended service at high temperatures.
3. It must be compatible with the base polymer and exert minimal adverse effect on those properties that give the polymer its value. Some of these critical properties are tensile strength, impact strength, heat deflection temperature, shear strength, and flexural modulus.
4. Finally, the flame retardant must not interfere with attainment of desired product esthetics and form.

Because of the stringest thermal stability requirements, only a very few compounds have been identified which can meet the necessary performance and economic criteria. They are all halogenated aromatic compounds, namely:

1. Brominated biphenyls—decabromobiphenyl, octabromobiphenyl (OBBP), hexabromobiphenyl.
2. Chlorinated biphenyls (PCB)
3. Brominated diphenyl oxides—decabromodiphenyl oxide (DBDPO).

Of prime interest in our efforts are the brominated biphenyls and brominated diphenyl oxides. While polychlorinated biphenyls could be used in some applications, their environmental problems make their use very unattractive and further suggest that similar problems might occur with the brominated analogues. This paper will summarize the environmental and toxicological studies that have been carried out to date as a part of a continuing program to increase our knowledge of decabromodiphenyl oxide (DBDPO) that The Dow Chemical Company is developing under the designation of FR-300-BA and octabromobiphenyl (OBBP). Details of the

toxicological studies will be published in an appropriate journal at the completion of our investigation. Comparisons of environmental data on octabromobiphenyl and decabromodiphenyl oxide with the polychlorinated biphenyls have been included.

CHEMICAL AND PHYSICAL PROPERTIES

The structure and properties of commercially produced decabromodiphenyl oxide (DBDPO) and octabromobiphenyl (OBBP) are summarized in Table I.

Comparable properties for the polychlorinated biphenyls have already been thoroughly reported in the literature [1, 2, 3]. However, for the sake of direct comparison with OBBP and DBDPO, Table II contains selected data on the most common polychlorinated biphenyls. These are also the ones found to be widely dispersed throughout the environment.

Major differences exist between polychlorinated biphenyls and the brominated materials in several properties:

1. Both OBBP and DBDPO are high melting solids, whereas the common polychlorobiphenyls are liquids. The greater mobility of

TABLE I

Properties of Commercial Decabromodiphenyl Oxide and Octabromobiphenyl.

	DBDPO	OBBP
Structure	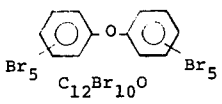 $C_{12}Br_{10}O$	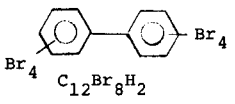 $C_{12}Br_8H_2$
Percent Bromine	83	82
Molecular weight	960	786
Melting Range, °C	290-306	200-250
Decomposition point, DTA	425°C	435°C
Volatility, TGA (10°C/min.)		
% Weight Loss		
< 1	300°C	250°C
<10	330°C	310°C
<50	370°C	350°C
Vapor pressure, mm Hg		
@250°C	<1 mm	
@278°C	2 mm	
@306°C	5 mm	
Solubility @ 25°C		
Water	20-30 ppb	20-30 ppb
Cottonseed oil	600 ppm	1,700 ppm
Solubility in Organic Solvents g/100 g solvent		
Acetone	0.05	1.80
Benzene	0.48	8.10
Chlorobenzene	0.60	18.70
Methylene bromide	0.42	7.40
Methylene chloride	0.09	3.90
o-Xylene	0.87	10.00
Octanol:Water Partition Coefficient	172,000	340,000

TABLE II
Polychlorinated Biphenyl Properties

PCB Trade Name	% Chlorine	Avg. No. Cl atoms per molecule	Water Solubility ppb @ 20°C	Boiling Range °C
Arochlor® 1242	42	3.10	200	325-366
Arochlor 1248	48	3.90	100	340-375
Arochlor 1254	54	4.96	50	365-390
Arochlor 1260	60	6.30	25	385-420

liquids combined with the large scale use of PCB's as functional fluids where leaks and spills can occur makes likelihood of their rapid, large scale loss into the environmental much greater.

2. The common PCB products exhibit much greater volatility than DBDPO. For example, Arochlor 1242 brand of PCB boils from 325–366°C (1 atm), while DBDPO exhibits 5 mm Hg vapor pressure at 306°C. Because of its low mobility and low vapor pressure, DBDPO should not volatilize significantly from plastics in which it is used, even upon exposure to temperatures > 250°C. Arochlor 1248, on the other hand, has been reported to volatilize from polyvinyl chloride in which it was used as a plasticizer at the rate of 19% of total PCB used after exposure to 87°C for 24 hours [4].
3. While the water solubility of the PCB's and the brominated compounds are similar, they differ markedly in solubility in organic solvents. Polychlorobiphenyls are readily soluble in most common organic solvents, but DBDPO and OBBP are far less soluble [5]. In cottonseed oil @ 25°C, DBDPO could only be dissolved up to 600 ppm, while stable 50:50 Arochlor 1242:cottonseed oil solutions were readily prepared.

TOXICOLOGY STUDIES

The toxicological properties of a fire retardant candidate are a major factor in determining suitability for large scale use. The toxicological studies, reported herein, were undertaken on one hand, to compare the toxicity of OBBP and DBDPO for the purpose of evaluating the toxicity of the materials and to assess the hazards associated with their manufacture and use; and, on the other hand, to determine if these materials, like the structurally similar polychlorinated biphenyls, are absorbed and retained by the body. The toxicological investigations have not been completed at the time of this writing, therefore, the information given in this paper is to be considered as an interim report on the studies.

The toxicological investigations include studies on the acute toxicity for different routes of exposure, rabbit ear bioassay tests for chloracnegenic activity, 30-day dietary feeding studies, ^{14}C metabolism studies and two

year dietary feeding studies on OBBP and DBDPO and special dietary feeding studies designed to give data on absorption and concentration, and on elimination of OBBP and DBDPO from the body. Additional studies on DBDPO which are reported on are a human skin sensitization study* and a teratology study.

The composition of the OBBP and DBDPO samples used in the toxicological studies was determined by vapor phase chromatography and mass spectrophotometry. The OBBP sample contained 45.2% OBBP, 47.4% nonabromobiphenyl, 5.7% decabromobiphenyl and 1.8% heptabromobiphenyl. The composition of the sample of DBDPO (Dow FR-300-BA, Specification No D37968) was 77.4% DBDPO, 21.8% nonabromodiphenyl oxide and 0.8% octabromodiphenyl oxide.

Acute Oral Toxicity of OBBP and DBDPO

Intragastric intubation of a single dose of a 10% corn oil suspension of OBBP or DBDPO to female Sprague Dawley (Spartan strain) rats that had been deprived of food for approximately 15 hours resulted in the survival of all rats at doses of 126, 252, 500, 1000 or 2000 mg/kg. There were no indications of toxicity among the OBBP or DBDPO treated rats directly after intubation or during the 14 day post-treatment observation period. All animals displayed body weight gains over the 14 day observation period. Gross pathological examination of one rat/dose level of OBBP or DBDPO, 24 hours after treatment, revealed no detectable pathological changes.

Skin Irritation of OBBP and DBDPO

Skin irritation studies conducted on shaved skin of New Zealand albino rabbits showed that OBBP or DBDPO, as dry solids, caused essentially no response on intact skin and a slight erythematous and edematous response on abraded skin after a single confined exposure of 24 hours. Repeating the exposures to intact skin for five days/week for two weeks and to abraded skin for three days did not alter the responses. OBBP moistened with water caused no response on intact skin and a moderate erythematous and slight edematous response on abraded skin after 24 hours of confined contact. Repeating the exposures caused a slight erythematous response on the intact skin and no alteration in the response of abraded skin. After cessation of treatment, the erythematous and edematous responses subsided and at the termination of the study all skin sites were normal in appearance.

Eye Irritation of OBBP and DBDPO

Eye irritation studies conducted on New Zealand albino rabbits showed that OBBP or DBDPO, as dry solids, caused transient irritation of the conjunctival membranes. The cornea, iris, and lens were unaffected. The eyes

* Study conducted by Industrial Bio-Test Laboratories, Inc., Northbrook, Illinois.

of the rabbits showed no conjunctival membrane irritation twenty-four hours after instillation of either experimental material.

Chloracnegenic Activity [6] of OBBP and DBDPO

Bioassay tests for chloracnegic activity were conducted on the ear of New Zealand albino rabbits. OBBP or DBDPO, as 10% chloroform solutions, caused a slight erythematous response and slight exfoliation during the month long study. There was no indication of the chloracne response on the ears treated with either experimental material at any time during or at the termination of the study.

30-Day Rat Dietary Feeding Studies on OBBP and DBDPO

Male Sprague Dawley rats maintained on diets containing 1.0, 0.1, 0.01, or 0% OBBP or DBDPO providing approximate doses of 800, 80, 8 or 0 mg/kg/day showed no overt indication of toxicity during the 30 day study. Inclusion of OBBP or DBDPO at any level in the diets did not influence the food consumption or body weight gains of the respective experimental animals. Hematology studies conducted during the terminal week of the study showed statistically significant decreased packed cell volume and total red blood cell count of rats on the 1% dietary level of OBBP. The hematology studies on OBBP were extended to include the rats on the 0.1 and 0.01% dietary levels. The hematological determinations of these rats and of rats receiving diets containing 1.0% DBDPO were not statistically different than the rats on the control diet.

Urinalyses made during the terminal week of the study showed no difference in total solids, pH, sugar, albumin, occult blood, and ketones of rats on diets containing OBBP or DBDPO when compared with rats on the control diet.

A comparison of organ weights showed no dose-related statistical difference in heart, testes and brain from rats on diets containing OBBP or DBDPO or in the weight of kidneys from rats on diets containing DBDPO. Enlarged livers were found in the rats on all dietary levels of OBBP and those rats on the 1.0 and 0.1% levels of DBDPO. Increased kidney weights were found in rats on diets containing 1.0 and 0.1 OBBP.

Gross pathological changes that were observed at necropsy were limited to dose related liver enlargement in rats at all dose levels of OBBP and those on the 1.0% dietary level of DBDPO. Kidney changes, consisting of petechial hemorrhage, enlargement, and mottling, were noted only in some of the rats on diets containing OBBP.

The histopathological examination of organs and tissues of the rats on the experimental diets revealed liver and kidney lesions at all levels of OBBP and at the 1.0% dietary level of DBDPO. The liver lesions consisted of centrilobular cytoplasmic enlargement and vacuolation and the kidney lesions consisted of hyaline degenerative cytoplasmic changes. The other

dose related pathological finding was thyroid hyperplasia which was observed in rats on all levels of OBBP and those rats on the 1.0 and 0.1% dietary levels of DBDPO.

^{14}C Metabolism Studies on OBBP and DBDPO

^{14}C labeled OBBP and DBDPO used in these studies had specific activities of 1.1 μCi/mg. The level of radioactivity found in the urine and expired air of three male and three female Sprague Dawley rats dosed with 1.0 mg of OBBP or DBDPO suspended in corn oil, and measured at 24-hour intervals over a 16-day and 4-day period, respectively, was less than 1%. The principal route of excretion for these materials was via the feces. The respective rates of excretion of OBBP or DBDPO were the same for both sexes. The mean values of ^{14}C activity found in the feces of the group of three male rats/experimental material are graphed in Figure 1. Within the first 24 hours, 90.6% $\pm$1.21* of the ^{14}C activity of the dose administered to the DBDPO treated rats was found in the feces and all the ^{14}C activity was accounted for by day 4 of the study.

In contrast, 61.9% $\pm$ 2.39 of the ^{14}C activity administered to the OBBP treated rats was found in the feces after the first 24 hours. From day 2 through day 16, there was a gradual elimination of approximately 11 additional percent, 7% of which was accounted for during the second 24-hour period after treatment. At the termination of the study, on day 16, 26.42% $\pm$ 1.43 of the ^{14}C activity in the administered dose had not been recovered.

Examination for radioactivity of various tissues taken from three male rats/time period following administration of the experimental materials, revealed ^{14}C activity in all tissues taken from the OBBP treated rats on day 1, and, at lower levels, in tissues taken from the DBDPO treated rats.

On day 16 ^{14}C activity was found in adrenal, adipose, heart, and skin at levels ranging from 0.14–0.25% of the administered dose/gram of tissue from the OBBP treated rats. Lesser amounts were found in liver, pancreas and spleen (0.01% $\pm$ 0.00, 0.06% $\pm$ 0.07, and 0.03% $\pm$ 0.04, respectively).

In contrast, the tissues taken from DBDPO treated rats on day 16 showed no ^{14}C activity with the exception of questionable amounts in adrenal (0.01% $\pm$ 0.06 of the dose administered/gram of tissue) and splenic tissue (0.06% $\pm$ 0.07 of dose administered/gram of tissue).

Two-Year Dietary Feeding Studies on OBBP and DBDPO

These studies, designed to run for two years, are now in progress. During the first 180 days, the male and female Sprague Dawley rats being maintained on diets of 1.0, 0.1, 0.01, or 0 mg of OBBP or DBDPO/kg/day have shown no overt indications of adverse effects due to treatment. There have been no dose related deaths among the rats on either experimental diet. The body weights and food consumption of the rats on the experimental diets are not different than the control rats.

* Mean and standard error.

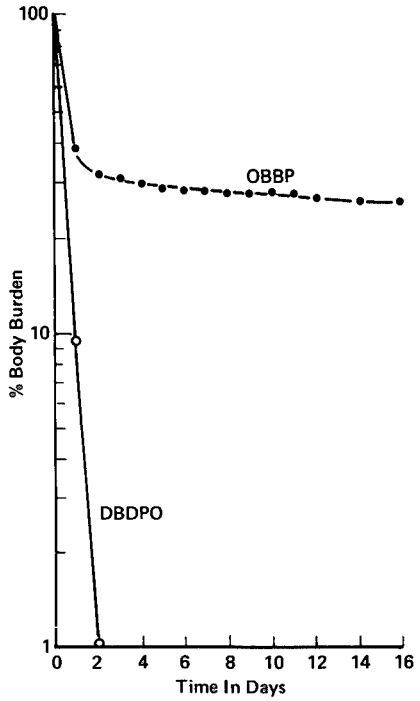

FIG. 1. ^{14}C Activity in Feces Excreted by three male rats/experimental material following administration of 1.0 mg of labeled octabromobiphenyl or decabromodiphenyl oxide/kg.

Tissue Accumulation Studies on Rats Maintained on Diets Containing OBBP or DBDPO

These studies, designed to run for two years, are now in progress. Three male and three female Sprague Dawley rats/dose level are being maintained on diets providing 1.0, 0.1, 0.01, and 0 mg of OBBP and

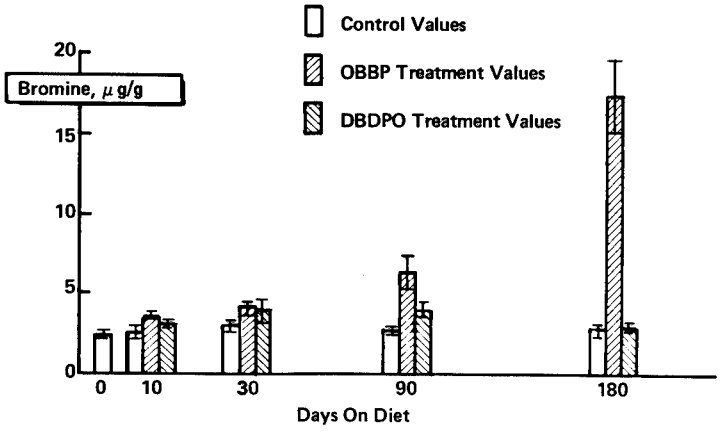

FIG. 2. Bromine content of liver tissue from rats maintained on diets providing a dose of 0.1 mg/kg/day of octabromobiphenyl or decabromodiphenyl oxide.

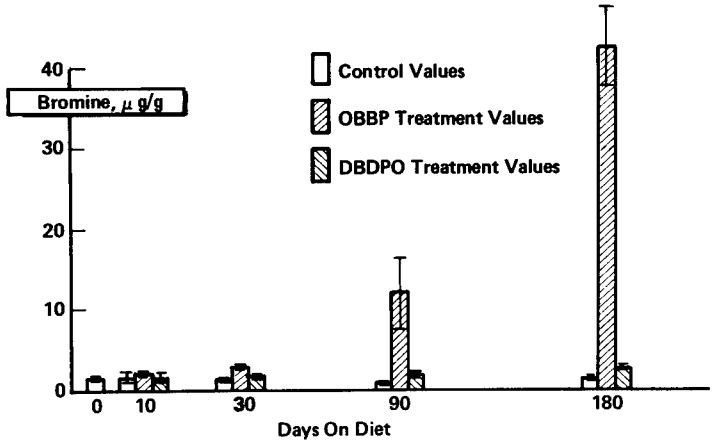

FIG. 3. Bromine content of adipose tissue from rats maintained on diets providing a dose of 0.1 mg/kg/day of octabromobiphenyl or decabromodiphenyl oxide.

DBDPO/kg/day for designated periods of time before being sacrificed for tissue analysis for bromine by Neutron Activation analysis. The tissues analyzed are adipose tissue, liver, kidney, skeletal muscle, serum and testes. At this time, sufficient data for interim reporting has been accumulated only on those rats receiving 0.1 mg/kg of the experimental materials at time intervals of 10, 30, 90, and 180 days.

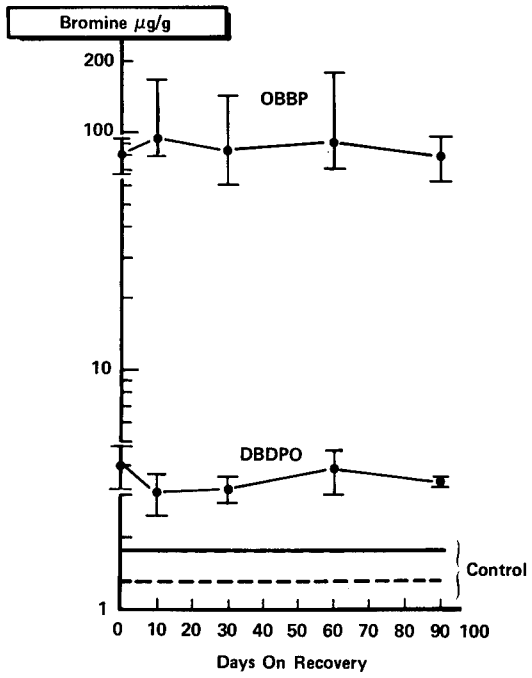

FIG. 4. Bromine content of adipose tissue from rats on recovery following 90 days on diets providing 1.0 mg/kg/day of octabromobiphenyl or decabromodiphenyl oxide.

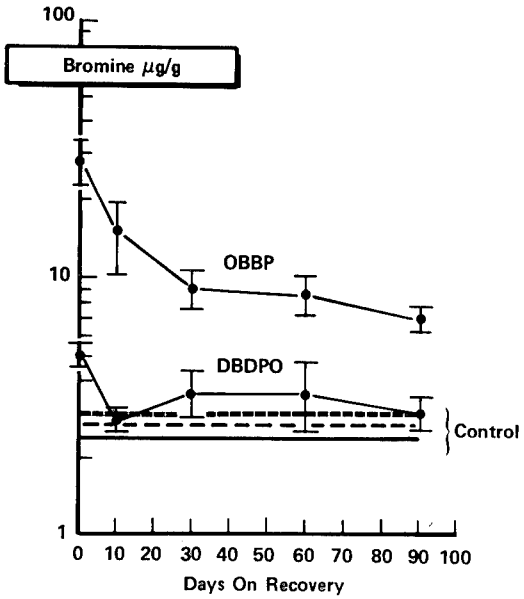

FIG. 5. Bromide content of liver tissue from rats on recovery following 90 days on diets providing 1.0 mg/kg/day of octabromobiphenyl or decabromodiphenyl oxide.

The bromine values obtained on kidney, skeletal muscle, serum, and testes from the rats receiving OBBP or DBDPO were not different than those values for the respective tissues from control rats. The mean bromine content of liver and adipose tissue of rats on OBBP or DBDPO diets is presented in Figures 2 and 3, respectively. Statistical analysis, by regression analysis and Student's t test, showed that the bromide concentration in the adipose and liver tissue of the OBBP treated rats was significantly increased at the $P < 0.01$ level, when compared with the controls. The bromine content of the liver of DBDPO treated rats was not significantly different than the control; whereas, the bromine content of the adipose tissue from these rats was statistically increased at the $P < 0.05$ level, but not at the $P < 0.01$ level when the data was analyzed for difference in slope using a log linear relationship.

Studies on the Elimination of Bromine from Tissues of Rats Maintained on Diets Containing OBBP or DBDPO

Male Sprague Dawley rats were maintained for 90 days on diets providing a dose of 1.0 mg of OBBP or DBDPO/kg/day and then placed on control diets of untreated feed for designated periods for recovery. Four rats from each group were sacrificed on the last day on the experimental diets, recovery day 0, and on recovery days 10, 30, 60, and 90 and tissues were collected for bromine analysis by neutron activation. The tissues analyzed were kidney, serum, adipose, and liver. On recovery day 0, there was no difference in bromine content in kidney or serum of rats on

the OBBP or DBDPO diets when compared with the respective tissues of control rats. Bromine was accumulated, but at different magnitudes, in the adipose and liver tissue of the rats on the OBBP and DBDPO diets. The bromine content in these tissues on the various recovery days is given in Figures 4 and 5.

Human Skin Sensitization Study on DBDPO [7]

Repeated application of a homogenous suspension of 5% DBDPO in petrolatum, three times a week for three weeks, to the skin of 50 human subjects resulted in no skin sensitization response during the "sensitizing" period or on challenge two weeks subsequent to the last application.

Teratology Study on DBDPO

Daily intubation, by intragastric gavage, of pregnant females on gestation days 6–15, with 1000, 100, 10, or 0 mg of DBDPO/kg, suspended in corn oil, caused no teratogenic response at any dose level. There were no indications of toxicity among the rats during gestation. The maternal body weights and food consumption of the DBDPO treated rats did not differ from control rats.

The terminal liver weights of the DBDPO treated rats, obtained at the time of cesarean section, were not different than the controls. Similarly, no differences were seen between the treated and control rats with respect to (1) the position and number of fetuses in utero, (2) the number of corpea lutea, (3) individual pup weight, crown-rump length, and male to female sex ratio. Significant incidences in resorptions occurred at the low dose levels but not at the high dose level.

No gross external abnormalities were seen in the fetuses from dams treated at any dose level of DBDPO. Soft tissue [8] and skeletal examinations [9] revealed an increased number of litters with subcutaneous edema and delayed ossification of normally developed bones of the skull of the fetuses of dams at the 1000 mg/kg level of DBDPO but not at the 100 mg/kg level.

Analysis of the maternal and fetal livers for bromine revealed statistically significant increased concentration in the livers of the maternal animals receiving 1000 mg/kg/day of DBDPO. The concentrations in maternal livers at the two lower dose levels were not different than the controls. Likewise, there was no difference in the bromine concentration in the livers of the fetuses from dams receiving any dose level of DBDPO when compared with the controls.

SUMMARY AND DISCUSSION OF THE TOXICOLOGICAL INVESTIGATIONS

Octabromobiphenyl and decabromodiphenyl oxide may be considered to present a low degree of hazard from acute exposure. Both experimental materials are low in acute oral toxicity. They are neither eye nor skin ir-

ritants nor skin sensitizers [7, 10]. OBBP and DBDPO are not absorbed through the skin in acutely toxic amounts and they do not possess chloracnegenic activity.

Dietary feeding studies conducted over a wide range of high dosage levels for 30 days to elucidate the potential hazard that might be incurred through long term repeated exposure, resulted in an unequivocal no effect level of 0.01% in the diet (approximately 8 mg/kg/day) for DBDPO, with a marginal effect level of 0.1% (approximately 80 mg/kg/day). In contrast, a no effect level was not established for OBBP in this 30-day period at these high dose levels. Thyroid hyperplasia seen in rats at all dose levels of OBBP and the top two dose levels of DBDPO was quite possibly a physiological response to competition between bromine and iodine in the thyroid gland. Such a response is not unexpected at high dosage levels with materials containing bromine in quantities as great as in OBBP and DBDPO.

DBDPO did not cause any teratogenic response in fetuses of rats administered 1000, 100, or 10 mg of DBDPO/kg/day on gestation days 6–15. No indications of toxicity, adverse effects on food consumption, or body or liver weights were observed in the maternal rats at any of the doses of DBDPO. At the high dose level the bromine content of the maternal livers was increased. The bromine content of fetal livers, was, however, unaffected by the administration of DBDPO to maternal rats at any dose level included in this study.

The teratological examination confirmed the 100 mg of DBDPO/kg/day as the unequivocal no effect level in this study. The number of resorptions occurring at the two lower levels of DBDPO was statistically greater than the controls. However, as this effect did not occur at the high dose level, it was probably due to chance rather than treatment.

Fetal toxicity in the form of subcutaneous edema was noted in fetuses of dams at the high dose level of DBDPO. The only other effect noted was delayed ossification of normally developed bones of the fetal skull occurring similarly at the high dose level.

Aftosmis et al [11] have reported that OBBP administered in diets of pregnant rats caused a teratogenic response, gastroschisis, in some of the fetuses of dams on diets containing 0.1 and 1.0% of OBBP. The bromine content was increased in the liver and fat of the OBBP treated maternal rats and also in the whole fetus.

The data from the 30-day dietary feeding study and the teratology study indicate the degree of hazard that exists from long term exposure to DBDPO is significantly less than to OBBP. The ^{14}C metabolism study and the special studies on absorption, accumulation, and elimination, which were subsequently conducted, offer additional substantiation for this observation.

The results of the ^{14}C metabolism study show that the half life for the disappearance of ^{14}C activity from the body of DBDPO treated rats was less than 24 hours. The disappearance of ^{14}C activity from the body of OBBP treated rats was biphasic. The half life of the first phase was less

than 24 hours, the second phase greater than 16 days. The principal route of excretion for both experimental materials was via the feces. No appreciable ^{14}C activity (less than 1%) was found in either urine or expired air. There were no sex-related differences in the way these materials were excreted by the rats.

Examination of the various tissues for radioactivity at 1, 3, and 16 days following administration of OBBP and DBDPO labeled with ^{14}C revealed that absorption had occurred with both materials. The levels of ^{14}C activity in the various tissues of the OBBP treated rats were greater than those found in the respective tissues of DBDPO treated rats. The ^{14}C activity readily cleared from the tissues of the DBDPO treated rats whereas on day 16, the last day of the study, ^{14}C activity persisted in the adrenal tissue, skin, adipose, and heart of the OBBP treated rats.

The results of the metabolism study further suggest that DBDPO does not have the potential of OBBP to bioaccumulate. The special tissue accumulation study revealed that after 180 days, there was no accumulation of OBBP or DBDPO in serum, kidney, skeletal muscle or testes of rats on diets providing a dose of 0.1 mg/kg/day. The sites of deposition were the liver and adipose tissue. The bromine content increased rapidly in both these tissues of the OBBP treated rats. The bromine content of the livers of the DBDPO treated rats plateaued after 30 days. The bromine values in the livers of the DBDPO treated rats sacrificed after 180 days on test were not statistically different than the control. Analysis of the data on the bromine content in adipose tissue of DBDPO treated rats revealed a trend, that was statistically significant, toward low level accumulation.

The special study on the elimination of bromine from various tissues of rats maintained for 90 days on diets containing 1.0 mg of OBBP or DBDPO/kg/day revealed high level accumulation of bromine in the liver and adipose tissue of the OBBP treated rats and low level accumulation in the DBDPO treated rats. Bromine was not eliminated from adipose tissue of the OBBP treated rats and only partial elimination from the liver of these rats after 90 days on recovery.

The low level of bromine accumulated in adipose tissue of the DBDPO treated rats remained unaffected during the 90 days on recovery diets. Bromine was readily cleared from the liver of these rats during the first 10 days on recovery.

Since the rats on the DBDPO two-year dietary feeding study have thus far exhibited no adverse effects related to treatment, and the body weights and food consumption data of the treated rats are comparable with the controls, coupled with the fact that 8 mg/kg/day was an unequivocal no effect dose in the 30-day dietary feeding study and 80 mg/kg/day only a marginal effect dose, the trend of DBDPO to accumulate in the adipose tissue of the rats receiving 1 mg/kg/day is judged at this time to be neither toxicologically nor physiologically significant.

An in-depth toxicological investigation on DBDPO is continuing to be pursued by The Dow Chemical Company. The investigation on OBBP has

TABLE III
Water Extraction of DBDPO from Polymers

Time (hrs)	ABS (10% DBDPO) Br, ppm	Polystyrene (10% DBDPO) Br, ppm
3	1.8	<1
19	1.3	<1
27	<1.0	<1
43	3.7	<1
51	not detected[a]	not detected[a]
75	" "	" "
99	" "	" "
187	" "	" "

[a] Detection limit 0.5 ppm.

been terminated because of the likelihood that this material will accumulate in the environment in a manner similar to the polychlorinated biphenyls.

ENVIRONMENTAL STUDIES

Leaching From Polymers

A series of studies were performed to measure the amount of DBDPO leached out of polymers upon exposure to water and other solvents. In the first experiment, pellet of ABS (acrylonitrile-butadiene–styrene) terpolymer and polystyrene containing 10% DBDPO were placed in 2 liters of water and shaken mechanically. Analysis of aliquots of the solution for bromine by neutron activation is given in Table III. Extraction of DBDPO was below limits of detection for Br (0.5 ppm) in many of the aliquots. The lack of increase of Br concentration with time and the erratic values of bromine determined are best explained by assuming that extraction of DBDPO was primarily due to erosion of surface particles. Evidently, migration of DBDPO within the plastic was not significant.

In static extractions of ABS containing 4.25% DBDPO with water, acetic acid, and cottonseed oil at elevated temperatures, the results shown

TABLE IV
Solvent Extraction of DBDPO from ABS

Solvent	Time (days)	Temp.°F	ppm DBDPO in solvent
Water	1	120	Not detected[a]
3% Acetic acid	1	120	Not detected[a]
	7	120	Not detected[a]
Cottonseed oil	7	135	1

[a] Detection limit 0.075 ppm.

in Table IV were obtained. In this case, only about .03% of total DBDPO was extracted by cottonseed oil at elevated temperatures. DBDPO content of the other solutions was below detection limits. By contrast, many of the unusual contaminations of food and milk by PCB's have been caused by their extractability from packaging containers, coatings, and even silo sealants [12].

Combustion Products

An apparatus was constructed to determine the relative amounts of bromine from DBDPO and OBBP converted to HBr during combustion when these materials were used as additives in thermoplastic resins.* Samples of polypropylene containing 5% DBDPO and 5% OBBP were burned in an oxygen rich (28%) atmosphere (to facilitate combustion). The combustion gases were titrated potentiometrically for halide ion and this value was used to calculate the amount of Br in the consumed part of the sample which was converted to HBr. In both cases, essentially all the bromine present in the fire retardant chemicals was converted to HBr (Table V). Subsequent runs using a starch–KI solution to qualitatively identify the presence of free bromine gave negative results.

An attempt was made to further determine the concentration and identify of the gaseous combustion products using long path infrared spectroscopy and mass spectrometry. While non-halogenerated combustion products such as carbon monoxide, carbon dioxide, ethylene, and acetylene were readily identified and measured, neither HBr or Br_2 was detected. This was due to the rapid absorption of HBr in condensation water formed in the apparatus. Bromide ion was confirmed in this water by testing with dilute silver nitrate solutions.

TABLE V
Polypropylene Combustion Data

F.R. Agent	Wt. sample burned, gm	ml 0.1M $AgNO_3$	%Br converted to HBr
None	0.1135	None	None
5% OBBP	0.0941	0.46	96%
5% DBDPO	0.1337	0.70	101%

* A detailed description of the experimental method is given in the Appendix.

Fish Bioconcentration

A fish bioconcentration study was performed by exposing Rainbow trout to DBDPO and OBBP under static conditions. 2,2′4,4′ Tetrachlorobiphenyl, a PCB isomer with known bioconcentration properties, was used as a positive control. ^{14}C labeled DBDPO and OBBP were used to facilitate

TABLE VI
Fish Bioconcentration Study Water Analyses

Compound	Water Concentration, ppb			
	Theoretical	0 Hour	48 Hours Without Fish	48 Hours With Fish
^{14}C-Octabromobiphenyl	20	23	26	20
^{14}C-Decabromodiphenyl Oxide	20	18	20	21
2,2', 4,4'-Tetrachlorobiphenyl	16	13	9	1

low level measurements while the tetrachlorobiphenyl was measured by electron capture gas chromatography.

Analysis of the water samples containing the brominated compounds showed (Table VI) little change in chemical concentration during the experiment. The lack of concentration change reflects minimal uptake by the trout and insignificant losses by other means, e.g., volatilization, absorption upon the surfaces of the tank. The PCB samples did show significant differences in chemical concentration, indicating uptake by the fish as well as losses by other means.

Analyses (Table VII) of filleted flesh from the exposed fish show that DBDPO and OBBP did not bioconcentrate to a measurable extent. (The negative values indicate counting levels below background). 2,2′4,4′ Tetrachlorobiphenyl did bioconcentrate at least 50 times over initial exposure levels within four hours.

Photolytic Degradation

Of the possible degradation routes of halogenated aromatic compounds in the environment, photolytic degradation is of prime importance since these materials do not appear to be readily metabolized by microorganisms. Until recently, this subject received very little attention in terms of the halogenated aromatic compounds. Because studies of this type are complicated by the very low water solubility of the materials in question, most have been performed using nonpolar organic solvents

TABLE VII
Fish Bioconcentration Study Flesh Analyses

Time Hours	^{14}C-Octabromobiphenyl Fish Flesh, Fish Flesh, ppb	^{14}C-Decabromodiphenyl Oxide Fish Flesh, ppb	Tetrachlorobiphenyl Fish Flesh, ppb
0	—	—	<100
1/2	1	-7[2]	150
1	6	1	330
2	14	1	520
4	1	3	1,000
6	-11[2]	1	1,200
12	-3[2]	-2[2]	1,300
24	13	3	1,200
48	8	6	1,000

[2] Below background.

instead of water. Also, the wide variety of ultraviolet sources used makes it very difficult to compare data from one study to another.

Available literature indicates that halogenated aromatics photodegrade by reduction in solvents capable of proton transfer [13, 14]. However, in water, the expected route is an oxidative process of photohydroxylation leading to the formation of phenolic compounds [15].

Modes of Photolytic Degradation

Photoreduction

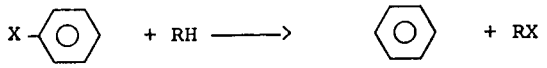

Photohydroxylation

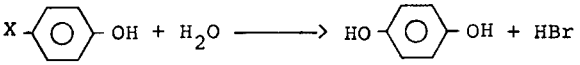

Once photodegradation of a polyhalogenated aromatic molecule in water is initiated, it should accelerate as electron withdrawing halogens are replaced by electron releasing hydroxyls. Also, as hydroxyl replacement of halogen proceeds, the resulting species would be expected to absorb more strongly in the longer wavelengths and this ultimately could result in rupture of the aromatic ring.

Another factor that must be considered is the relative photolability of bromine and chlorine on aromatic rings. C–Cl (85.6 kcal/mole) and C–Br (71 kcal/mole) bond energies suggest that brominated aromatics will be more susceptible to UV degradation [16]. A recent comparative study of photodegradation rates of monobromobenzene and monochlorobenzene in methanol showed that bromobenzene degraded at about 100 times the rate of chlorobenzene. (Iodobenzene degraded at about eight times the rate of bromobenzene) [17].

Comparative data on the photodegradation of hexachlorobenzene and hexabromobenzene in hexane under identical UV exposure showed that hexabromobenzene degraded with a half life of three hours and was completely degraded with ring rupture within 24 hours. Hexachlorobenzene, on the other hand, showed no detectable degradation during 24 hours exposure.

Under rather severe laboratory conditions at an irradiation wave length of 310 mu, polychlorobiphenyls dissolved in hexane have been reductively dechlorinated [18]. In the presence of air and water, polar products were observed. 2,2′,5,5′ Tetrachlorobiphenyl, when exposed to sunlight as a thin film in contact with oxygen and water, gave indication of the presence of hydroxy containing degradation products [19].

An initial study performed on DBDPO dissolved in octanol (7ppm) and exposed to artificial sunlight from a GE sunlamp showed DBDPO to decompose with a half life of four hours.*

* Detailed experimental procedures for the photodegradation studies are given in the Appendix.

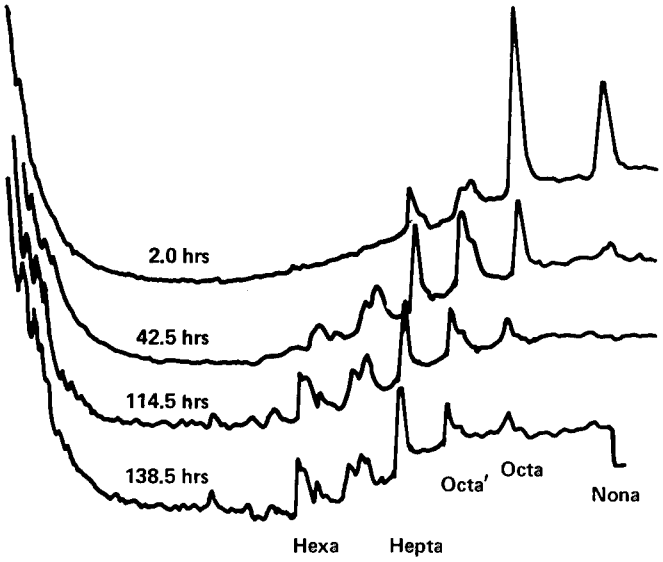

FIG. 6. Octabromobiphenyl (OBBP) Chromatograms after ultraviolet irradiation for different periods.

In order to make a direct comparison of the degradation rates and products of DBDPO, OBBP, and chlorinated biphenyls, parallel experiments were run using xylene as a solvent and exposing the samples in a stirred photochemical reactor to a 125 watt Hg lamp in a water-cooled quartz well. While xylene itself is a strong absorber of UV light, it was one of the best solvents available for DBDPO and OBBP. Gas chromatography and mass spectrometry showed that both DBDPO and OBBP photodegraded in xylene by reductive debromination with half lives of 15 hours and 40 hours

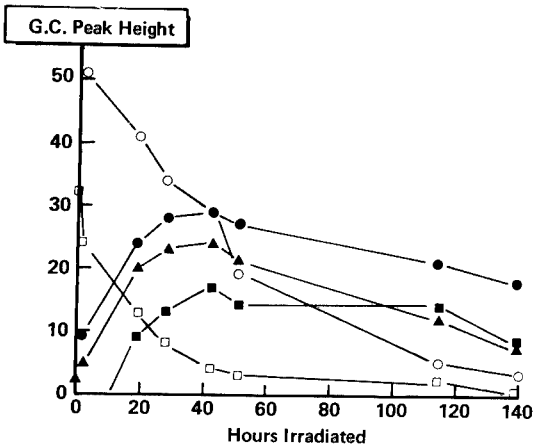

FIG. 7. Photodegradation of OBBP (octabromobiphenyl) in xylene; gas chromatogram peak height vs hours exposure. ○ is octabromobiphenyl; □ is nonabromobiphenyl; ▲ is octabromobiphenyl; ● is heptabromobiphenyl; and ■ is hexabromobiphenyl.

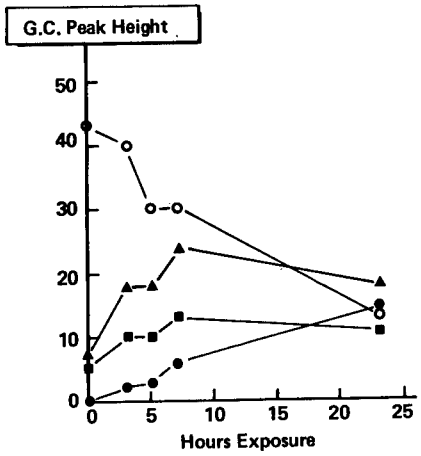

FIG. 8. Photodegradation of DBDPO (decabromodiphenyl oxide); gas chromatogram peak height vs hours exposure. O is decabromodiphenyl oxide; ▲ is nonabromodiphenyl oxide; ■ is nonabromodiphenyl oxide; and ● is octabromodiphenyl oxide.

respectively (Figs. 6, 7, 8). This was also confirmed by Volhard titration of the DBDPO solution for bromide ion (Fig. 9). When exposed under identical conditions, neither Arochlor 1242 nor 1260 showed any evidence of degradation after 350 hours of exposure (Fig. 10).

Even though the above study showed that the brominated aromatics do photodegrade readily, it did not provide any indication of the nature or stability of the decomposition products of DBDPO or OBBP in an aqueous environment. The stepwise photoreduction of DBDPO and OBBP in xylene leads to the formation of a variety of lower brominated diphenyl oxides and biphenyls which may be more stable to UV light than the parent compounds and cause toxicological and environmental problems in their own right. However, previously mentioned studies indicated that in water photohydroxylation would be the favored route and the hydroxyl substi-

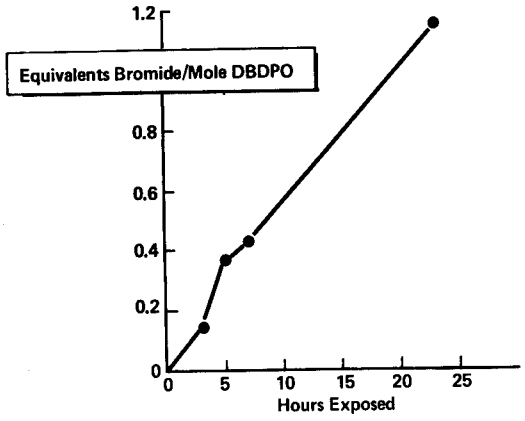

FIG. 9. Photodegradation of DBDPO; bromide formation vs hours exposure.

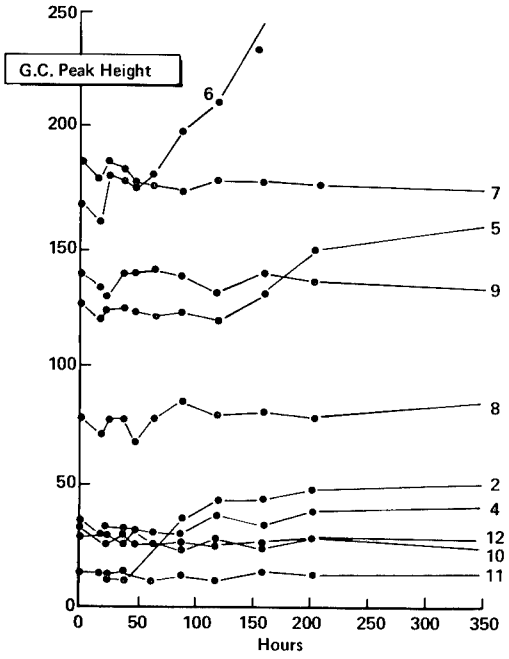

FIG. 10. Ultraviolet irradiation of Arochlor 1242; height of gas chromatogram peaks vs duration of ultraviolet exposure. (Peaks are numbered in order of increasing retention time on column.)

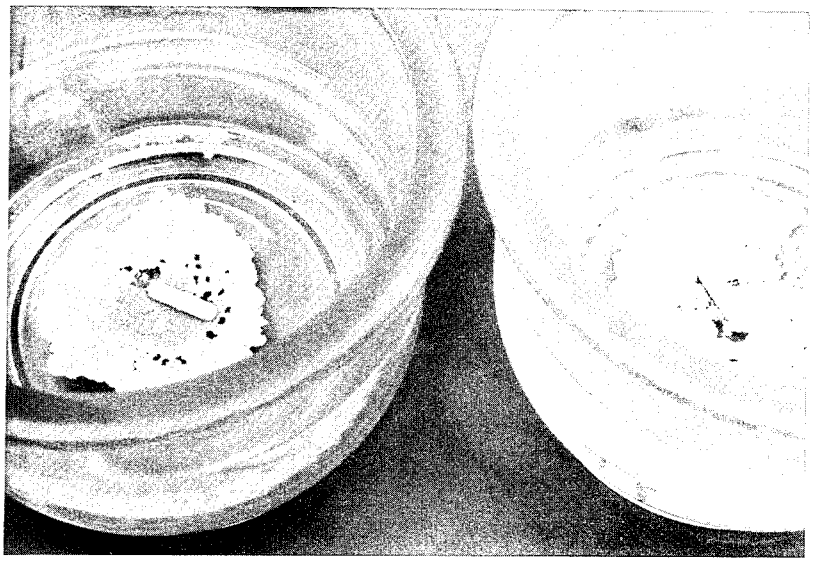

FIG. 11. DPDPO in water after the left sample was exposed to sunlight for 98 days; the right sample was shielded for the same period.

TABLE VIII
Total Bromine Concentration in Water in Sunlight Exposed DBDPO Study

Sample	Bromine, ppm
Dark - 98 days	0.2
Exposed - 31 days	2.6
Exposed - 66 days	5.6
Exposed - 98 days	7.3

tuted degradation products would decompose rapidly via increased UV absorption.

An actual sunlight exposure of DBDPO in water was carried out over a three month period in order to determine if stable lower brominated diphenyl oxides were formed which would show increased persistance over DBDPO. At the end of the exposure period visual comparison of the covered control and exposed sample showed significant discoloration for the exposed sample (Fig. 11). Analysis of the exposed water solution after 31, 66, and 98 days showed a significant increase in bromine concentration relative to the unexposed 98 day sample (Table VIII). After 98 days, this

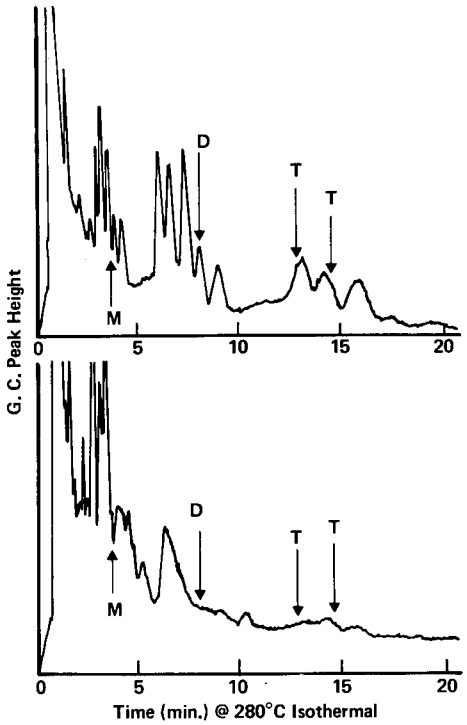

FIG. 12. The upper graph shows the effect of no sunlight exposure on decabromodiphenyl oxide in water for 98 days. The lower graph shows the effect of sunlight exposure on decabromodiphenyl oxide for 98 days.

corresponds to the bromine contributed by breakdown of about 300 times the initial amount of DBDPO soluble in water.

Xylene extracts of the water phase of both 98 day samples were analyzed by electron capture gas chromatography. Since a large excess of DBDPO was used in the experiment, peaks for deca- and nonobromodiphenyl oxide showed no change in intensity. However, the two samples differed markedly in the 0–20 minute retention time range (Fig. 12). The unexposed sample contained several major peaks in the 5–20 minute range that disappeared completely after sunlight exposure. The exposed sample, on the other hand, showed both new peaks and growth of existing peaks in the 0–5 minute retention time range.

Known samples of monobromodiphenyl oxide (4-bromo), dibromodiphenyl oxide (4,4′-dibromo-) and mixed tribromodiphenyl oxides were run under identical conditions and their retention times are shown as M, D, and T in Figure 12. These retention times were also confirmed for mono- and di- by adding known concentrations to the 98 day exposed sample and observing peak change. Based on known quantities added, the 98 day exposed sample was determined to contain < 5 ppb of 4-bromo-diphenyl oxide and < 2 ppb 4,4′-dibromodiphenyl oxide. While it appears that the original sample might have contained tribromodiphenyl oxide, the suspected peaks essentially disappeared after exposure. In no case did the exposed sample show an increase of any peak with retention time similar to those of the lower brominated diphenyl oxides. Also, no other peaks developed with longer retention times than 20 minutes but shorter than those of the highly brominated starting materials. Since the new peaks that appeared in the exposed sample were more volatile than monobromo diphenyl oxide, it appears that the end products of DBDPO degradation are not brominated diphenyl oxides. Subsequent analysis of the xylene extract of the 98 day exposed sample by gas chromatography/mass spectrometry did not indicate the presence of any aromatic bromine compounds in the 0–20 minute retention time range.

In summary, the photodegradation studies indicate that both DBDPO and OBBP are readily degraded by UV radiation when dissolved in organic solvents such as xylene and octanol. Under the same conditions, chlorinated biphenyls did not photodegrade. Exposure of DBDPO under "natural conditions" (in water using actual sunlight) caused it to degrade. The products of the photodegradation of DBDPO in water are not lower brominated diphenyl oxides. Because of this, photodegradation should be a realistic pathway for environmental degradation of DBDPO.

CONCLUSIONS

Based on the data available at this time, DBDPO (decabromodiphenyl oxide) appears to be both environmentally and toxicologically safe for use as a fire retardant additive in thermoplastics.

APPENDIX

Environmental Methodology

Combustion Products

An apparatus was constructed to burn polymer samples in a controlled oxygen environment, collect the combustion products, and automatically titrate for acids or halides. It consisted of an oxygen index flammability test unit as specified in ASTM-D-2863 fitted with air and oxygen supplies controlled by rotameters and a sealed cover with outlet. The oxygen index chamber gas outflow was passed through a trap to remove soot and then bubbled into water in a stirred three-necked 500-ml flask. Electrodes from a Sargent Recording Titrator Model D were inserted into the flask to determine halide concentration by potentiometric titration. An air flow of 2,500 cc/min and oxygen flow of 230 cc/min was used to provide and atmosphere of 28% oxygen (O.I. = 0.28) which would support combustion of the test samples containing OBBP and DBDPO.

Samples of polypropylene containing 5% DBDPO and 5% OBBP were prepared and molded into 5″ × 1/4″ × 1/8″ test bars. The sample was weighed and clamped in the oxygen index chamber. The air and oxygen flows were started through the dried glass system and the titrator was preset to maintain a constant potential. The sample was then ignited with a low temperature gas flame and the oxygen index chamber immediately clamped shut. In most cases, titration started soon after ignition. After approximately 0.15 g of sample was consumed, the oxygen flow was reduced to extinguish the sample. Sufficient air flow was maintained to continue the sweeping of combustion products through the scrubber. While water did condense in the soot trap, the air sweep removed it along with any dissolved halides. More than half of the titratable halide usually came out after the sample was extinguished. When titration was complete, the sample was removed from the combustion chamber and weighed.

Photolytic Degradation

A solution, .00728 mg/ml, of decabromodiphenyl oxide in octanol was placed in a 1 cm quartz spectrophotometer cell. The ultraviolet spectrum was run on a Cary 14 spectrophotometer from 350 mu to 210 mu using octanol as the reference. The cells were placed on a white background 0.5 m from a G.E. (RS 275) sunlamp to approximate the intensity of sunlight. The spectrum was run hourly to a total exposure time of four hours; results showed rapid decrease at 230 mμ and increases at 280–285 and below 230 mμ.

Solutions of 5 g of DBDPO, OBBP, Arochlor 1242 and Arochlor 1260 in one liter of xylene were charged to a photochemical reactor fitted with a

thermometer, magnetic stirrer, and a water jacketed quartz immersion well. A General Electric H-100 medium pressure lamp was suspended in the well. The solution was stirred during exposure and the temperature maintained at 25 ± 5°C. Samples were removed periodically and analyzed by gas chromatography using a flame ionization detector. The DBDPO samples were also extracted with water and the extract was analyzed for bromide ion using the Volhard titration method. For gas chromatography of the brominated compounds, a 4′ × 3/16″ column of 5% SE-30 on 30–60 mesh Chromosorb™ P was used. The temperature was programmed at 8°/minute from 190°C to 300°C. (Identity of the brominated peaks was established by mass spectrometry). The PCB's were analyzed with a 10′ × 3/16″ column of 12% DC-200 on 30–60 mesh Chromosorb P at 225° isothermal. A flame ionization detector was used in all cases.

Two large desiccators which had been thoroughly washed and rinsed successively with acetone, methylene chloride, methanol, water, and left filled with distilled water for eight days, were emptied, then charged with 10 grams of DBDPO (98% deca, 2% nona, which had been recrystallized three times from o-xylene, rinsed with methanol, boiled with water, and dried under hard vacuum overnight) and filled with 8 liters of distilled water. One desiccator was fitted with a standard lid, cased in a desiccator shield, and wrapped in foil. The second was fitted with a tight polyethylene film lid held in place by stretched latex tubing. The two filled containers were placed side by side on the roof of a four story building. One liter of each solution was carefully removed after 31, 66, and 98 days. A 10 ml aliquot of each was decanted and analyzed for bromine using neutron activation analysis. Five hundred ml of each of the 98 day aliquots was extracted with 10 ml of o-xylene. The xylene was separated, dried with $MgSO_4$, and concentrated by evaporation. Gas chromatography was performed using an F&M 5750 Gas Chromatograph equipped with a ^{63}Ni electron capture detector. The column used was a 10′ × 1/8″ stainless steel containing 10% DC-410 Gum on Chromosorb W (60–80 mesh). While separation of the more volatile fraction was obtained by isothermal chromatography at 280°C, it was necessary to use 310°C column temperature to reduce the long retention times of deca-, nona-, and octabromodiphenyl oxide.

REFERENCES

[1] O. Hutzinger, S. Safe, and V. Zitko, "Photochemical degradation of chlorobiphenyls (PCB's)," *Environ. Health Perspect., 1*, 3 (1972).

[2] H. L. Hubbard, in *Kirk-Othmer Encyclopedia of Chemical Technology*, A. Standen (Ed.), Second Edition, Interscience, New York, 1964, p. 289.

[3] I.C.T. Nisbet and A. F. Sarafim, "Rates and Routes of transport of PCB's in the environment," *Environ. Health Perspect., 1*, 21 (1972).

[4] "Arochlor Plasticizers," Technical Bulletin O/Pl-306, Monsanto, 1968.

[5] H. L. Hubbard, in *Kirk-Othmer Encyclopedia of Chemical Technology*, A. Standen (Ed.), Second Edition, Interscience, New York, 1964, p. 290.

[6] E. M. Adams, D. D. Irish, H. C. Spencer, V. K. Rowe, "The response of rabbit skin to compounds reported to have caused acneform dermatitis," *Industrial Medicine*, January, 1941.

[7] Communication from Industrial Bio-Test Laboratories, Inc., Northbrook, Illinois.
[8] J. G. Wilson, "Methods for Administering Agents and Detecting Malformations in Experimental Animals," in *Teratology Principles and Techniques*, J. G. Wilson and T. Warkany (Eds.), The University of Chicago Press, Chicago, 1965, pp. 262–277.
[9] A. B. Dawson, "A note on the staining of the skeleton of cleared specimens with Alizarin Red-S," *Stain Technol., 1*, 123 (1926).
[10] J. G. Aftosmis, O. L. Dashiell, F. D. Griffith, C. S. Hornberger, M. E. McDonnell, H. Sherman, F. O. Tayfun, and R. S. Waritz, "Toxicology of brominated biphenyls. II. Skin, eye and inhalation toxicity and an acute test method for evaluating hepatotoxicity and accumulation in body fat," (Company report), E. I. du Pont de Nemours and Company, Inc, Newark, Delaware.
[11] J. G. Aftosmis, R. Culik, K. P. Lee, H. Sherman, and R. S. Waritz, "The toxicology of brominated biphenyls. I Oral toxicity and embryotoxicity" (Company report), I. E. du Pont de Nemours and Company, Inc., Wilmington, Delaware.
[12] R. F. Skrentny, R. W. Hemken, and H. W. Dorough, "Silo sealants as a source of polychlorobiphenyl (PCB) contamination of animal feed," *Bull. Environ. Contamin. Toxicol., 6*, 409 (1971).
[13] N. Kharasch and P. Friedman, "Photochemically induced hydrogen transfer reactions of iodoaromatic compounds in methanol," *Abstracts, 148th ACS Meeting*, 26S (1964).
[14] R. F. Bridger and G. A. Russell, "Directive effects in the attack of phenyl radicals on carbon-hydrogen bonds," *J. Am. Chem. Soc., 83*, 3754 (1963).
[15] H. I. Joschek and I. Miller, "Photocleavage of phenoxyphenols and bromophenols," *J. Am. Chem. Soc., 88*, 3269 (1966).
[16] T. L. Cottrell, *Strength of Chemical Bonds*, Butterworth, London (1954).
[17] J. H. Plonka,Dow Chemical Company, private communication.
[18] S. Safe and O. Hutzinger, "Polychlorinated biphenyls: photolysis of 2, 4, 6, 2′,4′,6′-hexachlorobiphenyl, "Nature, 232, 641 (1971).
[19] O. Hutzinger, S. Safe and V. Zitko, "Polychlorinated biphenyls: photolysis of 2,4,6,-2′,4′,6′-hexachlorobiphenyl," *Nature, 232*, 15 (1971).

RELATIONSHIP OF THERMOCHEMICAL CHAR-YIELD TO THE FIRE RETARDANT PROPERTIES OF FOAMED POLYMERS*

R. H. FISH and J. A. PARKER

Ames Research Center, National Aeronautics and Space Administration, Moffett Field, California 94035

SYNOPSIS

Early polymer development at NASA-Ames paralleled spacecraft heat-shield development. Polymer characterization, therefore, has emphasized the thermal performance of char-forming ablative materials. Later, as the primary thermochemical char-yields (percent ash residues) were measured, polymer char-yield was found to be a function of molecular structure, i.e,, the number of aromatic equivalents per gram of polymer.

Because this relationship is a powerful general rule, it is applied in this study to a number of low-density polymer foam systems. These foam systems are classed, generally, as polyurethanes, polyisocyanurates, polyimides, and polybenzimidazoles and they cover a wide range of char-yields (20 to 76% at 800°C). Because the polymer char-forming process is much the same, whether reacting as an ablative heat-shield for spacecraft re-entry or as a thermal protective barrier in a fire environment, heat-shield technology has been used in devising fire-protection systems. Polymers exposed to a fire exhibit a number of measurable fire-associated properties, such as ignition, flammability, smoke production, and thermal insulation efficiency. In this study these properties are compared to the primary thermochemical char-yield of the foamed polymers tested.

The properties of ignition ease measured by the limiting oxygen index, flammability measured by a 2-foot flame tunnel, and smoke production measured by a modified NBS smoke chamber decreased with increasing char-yield. Because the efficiency of an ablative thermal barrier depends not only on reradiation of heat by the char-surface, but also on the transpiration cooling of the char zone by the outgassing products of decomposition, the property of thermal insulation efficiency, measured by exposure to a JP-4 fuel fire, will optimize as vapor production diminishes with increasing char-yield. Efficiency can be increased in the lower char-yielding polymers by addition of inorganic fibers to stabilize the char and increase the residence time of the cooling vapors. Efficiency can increase in the higher char-yielding polymers by addition of non-toxic vapor producing components, to provide additional transpirational cooling. Although not a part of this study, current work indicates that the relative toxicity of the vapor products of polymer decomposition decreases with increasing char-yield.

The char-yield of a polymer may be used as a guide to predict polymer behavior in a fire and will indicate which classes of polymers must be considered if ignition, flammability, smoke production, and relative toxicity must be minimized.

* Presented also at the National SAMPE Symposium and Exhibition, Los Angeles, California, April 11–13, 1972.

Applied Polymer Symposium No. 22, 221 (1973)

ULTRATHIN MEMBRANES FOR TREATMENT OF WASTE EFFLUENTS BY REVERSE OSMOSIS

L. T. ROZELLE, J. E. CADOTTE, B. R. NELSON, and C. V. KOPP

North Star Research and Development Institute, Minneapolis, Minnesota 55406

SYNOPSIS

Ultrathin membranes with thicknesses from 500 to 6000 Å were investigated for reverse osmosis treatment of municipal and metal finishing wastewaters. Several of these membranes consisting of polysaccharide mixed esters and ethers and a non-cellulosic condensation polymer were found to be highly suitable for this application. Ultrathin membranes prepared from cellulose acetate o-propyl sulfonic acid (CAOPSA) exhibited the following results using secondary effluent feeds under 600 psi pressure for 150 hours: an average water flux of 34 to 36 gallons per square foot (of membrane) per day (gfd) over the last 100 hours, and rejections of 96% for total dissolved solids, 94% for ammonia, and 83% for total organic carbon. Treatment with an enzyme-active laundry presoaking product was found to be effective in cleaning the membranes and restoring the flux to levels existing before fouling.

Several membranes were tested for treating metal finishing waste effluents using acidic solutions of metal ions at concentrations to simulate plating bath rinse waters. For nickel, iron, zinc and copper, ultrathin membranes of three polymers were promising: cellulose acetate, CAOPSA, and β-glucan acetate dimethylaminoethyl ether. Water fluxes were generally above 30 gfd at metal ion rejections up to 99.9%. For chromic acid an effective polymer membrane was CAOPSA. This membrane exhibited a water flux above 25 gfd at rejections of chromium above 90%. A new non-polysaccharide membrane was shown to be an excellent candidate for treating alkaline cyanide waste solutions. After several 500- and 340-hour tests on alkaline copper and zinc cyanide simulated rinse baths at pH's of 11.8 and 12.9, respectively, these membranes (designated NS-1) exhibited an average water flux of 10.1 and 11.8 gfd, respectively, greater than 95% rejection, and no membrane degradation.

INTRODUCTION

Reverse osmosis has high potential to be a major process for removal of contaminants from municipal and industrial waste streams and for reuse of the purified water. Although originally developed for demineralization of sea and brackish waters to obtain potable water supplies, reverse osmosis is finding applications in the treatment of a variety of domestic and industrial effluents [1, 2, 3, 4]. The reverse osmosis process of purification physically separates impurities in solution by circulating waste effluents at high pressures over the surface of semipermeable membranes. It is this

Applied Polymer Symposium No. 22, 223–239 (1973)

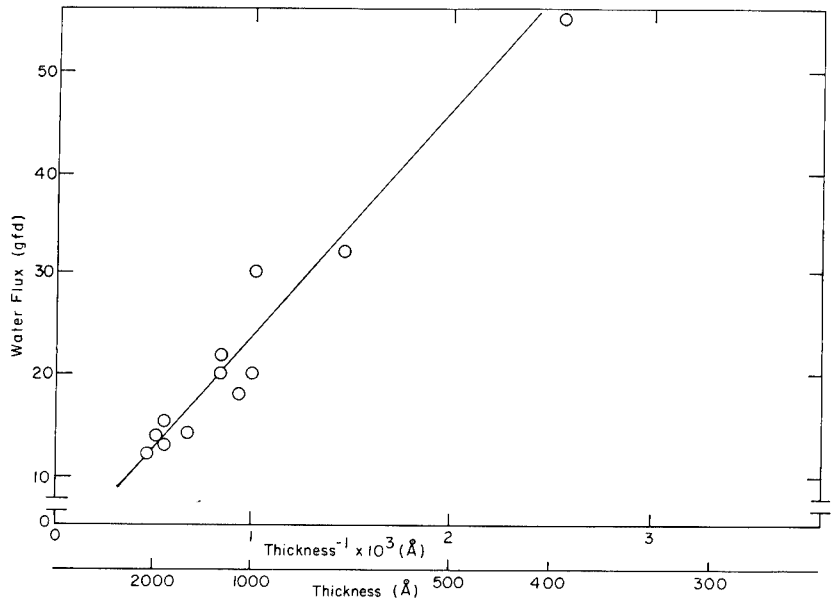

FIG 1. Effect of membrane thickness on water flux for cellulose acetate (E398-10).

membrane which largely determines the degree to which contaminants are rejected and the rate at which the purified water is passed (water flux).

The polymer used most often as a membrane for water desalination by reverse osmosis has been cellulose acetate. Reid and Breton [5] originally showed that this material had excellent potential as a reverse osmosis membrane. Loeb and Sourirajan [6] later developed the asymmetric cellulose acetate membrane that is used most extensively at the present time.

Ultrathin Membranes

In the work reported here unique membranes—ultrathin in nature—of various polymers were evaluated for the reverse osmosis treatment of municipal and metal finishing waste effluents. One type of ultrathin membrane can be prepared by pouring a solution of a polymer (*e.g.*, cellulose acetate) dissolved in a suitable solvent (*e.g.*, cyclohexanone) onto a water surface and allowing it to spread. A gelled ultrathin polymer membrane remains after evaporation of the solvent. In earlier desalination studies, flat sheets of ultrathin cellulose acetate membranes, with thicknesses under 2000 Å, were placed upon a suitable microporous support film (*e.g.*, polysulfone or Millipore VFWP filters) and were shown to exhibit significantly higher reverse osmosis performance than asymmetric cellulose acetate membranes [7, 8].

An advantage of the water-cast ultrathin membranes is the ability to control thickness and, hence, water flux. The solution diffusion model [9] predicts that the plot of flux versus reciprocal thickness should yield a

straight line through the origin. Figure 1 illustrates the effect of thickness on the water flux of an ultrathin cellulose acetate (E398-10) membrane. The relationship was linear with inverse thickness over the thickness range studied (400 Å to 2000 Å). These ultrathin membranes thus have considerable potential for high flux without affecting the rejection. Ultrathin cellulose acetate membranes have been characterized in earlier work [8, 10, 11].

The other type of ultrathin membrane is prepared by coating a non-polysaccharide polymer (designated NS-1) directly onto the microporous support, and insolubilizing it by crosslinking. In previous work the NS-1 membranes were shown to be one of the top candidates for single-stage seawater desalination [12].

The support used for the ultrathin membranes is a microporous film of polysulfone. These films, unlike the porous backing of the asymmetric membrane, are relatively resistant to pressure compactions, can be air dried without loss of porous properties, and are resistant to biological and chemical degradation [8, 11, 13]. They are also easy to prepare and handle.

Polymers

Transport properties of materials across polysaccharide membranes are grossly affected by substitution of functional groups (*e.g.*, esters and ethers [14, 15, 16]. Polysaccharide derivatives with a high degree of substitution of ester groups (*e.g.*, acetate) and, in addition, a minor proportion of highly hydrophylic substituent (*e.g.*, an alkyl sulfonic acid), were considered desirable for this work. The hydrophylic substituent would increase water transport rates.

A new non-polysaccharide membrane was shown in earlier work to be a prime candidate for wastewater treatment [12]. This new membrane (referred to as "NS-1") consists of a polysulfone support film with a 6000-Å thick coating of polyethylenimine reacted with tolyene diisocyanate. The structure is believed to be highly branched and crosslinked. Used with synthetic seawater at 1500 psi, the NS-1 membrane provides over 20 gfd flux at 99.5% salt rejection. Stability of the membrane to alkaline feed waters (pH 7 to 13) is excellent, which in turn, provides a possible new membrane for highly alkaline wastewaters.

Ultrathin membranes were prepared from a variety of polymers used for the reverse osmosis treatment of effluents from a high-rate activated sludge municipal treatment plant and simulated metal finishing processes. These polymers consisted of ultrathin polysaccharide mixed esters and ethers, ultrathin membranes of commercial polymers, and commercially available membranes. Membranes from four polymers exhibited the greatest potential for ultimate use, cellulose acetate o-propyl sulfonic acid, β-glucan dimethylamino ethyl ether, cellulose acetate methyl sulfonate, and NS-1. The reverse osmosis results of these four membranes are reported in this paper.

EXPERIMENTAL

Preparation of the Polysaccharide Derivatives

The procedure for the preparation of the polysaccharide derivatives followed two basic techniques:

1. The starting material was cellulose acetate with free hydroxyl groups. The cellulose acetate was reacted with a suitable hydrophylic reagent to produce the desired derivative for film casting. Cellulose acetate methyl sulfonate (CAMS) was prepared by reacting Eastman cellulose acetate (398–10) in pyridine solution with an excess of methane sulfonyl chloride.
   Completion of the reaction was determined in the product from the infrared absorption of a one-mil film at 3500 cm^{-1} (absence of the hydroxyl absorption peak indicated virtually complete substitution). The substitution of the new group was then estimated by subtraction of the known acetyl content from 3.0.
2. The starting material was pure polysaccharide. A given amount of hydrophylic reagent was used to etherify the polysaccharide to achieve a desired degree of substitution (DS). The partially substituted polysaccharide was then acetylated to full substitution. For preparation of cellulose acetate o-propyl sulfonic acid (CAOPSA), cellulose (cotton linters) was etherified with 1,3 propane sultone in an aqueous NaOH medium. The cellulose propyl sulfonate was acetylated in an acid-acetic anhydride media using perchloric acid as a catalyst.
   A procedure similar to CAOPSA was used to prepare β-glucan acetate dimethylaminoethyl ether (β-GADE). β-glucan was dissolved in aqueous alkali to react it with 2-dimethylaminoethyl chloride hydrochloride. The etherified product was isolated and acetylated in an acetic acid-acetic anyhydride media using a perchloric acid catalyst.

Preparation of Water-Cast Membranes

The polymeric derivative was dissolved in an organic solvent and filtered through a Seitz K-5 filter pad to remove gel particles. The solution with up to five percent by weight polymer was poured onto a water surface. The solution spread quickly and gelled to form an ultrathin membrane. The thickness was controlled by pulling the gelling membrane across the water surface at a constant rate. The solvents included cyclohexanone or a 90:10 mixture of dichloromethane:methanol. Either a Millipore VFWP filter or a microporous polysulfone film was used as a support for the ultrathin membranes in the reverse osmosis tests. Details of the preparation procedures for flat-sheet ultrathin membranes and polysulfone films are

described elsewhere [1,3]. The support was laminated to the ultrathin membrane by immersing the support in the water underneath the ultrathin memabrane and pulling it out of the water with the ultrathin membrane on its surface. The thickness of the ultrathin membranes was measured by interferometry techniques using a Reichert Metallograph equipped with a Normaskii polarization interferometer [10].

The preparation of the NS-1 membranes for both tubes and flat sheets was based on a coating process. A polysulfone support film was coated with a polyethylenimine (PEI) solution. The PEI-coated polysulfone film was then immersed in a tolylene diisocyanate solution for the crosslinking step [12]. For tubes, polymers were coated inside 0.5 in. id fiber glass tubes (Abcor, Inc.) that had been previously lined with a microporous polysulfone support.

Reverse Osmosis System

The reverse osmosis test loop (Fig. 2) contained a 20-liter reservoir, a Model 214-144B Milton Roy Pump, an accumulator (surge tank), a heat exchanger, six stainless steel test cells, a 100-mesh, high-pressure filter, a needle valve for system pressure control, and a Rotameter-type flow meter.

The design of the flat test cell is shown in Figure 3. The cell was machined from AISI 316 stainless steel. Mechanical support for the membrane was supplied by a 2-in. diameter sintered stainless steel plate, 1/4 in. thick. A Kraft paper support was placed between the porous plate

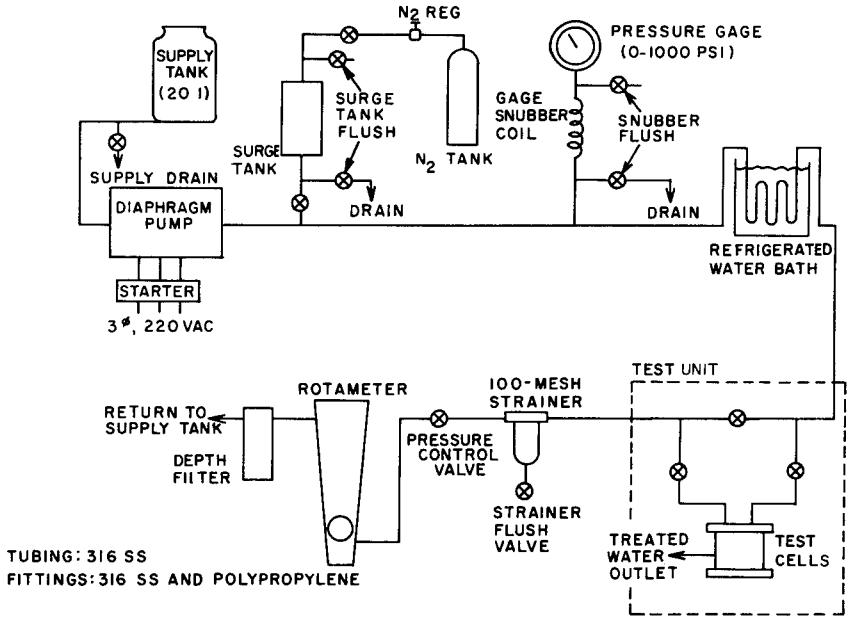

FIG 2. Schematic diagram of reverse osmosis test apparatus.

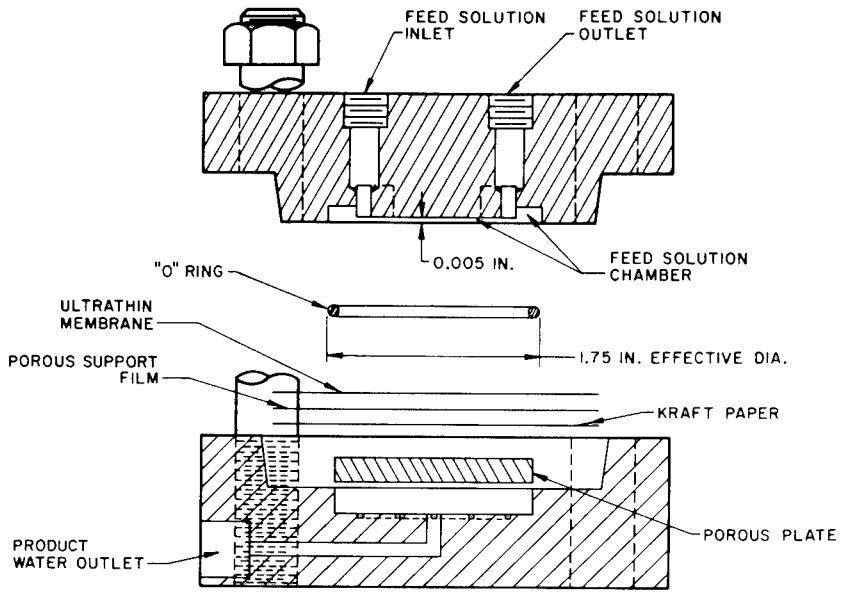

FIG. 3. Dynamic flat test cell for reverse osmosis.

and the membrane-support composite to protect the membrane from the rough surface of the plate. A seal was obtained with a 1.75 in. (id) "O" ring. The two end plates were held together by four nuts.

MUNICIPAL WASTE EFFLUENTS

Reverse Osmosis Tests

In the extended-term reported here the experimental procedure consisted of circulating secondary effluent (which had been filtered through a glass fiber mat and the pH adjusted to 5) at 600 psi through the test cells containing the membranes. After twenty hours, the membranes in the test cells were cleaned for 1.5 hours with a solution of 20 g of an enzyme active detergent. Deionized water was then circulated through the cells briefly under 600 psi, and fresh, filtered secondary effluent was again circulated through the cells under 600 psi for twenty hours. These twenty-hour test cycles, with the cleaning and deionized water procedures, were repeated seven times (150 hours). Each cycle was designated as a "test section" and given a number.

The secondary effluent was obtained from the Minneapolis-St. Paul Sanitary District plant. To prevent excessive biological activity, the effluent was stored at 4°C prior to use. Typical analytical data on the treated secondary effluents are given in Table I.

The feed and product waters were analyzed for total organic carbon (Beckman Instruments), ammonia nitrogen [17] total suspended solids (TSS) [10] and total dissolved solids (TDS) [17]. Except for suspended solids, the feedwaters were filtered through a 0.45μ filter before analysis.

Results and Discussion

Three polymers, cellulose acetate o-propyl sulfonic acid (CAOPSA), cellulose acetate methyl sulfonate, and cellulose acetate (CA), formed ultrathin membranes that exhibited water fluxes significantly higher than asymmetric cellulole acetate control membranes. The solute rejections were generally similar for all four membranes. Table II gives the results of reverse osmosis tests of approximately one week's duration using secondary effluent for these three polymer membranes and an asymmetric membrane control. The ultrathin membranes were all in the 400 to 600 Å thickness range. The data for important reverse osmosis parameters are summarized below.

Average Water Fluxes

The highest average flux—43 gfd—was observed for the CAOPSA membrane in the first test section. After forty hours, the average water flux for this membrane remained at about 36 gfd for the remainder of the test. The ultrathin cellulose acetate membrane exhibited a comparable average flux (34 gfd) in the third test section. Much lower average fluxes were observed for the cellulose acetate methyl sulfonate and the asymmetric cellulose acetate control membrane (20 gfd and 13 gfd, respectively, over the last two-thirds of the test).

TABLE I
Representative Analytical Data on Minneapolis-St. Paul Sanitary District Secondary Effluent[a]

Analysis	Average Values (mg/liter)
Chemical oxygen demand (COD)	127 - 159
Biochemical oxygen demand (BOD)	56
Ammonia -N	9 - 13
Nitrate -N	11 - 25
O-Phosphate	10 - 14
Total suspended solids (TSS)	30 - 90
Total dissolved solids (TDS)	850 - 1000
Soluble organic carbon	30 - 90
pH	7.0 - 8.5

[a] From MSSD data, permission for use granted by the District, April 1970.

TABLE II
Reverse Osmosis Treatment of Secondary Effluent

	Average Water Flux Within Test Section (gfd)							Average Percentage Rejection		
Membrane	1	2	3	4	5	6	7	TDS	NH_3	TOC
CAOPSA (211-89A)	43	40	35	36	36	34	36	96	94	83
Cellulose Acetate Methyl Sulfonate (211-10C)	30	24	20	21	21	18	19	97	96	85
Cellulose Acetate (E398-10)[a]	39	37	34	—	—	—	—	93	92	83
Cellulose Acetate (RO-97)	14.5	13.	13.5	13.2	13.2	13.2	13.2	96	92	85

Feed Data [Average Concentration in Filtered Feed (mg/l)]			
TSS[b]	TDS	NH_3(N)	TOC
15	668	8.1	25.1

[a] An apparent membrane failure was observed after Test Section 3; the average rejections include only Test Sections 1, 2, and 3.
[b] TSS = 52 for unfiltered feed.

Fouling Flux Decline

The flux-versus-time data for two of the membranes is given in Figure 4. For the CAOPSA membrane, the initial water flux in each test section with the effluent was always two or more gfd less than the deionized water flux. These initial effluent water fluxes varied from 55 gfd to slightly less than 40 gfd. The water flux at the end of the 20-hour test sections varied from about 38 gfd to about 30 gfd. The drop in water flux between washes was caused by the deposition of solid material on the surface of the membrane. All four membranes had some deposits on their surfaces when they were inspected at the end of the test. This fouling flux decline can be reduced by improving the cell design (*e.g.*, tubular configuration with turbulence promoters), increasing the feed flow rate, and by increasing the suspended solids removal. The asymmetric cellulose acetate control membrane exhibited very little flux decline over this time period (Fig. 4), because of its considerably lower flux.

Rejection Performance

As indicated in Table II, the ammonia rejections were high: up to 96%. The TDS rejections were above 95% in most cases. The TOC rejections were observed at 84 $\times$1%. This rejection performance was consistent throughout the 150-hour test. Phosphate rejection in earlier years were always above 99% for these membranes [1].

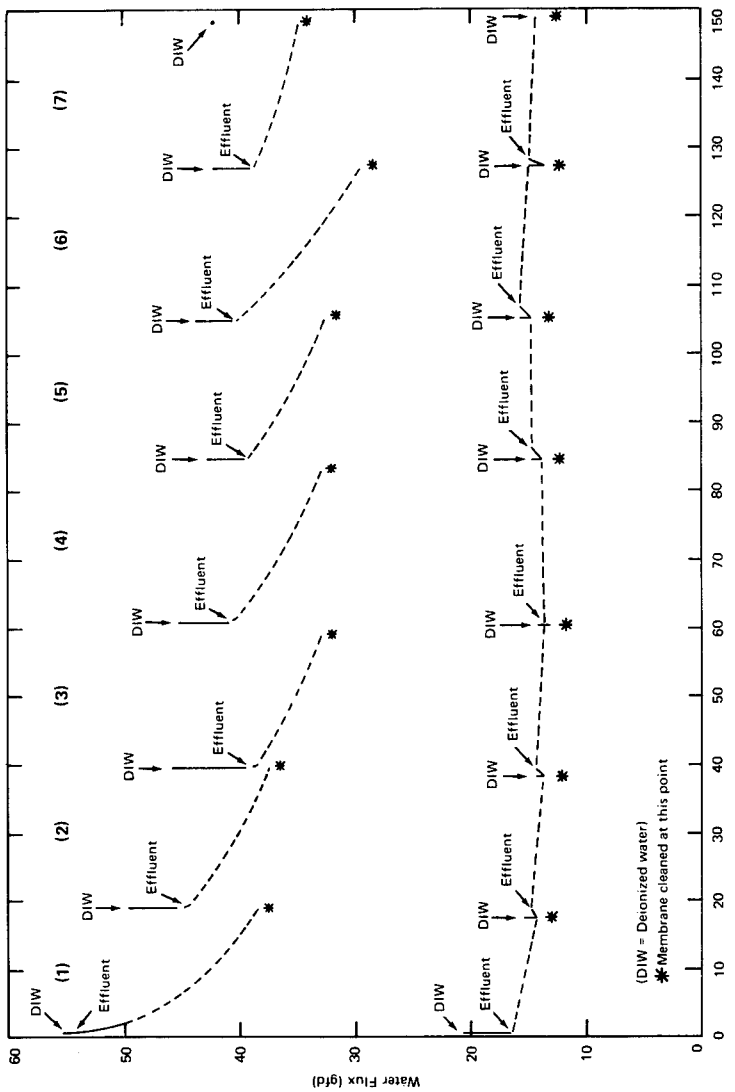

FIG. 4. Water flux data from secondary effluent test with ultrathin cellulose acetate o-propyl sulfonic acid and asymmetric cellulose acetate (RO-97).

METAL FINISHING WASTEWATERS

Water-Cast and Commercial Membranes

Reverse Osmosis Testing

The water-cast ultrathin membranes were tested in the flat reverse osmosis cells. The reverse osmosis tests were carried out under 600 psi pressure at 25°C and a feed flow rate of 1650 ml per minute. The simulated plating bath rinse solutions used in the membrane-testing procedures contained the most common as well as the most troublesome metal salts, acids, and bases. Solutions containing nickel, iron, copper, zinc, and chromium metal ions and cyanide ions represented the acid and alkaline electroplating rinses. The solution preparation procedures are given elsewhere [3]. The concentration of metal ions in the feed and product water were measured using a Varian AA-120 Atomic Absorption Spectrometer. The concentration of the cyanide ions was determined by total carbon analysis.

The metal ion concentrations in the feed solutions were maintained at 100 mg per liter by a recirculating system. The membranes were compressed with a 0.1% sodium chloride solution followed by testing with solutions containing nickel, zinc, iron, copper, and chromium, in that order, all at pH 5.0. This was followed by a chrominum solution at pH 2.5 and a mixed feed solution at pH 2.5. (Iron was omitted because of the precipitation of ferric oxide caused by the oxidation of the ferrous ion by the dichromate ion.) If it was suspected that the membranes had been damaged during the testing procedure, a final retest with the sodium chloride solution was made for comparison with the initial test. Figure 5 shows a typical water flux curve for two ultrathin cellulose acetate membranes during the testing procedure. The water flux curve was relatively smooth, despite changes in feed solutions.

Results and Discussion

For solutions of nickel, iron, copper and zinc, three polymers, cellulose acetate o-propyl sulfonic acid (CAOPSA), β-glucan acetate dimethylaminethyl ether (β-GADE), and cellulose acetate (E360–60), formed ulthrathin membranes that exhibited significantly higher water fluxes than the control asymmetric cellulose acetate membrane. Table III gives the results of these measurements. The rejections for the control and ultrathin cellulose acetate membranes were all higher than the β-GADE and CAOPSA membranes. However, the potential of greater chemical resistance and significantly high product water flux makes these membranes attractive for actual use. The thicknesses of all the ultrathin membranes in Table III were in the range of 900 to 1200 Å.

In Table III the results of two different variations of the CAOPSA polymer membrane are given. The 211-96B polymer exhibited a high flux

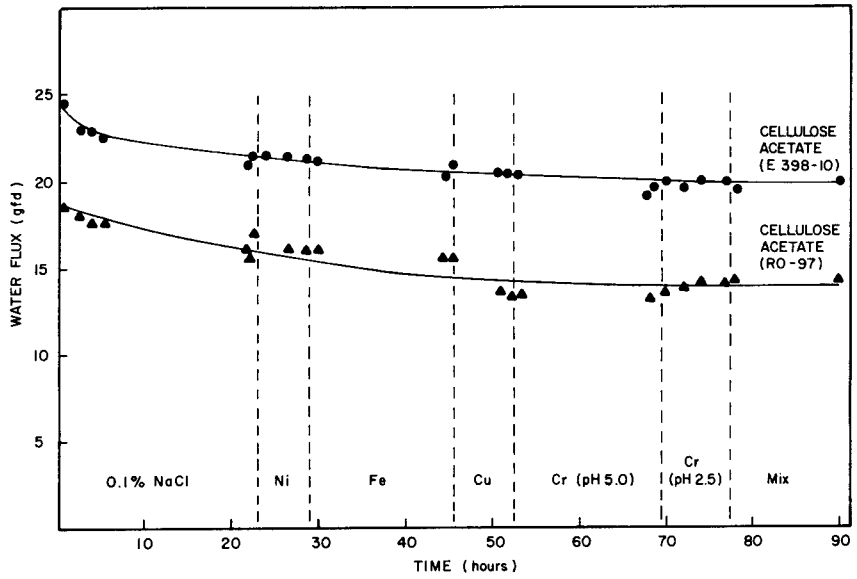

FIG. 5. Typical water flux behavior across membranes during reverse osmosis treatment of metal ion solutions.

(42 gfd), but the rejections were lower than those of the other membranes. The 211-89A polymer, which was prepared to contain a smaller amount of the hydrophylic o-propyl sulfonic acid than the 211-96B polymer, exhibited a reduced water flux of 19 gfd, but gave a high rejection for each metal species (above 97%). It is thus possible to vary the performance of the cellulose acetate o-propyl sulfonic acid membrane by varying the amount of the substituents on the cellulose unit.

The effect of feed water concentration on product water flux was investigated for several membranes ranging from low to high in water transport rates. The results are plotted in Figure 6. The flux of each membrane was

TABLE III
Reverse Osmosis Treatment of Nickel, Iron, Zinc, and Copper Solutions

Ultrathin Membrane	Water Flux (gfd) (70 hr)	Metal Ion Rejection (percent)			
		Ni	Fe	Cu	Zn
Cellulose Acetate (E360-60)	30	>99.9	>99.9	>99.9	98.7
β-Glucan Acetate Dimethyl-aminoethyl Ether (211-40A)	47	99.2	96.6	95.1	98.7
Cellulose Acetate O-Propyl Sulfonic Acid (211-96B)	42	94.5	91.2	82.9	99.2
Cellulose Acetate O-Propyl Sulfonic Acid (211-89A)	19	97.6	97.7	97.4	99.8
Cellulose Acetate (RO-97)	14	>99.9	>99.9	>99.9	>99.9

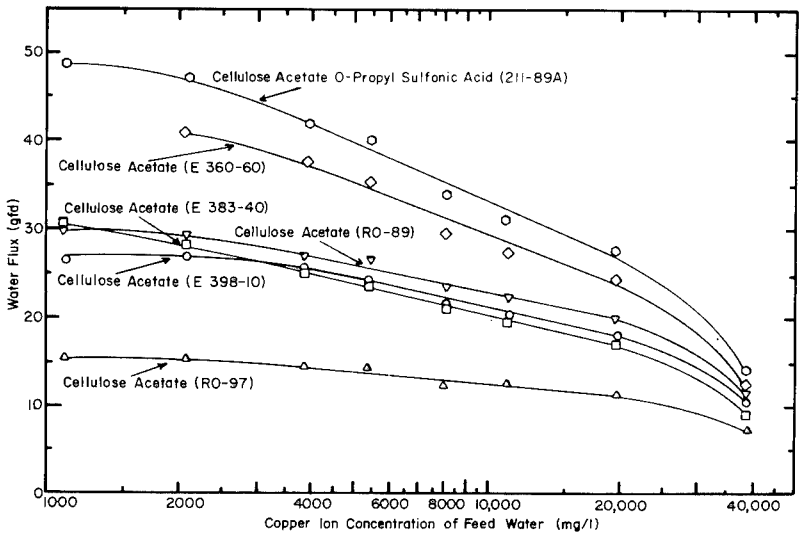

FIG. 6. Effects of increasing feedwater concentration on the water flux of reverse osmosis membranes.

corrected for a thickness of 1000 Å. The actual thicknesses varied from 500 to 1500 Å.

At a feed concentration of 2000 mg per liter copper, the water fluxes of all six membranes in Figure 6 began an approximately linear decline to a concentration of 20,000 mg per liter copper. Between 20,000 and 40,000 mg per liter copper, the water fluxes declined more rapidly. The linear portion of the curves in Figure 6 (2000 to 20,000 mg per liter copper) probably resulted from the increasing osmotic pressure in the feed water (from the increasing copper ion concentration). Since the operating pressure was not increased, the effective driving force would be reduced. For example, at a feedwater concentration of 20,000 mg per liter copper, the effective driving force was 378 psi instead of 600 psi.

The more rapid water flux decline in Figure 6 between feed water concentration of 20,000 and 40,000 mg per liter copper was probably caused by concentration polarization. This was evidenced by the fact that the high-flux membranes exhibited a sharper drop in flux than did the low-flux membranes. These sharper flux decreases of the high-flux membranes were attributed to greater concentration polarization effects which, in turn were caused by a relatively faster buildup of copper sulfate at membrane surfaces. It should also be noted that as the copper concentration of the feedwater increased, the difference in water flux between the lowest- and highest-flux membranes steadily decreased. In Figure 6, at 1000 mg per liter copper, water fluxes of the membranes varied from 15 to 49 gfd—a 34 gfd difference. At 40,000 mg per liter copper, they ranged from 9 to 15 gfd—a 6 gfd difference.

Chromic acid was observed to behave differently from the other metal

TABLE IV
Reverse Osmosis Treatment of Chromic Acid Solutions

Membrane	Membrane Thickness	Water Flux (gfd)			Percent Rejection of Cr^{+6} pH 2.5		pH 5.0
		65 hrs	140 hrs	170 hrs	65 hrs	140 hrs	170 hrs
Asymmetric Cellulose Acetate (RO-97)	4 mils	17	18	17	93.8	89.6	97.8
Ultrathin Cellulose Acetate O-Propyl Sulfonic Acid (211-89A)	500 Å	25	27	28	95.4	90.0	97.4
Ultrathin Cellulose Acetate (E398-10)	1200 Å	17	18	18	84.8	82.8	90.0

species. Table IV presents the results of reverse osmosis tests (up to 170 hours in duration) with three membranes using a chromic acid feed solution. The two pH's were chosen because pH 2.5 is the pH of a 100 mg per liter chromic acid (as chromium) solution, and pH 5.0 is the pH at which minimum hydrolysis of cellulose acetate membranes occurs [18].

The three membranes were exposed to chromic acid feedwaters (100 mg per liter chromium) for a total of 170 hours: 140 hours at pH 2.5, followed by 30 hours at pH 5.0. A decrease in the chromium rejection for all three membranes was observed in tests made at 65 and 140 hours at pH 2.5. A test of the membranes with a copper sulfate solution at 140 hours (pH 2.5) showed no serious degradation. The ultrathin cellulose acetate membrane

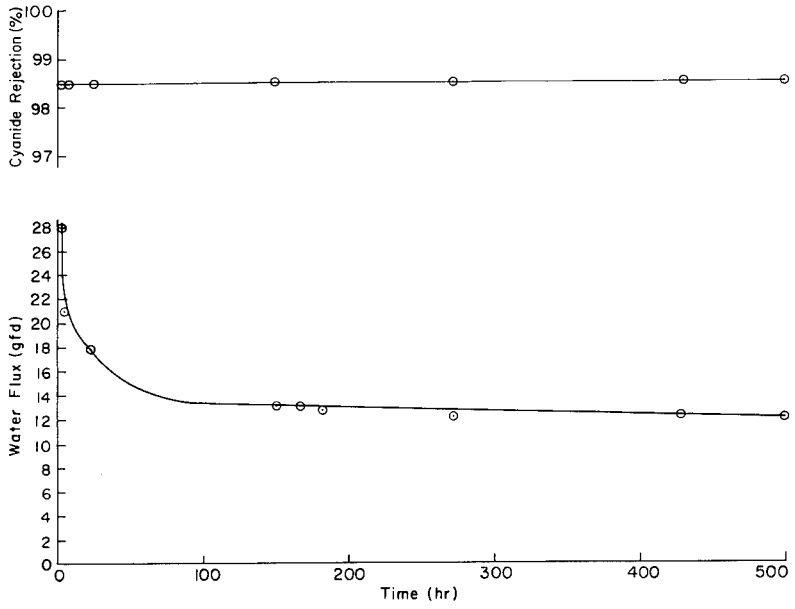

FIG. 7. Reverse osmosis performance of the NS-1 membrane on simulated copper cyanide rinse water.

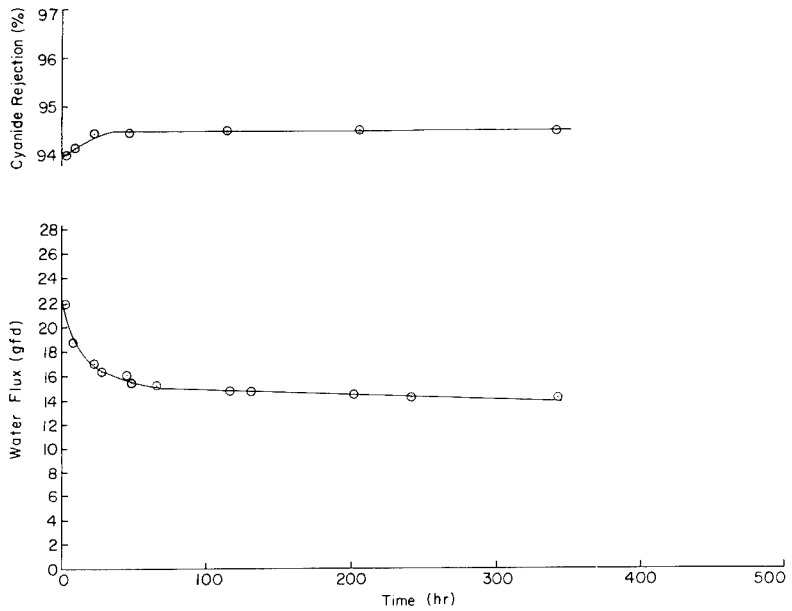

FIG. 8. Reverse osmosis performance of an NS-1 membrane on simulated zinc cyanide rinse water.

in Table IV would have exhibited higher water flux at a thickness comparable to the CAOPSA membrane. However, its chromic acid rejections were significantly lower than the other two membranes.

In Table IV an improvement in the rejection of the chromic acid with a change in pH from 2.5 to 5.0 was observed. The increase in ionization of the chromic acid at the higher pH apparently results in ionic species with decreased solubility in the membranes.

TABLE V
Comparison of Cyanide Rejection for Membranes with Zinc Cyanide Plating Rinse Waters

Membrane	Cyanide Rejection (percent)
Cellulose Acetate[a] Eastman RO-97	Membrane Deteriorated
Cellulose Acetate Butyrate* Universal Water Corporation	Membrane Deteriorated
Nylon Hollow Fibers* DuPont "Permasep B-5"	28.0
NS-1[b]	95.5

[a] Data on the cellulose acetates and hollow fibers given by A. Golomb [19]. Test solution for these membranes: zinc cyanide plating rinse at 1% of bath concentration, pH 11.8 at 600 psi.
[b] NS-1 results obtained at 10% of bath concentration, pH 12.9 after 340-hour operation.

NS-1 Membranes

Reverse Osmosis Testing

Each test reported here consisted of using four two-foot reverse osmosis tubes and one flat reverse osmosis test cell, containing NS-1 membranes. The tests were carried out under 600 psi pressure at 25°C. The simulated rinse water feed solutions consisted of 1/10 the average concentration of common copper and zinc cyanide plating baths. The copper-cyanide rinse waters contained 1.9 grams per liter copper and 3.1 grams per liter cyanide at a pH of approximately 11.8. The simulated zinc cyanide rinse water was prepared by a 1:10 dilution of an actual alkaline zinc plating bath solution obtained from Honeywell Inc. (approximately 1.3 grams per liter zinc, and 44.5 grams per liter sodium cyanide at a pH of 12.9).

Results and Discussion

Figure 7 is a typical plot of the water flux as a function of time in the copper cyanide system. For the four tubes and one flat cell the average percent copper and cyanide ion rejections after 500 hours were 99.9 and 98.7, with an average flux of 10.1 gfd. Figure 8 contains typical plots of water flux and cyanide rejection as a function of time for the zinc cyanide system. After the 340-hour test the average rejection of zinc and cyanide ions was 99.8 and 95.5% with an average water flux of 11.3 gfd (three tubes, one flat cell).

In both the copper and zinc cyanide tests the water flux at the end of the tests was between 50 and 70% of the initial readings. The water flux decline in both the copper and zinc cyanide tests was attributed primarily to fouling by colloidal iron oxide which was observed on the membrane surfaces after the 500- and 340-hour tests. This iron oxide is produced by chemical action on the stainless steel surfaces in the reverse osmosis system.

The results in Table IV demonstrated the absence of NS-1 membrane deterioration in the treatment of the highly alkaline zinc and copper cyanide plating bath rinse waters. Table V gives a comparison of NS-1 membranes with two commercially available membranes and one commercially available hollow fiber using zinc cyanide rinse waters. The data on cellulose acetate membranes and hollow fibers was given by A. Golomb [19]. In this latter work it was observed that the use of cellulosic membranes in the reverse osmosis treatment of simulated zinc cyanide resulted in rapid membrane deterioration, caused by alkaline hydrolysis. The rejection efficiency of the hollow fibers was too low for practical use.

Conclusions

Ultrathin membranes exhibit considerable promise for treating wastewaters by reverse osmosis. Ultrathin water-cast membranes formed from one polymer, cellulose acetate o-propyl sulfonic acid, were effective in

the reverse osmosis treatment of both secondary effluents and neutral-to-acidic simulated electroplating rinses. The ultrathin NS-1 membrane, formed by a coating process, is effective for reverse osmosis treatment of highly alkaline metal cyanide rinse waters.

The authors acknowledge the Environmental Protection Agency for partial support of this work under Program No. 12010 DRH.

REFERENCES

[1] L. T. Rozelle, E. M. Scattergood, B. R. Nelson, and J. E. Cadotte, *New and Ultrathin Membranes for Municipal Wastewater Treatment by Reverse Osmosis*, Environmental Protection Agency Program No. 17020 EFA, U.S. Government Printing Office, Washington, October 1970.

[2] A. C. F. Ammerlaan, B. F. Lueck, and J. W. Averill, "Membrane Process of Dilute Pulping Wastes by Reverse Osmosis," *TAPPI, 52* (January 1969).

[3] B. R. Nelson, L. T. Rozelle, J. E. Cadotte, and E. M. Scattergood, *Ultrathin Membranes for Treating Metal Finishing Effluents by Reverse Osmosis*, Environmental Protection Agency Program No. 12010 DRH, U.S. Government Printing Office, Washington, November 1971.

[4] F. E. McDonough and W. A. Mattingly, "Pilot Plant Concentration of Cheese Whey by Reverse Osmosis, *Food Technol., 24 (194)*, 88 (February, 1970).

[5] C. E. Reid and E. J. Breton, *J. Appl. Polym Sci., 133*, 1 (1957).

[6] S. Loeb and S. Sourirajan, "Advances in Chemistry Series No. 38," American Chemical Society, Washington, 117 (1963).

[7] L. T. Rozelle, J. E. Cadotte, and B. R. Nelson, *Ultrathin Membranes for Reverse Osmosis Water Desalination*, Office of Saline Water Research and Development Progress Report No. 725, U.S. Government Printing Office, Washington, December 1971.

[8] L. T. Rozelle, J. E. Cadotte, W. L. King, A. J. Senechal, and B. R. Nelson, *Development of Ultrathin Reverse Osmosis Membranes for Desalination*, Office of Saline Water Research and Development Progress Report No. 659, U.S. Government Printing Office, Washington, June 1971.

[9] U. Merten, *Desalination by Reverse Osmosis*, Chapter 2, U. Merten, ed., M.I.T. Press, Cambridge, Massachusetts, 1966.

[10] L. T. Rozelle, J. E. Cadotte, R. D. Corneliussen, and E. E. Erickson, *Development of New Reverse Osmosis Membranes for Desalination*, Office of Saline Water Research and Development Progress Report No. 359, U.S. Government Printing Office, Washington, June 1968.

[11] L. T. Rozelle, J. E. Cadotte, A. J. Senechal, W. L. King, and B. R. Nelson, "Tubular Ultrathin Membranes for Water Desalination," in *Reverse Osmosis Membrane Research*, H. K. Lonsdale and H. E. Podall (Eds.). Plenum Press, New York, 1972.

[12] J. E. Cadotte and L. T. Rozelle, *In Situ Formed Condensation Polymers for Reverse Osmosis Membranes*, Office of Saline Water Research and Development Progress Report, U.S. Government Printing Office, Washington, in press.

[13] L. T. Rozelle, J. E. Cadotte, and McClure, D. J., "Ultrathin Cellulose Acetate Membranes for Water Desalination," *J. Appl. Polym. Sci., Appl. Polym. Symp. No. 13*, 61 (1970), also presented at the 157th National Meeting of the American Chemical Society, Minneapolis, April 1969.

[14] L. T. Rozelle, J. E. Cadotte, and D. J. McClure, *Development of New Reverse Osmosis Membranes for Desalination*, Office of Saline Water Research and Development Report No. 531, U.S. Government Printing Office, Washington, June 1970.

[15] P. S. Francis and J. E. Cadotte, *Second Report on the Fabrication and Evaluation of New Ultrathin Reverse Osmosis Membranes*, Office of Saline Water Research and

Development Progress Report No. 247, U.S. Government Printing Office, Washington, April 1967.

[16] J. E. Cadotte, L. T. Rozelle, R. J. Peterson, and P. S. Francis, "Water Transport Across Ultrathin Membranes of Mixed Cellulose Ester and Ether Derivatives," *J. Appl. Polym. Sci., Appl. Polym. Symp. No. 13,* 73 (1970).

[17] *Standard Methods for the Examination of Water and Wastewater*, American Public Health Association, New York, 1965.

[18] K. D. Vos., F. O. Burris, and R. L. Riley, "Kinetic Study of the Hydrolysis of Cellulose Acetate in the pH Range of 2–10", *J. Appl. Polym. Sci., 10,* 825 (1966).

[19] A. Golomb, *Plating, 59,* 316 (1972).

REVERSE OSMOSIS MEMBRANES FORMED BY PLASMA POLYMERIZATION OF ORGANIC COMPOUNDS

H. YASUDA

Research Triangle Institute,
P.O. Box 12194,
Research Triangle Park, North Carolina 27709

SYNOPSIS

The plasma polymerization of organic compounds by an electrodeless (inductive coupling) glow discharge was used to prepare a composite reverse osmosis membrane which consists of an ultrathin semipermeable membrane deposited from plasma of organic compound(s) onto a porous substrate. This method has a unique advantage of being able to deposit semipermeable membrane onto porous substrates of various shapes (flat sheets, tublets, and hollow fibers) and of various materials (polymers, glass, ceramics, and metal). Many nitrogen-containing compounds (aromatic amines, heteroaromatic compounds, aliphatic amines, and derivatives of pyrrolidone) were found to yield excellent reverse osmosis membranes. The plasma polymerized semi-permeable membranes are highly crosslinked and are intimately bonded to the substrate (particularly to polymeric substrates). Consequently, composite membrane thus formed have excellent stabilities of reverse osmosis performance. The proper selection of membrane and substrate would lead to a superb composite membrane which would be suited to be used in severe and/or unusual conditions.

INTRODUCTION

Properties of Polymers for Reverse Osmosis Membranes

Recent studies [1, 2] on fundamental aspects of polymers as reverse osmosis membrane materials under the sponsorship of Office of Saline Water, U.S. Department of Interior have yielded useful guidelines which could be utilized in search of new materials and of new methods of membrane preparation. A very important factor—that the basic mode of water transport plays a predominant role in the performance of reverse osmosis membrane—has been demonstrated. [3, 4, 5, 6, 7] The behavior of ionic and nonionic polymer membranes in reverse osmosis can be summarized in a schematic representation given in Figure 1, where logarithms of water permeabilities of homogeneous polymer membranes are plotted against salt rejection obtained by the membranes (data has been presented

Applied Polymer Symposium No. 22, 241–253 (1973)

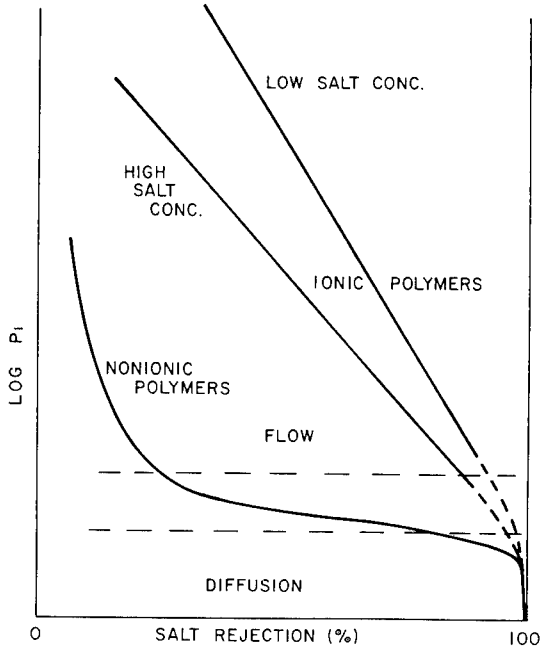

FIG. 1. Schematic representation of reverse osmosis characteristics of ionic- and nonionic-polymer membranes.

in [5, 7]). The trends seen in Figure 1 indicated several important aspects which provide useful guidelines for determining the direction of future research which could lead to improved reverse osmosis membranes. These are:

1. The water permeability and salt rejection are both functions of equilibrium water content of a polymer, and they cannot be considered two independent variables.
2. Ionic polymer has considerably higher water permeability in the relatively low salt rejection region.
3. At very high salt rejection region, however, the characteristic relation between water permeability and salt rejection for ionic polymers becomes nearly identical to that for nonionic polymers.
4. A good salt rejection can be obtained only with polymers in which water moves by diffusion under reverse osmosis conditions regardless of the ionic or nonionic nature of the polymer.

These observations further imply the following practical guidelines:

1. There seems to be a limit to improving the water permeability of a polymer while maintaining high salt rejection using synthesis of novel polymer structure and modification of polymers, though these approaches would lead to polymers which have improved mechanical and rheological properties.

2. Usefulness of a polymer as a reverse osmosis membrane, therefore, depends heavily on the geometrical factors of a membrane such as (a), a reduction of effective thickness by utilizing an asymmetric or composite structure, (b), an improvement of surface/volume ratio by using tubular or hollow fiber membranes, and (c), a combination of structures in (a) and (b). In this sense, a polymer which has good reverse osmosis characteristics may have no practical value unless the polymer can be formed into a functional membrane as mentioned above.

The method under investigation is based on the preparation of a highly cross-linked ultrathin salt rejecting membrane intimately bonded to an appropriate porous substrate. In this approach, a polymer is formed into an ultrathin membrane intimately bonded to an appropriate porous substrate during the process of polymerization, instead of preparing a thin membrane from a polymer. A highly crosslinked ultrathin membrane is formed on the surface of a porous substrate; accordingly, the final shape of the composite membrane depends on the shape of the porous substrate; i.e., flat sheet, tubulet, or hollow fibers. This approach is distinctly different from (1), conventional asymmetric membranes such as Loeb–Sourirajan type of cellulose acetate membrane, and (2), a conventional composite membrane which consists of an ultrathin film and a porous substate.

Since, in asymmetric membranes, the salt rejecting (active) layer and the supporting layer are made of the same polymer, the performance of the membrane must depend on both the salt rejecting characteristics and mechanical properties of the same polymer. The transition from active dense structure to porous backing layer is gradual [8], and the membrane is generally susceptible to compaction under high operating pressure.

With composite membranes, more than two polymers can be combined to perform the individual task of each composite layer, i.e., the salt rejection for ultrathin film and the mechanical support for the porous substrate. The composite membranes, therefore, may provide a wider choice in selecting materials to be used. On the other hand, the technical procedure of composite membrane preparation is considerably more complicated than the essentially one-step process of asymmetric membrane preparation, and the placement of an ultrathin film on top of a porous substrate leaves some degree of uncertainty in achieving smooth and uniform contact between the two layers, a factor which seems to be important particularly under severe or unusual conditions.

In the preparation of a plasma polymerized membrane, the polymer deposits from the vapor phase and anchors onto the underlying porous substrate. Therefore, very intimate bonding of the deposited membrane to the porous substrate can be obtained. This intimate bonding of the salt rejection layer to the substrate undoubtedly plays an important role in the stability of the reverse osmosis performance of composite membranes.

Another important aspect of this approach is that the preparation of a composite membrane occurs in the dry state. Therefore, an extremely hy-

drophobic substrate can be efficiently utilized. Due to the lowering of the glass transition temperature of polymers by the sorption of a solvent (water), the best supporting layer for composite reverse osmosis membranes can be obtained with hyrophobic polymers which do not sorb water. The dry process provides further advantages; the simplicity of the membrane assembling process for a practical module and the ability to store a membrane indefinitely before using it.

Background Knowledge on Glow Discharge

It has been known for many years [9, 10, 11] that some organic compounds form polymers in plasma, though the polymers were recognized as byproducts of phenomena associated with electric discharge. It was only relatively recently (about the 1960's) that this phenomenon was practically utilized to make a special coating on metal [12].

Once some of the advantageous features of plasma coating (e.g., flawless thin coatings of polymers, unique properties such as low dielectric constant, and good corrosion resistance) were recognized, much applied research concerning the use of the process was done. Perhaps due to the interest in electrical properties of deposited polymer film, most of the studies appearing in the literature are concerned with polymer deposition onto metals which were used as an electrode in a low pressure glow discharge [9–21]. Although the reactions (polymer as a byproduct) of organic compounds in an electrodeless (inductive coupling) glow discharge [22, 23, 24] and the properties of polymer formed by an electrodeless (inductive coupling) glow discharge [25, 26] have also appeared in the literature, neither the detailed polymerization mechanism nor the structure of polymer as formed by electrodeless (inductive coupling) glow discharge had been investigated.

Glow discharge polymerization can be achieved by a number of methods; e.g., d.c. and a.c. discharge with electrodes, and electrodeless discharge with a.c. (radiofrequency and microwave) discharge.

The polymer deposition pattern (i.e., the physical location of polymer deposition, polymer deposition rates, and the kind of polymer deposit) is highly dependent on the type of discharge and the geometrical aspect of a reactor (discharge vessel). Although it is difficult to generalize, the following trends can be drawn from results obtained by various types of discharge appearing in the literature:

1. In dc discharge, the deposition of polymer takes place almost exclusively on the cathode [13, 20], indicating that positive ions formed in glow discharge play an important role in plasma polymerization.
2. In ac discharge with electrodes, polymer deposits on the surface of both electrodes but nearly exclusively on the electrode surface. When a flow system is employed, polymer deposits on the wall of the reaction vessel on the downstream side of flow at a very high flow rate [20]. Electrodeless glow discharge with capacitive coupling (electrodes on the outside of reaction vessel) can be considered

similar to electrode discharge. In this case, polymer deposits on the wall of the reaction vessel, but the deposition seems to be limited to the region between the two electrodes and slightly on the downstream side.

3. In electrodeless discharge (with inductive coupling), the discharge tube is placed inside a solenoid through which an alternating current is passed. A discharge will be established when the current and frequency are sufficiently high. This type of discharge is referred to as "electrodeless discharge" in this paper. The electrodeless discharge requires higher frequency than electrode discharge, and either radiofrequency (RF) or microwave is generally used. In electrodeless discharge, polymer deposits on the wall of the reaction vessel in the glow region with exceptionally heavy deposition on the portion in the solenoid. In a flow system, polymer deposits also on the wall in the nonglow region on the downstream side. These four major types of discharge and the positions at which polymer deposits are summarized by schematic representation shown in Figure 2.

Buck and Davar [27] used glow discharge polymerization of vinyl monomer vapor using 40 kHz RF to prepare reverse osmosis membranes by depositing polymer onto the surface of a porous support membrane (Millipore filter) fixed tightly on the surface of an electrode. Salt rejection of approximately 95% with low water flux was reported with vinyl carbonate with addition of 8% acrylonitrile. Acryonitrile-vinyl acetate copolymer (2:1) was reported as next best. It was also recognized that only a small number of monomers give water-permeable polymer films.

It developed that the mechanisms of polymerization in electrode discharge and in electrodeless discharge seem to be quite different, and that the monomers reported by Buck and Davar to give best and next best results do not polymerize well in the electrodeless glow discharge employed in this study. However, the finding that only a small number of monomers yield water-permeable polymer in a limited sense, was also confirmed by this study, although the total number of monomers which yielded good reverse osmosis membranes exceeds a dozen.

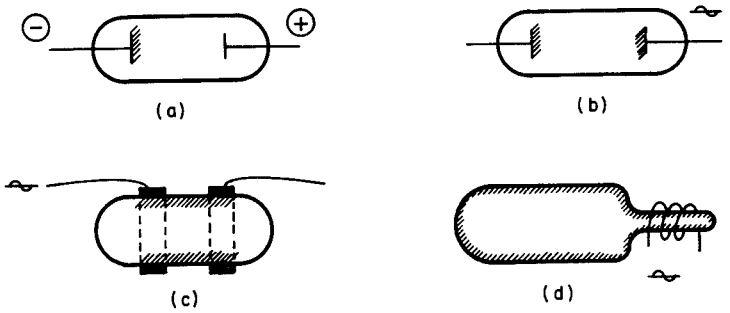

FIG. 2. Schematic representation of types of electric discharge and the pattern of polymer deposition.

The size and shape of a membrane which can be prepared by the glow discharge deposition onto the electrode are limited by the size and shape of the electrode. For this reason, an electrodeless glow discharge (by inductive coupling) seems to be a better way to prepare membranes, since polymer deposition occurs on any surface exposed to the glow discharge. The details of membrane preparation may be seen in Reference 28.

FACTORS INVOLVED IN THE MEMBRANE PREPARATION

Selection of Monomers

The organic compounds which can be used as the monomer of plasma polymerization are not limited to the conventional monomers such as vinyl compounds, but include nearly any kind of organic compounds which have high enough vapor pressure either at the ambient temperature or in the condition of glow discharge.

The mechanism of plasma polymerization is complex and apparently depends on the discharge conditions. In electrode discharge, the adsorption of monomer vapor seems to play an important role on the polymer deposition, (at least with vinyl type monomers). In the electrodeless glow discharge, however, the polymerization in the plasma (vapor phase) seems to play an important role.

The polymerization of an organic compound can be achieved either by electric discharge of pure monomer vapor or by electric discharge of a mixture of monomer and plasma gas such as He, H_2, A, N_2. The polymerization mechanism, particularly the role of adsorbed monomer versus vapor phase polymerization, seems to be also dependent on whether or not a plasma gas is used.

All this dependence of polymer deposition on experimental conditions may be interpreted by the following two basic modes of polymerization:

1. Polymerization of excited species of monomer (in vapor phase).
2. Polymerization of monomer (both in vapor phase and in adsorbed phase) initiated by excited species of plasma.

The latter depends highly on the polymerizability of a monomer. For instance, vinyl compounds will be polymerized by the second mechanism to a considerable extent; however, unconventional monomers such as saturated or stable aromatic and heteroaromatic organic compounds will not be polymerized by this mechanism.

In other words, in the electrodeless glow discharge, the first mechanism seems to be enhanced, and the second mechanism seems to play a more important role in electrode discharge. However, the possibility of either mechanism playing a role in a particular set of conditions cannot be neglected.

The rate of polymerization observed in the electrodeless glow discharge for vinyl monomers and corresponding saturated vinyl monomers are by

and large comparable as seen in Table I. Considering the fact that the saturated vinyl compounds do not polymerize by addition polymerization mechanism, yet their plasma polymerization rates are close to those of their corresponding vinyl compounds, the role of the first mechanism given is quite evident.

By the first mechanism, the polymerization seems to proceed by the recombination of primary radicals (or other excited species) and reexcitation of the terminated chains followed by the recombination. Consequently, plasma polymerization corresponds to the radical polymerization with extremely short kinetic chain length and reinitiation of terminated chain.

Organic compounds can be classified in two major groups so far as the behavior in plasma is concerned: one which polymerizes predominantly (Type A), and the other which decomposes in plasma with only a part of the original molecules polymerizing (Type B). Some structural factors were found to be responsible for the behavior of an organic compound in plasma. Although the effect is dependent on the neighboring structures or groups, those structures and groups—oxygen-containing (e.g., $-\overset{\overset{O}{\|}}{C}-$, $-\overset{\overset{O}{\|}}{C}-O-$, —O—, —OH), chlorine, aliphatic hydrocarbon chains, and cyclic hydrocarbon chains—decompose in plasma and tend to be absent in the polymer deposition.

In order to prepare a semipermeable membrane which allows transport of water, the polymer formed should be moderately hydrophilic [1, 4, 7]. Many hydrophilic organic compounds, however, contain structures and groups of Type B which do not remain in the resultant polymer deposition. For this reason, a very hydrophobic polymer deposition is often obtained from a very hydrophilic organic compound. Many vinyl and acrylate esters were found not suited for the preparation of reverse osmosis membrane by the electrodeless glow discharge. The most suitable monomers for the preparation of reverse osmosis by this method are Type A compounds

TABLE I

Comparison of Polymer deposition rates for vinyl and saturated vinyl compounds

Vinyl Monomer		Saturated Vinyl Monomer	
Compound	$a \times 10^4$ ($g/cm^2 \cdot min \cdot Torr^2$)	Compound	$a \times 10^4$ ($g/cm^2 \cdot min \cdot Torr^2$)
4-Vinylpyridine	16.4	4-Ethylpyridine	10.0
α-Methylstyrene	13.8	Cumene	10.4
Styrene	12.1	Ethylbenzene	9.4
2-Methyl,5-vinylpyridine	11.9	2-Methyl,5-ethylpyridine	12.9
N-Vinylpyrrolidone	9.7	N-Ethylpyrrolidone	4.6
Acrylonitrile	7.2	Propionitrile	4.9
Vinylidene Chloride	5.8	1,1'Dichloroethane	4.5

which are relatively hydrophilic. Among organic compounds investigated, only nitrogen-containing compounds, particularly amines, met this requirement.

Selection of Porous Substrate

Polymer deposition onto a porous substrate is considerably different from that onto a nonporous inert surface such as a glass slide and a metal plate. At least three major factors described below are found to play important roles in the preparation of reverse osmosis membranes by an electrodeless glow discharge of a monomer vapor.

Plasma Susceptibility of Substrate Materials

This factor is particularly important when polymeric porous substrates are used. All polymers degrade and lose weight when samples are exposed to a glow discharge. The dependence of polymer degradation (manifested by the weight loss rate) on the experimental factors has been described in Reference 28.

It was found that (a), the weight loss is proportional to the exposure time, (b), the pressure of plasma has little effect, (c), the rate of weight loss is highly dependent on the discharge wattage (the higher the wattage, the higher the rate of weight loss), and (d), the deposition of polymer from vapor of monomer plasma onto a (nonporous) polymeric substrate does not completely shield the substrate polymer from degradation and, particularly at higher wattage, the weight loss often exceeds the weight increase due to polymer deposition.

For preparation of reverse osmosis membranes, the plasma susceptibility of porous polymeric substrate and the discharge wattage necessary to maintain a glow discharge of a monomer play a very important interrelated role.

If the decomposition of substrate material is severe, it may lead to the change of transport properties of the substrate, particularly the change of pore size which could be detrimental to the transport properties of resultant composite membranes. The evolution of gaseous product by the decomposition may interfere with plasma polymerization of an organic compound to form an ultrathin membrane. Structures and groups considered as Type B in the behavior of organic compounds as monomer also play similar roles in degradation of polymers; i.e., polymers which contain Type B structures and groups are highly susceptible to plasma. Plasma susceptibility of some polymers are compared in Table II.

Adsorption (or Sorption) Characteristics of Porous Substrates

Another important factor that is encountered in polymer deposition onto porous substrate is the adsorption or sorption characteristics of a porous substrate. This factor influences the polymer deposition in the following manner.

Porous substrates, in general, have a large internal surface area and are good adsorbing material. Consequently, the degassing of the substrate to

maintain a desired vacuum level is dependent on how much and how strongly gases and vapors (particularly water vapor) are held by a porous substrate. Some of the vapors, particularly water vapor in a hydrophilic porous substrate, are difficult to degas by pumping. Thus, they will be evolved when the plasma is initiated, causing an uncontrollable effect due to this additional vapor plasma. In this respect, the hydrophilicity of the porous substrate plays an significant role in determining the reproducibility of polymer deposition.

When monomer vapor is introduced into the reaction system, some monomers will be adsorbed or sorbed by a porous substrate. The partition between vapor phase and sorbed phase is dependent upon the adsorbing capability of a porous substrate. For instance, when a porous glass tube is used as a substrate, nearly 100% of the monomer fed into a closed system is adsorbed, and it is difficult to establish a high enough pressure of monomer vapor until the substrate is saturated with the monomer.

Pore Size of Porous Substrate

The minimum thickness of polymer deposition needed to form a homogeneous flawless membrane is the radius of the pore it must bridge. Consequently, the reverse osmosis property of a composite membrane is greatly dependent on the pore size of a porous substrate.

The use of Millipore filter VC (nominal pore size 1,000Å) as a substrate failed to produce good reverse osmosis membranes, whereas Millipore filter VS (nominal pore size 250Å) yielded excellent reverse osmosis membranes.

REVERSE OSMOSIS CHARACTERISTICS

Some reverse osmosis results of composite membrane prepared by plasma polymerization are summarized in Tables III and IV. It is interesting to note that very hydrophobic polymers, such as one made from

TABLE II

Plasma Susceptibility of polymers measured by the rate of weight loss in helium plasma

Polymer	Weight Loss Rate[a], mg /cm^2 - min x 10^3
Poly(oxymethylene)	17.0
Poly(acrylic acid)	16.2
Poly(methacrylic acid)	15.4
Polyvinylpyrrolidone	11.9
Polyvinylalcohol	9.4
Poly(ethylene terephthalate)	1.7
Polyethylene	1.2
Nylon 6	1.1
Polypropylene	0.8

TABLE III
Reverse osmosis results of plasma polymerized polymer from hydrophilic type A monomers

Monomer	Substrate	NaCl Concentration (%)	Applied Pressure (psi)	Salt Rejection (%)	Water Flux (gfd)
4-vinylpyridine	porous glass	1.2	1200	90	.49[a]
	porous glass	1.2	1200	96	.81[a]
	porous glass	1.2	1200	87	.51[a]
	porous glass	1.2	1200	96	.72[a]
	polysulfone	1.2	1200	97	3.7
	polysulfone	1.2	1200	98	7.0
	polysulfone	1.2	1200	89	4.0
	polysulfone	1.2	1200	95	1.6
	Millipore-VS	1.2	1200	99	38.
	Millipore-VS	1.2	1200	98	4.0
	Millipore-VS	1.2	1200	95	24.0
	Millipore-VS	1.2	1200	97	7.4
N-vinylpyrrolidone	polysulfone	1.2	1200	91	10.6
4-picolin	polysulfone	1.2	1200	98	6.4
4-ethyl pyridine	polysulfone	1.2	1200	98	9.6
4-picolin	polysulfone	3.5	1500	96.	7.6
4-methylbenzylamine	polysulfone	3.5	1500	96.	2.2
n-butylamine	polysulfone	3.5	1500	94.	2.7
4-vinylpyridine	polysulfone	3.5	1500	97.	4.9
4-vinylpyridine	porous glass	3.5	1500	96.	0.80[a]
3-5 lutidine	polysulfone	3.5	1500	99.	12.

styrene, showed marginal salt rejection with measurable water flux. Since conventional polystyrene has very low water flux, the results may be reflecting the considerable hydrophilicity of plasma polymerized sytrene due to incorporation of carbonyl and hydroxyl groups by the trapped radicals. The partial hydrophilicity of plasma polymerized styrene agrees with observation of the surface of polystyrene deposited on glass slide.

The surface of polystyrene freshly plasma deposited on a glass plate is completely smooth under microscope observation, and shows a faint rainbow pattern in reflected light. However, the roughness of the surface develops when the surface is exposed to moisture in the air, and the rainbow pattern becomes clearly visible. This roughness often starts from

the slide edges and propagnates, which can be observed under microscope. The pattern of propagation resembles a quite regularly winding river. It seems that a portion of the film is buckling up; however, it has not yet been determined whether the film is peeling off from the glass surface or if the distortion occurs within the layer of the deposited polymer. The following factors were observed concerning the buckling pattern development:

1. The higher the amount of deposition, the faster the development.
2. The buckling does not occur when the polymer deposited slides are kept in a desicator.
3. The precoating of a glass slide with water soluble polymers changes the buckling development, and its extent is dependent on the type of precoating polymer. Poly(acrylic acid) does not alter the buckling development as compared to a glass surface. Poly(methacrylic acid) shows resistance against buckling development. Poly(vinyl alcohol) showed a different pattern than observed on the glass surface. No buckling was observed with polystyrene film deposited on poly(vinyl pyrrolidone). In most cases, the buckling development can be initiated by scratching the surface. The scratching of the surface does not cause the buckling of polymer layer deposited on poly(vinyl pyrrolidone) but does cause crazing.
4. The thinner layer of polystyrene deposited on glass plates under the conditions of low monomer flow rate and low wattage (e.g., 30 watts) for a short period of time (e.g., 10 min) did not show any buckling development (by moisture or by scratching the surface).

The reverse osmosis membranes of glow discharge polymers have quite unique features which are completely opposite to generally found trends. These are:

1. Steady increase of salt rejection and water flux with time of reverse osmosis run.
2. Very stable water flux after the initial incline is stabilized; practically no water flux decline is observed with many membranes.

TABLE IV

Reverse osmosis results of plasma polymerized polymers from hydrophobic and/or type B monomers

Monomer	Substrate	NaCl Concentration (%)	Applied Pressure (psi)	Salt Rejection (%)	Water Flux (gfd)
Styrene	Polysulfone	1.2	1200	24	4.9
Glycydylmethacrylate	Polysulfone	1.2	1200	47	4.0
Vinylacetate	Polysulfone	1.2	1200	31	4.6
2-Methyl Furan	Polysulfone	1.2	1200	42	16
Morpholin	Polysulfone	1.2	1200	56	42
Furan	Polysulfone	1.2	1200	31	54
Methacrylic Acid	Polysulfone	1.2	1200	30	13

3. Excellent performance at high salt concentration and under high pressure.

Buck and Davar [27] reported that water flux increased steadily for the first eight days with plasma polymerized membrane of vinylene carbonate and acrylonitrile mixture (deposited onto a Millipore VS fixed to an electrode at 40 KHz). Membrane prepared in this study showed more pronounced increase of both water and flux and salt rejection. The salt rejection generally reaches its maximum plateau value within approximately 20 days; however, water flux continued to increase up to approximately 100 days. Once the water flux reaches its plateau value, the flux is very stable and no flux decline was observed within the test period of approximately 30 additional days, though no true long test has been carried out.

These trends (i.e., increase of water flux and salt rejection with time) are found regardless of type of substrate, type of monomer used, and the concentration of salt and pressure. Therefore, this feature is a unique characteristic of glow discharge polymer and is probably due to chemical changes in the membrane as suggested by Buck and Davar [27].

Polymers formed by plasma polymerization generally contain considerable amounts of trapped radicals, and it has been reported that polymers which do not have hydroxyl and carbonyl group showed infrared absorption attributable to these groups after the polymers were exposed to air. Membranes prepared in this study were kept in the air from 30 minutes to several hours without any special attempt to control the exposure time. Buck and Davar [27] kept samples in water for a day before the testing. The factors which might be responsible for the change of reverse osmosis characteristics are obviously much slower processes than those that can be observed in infrared spectrum; however, no attempt has been made to elucidate the cause.

Examination of the surface by a scanning electron microscope of the porous polysulfone substrate, polymer deposition on the substrates which are kept in air, and polymer deposition on the substrates which are kept in 3.5% NaCl solution for two weeks has failed to show any significant differences observable at the magnification of 14,500. All surfaces were smooth without detectable structure and only gradual change of hill and dale could be observed when samples were tilted 40° to the electron beam. This observation at least proved that the polymer deposition occurs as a flawless uniform layer covering the texture of the substrate.

Water flux of many conventional polymers declines with time due to compaction of the membrane and the trend is more pronounced with high salt concentration and with high pressure. The composite membranes prepared by this method showed equally good performance under conditions for sea water conversion and brakish water treatment. In this respect, the glow discharge polymers seem particularly suited for reverse osmosis under severe conditions.

This study was supported by the U.S. Department of the Interior, Office of Saline Water, Contract No. 14-30-2658. The author's special thanks are due Dr. A. Peterlin, Director,

Camile Dreyfus Laboratory, Research Triangle Institute, for stimulating discussion during the course of the study. The author is indebted to Mrs. C. E. Lamaze for carrying out most of the experiments described in this paper.

REFERENCES

[1] *Research and Development Progress Report No. 473*, Office of Saline Water, Dept. of Interior.
[2] *Research and Development Progress Report No. 689*, Office of Saline Water, Dept. of Interior.
[3] H. Yasuda, C. E. Lamaze, and A. Peterlin, *J. Polym. Sci., A-2, 9*, 1117 (1971).
[4] H. Yasuda and C. E. Lamaze, *J. Polym. Sci., A-2, 9*, 1537 (1971).
[5] H. Yasuda, C. E. Lamaze and A. Schindler, *J. Polym. Sci., A-2, 9*, 1579 (1971).
[6] H. Yasuda, H. G. Olf, B. Crist, C. E. Lamaze, and A. Peterlin, *Water Structure at the Water-Polymer Interface*, H. H. G. Jellinek (Ed.), Plenum Press, New York, 1972.
[7] H. Yasuda and A. Schindler, *Reverse Osmosis Membrane Research*, H. K. Lonsdale and H. E. Podall, (Eds.) Plenum Press, New York, 1972.
[8] H. Yasuda and C. E. Lamaze, *Appl. Poly. Symposia, 13*, 157 (1970).
[9] C. S. Schoopfle and L. H. Connell, *Ind. Eng. Chem., 21*, 529 (1929).
[10] W. D. Harkins and D. M. Gans, *J. Amer. Chem. Soc., 52*, 5165 (1930).
[11] E. G. Linder and A. P. Davis, *J. Phys. Chem., 35*, 3649 (1931).
[12] J. Goodman, *J. Poly. Sci., 44*, 551 (1960).
[13] T. Williams and M. W. Hayes, *Nature, 29*, 769 (1966).
[14] K. Jesch, J. E. Bloor, and P. L. Kronick, *J. Poly. Sci.*, A-1, *4*, 1487 (1966).
[15] T. Hirai and O. Nakada, *Jap. J. of Appl. Phys. 7*, No. 2 112 (1968).
[16] A. R. Denaro, P. A. Owens, and A. Crawshaw, *Europ. Polym. J. 4*, 93 (1968).
[17] P. L. Kronick, K. F. Jesch, and J. E. Bloor, *J. Polymer Sci., A-1, 7*, 767 (1969).
[18] A. R. Denaro, R. A. Owens, and A. Crawshaw, *Europ. Polym. J., 5*, 471 (1969).
[19] A. R. Denaro, R. A. Owens, and A. Crawshaw, *Europ. Polym. J., 6*, 487 (1970).
[20] A. R. Westwood, *Europ. Polym. J., 7*, 363 (1971).
[21] A. R. Westwood, *Europ. Polym. J., 7*, 377 (1971).
[22] F. Swift, Jr., R. L. Sung, J. Doyle, and J. K. Stille, *J. Org. Chem. 30*, 3114 (1965).
[23] J. K. Stille, R. L. Sung, and J. Vander Kooi, *J. Org. Chem., 30*, 3116 (1965).
[24] J. K. Stille, and C. E. Rix, *J. Org. Chem., 31*, 1591 (1966).
[25] R. A. Connell and L. V. Gregor, *J. Electrochem. Soc., 112*, 1198 (1965).
[26] G. Smolinsky and J. H. Heiss, paper presented at the 155th American Chemical Society Meeting, San Francisco, Calif., April 1968; *Division of Organic Coating and Plastic Chemistry Preprints, 28*, (1), 537 (1968).
[27] K. R. Buck and V. K. Davar, *Br. Polym. J., 2*, 238 (1970).
[28] Research Triangle Institute's Final Report to Office of Saline Water, U.S. Department of Interior, Contract NO. 14-30-2658, May 1972. to be published as a Research and Development Progress Report of Office of Saline Water.

THIN-FILM COMPOSITE MEMBRANE FOR SINGLE-STAGE SEAWATER DESALINATION BY REVERSE OSMOSIS

R. L. RILEY, G. R. HIGHTOWER, and C. R. LYONS

Gulf Environmental Systems Company,
San Diego, California 92138

SYNOPSIS

Recent advances in the continuing development of the cellulose acetate thin-film composite membrane have made it possible to produce potable water from seawater by reverse osmosis in a single stage at water recoveries in excess of 50%. Stable long-term fluxes of 1.02 M^3/M^2-day (25 gal/ft^2-day) and sodium chloride rejections of greater than 99.5% are attained with seawater at an applied pressure of 102 atm (1500 psi). Improvements in large-scale, continuous membrane production combined with the excellent seawater performance of spiral-wound modules demonstrate a significant advance toward the practical application of the thin-film composite membrane.

INTRODUCTION

Economical desalination of seawater by reverse osmosis requires a membrane approaching theoretical semipermeability that is sufficiently thin to provide a rapid transport of water at practical pressures. The thin-film composite membrane, under development since 1968, offers a new route for the preparation of such membranes [1–6].

Structurally, the composite membrane is similar to the asymmetric Loeb–Sourirajan brackish water membrane [7] in that it possesses a very thin, semipermeable barrier supported by a finely porous substrate. The structural similarities of the membranes are shown in Figure 1; the methods of preparation, however, are distinctly different.

The conventional Loeb–Sourirajan approach is to form the entire membrane from a single material, cellulose 2.45 acetate (39.8% acetyl), by a procedure which produces a 2000-Å semipermeable barrier on one surface of the membrane that is supported by a graduated porous substrate [8, 9]. Unfortunately the procedure is empirical, and adaptation to new materials has been difficult and often unsuccessful. The membrane, while quite successful for brackish water applications, is not sufficiently selective for single-stage seawater desalination and exhibits a loss in water productivity with time at high pressures.

Applied Polymer Symposium No. 22, 255–267 (1973)

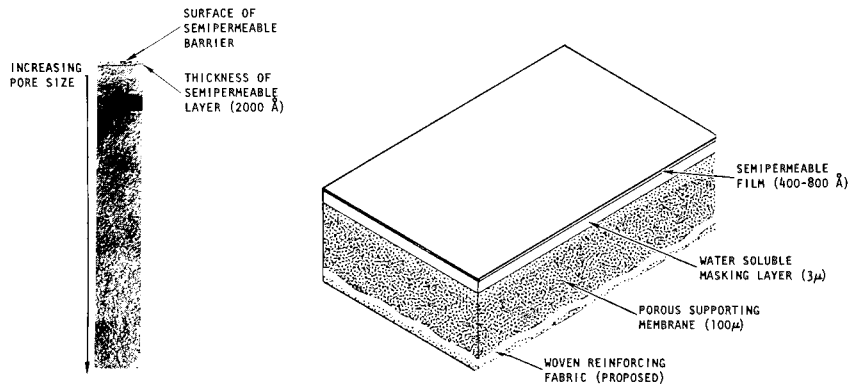

FIG. 1. Electron photomicrograph of a 30-μ cross section of a Loeb–Sourirajan modified membrane (left) and a cross-sectional drawing of the thin-film composite membrane (right).

The composite membrane, on the other hand, is prepared from one or more materials by forming a very thin film of polymer, generally cellulose acetate of a moderate degree of substitution, directly upon the polyacrylic-acid-masked surface of a finely porous supporting membrane by dipping from a dilute solution. The thickness of the thin film, generally 400 or 800 Å, is controlled by the withdrawal rate and the concentration of the polymer in the dilute solution. This more general method of asymmetric membrane preparation provides several additional degrees of freedom. These include the following:

1. Independent selection of materials from which to prepare the thin semipermeable barrier and the finely porous supporting membrane.
2. Independent preparation of the thin film and the porous supporting membrane, thereby making it possible to optimize each component for its specific function.
3. The ability to reproducibly vary and control the thickness of the thin film.
4. Control over the porosity and the perfection of the thin semipermeable barrier that is required to attain the intrinsic semipermeability of the material.

TRANSPORT PHENOMENOLOGY

The transport process through both the 400- and 800-Å cellulose acetate thin film of the composite membrane is diffusion controlled and can be described by means of a solution-diffusion model [10]. Thus, the water flux J_1 is given by

$$\mathcal{J}_1 = \frac{D_1 c_1 \bar{v}_1 (\Delta P - \Delta\pi)}{RT\Delta x} \equiv A(\Delta P - \Delta\pi) \tag{1}$$

where

D_1 = the diffusion coefficient of water in the membrane (cm^2/sec),
c_1 = the concentration of water in the membrane (g/cm^3),
v_1 = the partial molar volume of water in the external phase ($cm^3/mole$),
ΔP = the applied pressure (atm),
$\Delta\pi$ = the osmotic pressure difference across the membrane (atm),
R = the gas constant (cm^3 -atm/mole-°K),
T = the absolute temperature (°K), and
Δx = the effective membrane thickness (cm).

The proportionality factor A, referred to as the membrane constant, is a measure of the water flux per unit net pressure (g/cm^2-sec-atm).

The salt flux J_2 through the imperfection-free film is similarly given by

$$\mathcal{J}_2 = \frac{D_2 K \Delta\rho_2}{\Delta x} \tag{2}$$

where

D_2 = the diffusion coefficient of salt in the membrane (cm^2/sec),
K = the distribution coefficient for salt between membrane and solution [(g/cm^3 membrane)/(g/cm^3 solution)], and
$\Delta\rho_2$ = the difference in salt concentration across the membrane (g/cm^3).

The quantities D_1c_1 and D_2K are permeability coefficients.

The salt rejection is defined by

$$S = (\rho_2' - \rho_2'')/\rho_2' \tag{3}$$

where ′ and ′′ refer to feed and product solutions, respectively. In terms of the flux equations, salt rejection is given for dilute solutions by

$$S = 1 - \frac{\mathcal{J}_2}{\mathcal{J}_1\rho_2'} = \left[1 + \frac{D_2KRT}{D_1c_1\bar{v}_1(\Delta p - \Delta\pi)}\right]^{-1} \tag{4}$$

The transport properties of thick, dense cellulose acetate membranes of varying acetyl content have been measured by direct osmosis in earlier studies [11]. It was shown that the permselectivity increases and the water permeability decreases as the acetyl content of the membrane increases.

The water flux through the thin film of the composite membrane, with a given difference in water activity, depends on the water permeability D_1c_1 of cellulose acetate, the thickness of the thin film, and the characteristics of the surface pore properties of the supporting membrane [12].

Salt rejection, on the other hand, does not vary with thickness if the thin film is homogeneous. Hence, rejection depends only on the salt permeability D_2K and the perfection of the thin cellulose acetate film.

In reverse osmosis with seawater (3.5 wt % sodium chloride) at 102 atm applied pressure, the expected sodium chloride rejection of a perfect cellulose 2.45 acetate (39.8% acetyl) thin film is 99.76%; the expected rejection

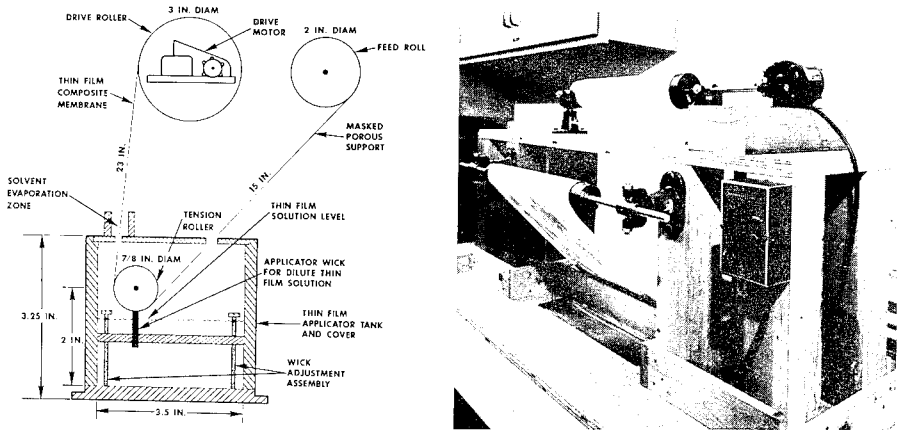

FIG. 2. A schematic drawing and photograph of the device used for continuously forming the thin semipermeable barrier of the composite membrane on the surface of the masked supporting membrane.

of a perfect cellulose 2.83 acetate (43.2% acetyl) thin film is 99.94%, Thus, most cellulose acetates of interest are intrinsically capable of desalinating seawater in a single stage. The expected water fluxes through 600-Å thin films of cellulose 2.45 acetate and cellulose 2.83 acetate are approximately 2.05 M^3/M^2-day (50 gal/ft^2-day) and 0.82 M^3/M^2-day (20 gal/ft^2-day), respectively.

EXPERIMENTAL

Techniques for preparing the composite membrane have been developed which are suitable for large-scale continuous production. Briefly, the membrane is prepared by forming a very thin film of cellulose acetate directly upon the polyacrylic-acid-precoated surface of a finely porous cellulose nitrate–cellulose acetate supporting membrane by dipping from a dilute chloroform solution. The continous dipping device, shown in Figure 2, vertically withdraws the masked membrane from the thin-film solution at a uniform and controlled rate. A wick, saturated with the cellulose acetate solution, applies the thin-film solution to the masked surface of the support membrane as shown in the schematic in Figure 2. The thin films described in this study were prepared from cellulose acetates of varying aceytl content and intrinsic viscosities supplied by Eastman Chemical Products, Inc. The acetyl contents were 43.2%, 41.6% and 41.4% with corresponding intrinsic viscosities of 2.04, 0.89, and 1.24, respectively. The masking layer, a 3-μ-thick water-soluble coating of 50,000 molecular weight polyacrylic acid (Rohm and Haas Acrysol A-1), was applied to the finely porous surface of the support membrane by airless spray from a 2.5 wt % solution of equal volumes of ethanol and water. The purpose of the masking layer is to fill or coat over the pores of the support so that the thin-film solution cannot intrude into the substrate. When the membrane is placed in operation, water diffuses through the thin film and dissolves the

polyacrylic acid which passes through the supporting membrane, thereby placing the thin film directly upon the finely porous surface of the supporting membrane. At this point, the thin film can no longer be removed from the substrate.

The thickness of the thin film, formed by drawing from the dilute chloroform solutions of cellulose acetate, is controlled by the concentration of the solution and the rate of withdrawal according to the Levich-Deryaguin theory [13]. The dry thin-film thickness, assuming a density of 1.50 g/cm^3 and a surface porosity of 26 dynes/cm for pure chloroform, is given by

$$\Delta X = 0.016\,(\mu v)^{2/3} c \tag{5}$$

where μ is the viscosity, v is the withdrawal rate, and c is the solution concentration expressed as g polymer/g solution.

The dependence of viscosity on the cellulose acetate concentration in chloroform at 25°C, determined with Cannon-Fenske viscometers, is given in Figure 3 for each of the cellulose acetates.

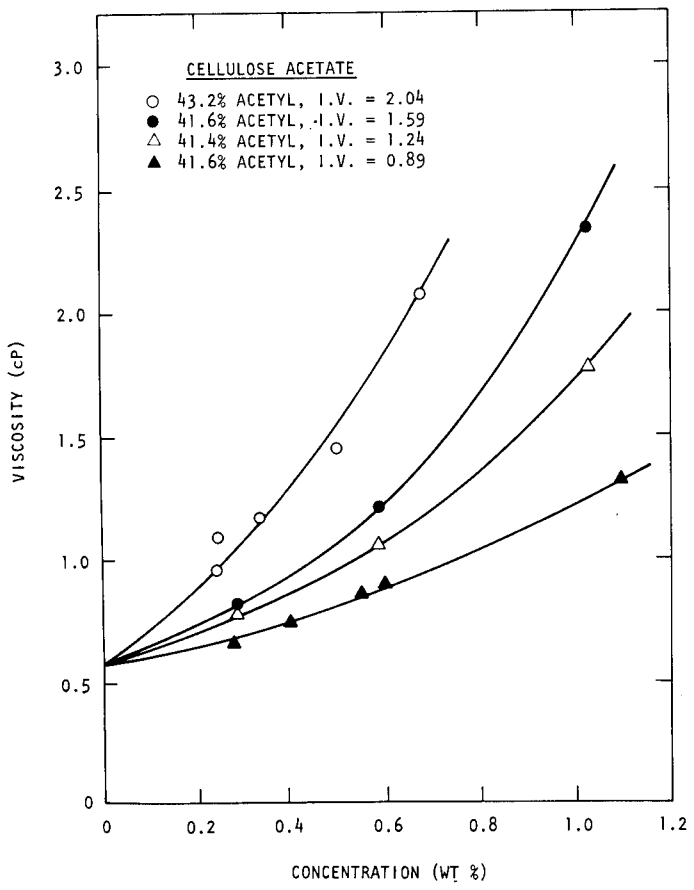

FIG. 3. Viscosities of thin-film cellulose acetates in chloroform at 25°C.

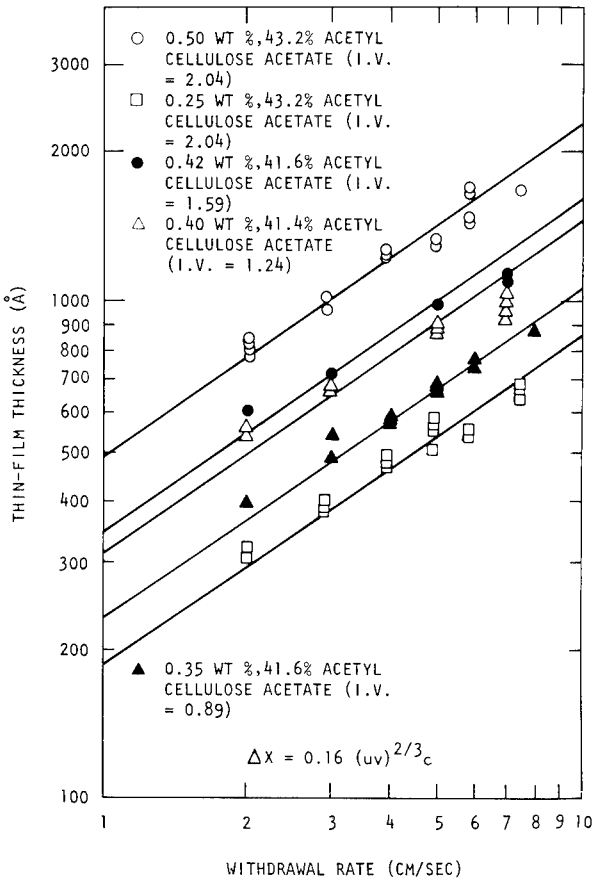

FIG. 4. Thickness of cellulose acetate thin films as a function of withdrawal rate and concentration in chloroform.

Observed thin-film thicknesses are presented in Figure 4 as a function of the withdrawal rate. Thicknesses were determined indirectly by preparing films on the surface of glass plates, floating a known area onto the surface of water, drying, and weighing.

The finely porous supporting membrane used in the preparation of the composite membrane is a mixed ester of cellulose nitrate and cellulose acetate that is prepared by the general method developed both in Germany and in the United States over the past 50 years [14–18]. The detailed procedure is described elsewhere [5]. The membrane used in this work was prepared continuously in 15-in. widths under experimental conditions aimed toward optimizing the surface pore number, size, and distribution. The finished membrane, with a bulk porosity of 70% to 80%, is typically 100 μ thick.

Electron photomicrographs, shown in Figure 5, were taken of the finely porous surface to characterize the membrane with respect to pore size, number, distribution, and total porosity. The bar charts, also shown in Fig. 5, summarize the pore size and area distribution of the pores.

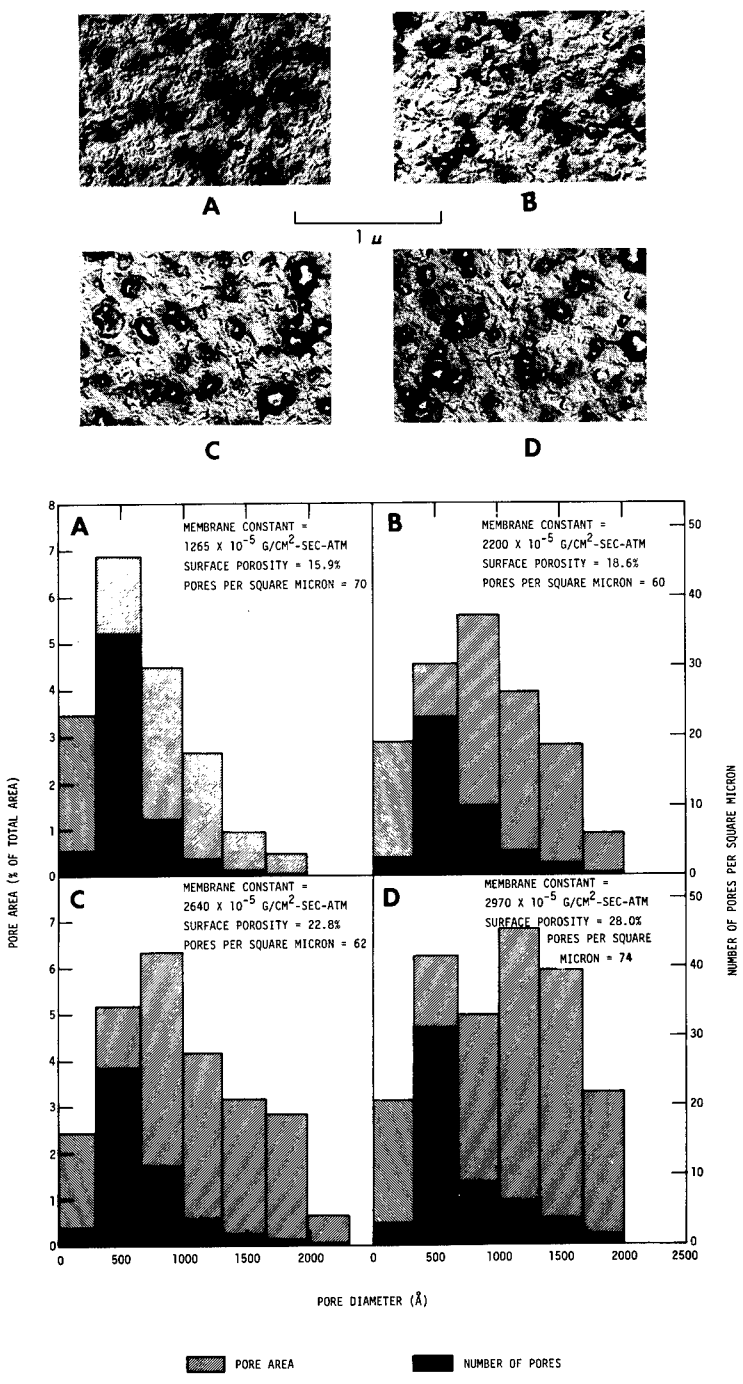

FIG. 5. Electron photomicrographs of palladium-shadowed carbon replicas of the finely porous surface of cellulose nitrate-cellulose acetate membranes with bar charts showing pore-size and area distribution of the pores on the surface supporting the thin, semipermeable barrier of the composite membrane.

TABLE I
Reverse Osmosis Performance of 41.4% Acetyl Cellulose Acetate Thin-film Composite Membranes as a Function of Thickness

Thin-Film Thickness (Å)	Membrane Constant (10^{-5} g/cm²-sec-atm)		Water Flux (gal/ft²-day)[a]		Sodium Chloride Rejection (%)		Flux Decline Slope After 121 hr on 3.5% NaCl (Log A vs Log Time)
	3.5% NaCl 121 hr	Seawater 150 hr	3.5% NaCl 121 hr	Seawater 150 hr	3.5% NaCl 121 hr	Seawater 150 hr	
400	1.55	1.49	24.4	24.9	99.43	99.46	-0.012 ± 0.006
400	1.70	1.62	26.8	27.2	99.30	99.34	-0.018 ± 0.006
600	1.15	1.10	18.2	18.3	99.63	99.44	-0.020 ± 0.004
600	1.19	1.14	18.8	19.0	99.61	99.65	-0.024 ± 0.005
800	0.93	0.89	14.7	14.9	99.66	99.65	-0.031 ± 0.004
800	0.89	0.84	14.1	14.0	99.71	99.62	-0.024 ± 0.005

[a]Gal/ft²-day × 0.041 = M³/M²-day.

The porosity of the 400-Å thin skin on the air-dried surface of the asymmetric support membrane ranges from about 15% to 30% [19]. The number of pores per square micron ranges from 60 to 75. Ideally, the pores should be as numerous as possible to minimize flow restriction through the thin semipermeable barrier. The diameter of the greatest number of pores is generally about 500 Å. The diameter of the pore should not greatly exceed the thickness of the thin semipermeable film to prevent the film from collapsing into the substrate.

REVERSE OSMOSIS

The desalination performance of the composite membrane was determined in closed loop reverse osmosis systems at 25°C with Pacific Ocean water, synthetic seawater, and 3.5 wt % sodium chloride brine. Synthetic seawater was prepared from a simulated sea salt mixture (ASTMD-1141-52), obtained from Lake Products Co., Inc., containing the elements found in natural seawater in quantities greater than 0.004%. The Pacific Ocean water was obtained several hundred meters offshore at Scripps Institute of Oceanography at La Jolla, California. Each of these brines, as far as as membrane performance is concerned, is interchangeable.

For seawater testing, the pH of the brine was reduced from 8.5 to 6.5 by the addition of small quantities of sulfuric acid. Occasionally, this reduction in pH was accompanied by a significant reduction in salt flux through the membrane.

The brine flow and velocity across the membrane, except where noted, were 2.0 gal/min and 170 cm/sec, respectively. The concentration of the brine was held constant during the experiments by returning the desalinated product to the brine stream. Consequently, the tests were carried out with essentially little or no recovery. Membrane foulants present in the system

with a particle size greater than five microns were removed by in-line cartride filters.

Membrane constants, as defined by eq. 1, were calculated from the water throughput rate and the salt rejection from the salt content of the feed and permeate in accordance with eq. 3. Atomic absorption, silver nitrate titration, and conductivity measurements were used to determine chloride and sodium chloride concentrations.

The dependence of water productivity with time was calculated according to the power law, $\log A = -m \log \text{time}$, where the constant m (the flux-decline slope) depends on membrane type, brine composition, brine concentration, foulants, operating pressure, and temperature.

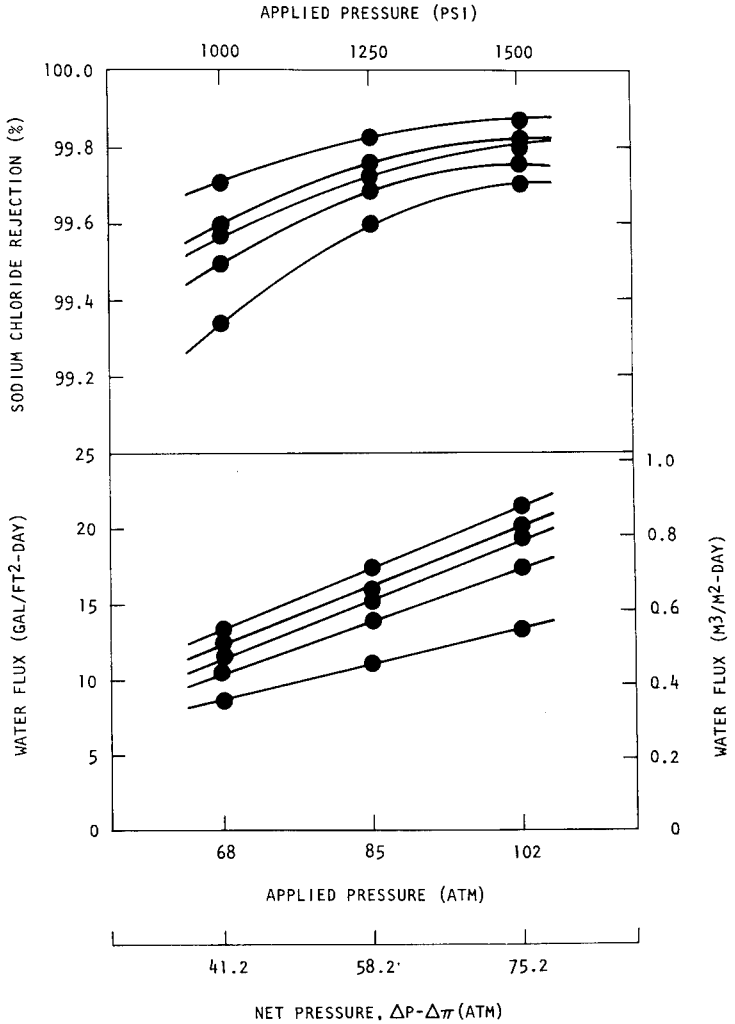

FIG. 6. Reverse osmosis performance for five 500-Å, 43.2%, acetyl-cellulose acetate, thin-film composite membranes as a function of applied pressure with 3.5 wt % sodium chloride.

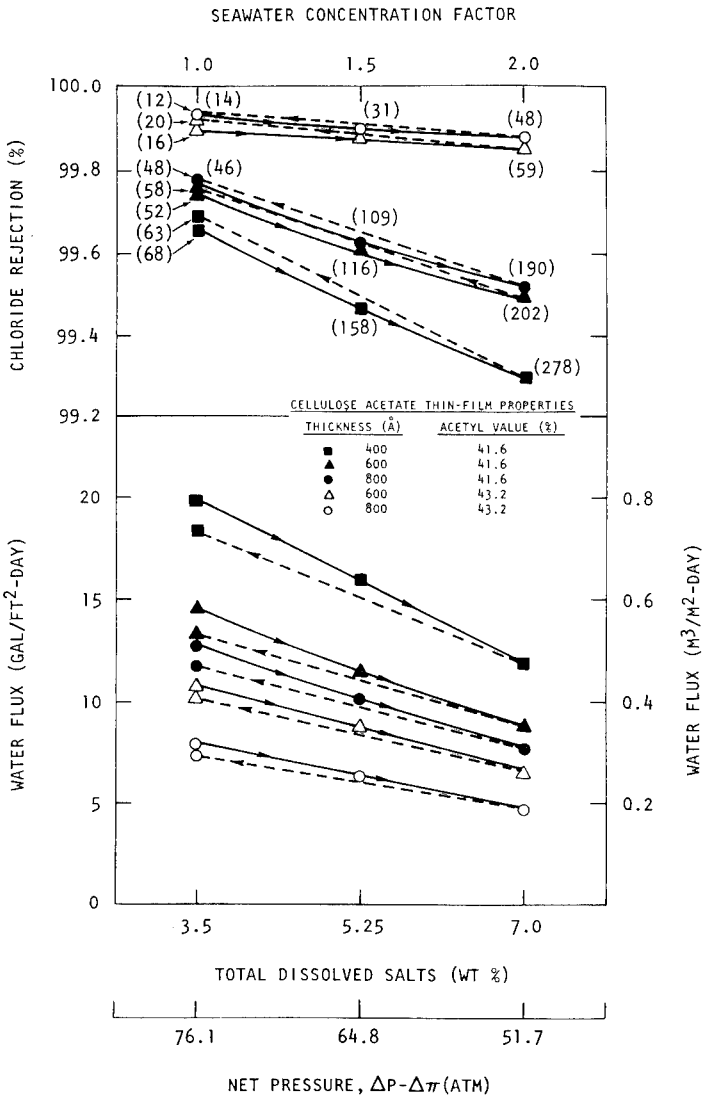

FIG. 7. Reverse osmosis performance for an average of two composite membranes with concentrated seawater at 102 atm applied pressure. Parts per million chloride in product shown in parentheses.

RESULTS AND DISCUSSION

Three reverse osmosis experiments are presented which characterize the transport properties of the composite membrane with respect to operating pressure, brine type, brine concentration (water recovery), and the thickness of the thin film. In addition, the effect of acetyl content and molecular weight of the cellose acetate thin film on composite performance was observed.

Composites, having 400-, 600-, and 800-Å thin films of 41.4% acetyl-cellulose acetate, were tested with seawater and 3.5 wt % sodium chloride brines at an applied pressure of 102 atm. The overall performance of the membranes presented in Table I was excellent with little, if any, dependence on brine type. The observed water flux, as predicted from eq. 1, is inversely proportional to the thickness of the thin film. Stable long-term fluxes of 25 gal/ft²-day were observed with 99.4% rejection of sodium chloride. However, the expected flux, based on the thickness of the 400-Å thin film and the water permeability of 41.4% acetyl-cellulose acetate, is about 45 gal/ft²-day. To realize this potential, additional improvements in the surface pore properties of the supporting membrane will be necessary to minimize flow resistance. The salt flux, contrary to that predicted by the solution-diffusion equations, increases with decreasing film thickness. This, of course, is attributed to an increase in the number of imperfections in the thin film.

The water and salt fluxes through composite membranes, as a function of applied pressure, are shown in Figure 6. Both are pressure dependent; that is, the salt flux increases with a corresponding decrease in water productivity at reduced pressures. Nevertheless, even at 68 atm applied pressure and a 3.5 wt % sodium chloride brine, the composite rejects an average of 99.5% of the sodium chloride at flux rates in excess of 10 gal/ft²-day. The composites prepared with 500-Å thin films of 43.2% acetyl-cellulose acetate are clearly capable of producing potable water from seawater in a single stage at practical operating pressures.

For seawater desalination to be economical, it is necessary to operate at high recovery rates, that is, 50% or more. Hence, to obtain potable water from seawater in a single stage, the membrane must reject about 99.5% of the sodium chloride. Recovery, defined as the percentage of brine which is recovered as product, is limited by the increase in osmotic pressure of the brine and by the degree of concentration permissible before precipitation of slightly soluble salts begins. Both phenomena, of course, determine the limit on discharge concentration and lead to decreased water productivity. The latter condition is generally controlled by acidifying the brine. The performance of composite membranes, as a function of seawater concentration or water recovery, is given in Figure 7 for ten membranes having thin films of varying thickness and acetyl content. All of the membranes produced potable water at 102 atm applied pressure even after the seawater had been concentrated by a factor of two (7.0 wt % total dissolved salts), well in excess of 50% recovery. The brine velocity across the membrane was 85 cm/sec. The highest flowing composites, having 400-Å thin films of 41.6% acetyl-cellulose acetate, exhibited stable long-term fluxes of 10 to 15 gal/ft²-day at twice the concentration of normal seawater.

Composities incorporated into the spiral-wound module configuration have also been tested successfully with seawater at pressures up to 81.6 atm. Generally, the performance has equalled that of composites tested as

flat sheets. However, the water flux per unit membrane area is lower, since the thickness of the thin film for this application is 1000 Å. A single module of this type, containing 2 ft^2 of membrane, operated for more than 2000 hours on seawater at an applied pressure of 68 atm with no deterioration in performance.

CONCLUSIONS

The thin-film composite membrane combines high water flux and stability with excellent selectivity. Even with cellulose acetate films as thin as 400 Å, the transport process is diffusion controlled. The water flux through the composite membrane depends on the water permeability of the thin-film material, the thickness of the thin film, and the number and characteristics of the pores in the surface of the cellulose nitrate–cellulose acetate supporting membrane. Long-term reverse osmosis tests have demonstrated that the composite membrane is capable of producing potable water from seawater in a single stage at high recovery rates. Initial testing of composite membrane spiral-wound modules with seawater has also demonstrated single-stage seawater capability. Techniques for preparing the composite have been developed which are suitable for producing pilot quantities for incorporation into an operational, single-stage, reverse osmosis seawater unit.

The authors would like to acknowledge R. Grabowsky, K. Tagami, and D. Want for important technical contributions, and G. Foreman for technical assistance in developing the spiral-wound module. The electron microscopy was performed by S. Liang. This work was supported by the Office of Saline Water, U.S. Department of the Interior, under Contract 14-30-3016.

REFERENCES

[1] R. L. Riley, H. K. Lonsdale, C. R. Lyons, and U. Merten, *J. Appl. Polymer Sci. 11*, 2143 (1967).

[2] R. L. Riley, H. K. Lonsdale, L. D. LaGrange, and C. R. Lyons, "Development of Ultrathin Membranes," U.S. Department of the Interior, Office of Saline Water, Research and Development Progress Report No. 386, Gulf General Atomic, May 1968.

[3] H. K. Lonsdale, R. L. Riley, L. D. LaGrange, C. R. Lyons, A. S. Douglas, and U. Merten, "Research on Improved Reverse Osmosis Membranes," U.S. Department of the Interior, Office of Saline Water, Research and Development Progress Report No. 484, Gulf General Atomic, December 1969.

[4] H. K. Lonsdale, R. L. Riley, C. E. Milstead, L. D. LaGrange, A. S. Douglas, and S. B. Sachs, "Research on Improved Reverse Osmosis Membranes," U.S. Department of the Interior, Office of Saline Water, Research and Development Progress Report No. 577, Gulf General Atomic, April 1970.

[5] R. L. Riley, C. E. Milstead, H. K. Lonsdale, and K. J. Mysels, "Research on Improved Reverse Osmosis Membranes," U.S. Department of the Interior, Office of Saline

Water, Research and Development Progress Report No. 729, Gulf General Atomic, March 1971.

[6] R. L. Riley, H. K. Lonsdale, and C. R. Lyons, *J. Appl. Sci. 15*, 1267 (1971).

[7] S. Loeb, and S. Sourirajan, *Advan. Chem. Ser. 38*, 117 (1962).

[8] R. L. Riley, J. O. Gardner, and U. Merten, *Science 143*, 801 (1964).

[9] Riley, R. L., U. Merten, and J. O. Gardner, *Desalination 1*, 30 (1966).

[10] Merten, U (Ed.), *Desalination by Reverse Osmosis*, the M.I.T. Press, Cambridge, Mass., 1966.

[11] H. K. Lonsdale, U. Merten, and R. L. Riley, *J. Appl. Poly. Sci. 9*, 1341 (1965).

[12] H. K. Lonsdale, R. L. Riley, C. R. Lyons, D. P. Carosella, Jr., *Membrane Processes in Industry and Biomedicine*, Plenum Press, New York, 1971, p. 102.

[13] V. G. Levich, *Physiochemical Hydrodynamics*, Prentice-Hall, Englewood Cliffs, N. J., 1962.

[14] Z. Zsigmondy, *Angew. Chem. 30*, 398 (1926); U.S. Patent 1,421,341 (1922).

[15] P. Grabar, *Compt. Rend. 198*, 1640 (1934).

[16] M. Vaughan, *Nature 183*, 43 (1959).

[17] W. Elford, *Proc. Roy. Soc. (London) B106*, 216 (1930).

[18] A. Goetz, U.S. Patent 2,926,104 (1960).

[19] R. L. Riley, G. Hightower, and C. R. Lyons, "Preparation, Morphology, and Transport of Composite Reverse Osmosis Membranes for Seawater Desalination," in *Reverse Osmosis Membrane Research*, H. K. Lonsdale and H. E. Podall (Eds.), Plenum Press, New York, in press.

MICROBIAL DEGRADATION OF POLYMER SOLIDS. II. A COMPARISON OF FUNGAL ATTACK IN CELLOPHANE AND AMYLOSE FILMS

S. A. BRADLEY, P. ENGLER, and S. H. CARR

Department of Materials Science
Northwestern University
Evanston, Illinois 60201

SYNOPSIS

Specimens of regenerated cellulose films (cellophane) and solution-cast amylose films have been subjected to microbial degradation. The degradation process was monitored by x-ray diffraction, infrared spectroscopy, and mechanical property tests. Crystalline index measurements of fungal degraded samples are found to increase, while cell-free enzymes disrupt both crystalline and non-crystalline regions, with a rise in weight average crystallite size and lattice distortion. Ultimate and yield tensile stress of amylose films decline during the degradation process. Enzymes appear to attack preferentially the non-crystalline regions of the two polymers investigated.

INTRODUCTION

Although most commercial, synthetic polymers are composed of organic repeat units, few polymers can act as the sole carbon source for microorganisms. Alkanes in the range of C_{18}–C_{24} are readily degraded [1], but only the low molecular weight components of polyethylene can support microbial growth [2]. Also, some polyesters [3] and several polyurethanes [4] can be degraded by microorganisms. In addition, the plasticizers of polyvinyl chloride sustain microbial growth by acting as a carbon source [3, 5, 6, 7], and thus, if an engineering polymeric solid is observed to support microbial growth, it may be the plasticizer, stabilizer, sizing agent, or processing aid that is being utilized, rather than the macromolecules present.

One technique for understanding how biodegradation of synthetic polymers would occur is to examine this process in naturally-occurring polymers. Polysaccharide polymers have glucose as the repeat unit, and amylose and cellulose are two members of this group that are excellent film formers. Although dissolved polysaccharides have been studied extensively as substrates for metabolic enzymes [8–10], little is known about how microbial degradation causes deterioration when the polymer exists as a re-

Applied Polymer Symposium No. 22, 269–286 (1973)

constituted solid. In the previous paper by Engler and Carr [11], several details in the degradation process were, in fact, elucidated. For example, it was shown that cellulase enzymes can diffuse appreciable distances in cellophane. Cellulolytic attack was described as being most extensive in disordered regions, with the result that crystallites appear to be more isolated and to become broken into segments, and both yield stress and ultimate tensile strength were shown to decrease progressively during the degradation process.

In a comparative study on amylose and cellulose, it is important to keep in mind the distinctly different morphologies each possesses. Cellophane film has essentially the same X-ray diffractogram as cellulose II [12], when allowance is made for effects due to orientation produced during processing. Cellophane is comprised of microfibrillar crystallites [11, 13], which have a diameter of a few hundred Angstroms and represent a bundle of 35 Å diameter protofibrils [13]. The cellulose chains are arranged parallel to the protofibril axis and are either in an extended [14] or folded [15, 16] chain conformation. Connecting the protofibrils and microfibrils is presumably a matrix of disordered material [11].

Amylose can assume either an extended-helix (B-complex) [17] or a helical (V-complex) conformation in the crystalline state. The V-complex is prepared by precipitation from aqueous solution with various complexing agents [18–20]. These complexing agents include alcohols, ketones, and fatty acids. The V-complex has also been precipitated from dimethyl sulfoxide [20, 21]. A folded chain crystallization mechanism has been proposed from electron microscopy studies on single crystals [22, 23], X-ray diffraction from films [24], and infrared spectroscopy of both single crystals and films [25]. The morphology is reported to vary from a rod-like to a spherulitic texture, depending upon the casting procedure or post-humidity treatment [26]. Fibrils of 40 Å diameter have also been reported [27].

Hydrolysis of amylose and cellulose by enzymes is not yet completely known from a mechanistic standpoint. Amylose can be degraded by either α or β amylase, while cellulose requires a collection of enzymes called the cellulase system. This system consists of enzyme C_1, an "activator" [28, 29] or "affinity factor" [30], exo- and endoenzymes C_x, the "hydrolytic factor" [28], and glucosidases to produce glucose. The amylase enzyme is similar to C_x in that it has a specific attachment site [31]. Non-ordered regions are assumed to be more readily attacked by the enzymes [11, 32, 33, 34]. For crystalline regions, degradation is a function of size [35] with the process starting on the crystallite surface and proceeding inward [36].

EXPERIMENTAL

The fungus used in this study was that already described by Engler and Carr [11]. The colonies were isolated from the soil by using a selective solid medium. All samples were incubated at 23°C for the prescribed length of

time and then sterilized in ethylene oxide gas to stop the degradative process. No detectable effect on strength, crystallinity, or infrared absorption spectrum was noted due to the sterilization process.

The regenerated cellulose film used was 1 mil thick DuPont PUD-O (E. I. Du Pont de Nemours and Co., Inc.) plain, nonmoisture-proof, unplasticized film. For microbial growth, films were placed directly on the agar medium [11] and inoculated with the fungus. Cell-free degradation of cellophane by cellulase enzymes was performed by placing specimens into 0.28% enzyme solution (4000 units per gram Nutritional Biochemical Company, Cleveland, Ohio) in 0.05 M sodium citrate buffer adjusted to pH 4.8. Following incubation at 40° C for predetermined time intervals, samples were removed, washed in distilled water, and dried under vacuum. Tensile specimens were made by cutting films that were clamped between two identical templates, producing films with a gauge length of 0.700 in. and width of 0.175 in. Tensile samples were cut in both the longitudinal and transverse directions.

Amylose films were cast at 60°C from 6% w/v aqueous solution that contained both n-propanol and dimethyl sulfoxide. The amylose used was Nepol 300 (A. E. Staley Co.), which is reported to contain 10% amylopectin. Exceedingly thin layers of silicone lubricant were applied to the stainless steel casting pan to facilitate film removal after oven drying at 60°C. The resulting films were 4 ± 1 mil thick and were slightly turbid due to microscopic surface roughness. The agar medium utilized was specified in ASTM Test G-21 [37]. All specimens were placed on to the agar medium with silicone side down. Tensile films had gauge lengths of 0.700 in. and widths of 0.175 in.

Tensile studies were performed with a floor model Instron Tensile Tester at 23 ± 1°C and 53 ± 6% relative humidity. The strain rate for all samples was 0.03 in./in. X-ray diffractogram studies were made with a Norelco diffractometer, which had been calibrated with a powdered sucrose standard. Copper K_α radiation generated at 20ma and 40KV was utilized, and diffracted intensity was measured with a scintillation counter at a scan rate of 1/2°/min; 1° divergence and 0.2° receiving slits were used. The cellophane samples were oriented so that the machine direction was perpendicular to the x-ray beam. X-ray diffraction patterns were also produced from a two-hour exposure of copper K_α at 19ma and 40KV with the films mounted in a cylindrical camera.

Transmission electron microscopy utilized an Hitachii HU-11A microscope to examine surface replicas, which were prepared by shadowing the samples with a carbon-platinum mixture at an elevation of 30° and reinforced with carbon. Replicas were isolated by decomposition of the underlying specimen by concentrated sulfuric acid. The pan side of the amylose film was never shadowed.

Infrared spectroscopy measurements were performed on a Beckman IR-9 infrared spectrophotometer at a scan speed of 20 cm^{-1}/min. Although the cellophane films were sufficiently thin for this work, the amylose samples had to be dispersed in a potassium bromide pellet.

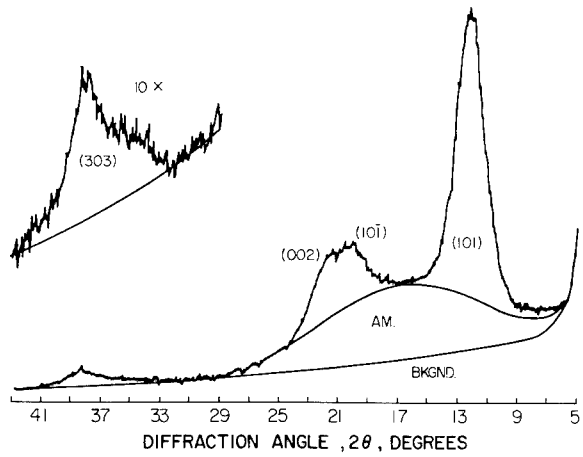

FIG. 1. X-ray diffractogram of 2-day fungus-degraded cellophane sample. Baseline and amorphous halo have been added graphically.

RESULTS AND DISCUSSION

Fungal Degradation of Cellophane

Although the concept of absolute crystallinity has been described as meaningless for cellulose [12], an internally consistent crystalline index can nevertheless be calculated [38, 39] and be used to follow the degradation processes. This index is measured by comparing the integrated intensity of the amorphous and crystalline scattering. Baseline and amorphous intensity must be graphically estimated, as depicted in Figure 1 for a 2-day degraded sample. The crystalline index was checked for consistency and found to

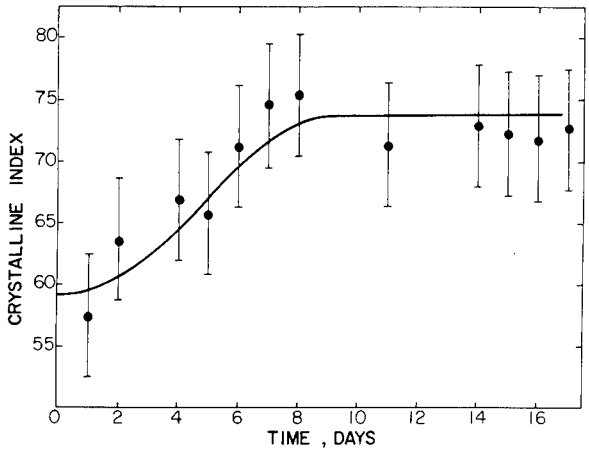

FIG. 2. Increase in crystalline index as measured by x-ray diffraction during fungal degradation of cellophane. Apparently fungus degradation is most vigorous in non-crystalline regions.

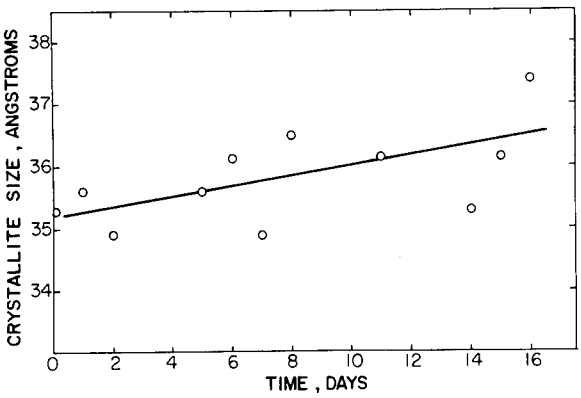

FIG. 3. Weight-average crystallite size as a function of time during fungal degradation of cellophane. Little, if any, significant change can be detected.

have a maximum of 3% deviation between doubly run samples. No correction for absorption or for Lorentz polarization factor was applied to the diffractogram, as these would presumably apply equally to discrete and diffuse scattering at each diffraction angle. Only the (101), (10$\bar{1}$), and (002) scattering maxima were used in the crystalline index determination for cellophane; the (303) peak was disregarded because it increased this index by 0.5%, which is equivalent to planimeter areal standard deviation. For fungal degraded cellophane the crystalline index sigmoidally increased from 55% initially to 73% at day 9, as shown in Figure 2. After 9 days new colonies were primarily concentrated around the edges of the film. The value of the crystalline index for the control specimen is lower than the "absolute" crystallinity of 70% for cellophane [12] and 74% for Fortisan [40].

The integral breadth of a given diffraction maximum is a function of residual strain, crystal defect density, and characteristic mosaic size [41].

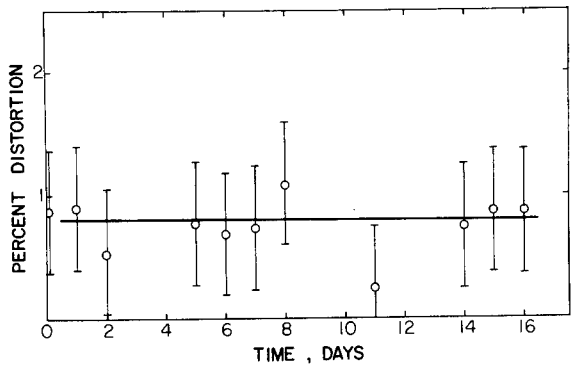

FIG. 4. Average lattice distortion in crystallites as a function of time during fungal degradation of cellophane. As in Figure 3, virtually no significant change can be detected.

TABLE I
Changes in Crystallite Size and Lattice Distortion During Fungal Degradation of Cellophane Films

	Buchanan and Miller Technique [44]	Schoening Technique [42]	Hosemann Paracrystalline Model [43]
Control			
Crystallite Size, Å	35.3	35.9	35.0
Lattice Distortion, %	0.88	1.75	2.40
Day 5			
Crystallite Size, Å	35.6	36.4	36.5
Lattice Distortion, %	0.76	1.42	2.15
Day 15			
Crystallite Size, Å	36.1	36.2	36.0
Lattice Distortion %	0.85	1.75	2.38

This last property, crystallite size, can be theoretically separated from residual strain if two reflections of the same order can be identified [42–44]. Three alternative bases can be employed when measuring contributions of mosaic size and defect density. The first procedure by Schoening [42] assumes that the size profile is Cauchy while the distortion profile is Gaussian. A second procedure, the Hosemann paracrystalline model [43], uses a Gaussian profile for size and different kinds of lattice displacements. Buchanan and Miller's technique [44] also assumes that size and distortion profiles are Gaussian and utilizes either Fourier transformations or integral peak breadths in the analysis of data. The integral breadth of Buchanan and Miller's microstrain procedure was chosen to illustrate results obtained in work reported here. All profiles were assumed to be Gaussian and were specially corrected for instrumental broadening but not for geometrical factors. The (303) peak was increased tenfold by electronic amplification.

Both weight-average crystallite size and defect density for these samples were determined using the (101) and (303), and, as shown in Figure 3, crystallite size is found to increase very slowly, as judged by a linear

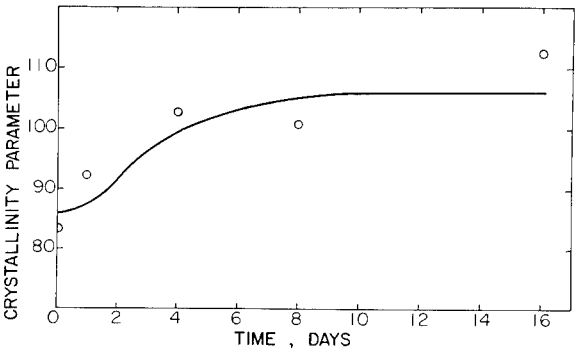

FIG. 5. Increase in crystallinity parameter as measured by infrared spectroscopy of fungus-degraded cellophane samples. Values above 100% may result from confounding effects due to excessive fungal overgrowths.

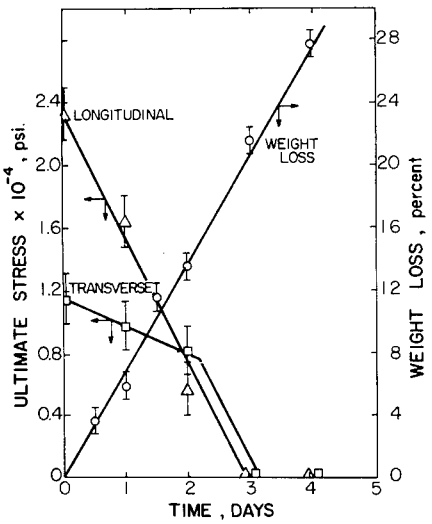

FIG. 6. Degradation of cellophane samples suspended in cellulase enzyme solution. Accompanying a progressive loss of material (circles) is a rapid weakening of the cellophane, as seen by a decline in ultimate tensile stress at failure for both longitudinal (triangles) and transverse (rectangles) samples.

regression line drawn through these data. The crystallite size for as-received samples is approximately 35 Å, which is in excellent agreement with values measured from regenerated cellulose [13] and Fortisan fibers [40]. Average lattice distortion for these degraded samples remained essentially constant at 0.80%, as shown in Figure 4. In Table I are listed some typical results of applying the Schoening and paracrystalline techniques to diffractometer scans made from cellophane used in these studies. With either procedure the same trend is observed, although the lattice distortions can be seen to fluctuate considerably. The integral breadth for the (101) remains relatively constant during the degradation, while the integral breadth for the (303) increases.

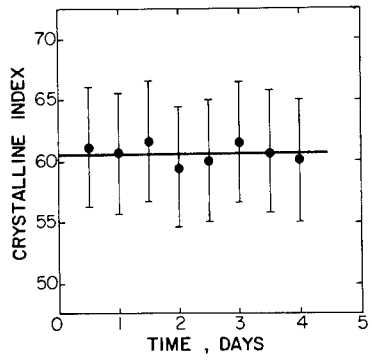

FIG. 7. Crystalline index change as measured by x-ray diffraction during cell-free cellulase enzyme degradation. No apparent change in crystalline index may indicate that crystallites are being consumed at the same rate as noncrystalline regions.

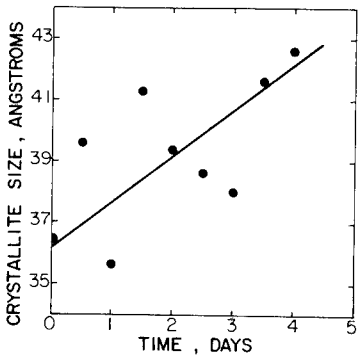

FIG. 8. Increase in weight-average crystallite size during cell-free cellulase enzyme hydrolysis of cellophane. The line is a result of linear regression analysis of these data.

Infrared spectroscopic analysis of cellophane was also conducted as an alternate technique to measure a crystalline index. Nelson and O'Connor [45] suggest that the ratio of absorbance at 1372 cm^{-1} and 2900 cm^{-1} can be correlated with a crystallinity parameter. As illustrated in Figure 5, the crystallinity parameter starts at 83% for the control and increases to 112% after 16 days of degradation. It is possible that the values beyond 4 days may be slightly high due to the fungal material itself.

Cell-Free Cellulase Enzymatic Hydrolysis of Cellophane

Cell-free enzymatic hydrolysis of cellophane was performed in order to examine enzyme damage in absence of effects due solely to fungal growth. Cellophane is suspended in a cellulase solution, enzyme molecules are presumed to adsorb onto the film surfaces and begin to diffuse into its bulk. A constant rate of weight loss, as shown in Figure 6, occurs during

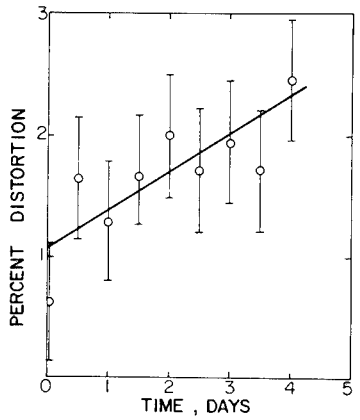

FIG. 9. Increase in average lattice distortion of crystallites during cell-free cellulase enzyme hydrolysis of cellophane.

the subsequent time of degradation. Concurrently, cellophane loses most of its mechanical anisotropy by the time about 15% of the material has been solubilized and all of its strength after 20% of the cellulose is gone.

This cell-free enzymatic degradation was also examined by x-ray diffraction techniques, as shown in Figure 7. The crystalline index remains essentially constant at 61% during the first 4 days of degradation, even though more than 25% of the cellulose has been solubilized. This is in contrast to the sigmoidal increase in crystalline index found in the fungal degraded samples and is possibly due to swelling of the film by water during the experiment. In this way, cellulase enzymes can have access to more of the ordered regions of a sample. Once this occurs, enzymes can disrupt and hydrolyze the highly ordered microfibrils at a rate comparable to that in the less ordered regions. These observations are consistent with work by Rateula and King [36], in which little x-ray crystallinity changes during cell-free degradation for various forms of cellulose were observed.

Crystallite size and distortion computations were also performed with these x-ray data. The weight-average crystallite size is measured to increase from 36.5 Å to 42.6 Å after 4 days of degradation (Figure 8). From weight loss data and the unchanging crystalline index, there is therefore an indication that both highly crystalline material and disordered regions become solubilized simultaneously. The observed increase in average crystallite size might be due to smaller crystallites being preferentially degraded or due perhaps to interfibrillar chains being cleaved and subsequently joining crystallites. In support of the first proposition, it should be noted that the degradation velocity has been related to particle size of crystalline hydrocellulose [35], with the smaller particles being more readily attacked than the larger ones. It is also possible that a free cellulose molecule could join a crystallite by the formation of hydrogen bonds and a concommitant reduction in its configurational entropy. As illustrated in Figure 9, the crystallites also become more distorted during degradation. Table II shows a comparison of the various techniques used to separate average crystallite size and distortion. There seems to be no indication that

TABLE II
Changes in Crystallite Size and Lattice Distortion During Cell-Free Cellulase Degradation of Cellophane Films

	Buchanan and Miller Technique[44]	Schoening Technique[42]	Hosemann Paracrystalline Model[43]
Control			
Crystallite Size, Å	36.5	36.7	37.8
Lattice Distortion, %	0.62	1.10	1.98
Day 2			
Crystallite Size, Å	39.2	40.1	39.0
Lattice Distortion, %	2.02	5.50	3.51
Day 4			
Crystallite Size, Å	42.6	42.5	41.0
Lattice Distortion, %	2.45	6.05	3.15

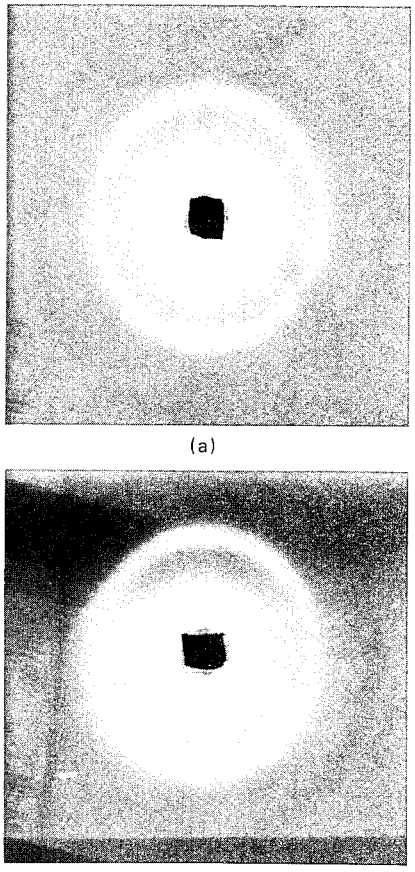

FIG. 10. X-ray diffraction patterns of Cellophane films. (a) Control sample with beam passing perpendicular to the film, $(10\bar{1})$ and (002) rings appear as one intense ring with (101) missing. (b) Control sample with beam inclined 20° with respect to the film; $(10\bar{1})$ and (002) rings appear as one intense ring with maxima 90° to equator, while (101) appears as a strong arc on the equator. This observed crystal texture is reasonably close to the "selective uniplanar orientation" described in Reference 47.

more highly strained crystallites are being degraded first, but it does appear that the crystallites do become more disorganized, on average, after degradation. Engler and Carr [11] observed by electron microscopy of enzyme digested films that interfibrillar material was degraded and microfibrils were broken into short segments. King [35] likewise reported fragmentation and surface erosion of crystalline hydrocellulose particles during degradation.

Enzyme hydrolysis has been found also to create small changes in the crystal texture of cellophane films, as revealed by cylindrical camera x-ray diffraction photography. If the x-ray beam is perpendicular to undegraded film, virtually no (101) scattering is observed; while the $(10\bar{1})$ and (002) show the random orientation illustrated in Figure 10a. When the beam is

normal to the machine direction but makes an angle of 20° with the film surface, the (101) line appears as two strong maxima on the equator. The ($10\bar{1}$) and (002) lines have intensity minima along the equator with intensity maxima at 90° to the equator (Fig. 10b). After three days of cellulase enzyme degradation, a small textural change can be detected, as shown in Figure 11. When the beam is perpendicular to the film, the ($10\bar{1}$) and (002) develop a slight maxima at the equator, but when the beam makes an angle of 20° with the film, then the (101) appears to have stronger but slightly shorter maxima on the equator. The ($10\bar{1}$) now has a strong intensity maximum 90° to the equator while the (002) has two relatively weak maxima near the ($10\bar{1}$) maxima. The integrated intensities and relative peak maxima of the diffractograms are changing in an analogous manner

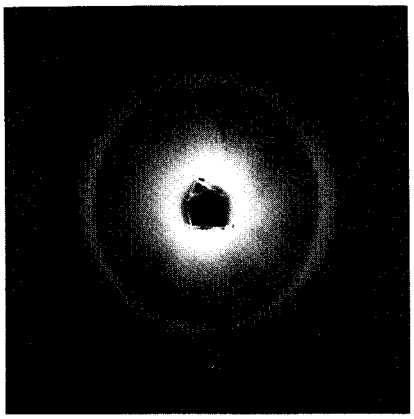

(a)

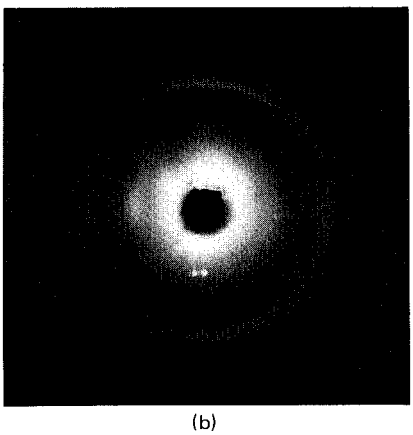

(b)

FIG. 11. X-ray diffraction patterns of cellophane film degraded three days by cellulolytic enzymes. (a) Sample with beam passing perpendicular to film; ($10\bar{1}$) and (002) rings are more distinct than in Figure 10a while (101) is missing. (b) Sample with beam passing 20° to the film, ($10\bar{1}$) and (002) rings are more distinct and the (101) appears as a stronger arc on the equator than in Figure 10b.

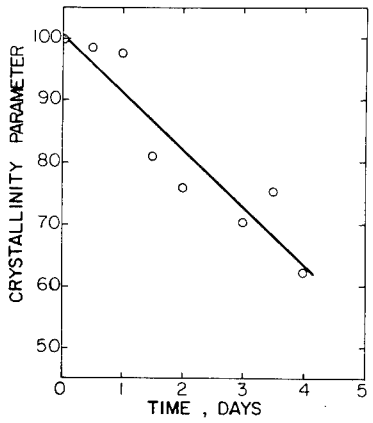

FIG. 12. Decrease in crystallinity parameter [45] as measured by infrared spectroscopy of cellophane by cell-free cellulase enzyme degradation. This indicates that crystalline and non-crystalline regions are being degraded.

to the x-ray diffraction pattern. This can be attributed to a small textural change occurring during cell-free cellulase degradation.

The initial crystal texture which is produced during processing [46, 47] has been described as being uniplanar combined with a degree of uniaxial orientation in the machine direction. Engler and Carr [11] found from birefringence profiles that a detectable orientation gradient existed in these films in addition to the selective uniplanar crystal texture, and they were able to show that core material would be consumed completely, while the partly hydrolyzed surface layers remained coherent. Thus, the textural changes observed may be due to cellulase enzymes preferentially degrading less oriented crystallites inside these samples. It might be that oriented layers of the film may be physically inaccessible to the enzyme molecule or that some stereo-specific mechanism as described by Hollo [31] for β-amylases may likewise be involved in cellulase enzyme degradation.

Infrared spectroscopic analysis of crystallinity parameter should not be so sensitive to textural changes as might be the x-ray crystalline index. Utilizing the absorbance ratio that was previously mentioned, the crystallinity parameter, as shown in Figure 12, tends to decrease during cell-free cellulase degradation. This suggests that crystallites are being disrupted, as was indicated by x-ray defect density data in Figure 9. No residual protein could be detected by infrared absorption spectroscopy.

Several differences can be noted between fungal and cellulase enzyme degradation. The fungus requires an induction period to produce enzymes sufficient to initiate degradation of cellophane. Conversely, for cell-free cellulase degradation no induction period is needed. The fungus primarily metabolizes the less crystalline material with a slight increase in average crystallite size and no apparent change in average crystallite distortion. The cell-free cellulase enzymes, however, degrade both ordered and disordered regions, with the result being an increase in both average crystallite size and distortion level. For the fungally degraded samples, a much smaller

texture change is observed, and might actually be the reason for changes in crystalline indices. The variance might also be explained in terms of differences in size and diffusibility of the two enzyme systems studied [8], or increased physical accessibility of crystalline regions due to swelling in the cell-free enzyme solution.

Fungal Degradation of Amylose Film

Degradation of another polysaccharide film, amylose, was also studied in the work reported here. The mechanical properties of amylose were found to change considerably after one day. Ultimate tensile strength, as shown in Figure 13, decreases by 36%; the yield strength drops by 18%; and the tensile modulus increases by 40% after 48 hours of degradation. Percent changes have been utilized because small differences in sample preparation lead to various levels of initial strength and modulus. Typical mechanical properties for a control sample were 5500 psi ultimate tensile strength, with a yield strength of 2900 psi and a tensile modulus of 430,000 psi. By the end of 60 hours, a tensile specimen could not be removed from the agar plate without tearing the film. This behavior is in contrast to cellophane films which could readily be removed from agar plates after as many as seventeen days of fungal degradation.

An x-ray diffraction analysis of successively degraded films was also performed. A typical x-ray diffractogram, with the estimated amorphous contribution superposed, is illustrated in Figure 14. The crystalline index

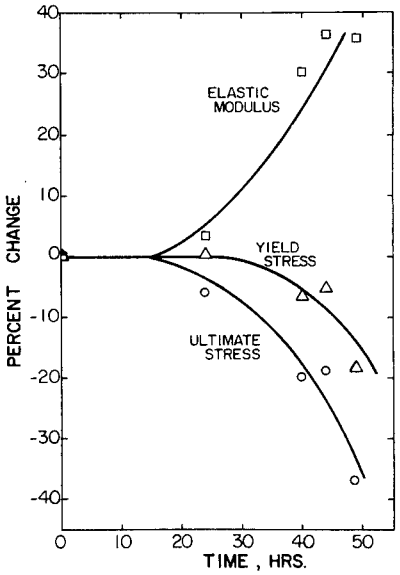

FIG. 13. Degradation of amylose films by fungus. A rapid decline in both yield and ultimate stress levels and an increase in tensile modulus can be seen to result from fungal degradation.

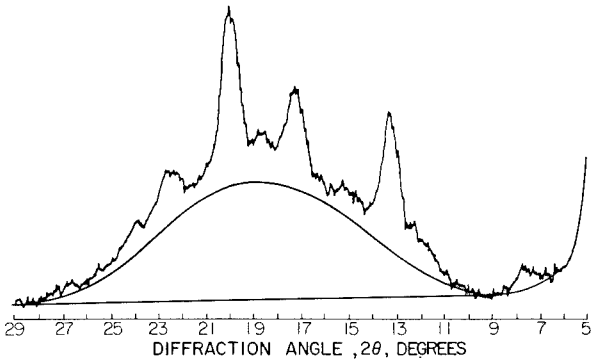

FIG. 14. X-ray diffractogram of 2-day fungus-degraded amylose film. Baseline and amorphous halo have been added graphically.

for the amylose films was determined as previously mentioned, and the diffraction peaks are in agreement with those found by Valletta et al. [18] for the n-propanol-amylose complex. For films with an initial crystalline index of 41 ± 2%, this parameter was found to increase during fungal degradation, as depicted in Figure 15. Interestingly, it was found that films with higher crystalline indices were associated with diminished rates at which crystallinity rose during degradation. This is depicted in Figure 16 where a crystalline index of 26% rises to 43% after two days of degradation. If, on the other hand, the initial index was 54%, it rose only to 60%. Thus, the degradation rate is a function of the crystalline index with the less ordered material removed preferentially in any case. Higher orders of a given

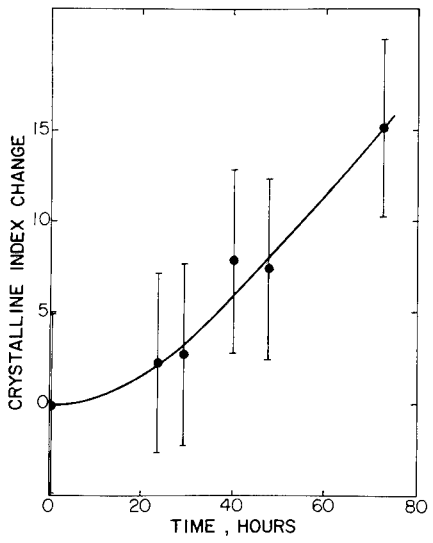

FIG. 15. X-ray crystalline index increase of fungus-degraded amylose. Initial crystalline index 41 ± 2%.

reflection could not be completely separated from the many diffraction peaks so that average crystallite size and distortion could not be measured.

An infrared spectroscopic analysis was conducted on amylose to detect changes in composition or in structure at the molecular level. No residual dimethyl sulfoxide could be detected, a fact which supports the X-ray studies. Koenig and Vasko [25] attribute the 1295 cm^{-1} cm band to a regular fold conformation and 855 cm^{-1} band to only crystalline contributions. When the relative absorbance ratio A_{1295}/A_{855} is examined during degradation of a 41 $\pm$ 2% (X-ray) crystalline sample, no significant change in the concentration of chain fold conformation is found. Apparently little degradation or addition of chain folds has occurred up to 74 hours degradation time.

Electron micrographs of surface replicas of amylose are shown in Figure 17. The original topography of lamellar crystallites (Figure 17a) becomes replaced by numerous hyphae (Figure 17b) lying on a surface of unidentified nature. Further work needs to be performed to determine whether the surface of degraded amylose becomes obscured by hydrolysis products or whether the features seen represent structural features associated with highly degraded amylose.

Although the same fungus was used to degrade both cellophane and amylose, the rapid amylolytic degradation may be due to the morphological variability of amylose, to greater amylase activity, to the less crystalline nature of amylose, or to the difference in accessibility of the anhydroglucose units. Borch, et al. [26] note that even small variations in relative humidity can produce reorganization in such solids. Any opening of the structure might possibly allow the enzyme to diffuse readily into the

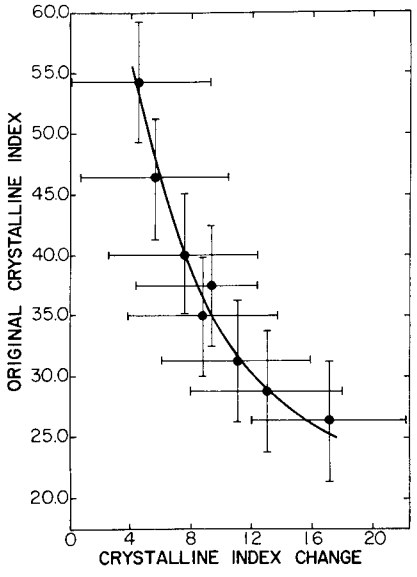

FIG. 16. Two-day crystalline index increase in fungus-degraded amylose films that had various initial crystalline indices.

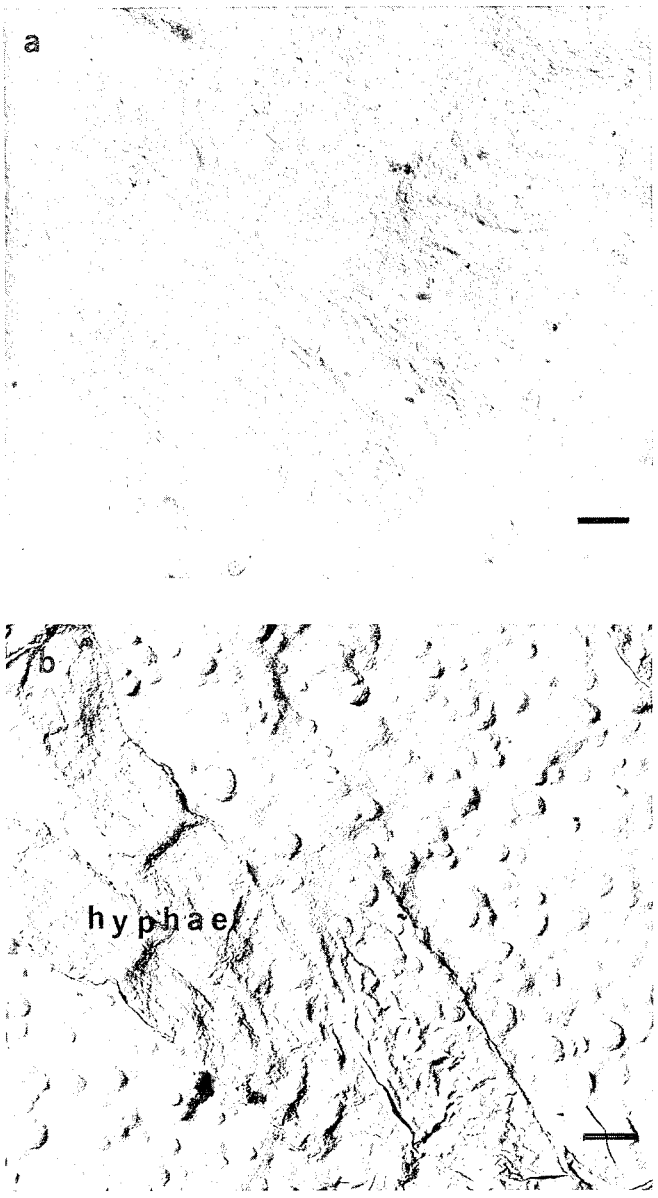

FIG. 17. Electron micrographs of surface replicas made from amylose films. (a) In the as-cast state fine striations can be seen which are presumably due to the intersection of lamellar crystallites with the film surface. (b) In the two day degraded sample the original surface has become obscured or degraded, and several hyphae can be observed. Bars represent one micron.

film and make the chains more accessible to the enzyme. The susceptibility of a polysaccharide film is also determined by the diffusibility and size of the enzyme molecule with respect to the spacing between crystallites and free volume in levels of noncrystalline regions [8]. As has already been

shown, the relative crystalline index of the substrate can determine the degradation rate.

CONCLUSION

Studies on cellophane and amylose films demonstrate a number of principles regarding the ways in which semicrystalline polymers can be degraded by fungi. By comparing the damage caused by degradative enzymes alone to damage which occurs when a fungus is growing on a film, it is observed that the enzymes are capable of diffusing considerable distances within a few days following inoculation. Enzymes appear to attack noncrystalline regions of the solid in preference to crystallites. It is also found that for fungus-degraded cellophane, the weight-average crystallite size and lattice distortion do not appreciably change. However, for cell-free cellulase enzyme degraded cellophane film there is an increase in weight-average crystallite size and lattice distortion. There is evidence that solutions of cellulase enzymes lead to preferential degradation of smaller crystallites. Cellophane films lose most of their mechanical anisotropy by the time about 15% of the material has been solubilized. Amylose films were likewise found to lose most of their tensile and yield stress rapidly, with low crystallinities leading to most rapid degradation rates.

The authors wish to express their gratitude toward the National Science Foundation for research support through grant GK32733 and the traineeship for one of us (P. E.) and toward the Advanced Research Projects Agency through the Northwestern Materials Research Center. We also appreciate discussions on starch-containing materials held with Dr. Charles Russell at the Northern Regional Laboratories, U.S. Department of Agriculture, and are grateful for helpful advice and assistance from Professors N. E. Welker and W. O. Pipes of Northwestern University.

REFERENCES

[1] M. Dostalek, V. Munk, O. Volfora, and K. Pecka, *Biotechnol. Bioeng., 10,* 33 (1968).
[2] L. Jen-hao and A. Schwartz, *Kunstoffe, 51,* 317 (1961).
[3] S. Berk, H. Ebert, and L. Teitell, *Ind. Eng. Chem., 49,* 1115 (1957).
[4] R. T. Darby and A. M. Kaplan, *Appl. Microbiol., 16,* 900 (1968).
[5] G. H. Booth, A. W. Cooper, and J. A. Robb, *J. Appl. Bacteriol., 31,* 305 (1968).
[6] R. E. Klausmeier, *Soc. Chem. Ind. (London), Monograph 23,* 232 (1966).
[7] G. Tirpak, *J. of SPE, 26,* 26 (July, 1970).
[8] E. B. Cowling and W. Brown, in *Cellulases and their Application,* Adv. Chem. Ser. No. 95, Amer. Chem. Soc., Washington, 1969, p. 152.
[9] E. T. Reese and M. Mandels, in *Cellulose and Cellulose Derivatives,* Vol. V, N. M. Bikales and L. Segal (Eds.), Wiley-Interscience, N.Y., 1971, p. 1079.
[10] W. J. Whelan, *Biochem. J., 122,* 609 (1971).
[11] P. Engler and S. H. Carr, *J. Polym. Sci., Polym. Phys. Ed., 11,* 313 (1973).
[12] A. Venkateswaran, *J. Appl. Polym. Sci., 13,* 2459 (1969).
[13] R. St. J. Manley and S. Inoue, *J. Polym. Sci. B, 3,* 691 (1965).
[14] V. E. Stockmann, *Biopolymers, 11,* 251 (1972).
[15] M. Chang, *J. Poly. Sci. C, No. 36,* 343 (1971).

[16] R. St. J. Manley, *J. Polym. Sci. A-2, 9,* 1025 (1971).
[17] J. Blackwell, A. Sarko, and R. H. Marchessault, *J. Mol. Biol., 42,* 379 (1969).
[18] R. M. Valletta, F. J. Germino, R. E. Lang, and R. J. Moshy, *J. Polym. Sci. A, 2,* 1085 (1964).
[19] F. J. Germino, R. J. Moshy, and R. M. Valletta, *J. Polym. Sci. A, 2,* 2705 (1964).
[20] A. D. French and H. F. Zobel, *Biopolymers, 5,* 457 (1967).
[21] W. Winter and A. Sarko, *Biopolymers, 11,* 849 (1972).
[22] R. St. J. Manley, *J. Polym. Sci. A, 2,* 4503 (1964).
[23] Y. Yamashita, *J. Polym. Sci. A, 3,* 3251 (1965).
[24] H. F. Zobel, A. D. French, and M. E. Hinkle, *Biopolymers, 5,* 837 (1967).
[25] J. L. Koenig and P. D. Vasko, *J. Macromol. Sci.-Phys., B4,* 347 (1970).
[26] J. Borch, R. Muggli, A. Sarko, and R. H. Marchessault, *J. Appl. Phys., 42,* 4570 (1971).
[27] H. Bittiger, E. Husemann, and B. Pfannemuller, *Staerke, 23,* 113 (1971).
[28] M. Mandels and E. T. Reese, *Develop. Ind. Microbiol., 5,* 5 (1964).
[29] K. Selby and C. C. Maitland, *J. Biochem., 104,* 716 (1967).
[30] J. M. Leatherwood in *Cellulases and Their Application*, Adv. Chem. Ser. No. 95, Amer. Chem. Soc., Washington, 1969, p. 53.
[31] J. Hollo and E. Laszlo, *Staerke, 23,* 272 (1971).
[32] B. Norkrans, *Physiol. Plant, 3,* 75 (1950).
[33] B. R. Porter, J. H. Carra, V. W. Tripp, and M. L. Rollins, *Tex. Res. J., 30,* 249 (1960).
[34] H. F. Zobel and F. R. Senti, *Cereal Chem., 36,* 441 (1959).
[35] K. W. King, *Biochem. and Biophys. Res. Commun., 24,* 295 (1966).
[36] G. S. Rautela and K. W. King, *Arch. Biochem. Biophys., 123,* 589 (1968).
[37] ASTM G 21-70, "Determining Resistance of Synthetic Polymeric Materials to Fungi," ASTM Standards, Part 30, Amer. Soc. Test Mater., Philadelphia, 1972, p. 1437.
[38] W. O. Statton, *J. Polym. Sci. C, 18,* 33 (1966).
[39] J. L. Mathews, H. S. Peiser, and R. B. Richards, *Acta. Cryst., 2,* 85 (1949).
[40] A. M. Hindeleh and D. J. Johnson, *Polymer, 13,* 423 (1972).
[41] J. B. Cohen, *Diffraction Methods in Materials Science,* MacMillan, New York, 1966, p. 301.
[42] F. R. L. Schoening, *Acta. Cryst., 18,* 975 (1965).
[43] R. Bonart, R. Hosemann, and R. L. McCullough, *Polymer, 4,* 199 (1963).
[44] D. R. Buchanan and R. L. Miller, *J. Appl. Phys., 37,* 4003 (1966).
[45] M. L. Nelson and R. T. O'Connor, *J. Appl. Polym. Sci., 8,* 1325 (1964).
[46] V. C. Haskell and D. K. Owens, *J. Appl. Polym. Sci., 4,* 225 (1960).
[47] W. A. Sisson, *J. Phys. Chem., 44,* 513 (1940).

THE USE OF POLYMERIC CATALYSTS IN ESTEROLYTIC REACTIONS—A COMPARISON WITH NATURAL ENZYMES*

C. G. OVERBERGER

University of Michigan,
Ann Arbor, Michigan 48104

SYNOPSIS

This lecture initially summarized the contribution of proximity and electrostatic factors in esterolytic reactions of poly-4(5)-vinylimidazole. The bulk of the lecture dealt with the highly exciting area of apolar forces in these reactions which is the third and most important factor.

Apolar forces are believed to be significant in structuring an enzyme with a substrate in various naturally-occurring systems. The hydrolysis of several anionic long-chain esters (I), catalyzed by poly-4(5)-vinylimidazole (PVIm), was observed to determine the extent of apolar forces.

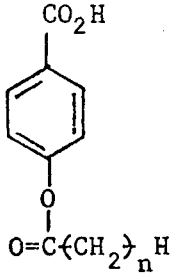

where n = 1, 6, 11 and 17

(I)

The esterolysis reactions were carried out in varying alcohol-water solvent systems. In all cases discussed, the substrate concentrations are below the critical micelle concentration.

Remarkable rate enhancements (ca. > 10^3) of the PVIm catalyzed reactions, relative to imidazole (Im), were observed in low alcohol content solvent systems (eg, 20% vol/vol ethanol–water). Further, ethanol–water mixtures were considerably more effective than 1-propanol–water mixture of the same composition.

In low alcohol content solvents, increasing the chain length of the substrate dramatically increased the rate enchancements of the PVIm reactions, in spite of increasing steric hindrance of the long-chain substrate. This trend is attributed to apolar attraction of substrate to the polymeric catalyst; it can be reversed in high-alcohol content of solvents in which the apolar forces are destroyed.

* A portion of this paper was presented at the International Symposium on Macromolecular Chemistry, Helsinki, July 1972 (Pure and Applied Chemistry, in press).

Applied Polymer Symposium No. 22, 287–288 (1973)

In certain systems Michaelis-Menten (saturation) kinetics were observed, indicating the formation of a catalyst–substrate complex prior to hydrolysis. Also, in some long-chain ester systems, an accelerative kinetic pattern was observed and is considered to be due to an acylated-PVIm intermediate.

THE INTERFACING OF POLYMERS WITH BLOOD

SUNG WAN KIM and DONALD J. LYMAN

Division of Materials Science and Engineering
University of Utah,
Salt Lake City, Utah 84112

SYNOPSIS

The adsorption of albumin, fibrinogen, γ-globulin, and prothrombin from their aqueous solution onto films of fluorinated ethylene/propylene copolymer, polydimethyl siloxane, and a segmented copolyether–urethane–urea were studied under both static and flow adsorption conditions. There appears to be a general agreement between the length of time to obtain a high concentration of albumin on the polymer surface and the thrombogenicity of the polymer, i.e., materials showing faster rates and greater concentrations of albumin are less thrombogenic. Platelet adhesion to these same surfaces using our ex-vivo flow through cell also shows a similar trend, i.e., less platelet adhesion on the less thrombogenic surfaces.

INTRODUCTION

During the last ten years, there has been a tremendous increase in types of surgical procedures to correct problems in the vascular system, such as patches to repair septal defects, vascular grafts, heart valves, etc., as well as extracorporeal treatment of the blood, such as the artificial kidney and the artificial lung. More recently, there has been much activity concerned with the actual assisting or replacement of the failing heart itself. These seem like worthwhile goals when one considers that, in the United States alone, heart deaths total more than 800,000 per year, with an anticipated loss to the economy of $9.7 billion each year [1]. Many of these lives could be saved and returned to productive life and the family if both a perfected heart assist device and a perfected artificial heart were available.

However, there are many basic problems which must be solved before this becomes a reality. Also, there is the alternate approach to the saving of human life, namely by gaining a basic understanding about heart disease. A more proper course may be a balance between basic knowledge (long term goal) and applied technology (the bringing of existing knowledge to the patient). Common to both of these approaches is the need for improved knowledge of blood coagulation on natural and synthetic surfaces. Our work has been directed toward gaining an understanding of these adverse interactions using synthetic polymers as the interface substrate.

Applied Polymer Symposium No. 22, 289–297 (1973)

EXPERIMENTAL

Platelet Adhesion

The adhesion of platelets to various polymer and protein coated polymer surfaces was determined using our ex vivo flow-through platelet adhesion cell [2]. The adhesion values are reported as the number of platelets adhering per 20,000 μ of surface area. While most data was obtained using uncoagulated, whole human blood, similar experiments were also done on calf and sheep blood in order to determine effects of flow rates anticoagulants, etc [3].

Protein Adsorption

Adsorption of proteins under static flow conditions were carried out in the absence of an air interface using a method similar to that previously described [4]. The adsorption experiments under flow conditions were accomplished by clamping the polymer films in a flow-cell, and circulating the protein solution through the cell by means of a non-occlusive tubing pump [5].

All films were rinsed to remove excess clinging solution. The amount of adsorbed protein was determined by multiple internal reflection infrared spectroscopy using ratios between the Amide I (C=O stretching) band at 1640 cm^{-1} to a standard band for each polymer substrate [4, 5].

Surface Energy Measurements

The measurements of contact angle and of surface tension were made using a contact angle Goniometer (Ramé-Hart, Inc.), and a Du Noüy Tensiometer. All experiments were conducted at room temperature.

Materials

The proteins (human and bovine) used were: albumin, crystalline; γ-globulin, fraction II; prothrombin, Cohn fraction III-2; and fibrinogen, Cohn fraction I (National Biochemicals Corp.).

The polymers used were: polydimethyl siloxane (Silastic Rubber, Dow Corning Corp.); Fluorinated ethylene/propylene copolymer (Teflon FEP, Du Pont); Polypropylene and polyethylene (Plastics Products of Utah), and a segmented copolyether–urethane–urea based on polypropylene glycol methylene bis (4-phenylisocyanated) and ethylene diamine [6].

DISCUSSION OF RESULTS

Platelet Adhesion

The first observable event in the formation of a thrombus is platelet adhesion and aggregation to the surface of the vessel or polymer implant. Our initial studies on platelet adhesion to a variety of neutral, hydrophobic polymers using the ex vivo flow-through cell, did indicate a direct relationship between platelet adhesion and the relative thrombogenicity of the

synthetic polymer [2]. However, there is a high concentration of proteins in blood, and one would expect that proteins would adsorb more rapidly onto the polymer surface, and the platelets would therefore be adhering to a protein coating. This rapid washing of the polymer surface with protein has been reported by others [7] using Zeta potential measurements. It was of interest, then, to determine the adhesion of platelets to preproteinated surfaces of known composition. A variety of surfaces were precoated with albumin using our static flow adsorption techniques [4], since it was felt that such a coating should give a non-thrombogenic surface [8]. These albuminated surfaces did show low platelet adhesion and appeared to be non-thrombogenic [9]. In addition, the albuminated surfaces appeared to be less hemolytic than the original polymer surface [10]. Similar studies on preproteinated surfaces of γ-globulin and fibrinogen showed a marked contrast to what was observed in the pre-albuminated surfaces [5]. Although initial platelet adhesion was low at one minute exposure time, there was a rapid increase with increasing time of exposure (2 to 6 min). Although coated Gott vena cava rings [11] of this type have not been implanted at this writing, it is expected that these γ-globulin and fibrinogen coated surfaces would be thrombogenic. This would be consistent with observations of others [12, 13] that have shown that both γ-globulin coated surfaces and fibrinogen coated surfaces are more active toward platelet adhesion, aggregation, and release reactions.

Protein Adsorption

It would thus appear that the nature of the protein coating achieved in situ would be the controlling factor in platelet adhesion, and this should be dependent on the chemical nature of the polymer surface. Therefore, the adsorption isotherms and adsorption kinetics of plasma proteins on various polymer surfaces should contribute much to our correlation of the relative thrombogenicity of these polymers.

A number of theoretical studies have been reported on the adsorption of macromolecules by Silberberg [14], Eirich [15], Frish [16], and Simha [17]. These involved flexible linear polymers, but little experimental work was done which could be applied to protein adsorption. Smith et al. [18] measured the adsorption of proteins on metal surfaces and on polyethylene by ellipsometric techniques. Stoner et al. [19] used electron microscopy techniques to determine the amount of adsorbed proteins on mica surfaces, for kinetic studies. While both methods were suitable for the adsorption of proteins onto highly dense, smooth substrates, they are not readily applicable for polymer surfaces since the polymer and the protein have similar refractive indices; the polymer surfaces are quite rough compared to the glass or metal surfaces used; and the low surface energy of many of thepolymers which resulted in migration of the replication material. The attenuated total reflectance method, which was earlier introduced by Lyman et al. [4] for the study of protein adsorption on polymer surfaces appears to surmount these problems and can be used for kinetics studies of protein ad-

TABLE I
The Langmuir Slope and Intercept Data[a] for Protein Adsorption on Selected Polymer Surfaces.

Protein: Surface[b]	Slope	Intercept	Deviation[c]
	$cm^2/g\ H_2O$	$cm^2/m\mu g$	%
Albumin:			
FEP	588	0.060	11
SR	119	0.012	235
PEUU-1	27.1	0.002	48
γ-globulin:			
FEP	326	0.034	24
SR	194	0.017	517
PEUU-1	32.5	0.004	105
Prothrombin:			
FEP	294	0.029	13
SR	62.2	0.002	227
PEUU-1	31.0	0.001	52

[a] Data from Langmuir verification curves plotting 1/a vs. 1/c.

[b] See results section for polymer codes.

[c] Measured as a percentage between the theoretical amount calculated for surface concentration by extending the Langmuir curve to that of the experimental amount determined on the surface.

sorption. Static protein adsorption isotherms were determined for the segmental copolyether urethane urea (PEUU-1), polydimethyl siloxane (SR), and fluorinated ethylene/propylene copolymer (FEP). The data are tabulated in Table I.

The adsorption isotherms obey nearly the Langmuir's adsorption equation, where 1/a has been plotted against 1/c, according to [20] $[1/a) = (1/a^{\infty}) + (1/a^{\infty}bc)$ where a^{∞} is the amount adsorbed in $\mu g/cm^2$ at saturation, a is the amount adsorbed at any time t, $b = k_1/k_2$, where k_1 and k_2 are the rate constants at adsorption and desorption respectively, and c is the concentration of protein in solution at equilibrium. The small deviation from linearity in the plotting is due to the lateral interaction between adsorbed proteins. The amount of protein adsorbed on the surface at saturation is greatest on the PEUU, and least on FEP. Examination of the rates of adsorption also show a similar trend (See Table II). That is, the most thrombogenic material, FEP, has much slower rate and a lower surface concentration than the non-thrombogenic PEUU. The SR is intermediate. If one then varies the flow conditions during protein adsorption, contrasting changes then begin to occur (See Table III). With the smooth PEUU, there is no change in the plateau concentration with changes in flow. However, at higher flow rates, the time to achieve this plateau concentration is increased from about 20 minutes to about 180 minutes. With the smooth FEP, there are changes in both plateau concentration and

time to achieve this plateau concentration. The rough SR also shows changes in both plateau concentration and time to achieve this plateau concentration. The existence of this surface roughness and pores in the SR (as determined by scanning electron microscopy) can affect the adsorption process, giving diffusion control of the rate at the interface [14]. The diffusion rate has a linear dependence upon flow rate, and theoretical equations are being set up on the basis of molecule and fluid dynamics. The slight changes in adsorption under flow conditions for the smooth FEP would appear to be due to possible order water effects [21] which again would give diffusion control of the rate at the interface. Because of the surface roughness of the SR, an actual surface area has not been determined. However, estimations of area would indicate that the same relative order, i.e., PEUU > SR > FEP, still exists.

In attempting to correlate these data with the highly complex phenomena of thrombosis formation on polymer surfaces, we find a general agreement between length of time to obtain a plateau concentration of albumin and thrombogenicity. Thus we would suggest that a more non-thrombogenic surface would form a protein monolayer faster than a relatively thrombogenic surface. The non-thrombogenicity of pre-albuminated surfaces is then explained, since on such a surface the plateau time is zero. Also, our previous work [22] demonstrates that a nonthrombogenic surface should have a relatively smaller heat of adsorption, as measured by the interaction energy and non-dispersion contributions at the interface. Theories and experimentation of the kinetics of protein adsorption are thus of great importance, but additional experiments are needed to verify that the observa-

TABLE II
Protein Adsorption to Various Polymer Surfaces Under Static Conditions

Protein: Polymer[a]	Plateau Conc., μg/cm²	Plateau time, min.	Bulk soln. conc.,[b] mg/l	First order rate constants,[c] k, min⁻¹	Relative rates of adsorption
Albumin:					
FEP	0.55	60	30	0.045	1
SR	1.0	25	12	0.115	2.6
PEUU-1	4.45	25	12	0.811	18
Fibrinogen:					
FEP	0.8	70	—	0.035[d]	1
SR	1.5	40	—	0.096[d]	2.7
PEUU-1	4.6	35	—	0.762[d]	22
γ-globulin:					
FEP	0.80	60	30	0.051	1
SR	1.25	30	25	0.135	2.7
PEUU-1	4.65	30	15	0.811	16
Prothrombin:					
FEP	0.85	25	30	0.149	1
SR	2.25	10	15	0.405	2.7
PEUU-1	4.75	10	15	0.811	5.4

[a] See Results Section for polymer codes.

[b] Concentration of bulk solution needed to get plateau concentration at equilibrium.

[c] Calculated from $kt = \ln\left(\frac{a\infty}{a\infty - a}\right)$ where $a\infty$ was plateau coverage on FEP, t was 1 minute, and a was actual coverage at 1 minute exposure.

[d] 20 mg% solution fibrinogen used in this work.

TABLE III
Protein Adsorption to Various Polymer Surfaces Under Flow Conditions

Surface: Protein	Plateau concentrations[a] and plateau times[b] at Reynolds Nos. of: 0	600	1200	1800	2400
Polydimethyl siloxane					
Albumin:	1.0 (25)	2.0 (100)	3.8 (160)	5.0 (180)	6.2 (230)
Fibrinogen:	1.5 (40)	— —	— —	— —	— —
γ-globulin:	1.3 (30)	2.5 (100)	4.0 (170)	5.5 (200)	6.4 (250)
Prothrombin:	2.1 (10)	3.7 (70)	4.9 (140)	6.4 (180)	7.3 (200)
Fluorinated ethylene/ propylene copolymer					
Albumin:	0.6 (60)	1.1 (60)	1.4 (70)	1.6 (70)	1.8 (60)
Fibrinogen:	0.8 (70)	— —	— —	— —	— —
γ-globulin:	0.7 (60)	1.1 (70)	1.6 (70)	1.8 (80)	2.0 (80)
Prothrombin:	0.7 (25)	1.3 (30)	1.5 (50)	1.8 (70)	1.8 (70)
Copolyether-urethane-urea PEUU-1					
Albumin:	4.5 (25)	4.4 (40)	4.5 (70)	4.6 (70)	4.4 (150)
Fibrinogen:	4.6 (35)	— —	— —	— —	— —
γ-globulin:	4.7 (30)	4.9 (50)	4.6 (100)	4.7 (160)	4.8 (190)
Prothrombin:	4.7 (10)	4.8 (20)	4.9 (70)	4.6 (100)	4.8 (140)

[a] Plateau concentration in $\mu g/cm^2$.
[b] Data in ( ) are plateau times in minutes.

tions made on single protein solution adsorptions do hold for adsorptions from mixtures, such as in whole blood. This work is in progress.

PROTEIN/POLYMER INTERFACE

It would appear that the nature of the protein adsorption does vary on different polymer surfaces and does not effect the thrombogenicity of the polymer. Therefore, if we are to synthesize new, non-thrombogenic polymers, we must understand the interaction at the protein–polymer interface.

The determination of the surface energy of a solid is of interest in fields such as adhesion and adsorption where forces at and across an interface operate. The concept of critical surface tension, which was introduced by Zisman [23] and has been used by many researchers, is the subject of many discussions and has led to various interpretations.

The Zisman technique is an empirical method of detemining the "wettability" of solid surfaces by plotting the cosine of the contact angle, θ, versus the surface tensions of a series of liquids. The resulting curve inter-

cepts the line, cos $\theta = 1$, and is called the critical surface tension, γ_c. Recent research [24] has shown that the Zisman type of cos θ versus γ_L plots can be misinterpreted when straight lines are plotted through scattered points or when long extra-polations of straight lines are made. This is since normal cos θ versus γ_L plots are not straight lines. However, Zisman's plotting is easier to obtain and, if one accepts the deviation from a true value due to the scattered points and nonlinearity, this method is more readily useful. Lyman et al. [25] obtained the critical surface tension, γ_c, of polymers from contact angle measurements and also used Good's equation to calculate the surface free energy of solid polymers.

These studies showed a definite relationship (inverse) between critical surface tension, γ_c, of various polymer surfaces and their in vitro coagulation time for human blood and dog blood. The values for polyethylene, polypropylene, fluorinated ethylene/propylene copolymer, polydimethyl siloxane, and the segmented copolyether–urethane are 31, 33, 18, 26, and 36 dyne/cm respectively. In general, the critical surface tension does correlate the coagulation behavior of a series of neutral, hydrophobic polymers, i.e., the lower the surface energy, the less thrombogenic is the material. The lowering of critical surface tension by protein coating is consistent with our general concept of a non-thrombogenic surface. However, the relationship does not necessarily hold, in the absolute sense, when we grossly change the generic type. For example, the relatively non-thrombogenic segmented polyurethane (PEUU) has γ_c of 36, while the thrombogenic FEP has that of 18. In addition to the concept of γ_c being related to blood clotting, the interaction of blood at the local level is also important. Therefore, our emphasis is on the interfacial phenomena between polymer and protein and between polymer and water rather than the polymer surface only.

The surface pressure [26], defined by $\pi = \gamma_{SW} - \gamma_{SL}$, gives the interfacial energy between the proteins and polymer surfaces. Here, γ_{SL} and γ_{SW} are interfacial tensions of polymer-protein solution and polymer-pure water, respectively, and following Young-Dupre Equation.

$$\gamma_{SW} = \gamma_{SV} - \gamma_{WV} \operatorname{Cos}\theta_W \tag{1}$$

$$\gamma_{SL} = \gamma_{SV} - \gamma_{LV} \operatorname{Cos}\theta_L \tag{2}$$

γ_{WV} and γ_{LV} are surface tensions of water and the protein solutions respectively. θ_W and θ_L are the contact angles of water and the protein solution on polymer surfaces. The surface tension of a protein solution is a function of the aging of the surface, and approximately five minutes elapsed until an equilibrium was obtained. It was found that a minimum surface tension occurred at certain solution concentrations. The surface pressure of the adsorbed protein, π, is then given by the difference between eqs. (1) and (2), or

$$\pi = \gamma_{SW} - \gamma_{SL} = \gamma_{LV} \operatorname{Cos}\theta_L - \gamma_{WV} \operatorname{Cos}\theta_W \tag{3}$$

TABLE IV
Water Adhesion and Surface Pressures of Protein at Various Polymer Surfaces

Polymer	θ_w	W_{sw}	γ_{sw}	Π	
				Albumin	γ-globulin
FEP	101°	58.7	31.5	48.8	43.7
PE	69°	97.4	5.8	15.8	24.5
PP	67°	99.4	7.8	23.3	21.6
SR	65°	102.5	4.2	20.6	17.3
PEUU	55°	113.5	5.50	11.8	5.4

W_{sw}, γ_{sw} and Π are in dynes/cm. Π values are at protein concentration 44.0 mg %.

The interfacial free energy of water and the surface pressure of protein at each polymer surface are tabulated in Table IV. Interfacial free energy of water at FEP is very high compared with other polymers, and PEUU shows the lowest interfacial free energy with water.

The proteins used here (albumin, γ-globulin) show the highest surface pressure with FEP and the lowest with PEUU, though FEP has the smallest surface free energy (18 dynes/cm) among the five polymers examined. It is also shown in Table IV that increasing water wettability and adhesion energy ($W_{sw} = \gamma_w + \gamma_w \cos\theta_w$) in the five polymers indicates decreasing surface pressure of proteins at the solution-polymer interface. The water contact angles on the polymers used in this work varies from 70° (SR) to 105° (FEP); however, they are decreased by 30–50° on the albuminated polymer surfaces [27]. This would indicate that the proteinated surface is more hydrophilic than the bare polymer surface. It is of interest that the thrombogenicity of these polymer surfaces is in the same relative order with the magnitude of the surface pressure at the interface, i.e., FEP > polyethylene > polypropylene > Silastic rubber > polyurethane. Also of note is the observation that, for any one polymer, π values of albumin and γ-globulin are similar, whereas prothrombin involved directly in blood clotting schemes has a higher π. Higher surface pressure π (higher interfacial energy) and higher interfacial energy of water means higher heat of adsorption provided the entropy effect is neglected. The value of this heat of adsorption would be expected to be small, but might contribute to platelet adhesion. The data here, as well as those obtained in the protein adsorption experiments indicate differences in the nature of the interfacial water on these hydrophobic polymers. According to Abdula's work [28] the ordered water triggers a two phase reaction in platelet aggregation: (a) initial immobilization of a few platelets around the "ice-forming molecule"; and (b) a chain reaction leading to activation of many layers of platelets onto the first formed layer. Based on this, we have recently proposed that the "iceberg formation" of water on the hydrophobic polymer surface can be a stimulus for platelet adhesion.

This work was supported in part by the National Science Foundation under Contract No. GK-29382 and the National Institute of Arthritis and Metabolic Diseases under Contract No. NIH-70-2017. We also wish to thank Mr. R. G. Lee and Ms. C. Adamson for their technical assistance.

REFERENCES

[1] M. S. Blumberg, K. W. Gardiner, D. J. Lyman, and P. M. Newgard, "Artificial Heart Devices and Systems: a Conceptual Phase Study", Government Printing Office, Washington, D.C.
[2] D. J. Lyman, K. G. Klein, J. L. Brash, and B. K. Fritzinger, *Thromb. Diath. Haen. 23,* 120 (1970).
[3] J. E. Lindberg, M. S. Thesis, University of Utah (1972).
[4] J. L. Brash, and D. J. Lyman, *J. Biomed. Mat. Res. 3,* 175 (1969).
[5] S. W. Kim, R. G. Lee, and D. J. Lyman, manuscript in preparation.
[6] D. J. Lyman, C. Kwan-Gett, H. H. J. Zwart, A. Bland, N. Eastwood, J. Kawai, and W. J. Kolff, *Trans. Amer. Soc. Artif. Int. Organs 17* 456 (1971).
[7] V. Mirkovitch, R. E. Beck, P. G. Andrus, and R. I. Leininger, *J. Surg. Res. 4* 395 (1964).
[8] *Chem. Eng. News, 37,* January 27, 1969.
[9] D. J. Lyman, K. G. Klein, J. L. Brash, B. K. Fritzinger, J. D. Andrade, and F. S. Bonamo, *Thromb. Diath. Haem.* (suppl.) *42,* 109 (1970).
[10] D. J. Lyman and S. W. Kim, *Fed. Proc. 30,* 1658 (1971).
[11] V. L. Gott, F. B. Ramor, J. C. Allen, and K. E. Becker, Proc. Artificial Heart Program Conference, R. J. Heggel, Ed., Washington, D.C., U.S. Govt. Printing Office, 1969, Chap. 17, p. 151.
[12] M. E. Glynn, M. A. Packham, J. Hirsh, and J. E. Mustard, *J. Clin. Invest. 45,* 1013 (1966).
[13] J. E. Mustard, M. F. Glynn, E. E. Nishizawa, and M. A. Packham, *Fed. Proc. 26,* 106 (1972).
[14] A. Silberberg, *J. Polym. Sci., Part C, 30,* 393 (1970).
[15] F. R. Eirich, R. Simha, and H. L. Frisch, *J. Phys. Chem. 57* 584 (1963).
[16] H. L. Frisch, *J. Phy. Chem. 59* 833 (1955).
[17] R. Simha, *J. Polym. Sci. 29* 3 (1958).
[18] L. E. Smith, C. A. Fenstermaker and R. R. Stromberg, *Polym. Prep. Amer. Urem-Soc., Div. Polym-Unem. 11* 1370 (1970).
[19] G. E. Stoner, S. Srinivasan and E. Gileadi, *J. Phys. Chem 75* 2103 (1971).
[20] J. F. Hubden and H. H. G. Jellinek, *J. Polym. Sci., 11* 365 (1953).
[21] W. Drost-Hansen, *Fed. Proc. 30* 1539 (1971).
[22] S. W. Kim, R. G. Lee, and D. J. Lyman, manuscript in preparation.
[23] W. A. Zisman, "Contact Angle, Wettability and Adhesion," *Adv. in Chem. Series* #43 ACS (1964).
[24] J. R. Dann, *J. Colloid, Surface Sci., 32* 321 (1970).
[25] D. J. Lyman, W. M. Muir, and I. J. Lee, *Trans. Amer. Soc. Artif. Int. Organs, 11* 301 (1965).
[26] S. Ghosh, K. Breese, and H. Bull, *J. Colloid Sci., 19* 457 (1964).
[27] D. J. Lyman and S. W. Kim, "Actualites Nephrologigues de l'hopital Necker," Flammarion Medicine Sciences, Paris (1972) p. 97.
[28] Y. H. Abdula, *J. of Atheros. Res., 7* 415 (1967).

BIOLOGICAL ACTIVITY OF IONENE POLYMERS*

A. REMBAUM

Jet Propulsion Laboratory,
California Institute of Technology
Pasadena, California 91103

SYNOPSIS

Ionene polymers are polyammonium salts with positive nitrogens in the backbone, resulting from the polycondensation of diamines with dihalides or from the polycondensation of halo amines. The mechanism of formation of ionene polymers of different structures and their biological activity is reviewed. The antimicrobial and antifungal properties are compared with low molecular weight ammonium salts. Ionenes were found to combine with DNA by means of ionic bonds to yield similar complexes to those obtained with polyamines (spermine and spermidine). They also combine with nerve cell receptors and exercise a more powerful and longer duration ganglionic blocking action than their monomeric analogs. The antiheparin activity of ionenes and the thromboresistance of elastomeric ionene heparin coatings is described. The enhanced biological activity of ionenes as compared with low molecular weight compounds is attributed to a co-operative effect of a large number of positve charges on the polymeric chains.

INTRODUCTION

Diamines react with dihalides to form polyammonium salts and since this reaction originates through the ionization of amines, the generic name of ionenes was suggested for these salts [1]. Ionenes are therefore polyelectrolytes with positively charged nitrogen atoms located in the backbone of polymeric chains and this type of polycation was first prepared by Marvel and coworkers from dimethylamino-n-alkyl halides [2]. Kern and Brenneisen were the first to report that ionenes are formed by the Menchutkin reaction from ditertiary amines and dihalides [3]. Although a number of patents were published since 1941 concerning the applications of ionene polymers [4] very little information was available on the mechanism, kinetics of their formation, or solution properties. The scope of this polycondensation reaction, the effect of concentration and solvent on rates and molecular weight of ionenes and a proposed mechanism were first

* This paper represents one phase of research performed by the Jet Propulsion Laboratory, California Institute of Technology, sponsored by the National Aeronautics and Space Administration, Contract No. NAS-7100.

Applied Polymer Symposium No. 22, 299–317 (1973)

y \ x	1	2	3	4	5	6
1						
2		CYCLIC DIAMMONIUM COMPOUNDS			LINEAR DIAMMONIUM COMPOUNDS	
3						
4	CYCLIC MONO-AMMONIUM COMPOUNDS			IONENE POLYMERS		
5						
6						

FIG. 1. Summary of results of x–y reactions.

reported in 1968, when it was realized that under well-defined conditions relatively high molecular weight ionenes were obtainable [1]. A light scattering study yielded a quantative relation between viscosity and molecular weight for the 3,4 and 6,6-ionene [5]. A study of the reaction products of diamines of structure I with dihalides of structure II, where Z is a halogen,

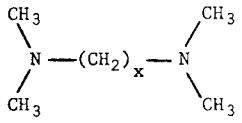

I

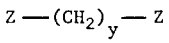

II

atom and x and y are the numbers of CH_2 groups in the amine and dihalide respectively, revealed that only with specfic values of x and y are ionene polymers formed [6]. Their unit segment is represented by III (x,y- ionene halide) where n is the degree of polymerization. Figure 1 summarizes the

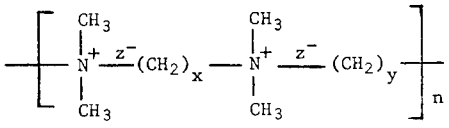

III

results of the reaction of I and II in which x and y varied from 1 to 6. An extension of the x and y values to 16 confirmed the results of Figure 1 and a physicochemical analysis of a large number of intermediates and final products permitted to postulate a reaction mechanism (Fig. 2).

The first step in the reaction of I with II is the formation of the intermediate IV, thermodynamically unstable when the values of x and y are

low, in which case chain scission occurs and linear or cyclic low molecular weight compounds are formed. The latter are also formed without the occurrence of chain scission when specific values of x and y are used. The formation of ring structure is governed by the fact that only five-, six- or seven-membered rings are stable when the positive nitrogens are separated by two or three methylene groups [7].

It became evident from this work that ionenes may be synthesized only under well-defined conditions and that compound V yields polymers when y = 3 or y ≥ 7. In this case symmetrical ionenes are formed (x = y) with repeat unit segment VII (y-ionene halide). An investigation of the kinetics

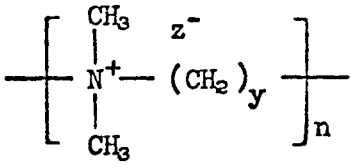

VII

of polymerization of VII with y = 3 and z = Cl by means of nmr spectroscopy proved [8] the existence of a cylic four-membered intermediate VIII and therefore the following polymerization mechanism was postulated;

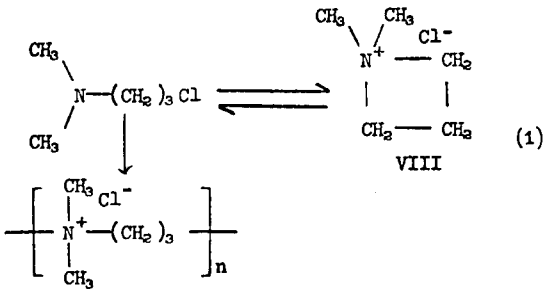

(1)

VIII

IX

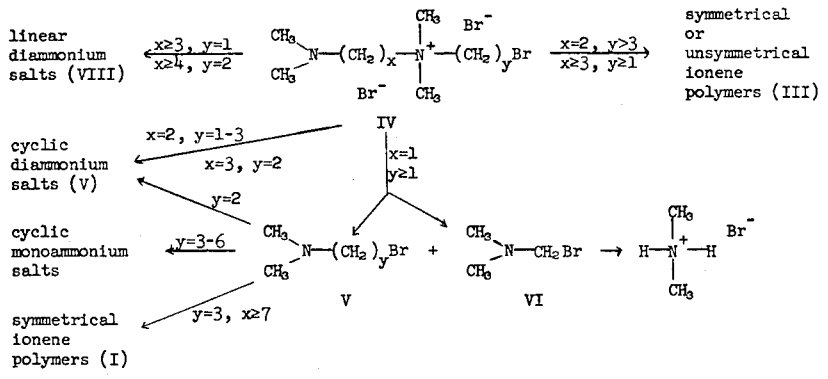

FIG. 2. Mechanisms of x–y reactions.

TABLE I
Toxicity of Polymeric Versus Monomeric Compounds[a]

	i.p.LD50 mg/kg	Oral LD50 mg/kg
3,3-ionene bromide	50-100	500-1000
2,4-ionene bromide	50-100	>1000
2,6-ionene bromide	50-100	>1000
6,3-ionene bromide *	50-100	>1000
6,4-ionene bromide	50-100	>1000
6,5-ionene bromide	50-100	>1000
6,6-ionene bromide	50-100	>1000
6,10-ionene bromide	10-50	500-1000
6,16-ionene bromide	50-100	>1000
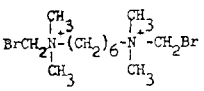	10-50	300-500
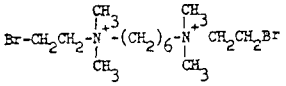	10-50	100-200
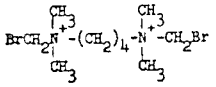	>1000	>1000
	100-200	>1000
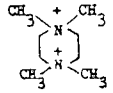	>1000	>1000

[a] For details see Reference 18.

The 3,3-ionene chloride (IX) = 3-ionene chloride of a molecular weight [9] of approximately 65000 is a polyelectrolyte with the highest charge density known and can be synthesized by means of a very simple technique.

A large variety of ionenes [10–16] including crosslinked ionene networks may be prepared by varying structure I and II. Linear as well as crosslinked ionenes are endowed with interesting pharmacological properties. These were investigated and compared with the pharmacological properties of monomeric ammonium salts, II (Fig. 2, Tables I and II) as well as with existing model compounds.

The biological activity of ionenes (e.g., the antimicrobial and antifungal effects, the action on synaptic junctions and the interaction with negatively charged biological polyelectrolytes, such as DNA and heparin) was several orders of magnitude more pronounced than of the low molecular weight model structures, which in many cases were devoid of any significant activity. Of special interest in the biomedical areas are ionenes containing urethane moieties which can be synthesized from diisocyanates [13, 17], modified by reaction with alcohols containing dimethylamino end groups. Specific diisocyanate prepolymers lead to elastomeric ionenes (cationic polyurethanes) which combine with heparin to yield thromboresistant ma-

TABLE II
Antimicrobial Activity of Polymeric Versus Monomeric Compounds

	S. Aureus ppm	P. Aerugi nosa ppm	P. vulgaris ppm	P. mirabilis ppm	E. Coli ppm	S. Typhimurium ppm
3,3-ionene bromide	1000	>1000	>1000	>1000	>1000	>1000
2,4-ionene bromide	1000	>1000	>1000	>1000	>1000	>1000
2,6-ionene bromide	1000	1000	>1000	>1000	>1000	>1000
6,4-ionene bromide	1000	>1000	>1000	>1000	>1000	>1000
6,5-ionene bromide	1000	>1000	>1000	>1000	>1000	>1000
6,6-ionene bromide	1000	>1000	>1000	>1000	>1000	>1000
6,10-ionene bromide	1000	1000	>1000	>1000	1000	1000
6,16-ionene bromide	1000	>1000	>	>1000	1000	1000

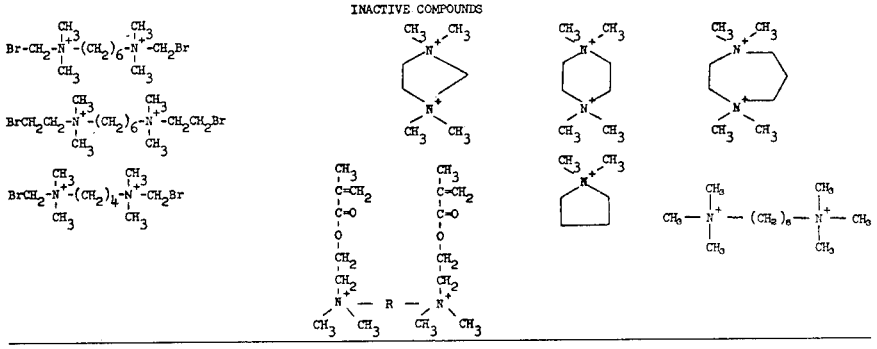

terials. In this paper the applications of crystalline and of elastomeric amorphous ionenes (cationic polyurethanes) in the biomedical area will be reviewed with particular emphasis on the elementary principles of their pharmacological action.

SOLUBLE INSOLUBLE AND CROSSLINKED BACTERICIDES AND FUNGICIDES

Ionene polymers exhibit toxic effects when injected into mice intraperitoneally(i.p.). The i.p. lethal dose for 50% survival (i.p. LD_{50}) is, however, comparable to that of a number of clinically used drugs. Oral adminis-

TABLE III
Minimum Inhibitory Concentration[a]

	S. Aureus ppm	E. Coli ppm
3,3 ionene bromide	> 128	> 128
6,6 ionene bromide	16	16
6,10 ionene bromide	4	4
2,10 ionene bromide	4	8
6,16 ionene bromide	4	32

[a] Similar values of minimum inhibitory concentration were found for P. Aeruginosa, B. Subtilis, C. Sporogenes and M. Smegmatis.

TABLE IV
Antifungal Activity of Monomeric Versus Polymeric Quaternary Ammonium Salts

	C. globosum ppm	M. verruca ris ppm	A. versicolor ppm	P. Citrinum ppm	F. oxysporum ppm	Alternaria Sp. ppm	R. Nigricans ppm
3,3-ionene bromide	(1000)	(1000)	>1000	>1000	(1000)	(1000)	>1000
2,4- " "	(1000)	(1000)	>1000	>1000	(1000)	(1000)	>1000
2,6- " "	(1000)	(1000)	>1000	>1000	(1000)	>1000	>1000
6.4- " "	(1000)	(1000)	>1000	>1000	(1000)	(1000)	>1000
6,5- " "	(1000)	>1000	>1000	>1000	(1000)	(1000)	>1000
6,6- " "	(1000)	>1000	>1000	>1000	(1000)	(1000)	>1000
6,10- " "	(1000)	(1000)	>1000	>1000	>1000	(1000)	>1000
6,16- " "	(1000)	>1000	>1000	>1000	(1000)	(1000)	>1000

Inactive Compounds

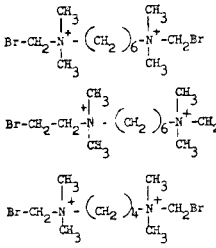

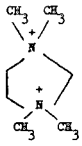

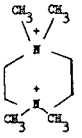

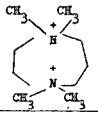

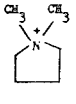

tration of ionene polymers is considerably less toxic than intraperitoneal. A comparison of i.p. LD_{50} with oral i.p. LD_{50} is shown in Table I in which the toxicity data for some low molecular weight ammonium salts are also included. Although the toxicity of some low molecular weight diammonium salts is higher than of most ionene polymers, the former exhibit much lower antimicrobial activity than the latter. In Table II are shown the results of a preliminary screening of the activity of ionenes against a variety of gram positive and negative bacteria. None of the low molecular weight ammonium salts (Table II) inhibited bacterial growth at 1000 ppm. The commonly tested bacteria are Escherichia Coli (E. Coli), a gram negative bacterium found in the large intestine of man and Staphylococcus Aureus (S. Aureus) a gram positive bacterium which causes boils, furuncles, abscesses and suppuration in wounds. The minimum inhibitory concentration in parts per million for these two representative bacteria is shown in Table III.

From Table III one concludes that the structure of the ionene polymers play an important role in the antimicrobial activity and that out of those

TABLE V
Minimum Inhibitory Concentration of Ionenes Against Alternaria Sp.

	Concentration ppm
3,3 ionene bromide	4
6,6 ionene bromide	8
6,10 ionene bromide	4

tested, the 6,10 ionene seems to have the optimum structure for efficient growth inhibition of E. Coli.

The ionenes were also found to inhibit the growth of the following fungi; C. Globosum, M. Verrucaris, F. Oxysporum and Alternaria Sp. The results of a preliminary screening are shown in Table IV.

The minimum inhibitory concentration for Alternaria Sp. is recorded in Table V.

A comparison of the antimicrobial with the antifungal activity leads to the conclusion that in both cases the polymeric nature is a condition sine qua non for the activity and that the monomeric analogues are inactive. In addition, the high charge density ionenes (e.g., 3,3-ionene) are just as active towards fungi as the low charge density ionenes (e.g., 6,10 ionene) in contrast to the behavior of ionenes towards bacteria.

The results of Table III were obtained by a dilution technique, i.e., the determination of the minimum concentration of the tested substance which inhibits growth of a bacterial culture [19]. A spectrophotometric technique which measures the growth of bacteria with time is more informative. This technique was used to observe the effect of 3,3- and 6,10-ionene on Pseudomonas BAL 31, a marine bacterium isolated off the coast of Chile and a host of bacteriophage PM2. PM2 is a virus which invades Pseudomonas BAL 31 and assumes control of the latter [20]. The bacteria may be stored on agar containing nutrient broth and salts and grown in clones, i.e., colonies originating from a single bacterium. When a clone is transferred to a new agar plate new clones are produced, one of which is removed for growth to an aqueous suspension containing nutrient. On bubbling air through the medium, bacteria grow to confluence, i.e., maximum concentration of bacteria permitted by the availability of nutrients, concentration of wastes, and the pH of the medium. At confluence a steady state is reached when the rate of bacterial formation is equal to the rate of

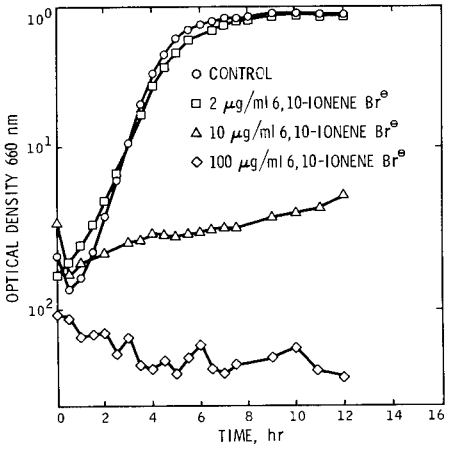

FIG. 3. Growth of Pseudomonas Bal 31 in presence of 6, 10-ionene bromide.

TABLE VI

Ionene	Concentration ppm	Half Life Time $t_{\frac{1}{2}}$ (hrs)
--	--	3.4
3-	2	3.6
3-	10	3.6
3-	100	3.6
6,10-	2	3.4
6,10-	10	23
6,10-	100	no growth

bacterial disappearance. The transfer of an aliquot of confluent culture to a fresh nutrient medium in presence of a known concentration of ionene polymers permits the determination of minimum inhibitory concentration as well as the half-life time of the first order growth reaction. Figure 3 is a plot of the logarithm of optical density at 660 nm, versus time in presence of 0, 2, 10, and 100 μg/ml (or 0, 2, 10 and 100 ppm) of 6,10-ionenes. The curves were obtained by withdrawal of small aliquots of sample into a microcell at half hour intervals and measurement of optical density of 660 nm. After a brief induction period (0.5 hour), cells begin to grow. In absence of ionenes, growth is logarithmic for 5 hours until confluence or the stationery phase is reached. In presence of 10 ppm of 6,10-ionene, growth is inhibited. A comparison of growth characteristics for 3,3- and 6,10-ionene is shown in Table VI. Table VI shows that at (a) 100 ppm the 3,3-ionene has no effect on growth, (b) at 100 ppm the 6,10-ionene inhibits growth completely and (c) at 10 ppm the growth is considerably reduced [21].

Insolubilized ionene polymers retain their antimicrobial properties. The insolubilization can be achieved either by exchanging the counterions or by an ionic crosslinking reaction. Thus addition of a KI, iodine aq solution to an aq solution of ionene chloride yields structure X, insoluble in water and in most organic solvents. The bactericidal activity of the polyammonium salt is here enhanced by a slow release of iodine, the antimicrobial activity of which is well known. Impregnation of textiles with ionenes followed by

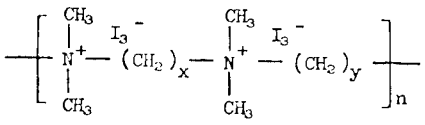

X

KI, I_2 treatment leaves under suitable conditions an antibacterial layer on various surfaces e.g., surgical sutures, cloth, etc. In addition, insoluble crosslinked systems are obtained by means of the following reaction:

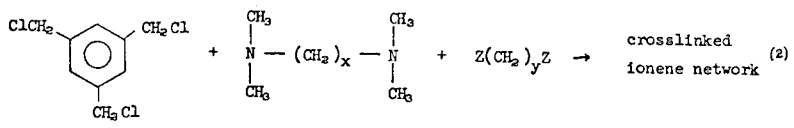

(a suitable commercially available crosslinking agent is 1,3,5-trichloromethyl mesitylene.) In both cases i.e., with polytriiodides as well as with crosslinked ionenes inhibition zones were obtained with E. Coli, S. Aureus, B. Subtilis etc. when tests were carried out by means of a disc technique [19].

The mechanism of ionene interaction with bacteria has not been established. The first step in growth inhibition may be either a flocculation phenomenon or adsorption of ionenes on the bacterial membranes. Most bacteria as well as living tissue cells of various organisms are negatively charged. Positively charged polyelectrolytes could therefore be partly adsorbed on bacterial cell surfaces by electrostatic attraction and flocculate bacteria by a similar mechanism postulated for the flocculation of colloidal suspensions [22]. This is, however, not likely at least for Pseudomonas Bal 31 where it was shown that addition of inhibitory concentrations of 6,10-ionene bromide after four hours of growth did not alter, at first, the optical density of the medium, although further growth was stopped and the optical density decreased slowly (50% decrease in O.D. after 12 hours). A sudden decrease of O.D. to zero or nearly zero would have been expected if flocculation of bacteria occurred. Adsorption of polyelectrolytes onto surfaces of membranes without the occurrance of flocculation and interference with transport across cell membranes or with the replicative system is therefore a more likely mechanism of inhibition.

Chemical interaction with bacterial DNA is a remote possibility which should, however, not be overlooked. In fact, ionenes form strong water insoluble complexes with DNA. An aqueous solution of calf thymus DNA (Na content of 5.9%) when mixed with an aqueous solution of 6,10-ionene bromide (Br content 33.9%) results in a solid fibrous precipitate which when dry contains only 0.3% of Na and 0.2% of Br. The complex can be obtained in form of fibers exhibiting strong birefringence in a polarizing microscope and this implies that the helical configuration of DNA was preserved [21]. The elemental analysis results indicate electrostatic bonding between the negative oxygen of the DNA phosphate groups and the positive nitrogens of the ionene and elimination of sodium bromide during complex formation. Although different structures of ionenes yield similar complexes, an examination of DNA molecular models (Fig. 4) show that that 6,10 ionene gives the best fit if we assume that the latter wraps itself around the DNA double helix.

The ionene-DNA complex is soluble in high ionic strength solutions (0.5 M NaCl) but its stability has not yet been determined. Similar complexes have been obtained with polyamines [23] of structures XI, XII and XIII.

$NH_2(CH_2)_3-NH-(CH_2)_4NH_2$

XI Spermidine

$NH_2(CH_2)_3NH(CH_2)_4NH(CH_2)_3NH_2$

XII Spermine

$NH_2-(CH_2)_4-NH_2$

XIII Putrescine

These polyamines, in spite of the fact that they exhibit high toxicity when injected in vivo, are present in most living organisms and affect a large

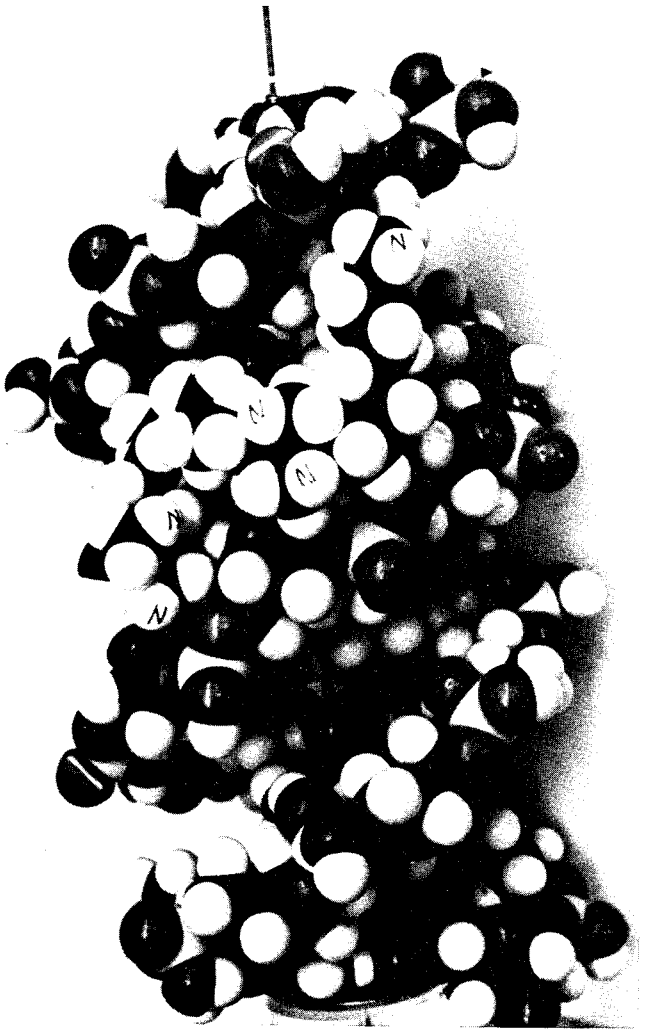

FIG. 4. Probable configuration of DNA-6, 10-ionene complex.

number of metabolic transformations. Spermine was discovered in the human semen as long as 1678 by Leeuwenhoek. It is now known that spermidine and spermine and the related diamine, putrescine, are ubiquitous in animals and plants, and at least one of these three amines is present in all microorganisms [24]. Spermidine and spermine bind to DNA and may be attached like the histones along sections of a DNA molecule. Polyamines also have a marked stimulatory effect on the enzyme synthesizing ribonucleic acid (RNA) that is DNA primed RNA polymerase. They also stimulate the DNA replicating enzyme (DNA-primed DNA polymerase) and may stabilize the low molecular weight RNA (transfer RNA). The polyamines interact also with ribosomes, the subcellular particles which are functional in protein synthesis. The role of polyamines in oncogenesis and diagnosis of cancer by the determination of

their concentration in the blood and urine of cancer patients was recently described [25].

Since at pH 7 the polyamines exist in the form of polycations their binding to DNA probably involves the same mechanism as proposed for ionene-DNA complexes and similar models to that in Figure 4 were previously postulated [24]. The 3,4-ionene can therefore be considered as a model for polyspermidine or polyspermine and since the molecular weight of ionenes and the number of positively charged nitrogens can be made considerably higher than in naturally occurring polyamines the number of electrostatic bonds between DNA and ionenes is necessarily higher, therefore the resulting complexes should be more stable. It must be, however, borne in mind that the 3,4-ionene, in contrast to Spermine, does not contain hydrogen atoms capable of hydrogen bonding with oxygens of the phosphate groups, and this fact may affect the stability of its complexes with nucleic acids or its biological activity.

GANGLIONIC AND NEURO-MUSCULAR BLOCKING ACTION

Some of the ammonium compounds (hypotensive agents) shown in Table VII are still clinically used against essential hypertension, i.e., the commonest variety of high blood pressure [26]. These compounds interact

TABLE VII
Structure of Hypotensive Agents

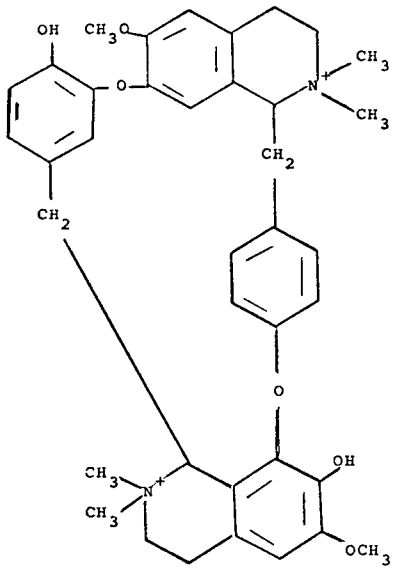

Tubocurarine

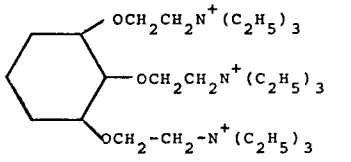

Gallamine Triethiodide

$(CH_3)_3N^+-(CH_2)_6-N^+(CH_3)_3$

Hexamethonium

Ganglionic Blocker

$(CH_3)N^+(CH_2)_{10}-N^+(CH_3)_3$

Decamethonium

Curarizing Activity

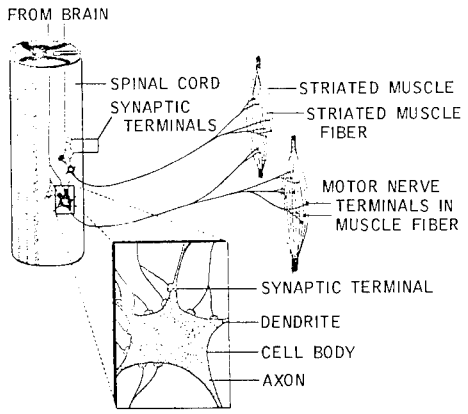

FIG. 5. Neurons and Synapses depicting the association between nerves in the spinal cord and extensions into muscle. The enlargement is a diagram of the synapse.

either with synaptic junctions in ganglia and/or with nerve cells motor ends. Nerves from the brain or spinal cord made up of preganglionic fibers run from the ganglion and terminate in the innervated organ (Fig. 5). Stimulation of preganglionic neurons results in release of acetylcholine which causes depolarization of synaptic membrane thereby stimulating the postganglionic fibers and consequently the peripheral organ. The mono–, di–, or triammonium compounds of Table VII inhibit nerve impulse transmission in the ganglia or motor end terminals which also have synaptic junctions. The activity of ganglionic blocking agents is strongly dependent on structure (Tables VIII and IX).

The mechanism of action of ammonium salts (Table VII) in the synapses of ganglia or at the junction of neuron dendrites with the muscle cells is believed to involve interferences with the release and binding of acetyl choline (XIV) to the receptor [27]. Upon arrival of an impulse, the motor

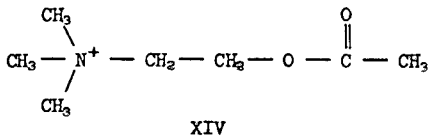

XIV

end terminals act like glands secreting acetyl choline, a chemical messenger that diffuses across the synaptic gap. Acetyl choline molecules then combine with receptor molecules in the contact area of the muscle fiber, and this results in trigering of an impulse in the muscle. The polyammonium salts probably act as inhibitors of the transmitter substance (acetyl choline). The ionenes were found to act as more efficient ganglionic blockers and have longer duration effects than their monomeric analogues [28]. Ionene of structure XV was less toxic to mice than the monomeric

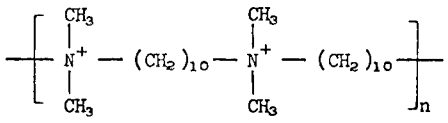

XV

TABLE VIII
Influence of Chain Length on Ganglionic Blocking

$(CH_3)_3N^+ - (CH_2)_nN^+(CH_3)_3$								
n	2	3	4	5	6	7	--	10
Activity	3.0	4.3	5.9	33.3	100	16.7		28.30

analogue XVI, yet its ganglionic blocking duration effects were manyfold

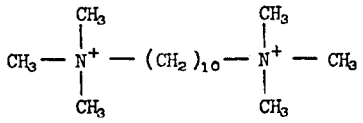

XVI

that of XV.

These increases in duration of action may be a result of more secure binding to the receptors because of a larger number of positive charges in XV than in XVI. Whatever the mechanism of the increase in duration of effect, it is of obvious practical interest, especially in pharmaceutical chemistry, for it suggests that polymerization of moieties may be a useful way to increase the duration of action of drugs.

INTERACTION WITH HEPARIN

Ionenes form water insoluble complexes with heparin. The solubility and the film forming ability of these complexes depend on the structure of ionene and the molecular weights of both components. Complex formation is probably the reason for the antiheparin activity of ionenes.

Interest in antiheparin agents arise from the belief that certain clinical hemorrhagic states may be associated with a heparin-like substance in the

TABLE IX
Effect of Size of Alkyl Groups

	Methyl	versus	Ethyl
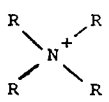	$R=CH_3$ ganglionic stimulation		$R=C_2H_5$ ganglionic blockade
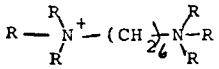	ganglionic blockade		no ganglionic blockade curarizing effect
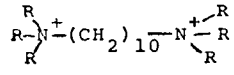	curarizing effect*		ganglionic blockade

blood. In addition, the value of antiheparin agents lies also in the treatment of post partum hemorrhage and the restoration of normal blood coagulability after open heart surgery and after hemodialysis, where administration of relatively large doses of heparin is a common practice.

Protamine sulfate and toluidine blue, neither of which are free of toxic effects, are clinically used as antiheparin agents. Although most ionene structures have antiheparin activity, extensive investigations of toxicology and effects on the circulatory system in laboratory animals were carried out only with 6,3-ionene bromide referred to as "polybrene" [18, 29]. The latter was found to be more toxic (i.v. LD_{50}, 28 mg/kg in mice and 20 mg/kg in rats. The i.p. LD_{50} in mice, 61.5 mg/kg) than toluidine blue (i.v. LD_{50} 45 mg/kg) and protamine sulfate (i.v. LD_{50}, 44 mg/kg). However, cumulative i.v. doses of 6,3-ionene bromide up to 5 mg/kg as 1% solutions could be given rapidly to anesthetize dogs without markedly affecting either the respiration or circulation i.e., without toxic symptoms.

Heparin offers a protective action in neutralizing the toxicity of 6,3-ionene bromide in both mice and dogs. Thus pretreatment of mice with heparin enabled them to survive doses of three times the LD_{50} values with only mild toxicity symptoms. This is not surprising considering the formation of relatively stable complexes between ionenes and heparin.

HEPARINIZED THROMBORESISTANT COATINGS

A number of polymeric materials containing either physically, ionically or covalently bonded heparin on the surface were recently reported [30]. A waxy coating made by complexing of tridodecyl methyl ammonium bromide (TDMAC) with heparin received particular attention [31]. The latter may be formed in situ by treating a polymeric surface first with the quaternary ammonium salt and then with heparin, which is thus insolubilized on the surface.

The various heparinized surfaces inhibit the blood clotting process [32]. It is still not clear, however, to what extent the thromboresistance is due to heparin release during contact with blood. A special class of ionene polymers based on urethane prepolymers has been found to yield (a), elastomeric materials to which heparin can be bonded on the surface [17], or (b), thromboresistant elastomeric complexes containing heparin in the bulk [33].

Elastomers with Surface Bonded Heparin

A commercially available triisocyanate (XVII = solithane, Triokol Co.) forms a crosslinked cationic polyurethane when reacted first with dimethylamino ethanol and then with dihalides (II). The reaction product may be cast into sheets exhibiting rubbery characteristics. The latter after immersion in a 2% solution of heparin in a mixture of water and tetrahy-

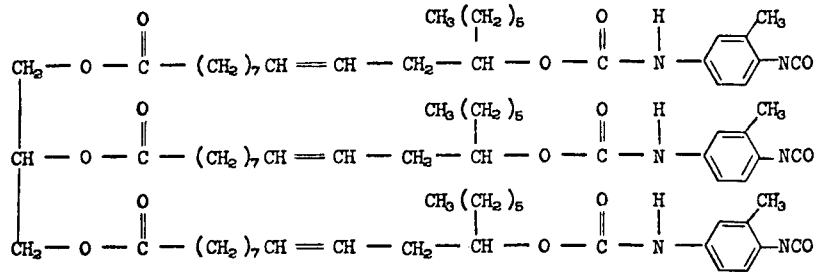

XVII

drofuran (1:1 by volume) for 12 hours and subsequent repeated washings with distilled water was found to be thromboresistant, i.e., no clots were observed for several hours, when whole human blood (0.5 cc) was placed on the surface (1 cm^2) of the specimen. Similar thromboresistant surfaces were obtained [17] by variation of the structure of reagents reacting with XVII.

Polyurethane–Heparin Complexes (PUHC)

Of special interest are cationic polyurethane complexes capable of forming thromboresistant coatings. The latter were synthesized from polyether polyurethanes according to the scheme shown below [33].

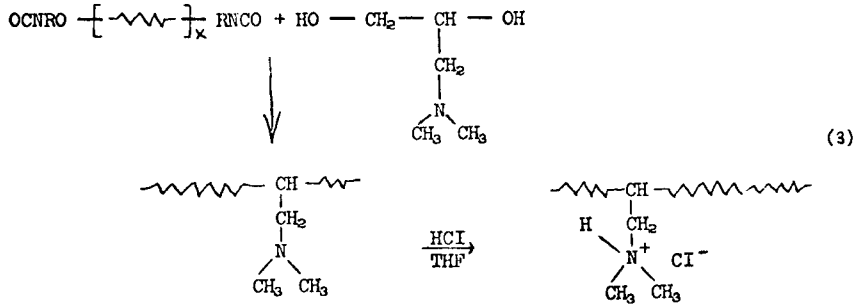

(3)

R = — OC — NH — (Aromatic or Aliphatic Residue)

The cationic polyurethanes thus prepared yielded elastomeric materials when combined with sodium heparin. The polyurethane heparin complexes (heparin content: 16%, referred to as PUHC) could be obtained in form of homogenous solutions. The latter were used to coat thromboresistant films on commercial polyurethane tubing. The thromboresistance was ascertained by modified Lee White tests carried out in PUHC coated tubing subjected to a water or saline extraction before test and by successful extracorporeal blood circulation.

In order to evaluate further the thromboresistance of PUHC coatings the rate of adhesion of blood platelets to coated and uncoated polyurethane was investigated by means of scanning electron microscopy (SEM).

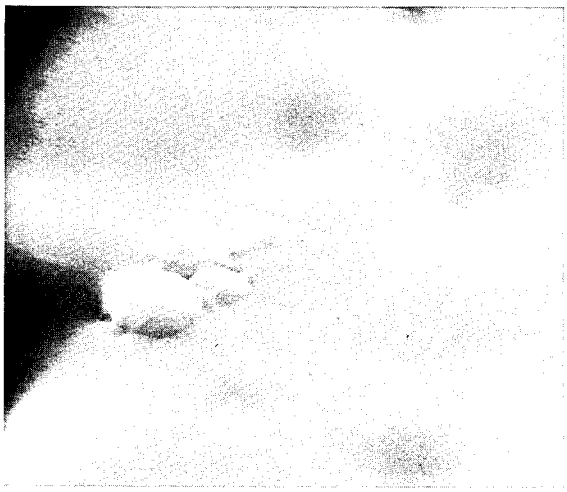

FIG. 6. Blood flow 3 min. (PUHC) 5000 ×.

Tubing sections were inserted into a beagle A-V shunt prepared by the Frasher technique [34] and blood was circulated through them for different times. The test specimens were treated with glutaraldehyde (3% aqueous solution) and photographed at representative locations by means of SEM.

The appearance [35] of platelets on a PUHC surface (Fig. 6) after blood circulation for an identical time (3 min) is remarkably different from that on the control sample (Fig. 7, uncoated commercial polyurethane). Figure 7 and the enlargement (Fig. 8) of activated platelets shows the development of pseudopods which have not formed on the heparinized coatings.

A plot of the number of platelets as a function of time on PUHC coated tubing shows that the buildup rate is just in the first 30 min. reaching a

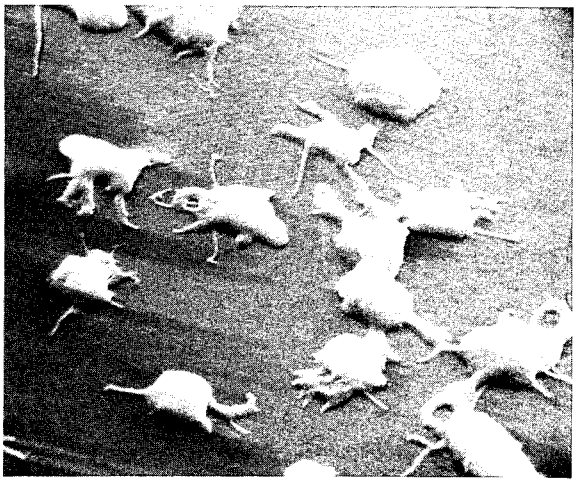

FIG. 7. Blood flow 3 min. (control) 5000 ×.

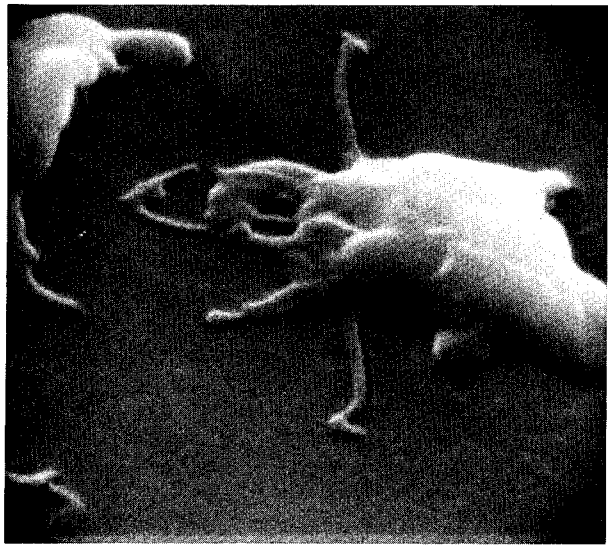

FIG. 8. Blood flow 3 min. (control) 2000 ×.

saturation limit of about 6×10^5 platelets/cm² at about 60 min. (Fig. 9). A quantitative comparison of the platelet deposition rate with a non-heparinized surface is impossible, since on commercial polyurethane the platelets are already agglomerated after 10 min. of blood flow. Since the first step in the process of blood coagulation by severance of tissues is the deposition of blood platelets followed by agglomeration and a viscous metamorphosis, the slow rate of platelet deposition on PUHC surfaces is indicative of thromboresistance.

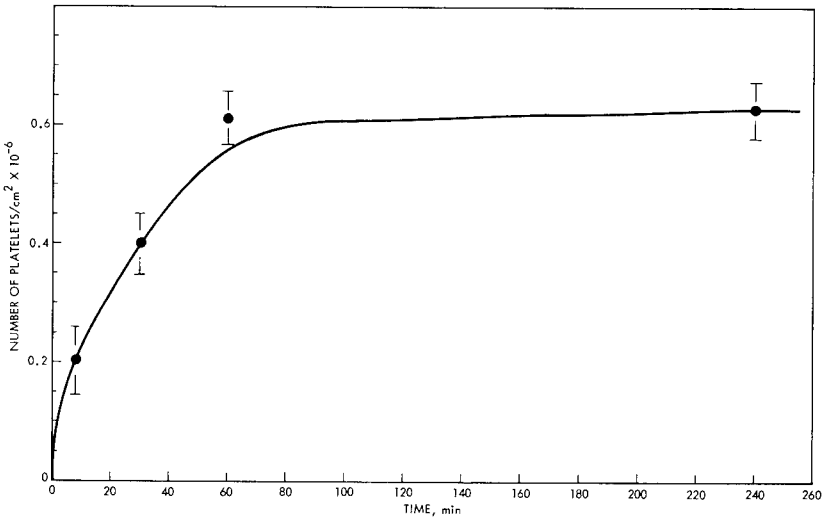

FIG. 9. Rate of platelet deposition on a PUHC tubing.

CONCLUSIONS

The survey of the recent investigations into the mechanism of formation, properties and applications of ionenes in biomedicine yields the following conclusions:

1. The ionenes constitute a unique system because their structure, their distances between positive charges, their counterions, and their molecular weight can be varied systematically. Since very small changes in structure frequently have drastic effects on the biological behavior, the ionenes when used as model compounds constitute a useful tool for the elucidation of the mechanism of biological processes. These considerations apply not only to the study of toxicity or antimicrobial activity, but also to the use of ionenes as model histones to understand the interaction of the latter with DNA or as model substances to elucidate the properties of membranes of tissue cells, blood corpuscles or viruses (A preliminary investigation has shown that the sensitivity of chick embryo cells to the Sindbis virus is significantly decreased in presence of ionenes [21]).
2. The cooperative effect of polyammonium salts as compared with low molecular weight mono or diammonium compounds is apparent in the antimicrobial and antifungal activity in the duration of neuro muscular blocking action, in the formation of ionene-DNA and ionene-heparin complexes. The differences in the biological properties or stability of the complexes may be explained in each case by a stronger electrostatic association between negative and positive species because in the latter, the molecular weight and consequently the number of bonding sites is relatively high.
3. The effect of molecular weight on toxicology, complex formation with DNA or neuromuscular blocking action is not known or has been only superficially examined. This is mainly because information on the synthesis of different molecular weight ionenes and correlations between molecular weight and their solution properties have become available only recently.

REFERENCES

[1] A. Rembaum, W. Baumgartner and A. Eisenberg, *J. Polym. Sci. B, 6*, 159 (1968).
[2] C. F. Gibbs, E. R. Littman and C. S. Marvel, *J. Am. Chem. Soc., 55*, 753 (1933).
[3] W. Kern and E. Brenneisen, *J. Prakt. Chem., 159*, 159, 194 (1941).
[4] D. M. Ritter, U.S. Patent 2,261,002, Oct. 28, 1941; N. E. Searle, U.S. Patent 2,271,378, Jan. 27, 1942; J. E. Kirby, U.S. Patent 2,375,853, March 15, 1945; J. G. Erickson, U.S. Patent 2,807,910, Oct. 1, 1957; C. Taube and K. Bockmann, U.S. patent 3,009,761, Nov. 21, 1961; L. H. Bock and A. L. Houk, U.S. Patent 2,454,547 Nov. 23, 1948; and L. P. McCarty, U.S. Patent 3,206,462 (Sept. 14, 1965).

[5] D. Casson and A. Rembaum, *Macromol. 5,* 75, (1972).
[6] A. Rembaum and H. Noguchi, *Macromol. 5,* 261 (1972).
[7] H. Noguchi and A. Rembaum, *Macromol. 5,* 253 (1972).
[8] S. P. S. Yen, D. Casson, and A. Rembaum, *Water Soluble Polymers,* N. Bikales (Ed.), New York, Plenum Press, 1973, p. 291.
[9] M. Schmir and A. Rembaum, *Water Soluble Polymers,* New York, Plenum Press, 1973, p. 327.
[10] J. C. Salamone and B. Snider, *J. Polymer Sci. A, 8,* 3495 (1970).
[11] E. Tsuchida, K. Samada and K. Moribe, *Makrom. Chemie., 151,* 207 (1972).
[12] T. Dolezal, D. C. Edwards and R. H. Wander, *Rubber World,* p. 46.
[13] D. Dieterich, W. Keberle and H. Witt, *Ang. Chem. (Intern. Ed) 9,* 40 (1970).
[14] J. C. Salamone, B. Snider and W. L. Fitch, *Polym. Prep. Am. Unem. Soc., Polym. Unem. Div. 11* 652 (1970).
[15] A. A. Berlin, L. V. Zherebtsova and Ye. F. Razvodovskii, *Polym. Sci. USSR, 6,* 67 (1964).
[16] A. Rembaum, S. Singer and H. Keyzer, *J. Polym. Sci., B, 7,* 395 (1969).
[17] A. Rembaum, S. P. S. Yen, R. F. Landel and M. Schmir, *Biomedical Polymers,* A. Rembaum and M. Shen, M. Dekker (Eds.), New York 1971.
[18] E. T. Kimura, P. R. Young, R. J. Stein, and R. K. Richards, *Toxicol. Appl. Pharmacol. 1,* 185 (1959).
[19] Hugo, W. B., *The Inhibition and Destruction of the Microbial Cell,* New York, Academic Press, 1971.
[20] R. T. Espejo and E. S. Canelo, *J. Bact., 95* 1887 (1968) and R. T. Espejo and E. S. Canelo, *Virology, 34,* 738 (1968).
[21] M. Schmir and A. Rembaum, unpublished results.
[22] A. Rembaum, D. Casson, and J. J. Morgan, *Environmental Science and Technology,* (in press).
[23] U. Bacharach, *Ann. Rev. Microbiol., 24,* 109 (1970).
[24] T. A. Smith, *Endeavor, 22* (1972).
[25] "Polyamines: Their Implications for Effective Cancer Regulation", Symposium held at Baltimore, Maryland, October 12–13, 1972, NCI Monograph (in press).
[26] S. Thesleff and D. M. J. Quastel, *Ann. Rev. Pharmacol., 5,* 263 (1965); W. Paton and E. J. Zaimis, *Pharmal. Rev., 4,* 219 (1952).
[27] A. Burger (Ed.), *Drugs Affecting the Peripheral Nervous System,* M. Dekker, New York, 1967; D. Edwards, J. J. Lewis, D. E. McPhail, T. C. Muir, and J. B. Stenlake, *J. Pharmacol. Suppl., 12,* 137 (1960).
[28] F. W. Schueler and H. H. Keasling, *J. Am. Pharm. Assoc. 45,* 192 (1956).
[29] F. W. Preston, *Proc. Central Soc. Clin. Res., 25,* 63 (1952).
[30] V. L. Gott, M. D. Ramas, F. B. Najjar, J. L. Allen, and K. E. Becker, Artificial Heart Program Conference, June 1–13, 1969.
[31] R. I. Leininger, J. P. Crowley, R. D. Falb, and G. A. Grode, ASAIO, *18,* 312 (1972).
[32] D. Stoffey, H. Lee, and W. Stone, *J. Macrom. Sci. Chem., A-3,* 119 (1969).
[33] S. P. S. Yen and A. Rembaum, *J. Biomed. Mater. Res., 1,* 83 (1971).
[34] W. G. Frasher, *J. Appl. Physiol., 22,* 348 (1967).
[35] A. Rembaum, S. P. S. Yen, M. Ingram, J. F. Newton, C. L. Hu, W. Frasher, and B. Barbour, *Biomater., Med. Dev., Artif. Organs, 1,* 199 (1973).

HISTOLOGIC ORIGIN OF AORTIC TISSUE MECHANICS: THE ROLE OF COLLAGENOUS AND ELASTIC STRUCTURES

C. D. ARMENIADES, L. W. LAKE and Y. F. MISSIRLIS

Department of Chemical Engineering
Rice University, Houston, Texas 77001

and

J. H. KENNEDY

Taub Laboratories for Mechanical Circulatory Support
Baylor College of Medicine, Houston, Texas 77025

SYNOPSIS

This study describes the stress/deformation behavior of aortic and aortic valve tissue on the basis of its main structural biopolymers, elastin and collagen. By selective removal of specific constituents from fresh specimens of bovine and human aortas and aortic valves, it was possible to obtain macroscopic tensile deformation data on the native tissue and its collagenous and elastin structures. It was found that at low extensions (less than 50%) the aortic wall mechanics are largely determined by the compliant elastin structures, while the high-modulus collagen assumes an increasing load-bearing role at high extensions, acting, thus, as a strain-limiting network. This behavior is consistent with the respective organization of the elastin and collagen networks, observed histologically in the bovine and human aortic tissue. The mechanics of both systems may be successfully described by a four-parameter model, based on a parallel linkage of unidirectional bundles of elastin and collagen fibers, with the parametric values determined independently from the known tensile moduli of pure collagen and elastin and from histological observations. Extension of these studies to the aortic root region reveals that the highly collagenous aortic ring serves as the structure that limits radial distention of the aortic sinus and valve leaflets under diastolic pressures. Histologic examination of the aortic ring and valve leaflets shows a biaxially oriented collagenous network as the main load-bearing constituent.

BACKGROUND

Normal functioning of the circulatory system is vitally dependent on the proper deformative response of the various blood vessels to the pulsatile stresses generated by the pumping action of the heart. Disfunctions involving abnormal compliance of the arterial walls, such as arteriosclerosis and aneurysm, often entail severe or fatal pathologic conditions. Since

Applied Polymer Symposium No. 22, 319–339 (1973)

these disfunctions are also associated with histologic changes in the arterial system, a correlative study of the mechanical properties and histology of arterial tissue is of obvious importance.

A number of previous studies have considered changes in the physical properties and histology of arterial tissue with various diseases. These include observations of a rise in incremental Young's modulus with aging [1], possibly caused by an increase in the ratio of collagen to elastin fibers [2]; a general deterioration in the quality of intra-arterial components in arteriolsclerosis [2]; a decrease in the crosslinking amino acid content of elastin in atheromatous tissue [3]; and a study of the morphological factors that are important in the response of the aortic media to hypertension [4]. In addition, Burton [5] has suggested that arterial aneurysms are caused by a decrease in elastin fiber content without a corresponding increase in collagen fibers. This hypothesis is reasonable even though Sumner et al [6] failed to detect a change in the quantity of collagen and elastin in aneurysmal human arteries. It has also been observed that absence of collagen from the aortic wall causes an increase in its extensibility [7]. Although most of these studies have considered the aortic mechanical properties to be determined mainly by the collagenous and elastic networks of the vessel wall, the actual role of each tissue component in the deformation process is still a matter of considerable speculation [3, 8]. It is, however, precisely this information that is needed in order to establish a structural basis for the mechanics of normal aortic tissue and determine, eventually, the histological origin of various arterial disfunctions.

A second application of aortic mechanics lies in the use of aortic tissue in homograft or heterograft replacement of cardiac valves. There is evidence that denaturation of the implanted collagen may be a significant problem in aortic valve heterografts. Indeed, a number of authors [9, 10, 11] have noted that the long-term success of these tissue implants is heavily dependent on the quality of their structural components. It is likely that a full understanding of aortic mechanics and its relation to the tissue components would help optimize the methods of selection, preservation, and implantation of cardiac valve grafts. In addition, comparative studies of the mechanics and histology of animal and human aortic tissue may help in the assessment of the relative merits of homografts and heterografts with respect to compatibility and long-term function.

A realistic approach to the development of structure-property relations for aortic tissue must deal with the fact that its response to mechanical stress depends in a complex manner on a large number of parameters [12]. In general, the properties of this tissue are directionally anisotropic, nonlinear, history-dependent, time dependent, temperature dependent, and affected by the surrounding medium. That the aortic wall is anisotropic is a reasonable deduction from the function of the vessel. This has been noted [13, 14], but rarely quantified [15]. History dependence, usually in the form of a strain-rate dependence, has often been alluded to [12, 16], but rarely measured. Time dependence has been quantified by stress relaxation measurements [13] or in terms of a phenomenological model [16]. The effects of the surrounding medium on tissue deformability are also generally

recognized [5, 17]. Most studies, the present included, have deformed the tissue in a constant environment (Ringer's solution). In vivo studies [5, 18], while providing valuable information about the operation of the intact aorta, do not characterize the individual aortic components as biomaterials. The above problems, particularly the anisotropy and the composite nature of the aortic wall, has rendered of little practical use the standard engineering formualations of stress and strain. Assemblies of springs and dashpots seem to exhibit reasonable fit to tissue mechanics [16] but they are, of course, only convenience parameters that are not directly related to the histology of the tissue.

It is reasonable to assume that the main load-bearing components of the aortic wall are collagen and elastin. These are extracellular, passive components in the sense that they do not respond to efferent nerve impulses. The active component, smooth muscle, is about fifty times more compliant than elastin (in terms of Young's modulus) when relaxed and thirty times more compliant when contracted [5, 16]. Thus the contribution of smooth muscle is measurable only at small strains (less than 20%) and only when it is contracted [16, 18] and decreases further in large arterial vessels, which are sparsely populated with smooth muscle cells. It has been generally, though not exclusively [13] assumed that the low-modulus elastin determines the mechanical properties of the aortic wall at low deformations, while the stiffer collagen forms a strain-limiting network at high deformations [5]. While this premise has been verified indirectly [16], there are no reported measurements of the individual contributions of collagen and elastin to arterial deformability. The effects of lipids and mucopolysaccarides on the overall tissue properties are also unknown. Though these components probably do not bear direct load, their presence and organization could affect the stress distribution among the load-bearing components of the aortic tissue.

In this paper we attempt to define quantitatively the mechanical properties of the human aortic wall in terms of parameters that are directly related to the organization of its major structural components, elastin and collagen. The role of these components is assessed by comparing the in-vitro stress/deformation behavior of a series of specimens, with various constituents selectively removed and by correlating these data with histological observations. The resulting stress–strain relations are based on an analytical treatment, derived from previous measurements on bovine aortic tissue [19] which has similar macroscopic properties and histology. Both the bovine and the human data are discussed here for comparative purposes. This treatment is extended to the aortic valve. Its deformation behavior during diastole is analysed in terms of the complex histology of the aortic root region.

EXPERIMENTAL

The aortic tissue specimens used in this work were obtained from the upper descending aorta of two bovine and three human subjects. This region has a relatively uniform composition over its length with a high

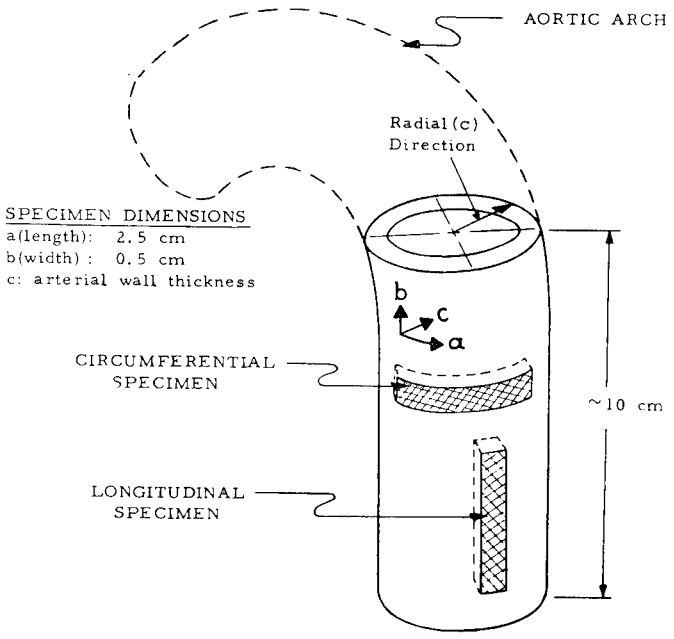

FIG. 1. Schematic diagram, showing the orientation of the two types of tensile specimens, cut from the wall of upper descending aortic segments.

elastin content. The bovine specimens were taken from approximately 6-month old animals while the human specimens came from a 22-year male who died of Ewing's sarcoma (1), a 15-year male drowning victim (2), and a 19-year female with cause of death unknown (3). Intact aortic roots, containing about 5 mm of tissue around the aortic ring and a 4–6 cm portion of the ascending aorta were also excized from these and four other subjects. All aortic valves were essentially nonregurgitant and showed no gross tissue pathology. These specimens were removed within 24 hours after death and stored in refrigerated saline with small amounts of penicillin or Gentocin at 3°C. It was found that storage under these conditions for periods of at least six weeks does not affect the mechanical properties of the extracellular tissue. Tensile specimens 1/2 cm wide were cut along the longitudinal as well as the circumferential direction of the aortic wall, as shown in Figure 1 and the adventitial layers removed by dissection. The lengths of all specimens were sufficient to avoid end effects (at least 2 cm).

Lipids were removed from the tissue by extraction with acetone for 24 hours in a soxhlet apparatus [20]. This technique is known to remove lipids completely and was found to cause no denaturation of the other tissue components. After lipid extraction the samples were reequilibrated for five days in Ringer's solution prior to any measurements. Collagen was removed by steam autoclaving of the tissue under water at 15 psig (120°C) until the extract became biuret negative (usually about 6 hours). This procedure was chosen over a number of others [21] as the least degradative on the remaining tissue components. Indeed, continued autoclaving of the

tissue for periods up to 15 hours produced no further changes in mechanical properties. The lipid and collagen content of the tissue was estimated from hydroxyproline determinations [22] of adjacent samples from the same aorta, autoclaved before and after lipid extraction. The amount of collagen in the defatted tissue estimated by this method agrees closely with the dry weight loss of the autoclaved tissue, indicating that the process removes only collagen. The autoclaved tissue always contained a hydroxyproline level of 2–4% and was considered to be essentially elastin [23]. It is possible that this material contains also a small amount of mucopolysaccharides (7–8%) and a carbohydrate–protein complex rich in polar aminoacids, which can be removed by treatment with dilute NaOH at 98°C [24]. This was not done for fear of elastin denaturation. Selective removal of elastin was accomplished by means of an enzymolytic treatment, using a 50–50 mixture of elastase and trypsin inhibitor (300 μg/ml buffer at a pH of 8.6) for 4 hours at 15°C. This treatment was found to remove over 50% of the elastin without causing observable degradation in the mechanical properties of the collagen present in the tissue.

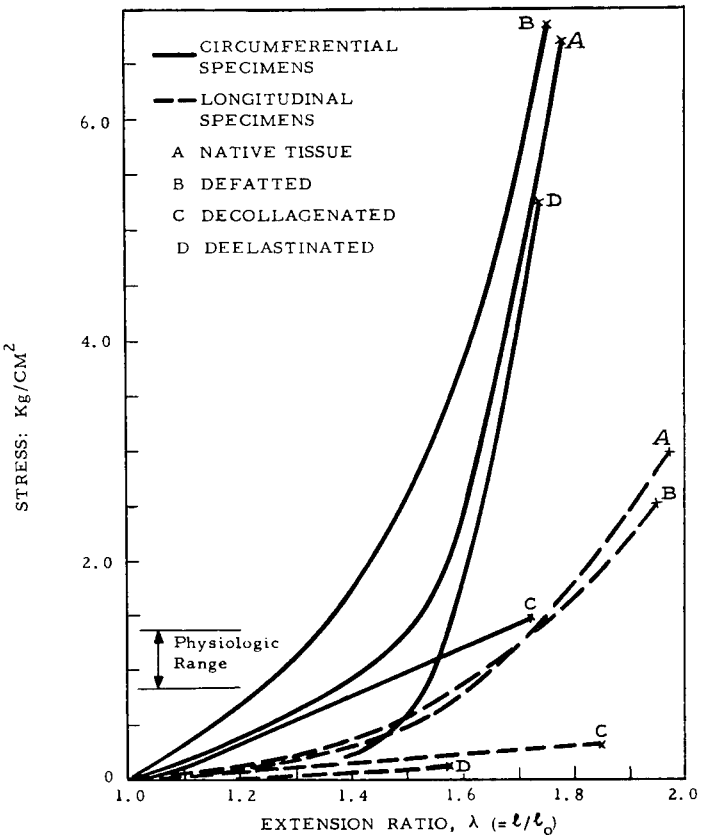

FIG. 2. Typical stress–deformation data for native, defatted, and decollagenated bovine aortic tissue.

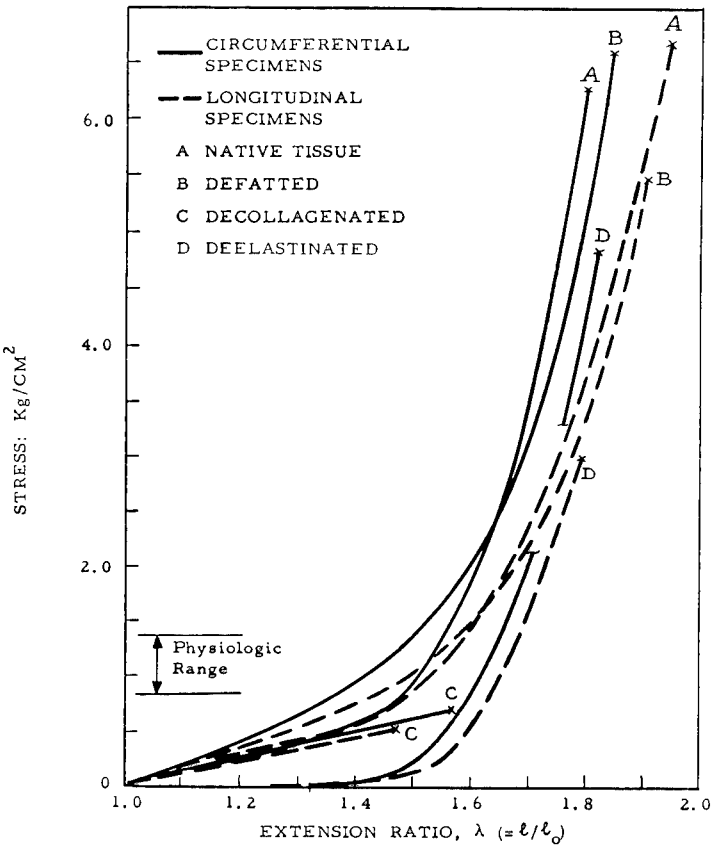

FIG. 3. Typical stress–deformation data for native, defatted, and decollagenated human aortic tissue.

All measurments of mechanical properties were performed on an "Instron TM-M" testing machine with the specimen immersed in Ringer's solution at 23°C. The reported tensile data were taken at a constant strain rate of 0.15 min^{-1}, although the tissues under consideration show modulus increases of less than 10% per decade increase in strain rate. The cross-sectional area (A_o) of the specimens was measured optically with the immersed specimen in position between the Instron grips at zero load. This technique yields A_o values that agree within 7%, on the average, with the wet and dry weight technique of Bergel [13]. No attempt was made to correct for voids [17]. In this work $l_{o'}$, the unstrained specimen length, was measured at the point of initial deflection of the load recorder pen. The strain-dependent "local modulus" was obtained from the slope of the stress–strain curve at the point under consideration.

RESULTS

Aortic Tissue

Figure 2 shows typical stress–deformation data of longitudinally and circumferentially oriented tensile specimens of bovine aortic tissue in the native state (Curve A) after removal of lipids (Curve B), after de-

collagenation (Curve C) or alternately, after removal of elastin (Curve D). Similar data for human aortic tissue and its main structural components are shown in Figure 3.

The response of the bovine tissue and its components to tensile stress is directionally anisotropic, the longitudinal specimens showing much lower moduli, and, in the native and defatted states, greater elongations at break than the corresponding circumferential specimens. This anisotropic behavior is most pronounced in the deelastinated bovine specimens (Curve D), which show a high modulus in the circumferential direction but disintegrate under very low stresses in the longitudinal direction. In contrast to the bovine specimens, human aortic tissue and its structural components show no appreciable directional anisotropy in their deformation behavior, as can be seen in Figure 2B.

A basic characteristic of the deformation behavior of native aortic tissue, both bovine and human, is the appearance of two distinct regions of nearly linear behavior, one at low extensions ($\lambda < 1.5$) and one at high extensions ($\lambda > 1.6$). This allows the definition of "low strain" and "high strain" tensile moduli, which are characteristic parameters of each specimen over most of its deformation range. The inflection between the two regions appears consistently around $\lambda = 1.5$ in the bovine tissue, but varies among human aortic specimens ($\lambda = 1.4$–1.7).

In the specimens with appreciable lipid content (all of the bovines and one of the humans) removal of the lipids results in an everywhere nonlinear deformation behavior, with a higher initial tensile modulus, which increases continuously with deformation. The defatted and decollagenated specimens, (Curve C), which are essentially pure elastin, show a strictly linear response throughout their entire deformation range in the bovine as well as the human aortic specimens. Their longitudinal and circumferential moduli have values indistinguishable from the respective low-strain moduli of the native tissue. In a similar manner the deelastinated specimens (Curve D), which are mainly collagenous, show after an extended initial "toe" region a high modulus, corresponding to the high-strain modulus of the native tissue.

TABLE IA

Variance in Low-strain Modulus of Native, Defatted, and Decollagenated Bovine Aortic Tissue.

		Native		Defatted		Decollagenated	
Subject[a]	Direction of Tensile Stress	$E_{ave.}$[b]	S.D.[c]	$E_{ave.}$	S.D.	$E_{ave.}$	S.D.
1(8)	Circumferent.	1.67	.268	4.20	1.63	.935	.082
1(8)	Longitudinal	.453	.089	.608	.442	.278	.084
2(4)	Circumferent.	2.20	.352	5.19	.292	1.97	.149
2(4)	Longitudinal	1.06	.160	3.25	1.44	1.13	.181

[a] Number in parenthesis denotes the tensile specimens taken from each subject.

[b] Average tensile modulus of specimens within group measured at $\lambda = 1.25$ for low strain and at λ = (1.6-failure) for high strain: kg/cm^2.

[c] Standard deviation of modulus measurements within group.

TABLE IB
Variance in High-strain Modulus of Native, Defatted, and Decollagenated Bovine Aortic Tissue

		Native		Defatted		Decollagenated	
Subject	Direction of Tensile Stress	$E_{ave.}$	S.D.	$E_{ave.}$	S.D.	$E_{ave.}$	S.D.
1(4)	Circumferent.	19.1	6.89	18.3	5.44	1.36	.160
1(4)	Longitudinal	2.08	.878	2.61	1.00	.590	.070
2(4)	Circumferent.	28.0	5.40	21.3	1.70	1.82	.110
2(4)	Longitudinal	7.32	5.67	5.08	1.43	1.13	.160

An indication of the statistical significance of individual measurements is given by Tables I (bovine) and II (human). Despite the large variance in modulus between specimens from the same subject (and the greater variance between subjects) the directional anisotropy of the moduli and the difference in properties between native, defatted, and decollagenated bovine tissue are (with one exception) significant to a confidence level of 0.99. The effect of lipid removal from bovine aortic tissue is significant ($p = 0.99$) at low extensions only. At high extensions the removal of collagen appears significant to a 0.999 confidence level.

The human aortic specimens do not show the directionally anistropic deformation behavior that is characteristic of the bovine tissue. This can be seen in Figure 3 as well as in Table II. At low extensions the observed moduli of the native human specimens are indistinguishable between the circumferential and longitudinal directions and have values, comparable to those of circumferentially oriented bovine specimens. Directional anisotropy in deformation begins to appear at high extensions, the longitudinal modulus having a lower value. This is significant in only two subjects, to a confidence level of only 0.9.

The effect of lipid removal in samples from human subjects (1) and (2)

TABLE IIA
Variance in Low-strain Modulus of Native, Defatted, and Decollagenated Human Aortic Tissue

		Native		Defatted		Decollagenated	
Subject Number	Direction of Tensile Stress	$E^a_{ave.}$	S.D.	$E_{ave.}$	S.D.	$E_{ave.}$	S.D.
1(4)	Circumferent.	1.55	.259	2.32	.418	1.50	.289
1(4)	Longitudinal	1.09	.263	1.38	.211	0.973	.189
2(4)	Circumferent.	1.57	.348	3.13	1.09	1.84	.505
2(4)	Longitudinal	1.35	.326	2.08	.579	1.41	.314
3(4)	Circumferent.	1.52	.267	2.69	.210	1.72	.094
3(4)	Longitudinal	1.44	.241	2.82	.492	1.44	.299

[a] Average tensile modulus within group measured at $\lambda = 1.25$ at low strain and $\lambda = \lambda_m$ at high strain: kg/cm².

TABLE IIB
Variance in High-strain Modulus of Native, Defatted, and Decollagenated Human Aortic Tissue

		Native			Defatted			Decollagenated		
Subject Number	Direction of Tensile Stress	$(E_{ave})_m$[a]	λ_m[a]	S.D.	$(E_{ave})_m$	λ_m	S.D.	E_f[b]	λ_f[b]	S.D.
1(4)	Circumferent.	30.1	1.90	10.3	27.9	1.90	9.62	1.99	1.9	.381
1(4)	Longitudinal	14.1	1.90	3.98	14.6	1.90	4.07	1.07	1.55	.278
2(4)	Circumferent.	20.0	1.80	2.22	24.2	1.88	5.88	1.84	1.65	.505
2(4)	Longitudinal	18.3	1.62	5.30	28.2	1.70	6.26	1.70	1.45	.610
3(4)	Circumferent.	21.9	2.00	4.07	11.8	2.00	3.10	1.88	1.53	.253
3(4)	Longitudinal	12.3	1.75	2.36	16.8	1.78	3.93	1.44	1.37	.340

[a] Average tensile modulus within group measured at $\lambda = 1.25$ at low strain and $\lambda = \lambda_m$ at high strain: kg/cm².

[b] E_f and λ_f are the tensile modulus and extension at failure for the decollagenated tissue.

which have a very low lipid content as shown in Table III, is either not significant (longitudinal specimens) or significant only to a 0.95 level (circumferential specimens). In contrast specimens from subject (3), which have a very high lipid content (20%) show very significant differences ($p = 0.999$) in low-strain modulus between the native and defatted specimens. The effect of lipid removal on specimens from this subject is very similar to that observed in bovine aortic tissue, which consistently shows this level of lipids. Removal of collagen in all the human aortic specimens is very significant ($p = 0.999$) at high extensions, as was also the case with bovine specimens.

The structural origin of the observed macroscopic behavior of aortic tissue may be inferred from histological examinations of microtomed sections at different directions. Representative optical micrographs are shown in Figures 4 through 8.

Figures 4 and 5 illustrate the respective organization of elastin structures in the native bovine and human aortic tissue. These structures consist of

TABLE III
Composition of Aortic Specimens

	Number	Number of Specimens	Per Cent Collagen	Per Cent[a] Lipids	Per Cent Elastin
BOVINE					
	1	4	17	21	52
	2	2	15	25	45
HUMAN					
	1	2	24	3	61
	2	2	13	0	52
	3	2	12	21	66

[a] Measured by hydroxyproline determination as by weight of the acetone-extracted fraction of native aortas. The two methods agree within +5%.

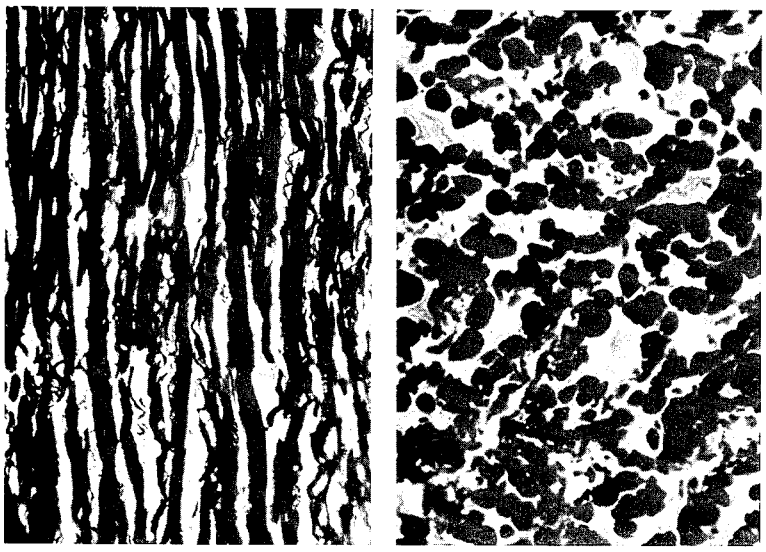

(a) (b)

FIG. 4. Optical micrographs of 5-micron sections, of bovine aortic wall tissue. Verhoeff stain (elastin black, collagen grey), 1500×. A. Circumferential section (plane ab, Fig. 1) B. Longitudinal section (plane bc, Fig. 1)

well-defined, somewhat wavy strands, 3–10μ in diameter. In the bovine aorta the arrangement of the strands is highly anisotropic, with preferential orientation in the circumferential direction. This anisotropy in the elastin network is hardly noticeable in the human tissue.

The organization of the collagen structures in the bovine and human aortic tissue is shown in Figures 6 and 7. They appear as diffuse, folded mi-

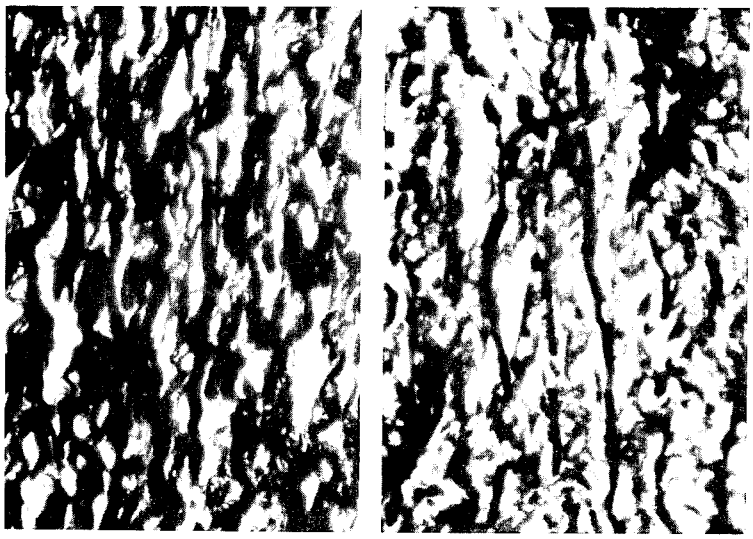

(a) (b)

FIG. 5. Optical micrographs of 5-micron sections of human aortic wall tissue. Verhoeff stain, 1500×. A. Circumferential section. B. Longitudinal section.

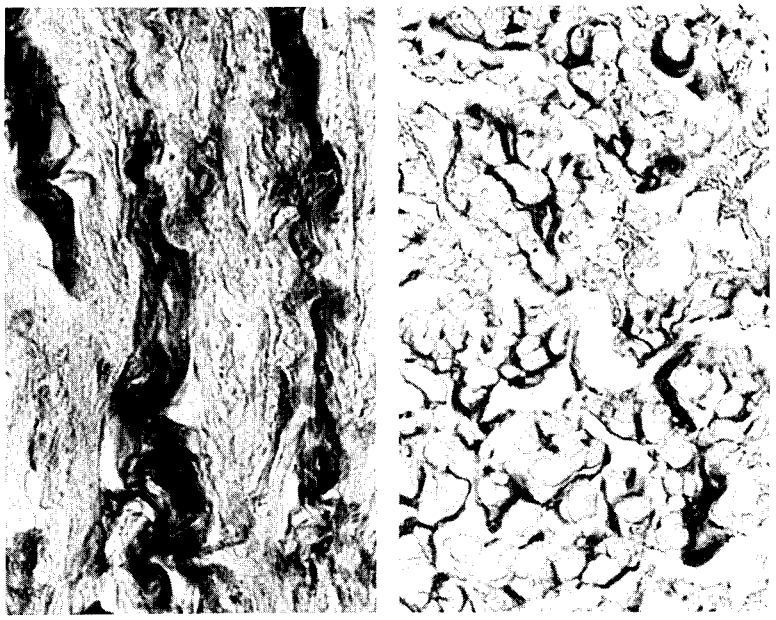

(a) (b)

FIG. 6. Optical micrographs of 5-micron sections of bovine aortic wall tissue. Aniline blue/orange G stain (collagen dark, elastin grey), 1500×. A. Circumferential section. B. Longitudinal section.

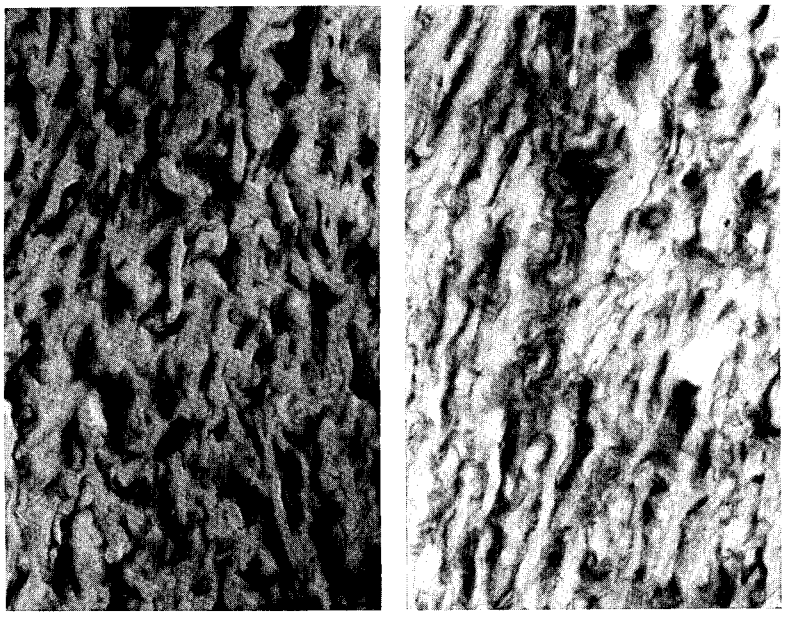

(a) (b)

FIG. 7. Optical micrographs of 5-micron sections of human aortic tissue. Aniline blue/orange G stain, 1500×. A. Circumferential section. B. Longitudinal section.

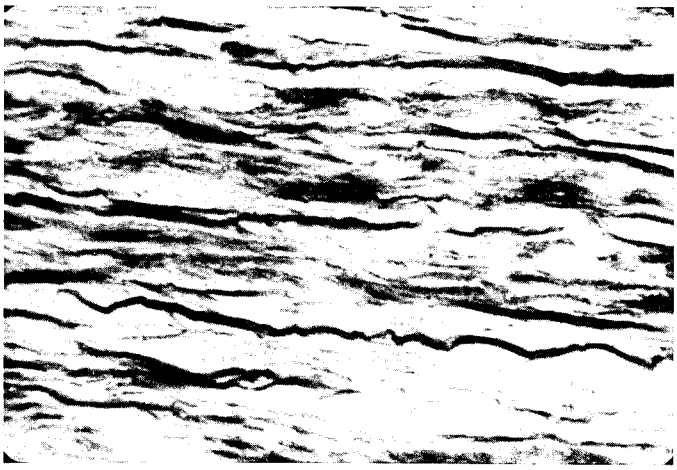

FIG. 8. Optical micrograph of 5-micron section cut in the ab plane from a circumferential bovine specimen, extended to = 1.5. Aniline blue/orange G stain, 1500×.

crofibril bundles, which often meander outside the focal plane of the micrograph. In the bovine tissue the collagen structures show the same high degree of circumferential orientation as the elastin structures of Figure 4. Human aortic collagen is only slightly anisotropic, but perhaps to a greater extent than the elastin networks (compare Figures 5 and 7).

These histological observations are in excellent agreement with the macroscopic stress/deformation behavior of the bovine and human aortic specimens, shown in Figures 2 and 3. At low extensions the stress is borne mainly by the elastin fibers; hence, the tensile modulus of the whole tissue is similar to that of pure elastin. Progressive straightening of the collagen fibril bundles causes the observed sharp increase in modulus at intermediate extensions ($1.4 < \lambda < 1.6$), while at high extensions the collagen

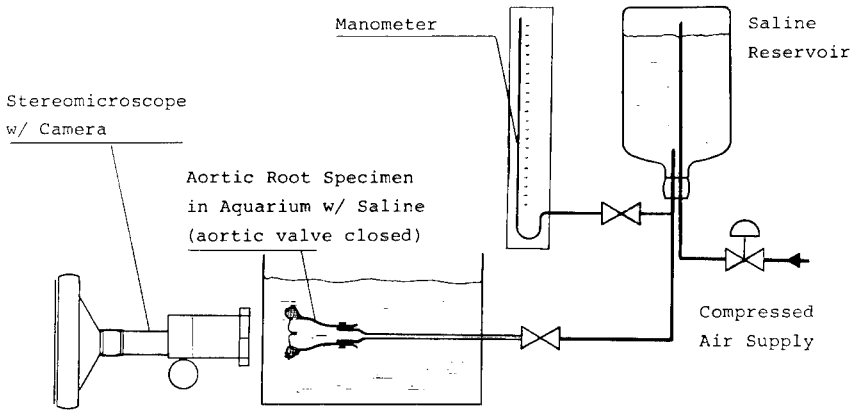

FIG. 9. Schematic diagram of apparatus for subjecting aortic valve specimens to simulated diastolic pressure.

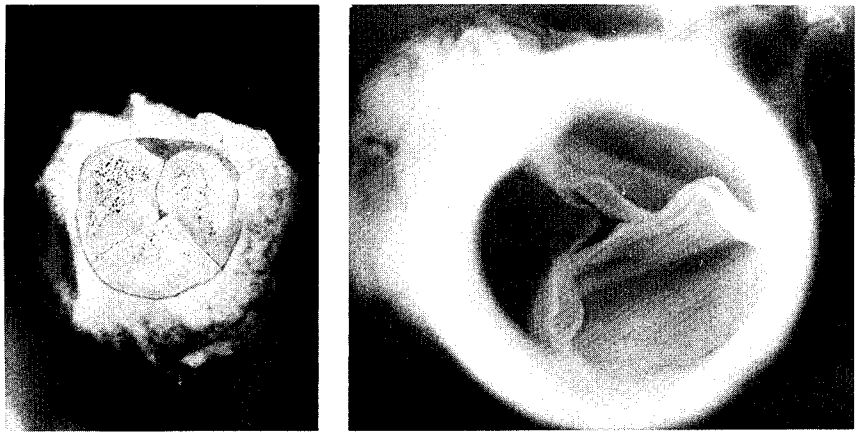

(a) (b)

FIG. 10. A. Ventricular view of closing aortic valve showing the India Ink microdots sprayed on the leaflets. 1.5×. B. Aortic view of valve showing coaptation of the closing leaflets along their free edge. 3×.

fibers begin to strain, and, because of their high modulus, become the main load-bearing component. This is illustrated in Figure 8, where, at an extension ratio of 1.5, the majority of the collagen fibrils in the bovine specimen are now straight, forming well-defined continuous bundles in the direction of stress. A similar straightening of the collagen fibers in the stress direction is also observed with human aortic tissue.

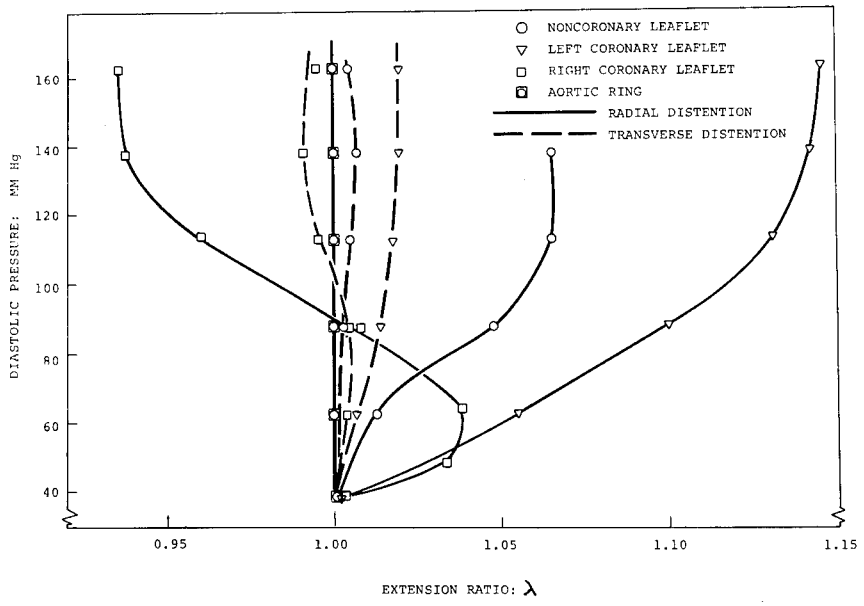

FIG. 11. Typical leaflet distention in the radial and transverse directions when the aortic valve is subjected to simulated diastolic pressures.

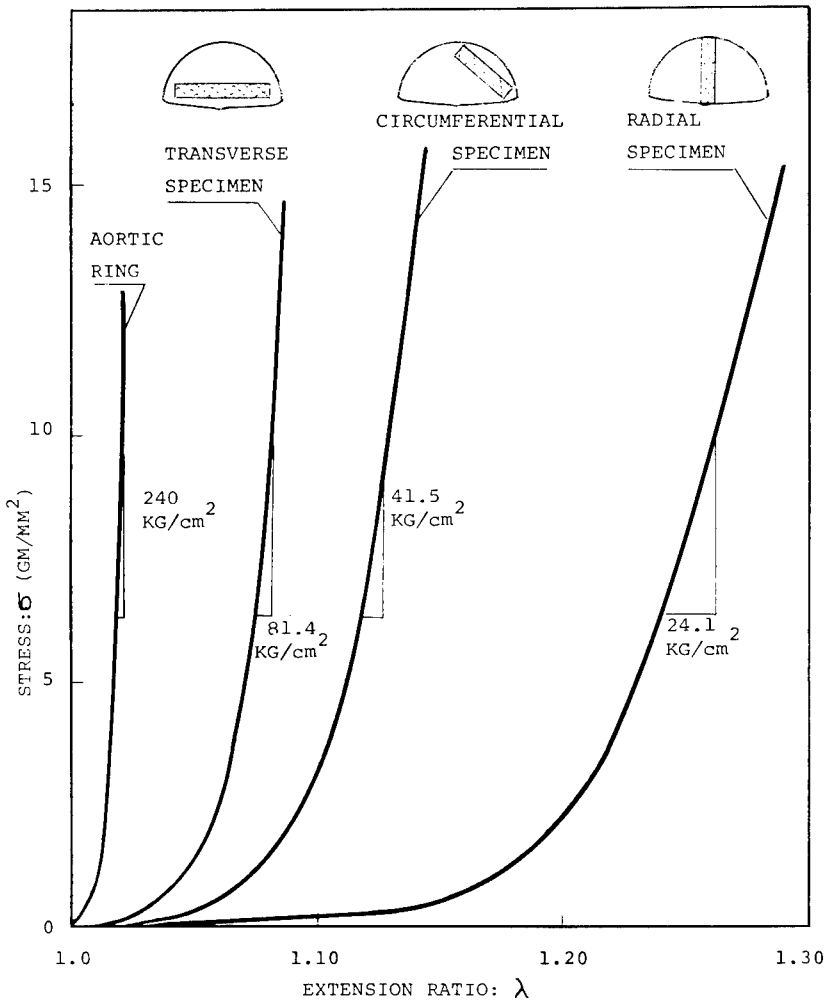

FIG. 12. Typical stress-deformation data for microtensile specimens, cut from the aortic valve leaflets in the radial, transverse and circumferential direction and from the aortic ring.

Aortic Valve Mechanics

The closing and distention of the human aortic valve under simulated diastolic pressure was observed in vitro by connecting the aortic root specimens (after ligation of the coronaries) to a saline system which can be pressurized, as shown in Figure 9. By careful dissection of the ventricular tissue around the aortic ring it was possible to expose the ventricular surface of the valve leaflets, without disturbing the anatomic configuration of the aortic root, which would render the valve regurgitant. A typical valve thus trimmed is shown in Figure 10. In order to monitor in detail the deformation of the individual valve leaflets under pressure, a random pattern of India Ink microdots was deposited on the ventricular surface of the valve

using an artist's spray gun. The valve was photographed through a stereomicroscope while subjected to different pressures and the change in the microdot patterns measured on the photographs. The aortic ring contour at each pressure was also measured. Dimensional changes of the leaflets in the radial and transverse directions could thus be plotted as a function of pressure. A typical plot is shown in Figure 11.

In general the seven normal aortic valves tested here show appreciable distention in the radial direction only. This reaches an average overall value of 14 $\pm$ 8% at pressures of 100–130 mm Hg and does not change with further increase in pressure (up to 210 mm Hg). Individual leaflets within a valve show greater or lesser radial distentions and they may even contract. Of considerable importance is the invariance of aortic ring contour length with pressure shown by all nonregurgitant valves and the extremely low (< 2%) distention of the leaflets in the transverse direction.

In order to investigate the mechanical properties of the aortic valve components, a series of microtensile specimens (2mm wide by 0.8–1.2 cm long) were cut from individual leaflets in the radial, transverse and circumferential directions and from the aortic ring. These were deformed in tension, while immersed in saline. Figure 12 shows typical stress–deformation data, while Table IV gives the statistical significance of the calculated tensile moduli. The remarkably high modulus of the aortic ring explains its dimensional invariance under pressure, while the relatively low modulus of the leaflet tissue in the radial direction is consistent with the observed radial distention when the valve is under diastolic pressure.

Preliminary histologic examination of the aortic valve and ring shows a complex network of collagen fibrils as the predominant structural component. While some preferential orientation of the fibrils in the transverse direction of the leaflet is observed in some sections, this is by no means prevalent over the entire leaflet. The elastin content of the leaflet is extremely low. A small number of elastin fibers are observed only near the free edge and at the ventricular surface. The aortic ring is almost entirely collagenous. These histological observations are consistent with the fact that removal of lipids and elastin from the leaflets and aortic ring causes no significant change in the mechanical properties of the microtensile specimens, while decollagenation of the tissue results in virtual disintegration.

TABLE IV
Mechanical Properties of Microtensile Specimens from Aortic Valve Leaflets

	Specimen Direction			
	Radial	Transverse	Circumf.	Aortic Ring
No. of Specimens	15	19	6	3
E_{ave}: kg/cm^2	25	85	36.6	243.6
Std. Deviation	12.2	32	16.6	54.9

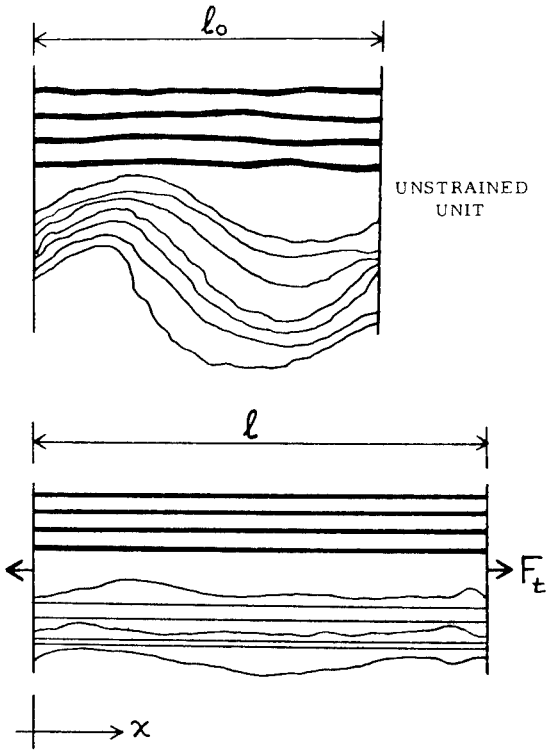

FIG. 13. Schematic diagram of the basic mechanical unit of aortic tissue, showing parallel arrangement of elastin fibers (heavy lines) and collagen fibrils (thin lines).

ANALYTICAL TREATMENT

A quantitative treatment of the deformation behavior of aortic tissue,based on histologic considerations is possible by assuming a parallel arrangement of elastin fibers and collagen microfibril bundles, as shown schematically in Figure 13. The elastin fibers have an initial (unstrained) length, l_o, equal to that of the overall unit, while the collagen fibrils are characterized by individual lengths, l_i, which are distributed about some mean value, $\bar{l}$ with characteristic spread s. Application of a tensile force, F_t on this unit causes an increase in length from l_0 to l. The contribution of the elastin and collagen to the retractive force is:

$$F_t = F_{\text{elast.}} + F_{\text{coll.}} = n_e E_e (l - l_0) + E_c \sum_{i=1}^{n_c} (l - l_i) \qquad (1)$$

In this expression E_e and E_c are spring constants, characterizing the rigidity of elastin and collagen respectively, while n_e represents the number of elastin fibers in the unit, all of which contribute equally to the retroactive force. With increasing tensile deformation of the unit the collagen fibrils start to strain, as l takes values within the distribution of l_i. The number of unstrained, fully extended fibrils at a given elongation of the unit is:

$$n(l) = n_c p(l; \bar{l}, s) \qquad l > l_0 \tag{2}$$

where n_c is the total number of collagen fibrils and p (l,l,s) denotes the probability of finding fibrils with unstrained lengths l, according to their length distribution, l(l;l,s), defined as:

$$l(l; \bar{l}, s) = \frac{\int_{l_0}^{l} xn(x)\,dx}{\int_{l_0}^{l} n(x)\,dx} = \frac{\int_{l_0}^{l} xp(x; \bar{l}, s)\,dx}{\int_{l_0}^{l} p(x; \bar{l}, s)\,dx} \tag{3}$$

where x is an integration variable. From histological observations the lower bound of fibril length can be set at l_o:

$$\lim_{l \to l_0+} l(l; \bar{l}, s) = \lim_{l \to l_0+} (l) = l_0 \tag{4a}$$

which makes the second term in eq. (1) negligible at low strains. From the definition of $\bar{l}$ we have:

$$\lim_{l \to \infty} l(l; \bar{l}, s) = \bar{l} \tag{4b}$$

Substitution of Equation (3) into (1), division by A_o (the unstrained cross-sectional area of the specimen) and substitution of the extension ratio, γ, for l yields:

$$\sigma_0 = \frac{F_t}{A_0} = \frac{n_e E_e l_0}{A_0}(\lambda - 1) + \frac{n_c E_c l_0}{A_0}\left(\lambda - \frac{l(l; \bar{l}, s)}{l_0}\right)$$

$$= E_{\text{low}}(\lambda - 1) + E_{\text{high}}\left(\lambda - \frac{l(l; \bar{l}, s)}{l_0}\right) \tag{5}$$

where E_{low} and E_{high} are the low and high strain moduli of the whole tissue. A reasonable distribution function for p(l;$\bar{l}$,s) is the Gaussian function (8):

$$p(l; \bar{l}, s) = \frac{1}{s\sqrt{2\pi}} \exp\left[-\frac{1}{2}\left(\frac{l - \bar{l}}{s}\right)^2\right] \tag{6}$$

This treatment gives an analytic description of the stress–deformation behavior of the aortic tissue, as well as its main structural components. The response of the defatted specimens is represented by increasing the value of s over that used for whole tissue, while by letting $n_c = 0$ the model gives the linear response of pure elastin. The response of the collagen network alone is obtained by setting $n_e = 0$.

DISCUSSION

The potential value of the in vitro measurements of this work lies in their extrapolation to predict in vivo properties of arterial tissue. It is possible to convert the stress–deformation data of tensile specimens into corresponding blood-pressure distension values for the whole vessel by means of a relation.

developed for the deformation of pressurized isotropic tubes with fixed ends. The expression requires knowledge of the thickness-to-diameter ratio of the tube and Poisson's ratio of the material [25]. Despite the known anisotropy of aortic tissue and its unknown Poisson's ratio, this conversion is often made [13, 15]. On this basis the physiologic blood pressure range is shown to correspond to the nonlinear stress/deformation region of the native aortic tissue (Figs. 2 and 3).

Comparison of the results of this work with previous measurements of human aortic tissue properties [1, 6, 26] is extremely difficult due to differences in testing techniques (pressure–distension vs stress–strain measurements) and reporting of data (incremental vs tangent modulus). There is also considerable variance in age and histopathology between the specimens studied by the different investigators. Within these uncertainties the results of the different studies (including the present) are in general agreement.

The effect of lipid removal on mechanical properties is of considerable interest. The significant difference in stress–deformation behavior between native and defatted tissue in bovine and human specimens with appreciable lipid content raises the possibility that lipids may participate in the stress-transfer mechanism of tissue deformation. A similar effect of lipids on aortic deformation behavior has been observed in vivo [27]. It should be noted here that the defatting process causes no measurable changes in the mechanical properties of either the collagenous or elastic components of the aortic tissue, indicating that the observed differences in behavior between the native and defatted tissue are not due to denaturation of structural components.

The observed behavior of the decollagenated tissue (Curve C, Figs. 2 and 3) is in agreement with previous stress–deformation measurements on elastin, purified from ligamentum nuchae [28]. These data clearly indicate that the response of elastin to tensile stress is indeed linearly elastic over its entire deformation range. This behavior cannot be described by the theory of rubber elasticity and raises serious doubts on the applicability of that theory to obtain estimates of molecular parameters of elastin from its mechanical properties [17].

The histologically observed orientation of the collagenous and elastic networks in the aortic tissue has a pronounced effect on the properties of the tissue at high deformations. In the case of the bovine tissue which is highly anisotropic, the circumferential specimens show little change in extension at failure (λ_f) upon removal of either collagen or elastin. This is in agreement with the histologically observed circumferential orientation of both structural networks and consistent with the parallel model assumed in our analytical treatment. In the longitudinal specimens, decollagenation causes a modest decrease in λ_f, while removal of elastin completely destroys the structural integrity of the remaining tissue. (Figure 2, Curve D). In the human tissue the essentially biaxial orientation of both structural networks causes a significant reduction in λ_f with removal of collagen or elastin in the circumferential as well as longitudinal directions (Figure 3, Table IIB).

The analytical treatment developed in this work provides a 4-parameter description of the aortic tissue mechanics. Its possible advantage over previous phenomenological models lies in the histological origin of its parameters. E_{low} corresponds to the tensile modulus of pure elastin, which is the prime loadbearing component at low extensions, while E_{high} is related to the tensile modulus of the collagen network. Values for both of these parameters may be obtained from mechanical property measurements of purified collagen or elastin from the respective species (bovine or human). The parameters $\bar{l}$ and s are defined in terms of tissue microstructure and can be directly obtained from histological observations. We have been able to estimate $\bar{l}/l_o$ (the normalized mean unstrained length of collagen fibril bundles) as well as s from careful measurements of the contour lengths of collagen bundles, which are seen in microtomed sections of unstretched circumferential specimens (Fig. 6). The values of $\bar{l}/l_o$ obtained from sections, microtomed along the (ab) or the (ac) planes of the circumferential specimens (Fig. 1) are similar, averaging 1.5. This indicates that the distribution of the collagen network is isotropic in these two directions.

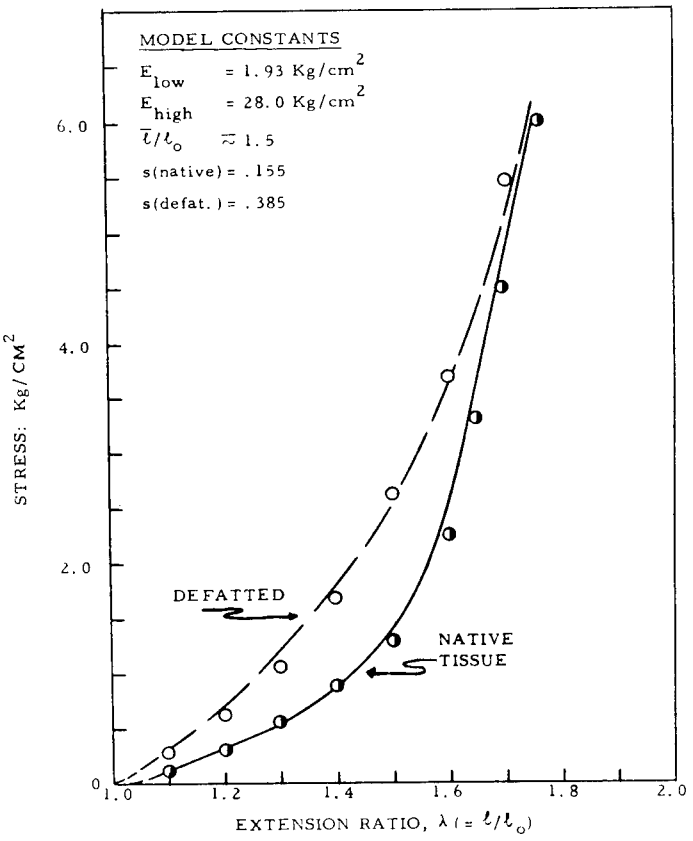

FIG. 14. Comparison of tensile stress–deformation behavior predicted by eq.(5) (solid and dotted lines) with experimental data for native (◑) and defatted (○) aortic tissue.

It is significant that the histologically determined parameters $\bar{1}$ and s, when substituted in eq. (5), along with values of E_{low} and E_{high} yield a curve, which is in excellent agreement with the observed mechanical behavior of the specimen. This is shown in Figure 14 with data of the native and defatted tissue specimens from Figure 2. The analytical expressions for the two curves differ only in the value of the parameter s, which was arbitrarily assumed for the defatted specimen. Thus the analytical treatment, developed in this work, gives an accurate structural model of the mechanics of "normal" aortic tissue, which is consistent with histological observations. This model may now be used as a basis for defining quantitatively the changes in structure and function associated with aging or various histopathologic conditions. Of primary interest are, of course, the effects of lipids in aortic tissue, which can be effectively investigated by this type of approach.

Our studies on aortic valve mechanics, although still preliminary in nature, indicate a mode of operation in which proper coaptation of the closing leaflets is the main factor determining valve sufficiency. In a physiologically functioning system, aortic pressure rises rapidly to its maximum value at the start of the diastolic cycle, thus causing rapid closure of the aortic valve with radial distention of the coapting leaflets. Deviations from this mode of operation would tend to make the valve regurgitant. These are observed in patients with syphllitic aortitis, where dilatation of the compliant aortic root prevents proper closure of the leaflets [29]. Regurgitation in normal valves can also be caused in vitro by a very slow increase in diastolic pressure. This hinders the initial high rate of flexure and radial distention of the leaflets, which characterizes physiologic valve operation and seems to cause improper leaflet coaptation.

The observed low modulus of the valve leaflets in the radial direction tends to minimize the concentration of flexural and shear stresses during valve motion upon opening and closing. These results are consistent with the analytical study of aortic valve motion by Swanson and Clark [30].

A detailed histologic study of the directional organization of the collagenous network of the aortic valve currently under way is expected to provide a firmer structural basis to the observed macroscopic behavior. Of considerable interest is also the nature of the highly compliant ground substance that surrounds the collagen structures and manifests itself macroscopically in the extensive toe regions of the stress–deformation data.

The financial support of this work by research grants HE 09251 and HE 13330 of the National Institutes of Health is gratefully acknowledged.

REFERENCES

[1] B. M. Learoyd, and M. G. Taylor, *Circ. Res., 18,* 278–292.
[2] G. Mack, A. Ebel, E. E. Kempf, V. Pantesco, J. L. Fontaine, and R. Fontaine, *J. Cardio. Surg. (Torino), 11,* 292–296.
[3] Kramsch, D., *Exp. Gerontol., 4,* 1–6.
[4] H. Wolinsky, and S. Glagov, *Circ. Res., 14,* 400–413.

[5] Burton, A. C., *Physiol. Rev., 34,* 619–642.
[6] D. S. Summer, D. E. Hokanson, and D. E. Strandess, *Surg. Gynecol. Obstet., 130,* 459–466.
[7] George M. Hass, *Arch. Pathol., 34,* 971–981.
[8] Stanley Middleman, *Transport Phenomena in the Cardiovascular Systems*, Wiley, New York, 1972, pp. 19–22.
[9] B. G. Boyes—Barratt, *Conc. Cardio. Dis., 36,* 1–6.
[10] A. Carpentier, G. Lemaigre, L. Robert, S. Carpentier, and Dubost, C., *Thor. Cardio. Surg., 58,* 467–483.
[11] D. Ross, and H. Magdi, *Progr. Cardio. Dis., 11,* (4), 275–293.
[12] Y. C. B. Fung, *Amer. J. Physiol., 213,* 1532–1544.
[13] D. H. Bergel, *J. Physiol., 156,* 455–457.
[14] W. E. Mortiz, M. Anliker, and E. Ogden, "Proceedings of the 8th Conference on Medical and Biological Engineering, July 20–25, 1969, Session 27–5."
[15] D. J. Patel, J. S. Janicki, and T. E. Carew, *Circ. Res., 25,* 765–779.
[16] J. T. Apter, M. Rabinowitz, D. H. Cummings, and E. Marquez, *Circ. Res., 19,* 104–121, *21,* 901–918, and *22,* 393–404.
[17] A. Hoffman, *Biomaterials,* Seattle University Press: 1971, pp. 285–312.
[18] L. H. Peterson, R. E. Jensen, and J. Parnell, *Circ. Res., 8,* 622–639.
[19] L. W. Lake, and C. D. Armeniades, *Trans. Amer. Soc. Artif. Intern. Organs, 18,* 202–208.
[20] G. C. Wood, *Biochim. Biophys. Acta, 15,* 311–324.
[21] S. M. Partridge, *Advances in Protein Chemistry,* Vol. 17, Academic Press, 1962, pp. 227–302.
[22] R. E. Neuman, and M. A. Logan, *J. Biol. Chem., 184,* 299–306, and *186,* 549–556.
[23] J. P., Bentley, and A. N., Hanson, *Biochim. Biophys. Acta, 175,* 339–344.
[24] L. Gotte, A. Fracissini-Serfini, and V. Moset, *J. Atheroscler. Res., 3,* 244–247.
[25] S. Timoshenko and J. N. Goodier, *Theory of Elasticity*, Wiley, New York,1951, p. 258.
[26] E. M. Krokosky and T. Krouskop, *J. Biomed. Mater. Res., 2,* 357.
[27] J. T. Nichol, Cand. *J. Biochem. Phys., 33,* 507.
[28] T. Weis-Fogh, and S. O. Anderson, *Nature, 227,* 718.
[29] R. F. Rushmer, *Cardiovascular Dynamics,* 2nd Ed., Saunders, 1961, p. 340.
[30] W. M. Swanson, and R. E. Clark, ASME paper No. 72-WA/BHF-5, Winter Annual Meeting, New York, Nov. 26, 1972.

AUTHOR INDEX

Published Applied Polymer Symposia

1965	No. 1	High Speed Testing, Vol. V Co-Chaired by A. G. H. Dietz and Frederick R. Eirich
1966	No. 2	Thermoanalysis of Fibers and Fiber-Forming Polymers Edited by Robert F. Schwenker, Jr.
	No. 3	Structural Adhesives Bonding Edited by Michael J. Bodnar
1967	No. 4	Weatherability of Plastic Materials Edited by Musa R. Kamal
	No. 5	High Speed Testing, Vol. VI: The Rheology of Solids Co-Chaired by Rodney D. Andreqs, Jr., and Frederick R. Eirich
	No. 6	Fiber Spinning and Drawing Edited by Myron J. Coplan
1968	No. 7	Polymer Modification of Rubbers and Plastics Edited by Henno Keskkula
1969	No. 8	International Symposium on Polymer Modification Edited by K. A. Boni and F. A. Sliemers
	No. 9	High Temperature Resistant Fibers from Organic Polymers Edited by J. Preston
	No. 10	Analysis and Characterization of Coatings and Plastics Edited by Claude A. Lucchesi
	No. 11	New Polymeric Materials Edited by Paul F. Bruins
	No. 12	High Speed Testing, Vol. VII: The Rheology of Solids Co-Chaired by Rodney D. Andrews, Jr., and Frederich R. Eirich
1970	No. 13	Membranes from Cellulose and Cellulose Derivatives Edited by Albin F. Turbak
	No. 14	Silicone Technology Edited by Paul F. Bruins
	No. 15	Polyblends and Composites Edited by Paul F. Bruins
1971	No. 16	Scanning Electron Microscopy of Polymers and Coatings Edited by L. H. Princen
	No. 17	Mechanical Performance and Design in Polymers Edited by O. Delatycki
	No. 18	Proceedings of the Fourth International Wool Textile Research Conference Edited by Ludwig Rebenfeld
1972	No. 19	Processing for Adhesives Bonded Structures Edited by Michael J. Bodnar
1973	No. 20	United States–Japan Seminar on Polymer Processing and Rheology Edited by D. C. Bogue, M. Yamamoto, and J. L. White
	No. 21	High-Temperature and Flame-Resistant Fibers Edited by J. Preston and J. Economy
	No. 22	Polymeric Materials for unusual Service Conditions Edited by Morton A. Golub and John A. Parker